University of Southampton

Faculty of Environmental and Life Sciences

School of Health Sciences

Bioengineering technologies to monitor movements in supported postures: a potential strategy to prevent pressure ulcers

Silvia Caggiari

Thesis for the degree of Doctor of Philosophy

March 2020

University of Southampton

Abstract

Faculty of Faculty of Environmental and Life Sciences

School of Health Sciences

Thesis for the degree of Doctor of Philosophy

Bioengineering technologies to monitor movements in supported postures: a potential strategy to prevent pressure ulcers

by

Silvia Caggiari

There are many clinical situations in which skin and soft tissues are subjected to sustained mechanical loading, particularly in individuals with restricted mobility. This can result in the breakdown of soft tissues in vulnerable areas, leading to the development of pressure ulcers (PUs). For several decades, interface pressure measuring systems have been employed to assess the magnitudes of pressures at the support surface interface of individuals at risk of developing PUs, typically to evaluate the short-term performance of pressure relieving systems (e.g. mattresses) and promote optimal postures. These technologies have recently been adapted to monitor over extended periods, providing the opportunity to estimate clinically-relevant temporal trends in posture and mobility. However, their ability to detect individual postural movements has not been established. Therefore, the present research was designed to assess the combination of pressure monitoring and intelligent data processing for the detection of postural changes during prolonged lying.

A series of experimental studies utilised biomechanical parameters derived from pressure distribution and signals representative of body segmental movements using actimetry systems. Continuous measures were taken in cohorts of healthy individuals during evoked lying postures involving a raised head of the bed (HOB) and automated lateral tilt. The sensitivity and specificity of parameters for detecting changes in defined lying postures were examined. Data optimisation with Receiver Operating Characteristics (ROC) and Principal Component Analyses were performed to establish the most robust parameters, thus reducing the large volume of data associated with long-term monitoring. In particular, contact area and centre of pressure signals at specific body regions i.e. whole body and buttock, proved the most accurate of the interface pressure parameters, with ROC curve values (AUC) exceeding 0.5 for the majority of evoked postures. Signals derived from actimetry at the sternum also proved accurate in detecting postural movements, with the majority of postures revealing high AUC values. These parameters were combined with an automated detection method and machine learning algorithms to develop a robust methodology capable of predicting the frequency and magnitude of postural changes.

The methodology was refined to accommodate a random sequence of postures on different support surfaces. The final automated methodology was then tested on pressure monitoring data from a small cohort of spinal cord injured subjects, who are vulnerable to PU development.

Prediction of lying postural changes was achieved with a derivative threshold – based method, which yielded an accuracy of 100% when pressure signals were combined with body angles, and >85% for pressure signals in isolation. Prediction of lying postures was achieved by applying machine learning classifiers to either a combination of actimetry and pressure data or the pressure parameters in isolation. The most accurate combination of clinically relevant parameters involved pressure signals and body angles, achieving an average accuracy of ≥88%.

The series of experiments and analytical approaches undertaken in this project contributed to the development of a semi-automated methodology based on robust biomechanical parameters for prediction of posture and mobility during prolonged lying. This was translated to a clinical data set, where long-term pressure monitoring was employed to evaluate previously unknown postures and provide the objective means to evaluate whether repositioning for pressure ulcer prevention adhered to international guidelines. Although further improvements are required for the analysis and visualisation of pressure data in clinical settings, this novel methodology has the potential to provide objective indication of posture and mobility which will inform effective personalised PU prevention.

Table of Contents

Table of Tables

Table of Figures

Research Thesis: Declaration of Authorship

Print name: Silvia Caggiari

Title of thesis: Bioengineering technologies to monitor movements in supported postures: a potential strategy to prevent pressure ulcers

I declare that this thesis and the work presented in it are my own and has been generated by me as the result of my own original research.

I confirm that:

1. This work was done wholly or mainly while in candidature for a research degree at this University;
2. Where any part of this thesis has previously been submitted for a degree or any other qualification at this University or any other institution, this has been clearly stated;
3. Where I have consulted the published work of others, this is always clearly attributed;
4. Where I have quoted from the work of others, the source is always given. With the exception of such quotations, this thesis is entirely my own work;
5. I have acknowledged all main sources of help;
6. Where the thesis is based on work done by myself jointly with others, I have made clear exactly what was done by others and what I have contributed myself;
7. Parts of this work have been published or are under peer review:
   Caggiari S, Worsley PR, and Bader DL (2019) A sensitivity analysis to evaluate the performance of temporal pressure – related parameters in detecting changes in supine postures. *Medical Engineering & Physics* 69: 33-42.

   Caggiari, S., P. R. Worsley, Y. Payan, M. Bucki, and D. L. Bader. Biomechanical response and machine learning for the detection of lying postures. *Journal of Clinical Biomechanics* – **under review**

Signature: Date:

Dissemination

Publications

Caggiari S, Worsley PR, Payan Y, Bucki M, and Bader DL**.** Biomechanical response and machine learning for the detection of lying postures. *Paper in reviewing process to Clinical Biomechanics Journal*.

Caggiari S, Worsley PR, and Bader DL. (2019) A sensitivity analysis to evaluate the performance of temporal pressure - related parameters in detecting changes in supine postures. Medical Engineering & Physics, 69, 33-42

Conference presentations

Caggiari S. (2019) Prediction of individual positioning in a range of lying postures. Medical Physics and Engineering Conference (MPEC), 21-23 September, Bristol

Caggiari S. (2019) A novel approach to identify individual positioning in a range of supine postures. European Pressure Ulcers Advisory Panel (EPUAP), 18-20 September, Lyon

Caggiari S. (2018) Can the efficacy of pressure relieving strategies be assessed through the magnitude of movements performed? European Pressure Ulcers Advisory Panel (EPUAP), 12-14 September, Rome

Conference Posters

Caggiari S. 2018 Pressure monitoring and actimetry systems to evaluate temporal biomechanical and spatial changes during lying postures. World Congress of Biomechanics (WCB), 8-12 July, Dublin

Acknowledgements

Firstly, I would like to express my limitless gratitude to my supervisors, Dan and Peter, for their guidance, help and support throughout this journey. Thank you both for having made your valuable expertise available to me at all time.

I would like to thank Engineering & Physical Sciences Research Council (EPSRC) and Sumed International for having funded and supported this research. In particular, my thanks go to Graham Collyer for his encouragement and support throughout the project.

My thanks also go to Professor Payan and his research group at the University of Grenoble, for having shared their valuable knowledge and experiences in using machine learning to analyse large data sets of interface pressures. This collaboration was facilitated by a financial grant from the European Pressure Ulcer Advisory Panel (EPUAP), which was greatly appreciated.

Last but not the least, my thanks go to whomever has contributed in several ways to help me achieve my end goal.

All the volunteers who took part in this study. Thanks for having taken 2 hours of your time to lying in a bed. My colleague Sarah for having shared the clinical data. A thank goes to the patients who have been involved in this study.

My mother for spiritually supporting me throughout these years away from home.

Martina and all other people I met in Southampton over the past three years, who have helped me on finding a new home.

My friends, who have given me carefree time during my awaited holidays.

My colleagues, who have provided a friendly environment to work in.

Grazie a tutti!

Abbreviations

APAM	Alternating pressure air mattress
ASIA	American Spinal Injury Association
AUC	Area under the (ROC) curve
B	Buttock
BMI	Body mass index
CA	Contact area
CLP	Constant low pressure
CLRS	Continuous lateral rotational system
CNN	Convolutional neural network
COP	Centroid of the pressure distribution
DTI	Deep tissue injury
EPUAP	European Pressure Ulcer Advisory Panel
FE	Finite Element
GUI	Graphical User Interface
HOB	Head of bed
HS	High sitting
I/R	Ischemic/reperfusion
IMU	Inertial motion unit
IQR	Interquartile range
IRAS	Integrated Research Application System
KNN	k-Nearest Neighbors
LB	Lower body
LDF	Laser Doppler Fluxmetry
MDRPU	Medical device-related pressure ulcer
MRI	Magnetic resonance imaging
NB	Naïve – Bayes
NPUAP	National Pressure Ulcer Advisory Panel

PC	Principal component
PCA	Principal component analysis
PP	Peak pressures
PPG	Peak pressure gradient
PPI	Peak pressure index
PPPIA	Pan Pacific Pressure Injury Alliance
PU	Pressure ulcers
PURPOSE T	Pressure Ulcer Risk Primary or Secondary Evaluation Tool
RAS	Risk assessment scale
ReLU	Rectified Linear Unit (layer)
RMS	Root mean square
ROC	Receiver Operating Characteristics (curves)
ROI	Region of interest
SCI	Spinal cord injury
SD	Standard deviation
SVM	Support Vector Machine
T_cPCO_2	Transcutaneous carbon dioxide tension
T_cPO_2	Transcutaneous oxygen tension
UB	Upper body
WB	Whole body

Chapter 1: Structure and function of skin and subcutaneous tissues in health and following mechanical damage

The present chapter aims to detail the structure, function and biomechanical aspects of healthy skin and underlying soft tissues. Additionally, the microcirculation, fundamental in maintaining the viability of these tissues, will be considered. The chapter will also discuss the state of art knowledge on the effects of mechanical loading on the integrity of skin and underlying soft tissues, where compromise can lead to the development of pressure ulcers (PUs). The aetiology, classification, risk factors, and prevalence and incidence of PUs are subsequently discussed, in conjunction with a range of preventive strategies.

1.1 Structure of the skin and subcutaneous tissues

The skin (Figure 1-1) represents the largest organ of the human body, with a surface area of approximately $2m^2$, accounting for approximately 15% of the total body weight in the adult human. It ranges in thickness from 0.5 to 4.0mm depending on anatomical location, where typically skin is thicker in weight bearing regions e.g. plantar aspect of the foot. Structurally, the skin is divided into three main layers, namely the epidermis, the dermis and the subcutaneous layers.

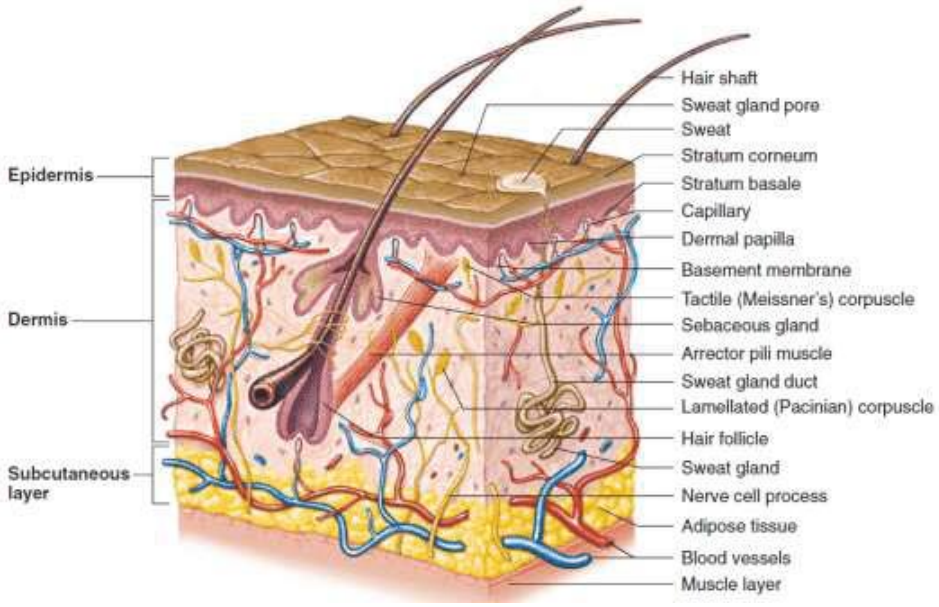

Figure 1-1: Schematic diagram of the skin and subcutaneous tissues (Shier et al. 2004).

The epidermis is the avascular outer layer of the skin, approximately 75–150μm thick, varying depending on the function and anatomical location. It consists of squamous epithelium, whose cells are stratified in different layers. The deepest is a region in which the keratinocytes, the

main epidermal cells, proliferate and slowly progress through the overlying strata. The most superficial layer, the stratum corneum, consists of cells that are tightly packed to provide a physical barrier to environmental pathogens and regulate water loss. These anuclear cells, termed corneocytes, are constantly being shed and replaced by cells from deeper layers. The epidermis also contains melanocytes responsible for the synthesis of the colour pigment, Langerhan cells responsible for the immune response and Merkel cells that provide tactile sensation.

The underlying dermis is the highly vascularised layer of skin, which provides structural strength and stiffness, water storage, and interaction with the epidermis through the basement membrane, in the form of an undulating epidermal – dermal junction. The dermis consists of two separate layers; a superficial layer called the papillary dermis and a deep layer called the reticular dermis. The main structural components of the dermis are collagen, elastin and proteoglycans, which interact to behave as a highly organised fibre-reinforced polymer gel. Sensory receptors are present throughout the dermis to provide touch, pain and heat sensation. In addition, the dermis contains blood capillaries, sebaceous glands and sweat glands, hair follicles and lymphatic capillaries (Figure 1-1). The vasculature of the dermis includes both superficial and deep architecture, which are interconnected (Figure 1-2). The former is comprised of paired arterioles and venules, with capillaries arising from the arterioles, extending upward within the papillary dermis and then looping back down to the venules. The deep vasculature consists of arterioles and venules of larger diameters that arise from the underlying muscles and subcutaneous fat. The two plexis are connected by paired ascending arterioles and descending venules, which supply the hair bulbs and sweat glands.

Subcutaneous tissue is the innermost layer of the skin, whose thickness varies with the presence of fat cells. This layer exhibits both insulating and cushioning properties, reducing cutaneous heat loss and protecting underlying structures. The subcutaneous blood vessels run parallel to the skin, whereas lymphatic vessels and nerves contained within the subcutaneous tissue are oriented perpendicularly, towards the skin. In addition, a proportion of mechanoreceptors responsive to pressure terminates in the subcutaneous tissue. In most sites, beneath the subcutaneous tissue lies skeletal muscle, composed of cells known as muscle fibres which are bundled and surrounded by connective tissue layers. This arrangement allows skeletal muscle to contract and release with minimal friction between the muscle fibres.

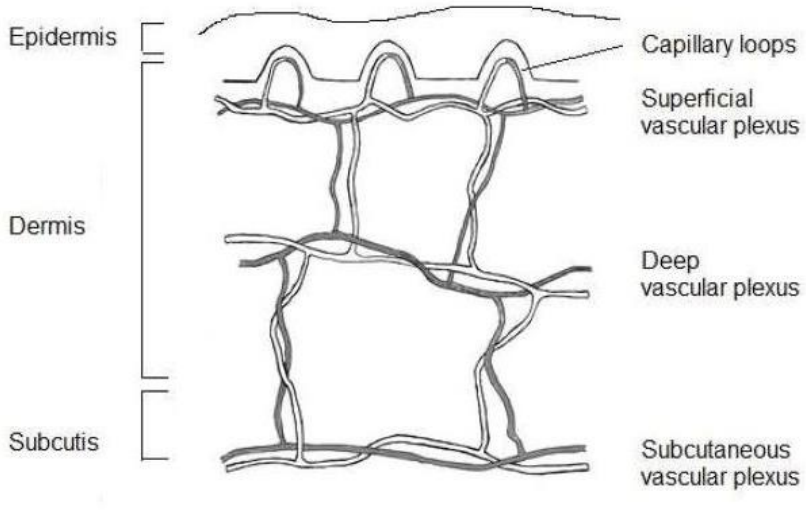

Figure 1-2: Schematic of the architecture of the vasculature in the skin (Liao et al. 2013).

1.2 Function of the skin

The skin has a range of functions, which can be classified as protective, thermoregulatory, sensory and biochemical in nature. Intact skin acts as a barrier, protecting the underlying tissues from external stimuli and mechanical damage. Accordingly, it maintains internal environment and prevents excessive fluid and moisture loss.

The heat-regulatory function occurs through thermoreceptors located within the skin. These transmit impulses to a specific region of the brain, the hypothalamus, which induces appropriate cutaneous vasodilatation or vasoconstriction. Vasodilatation causes heat loss from the surface by radiation and the release of sweat, cooling the surface of the skin. Vasoconstriction enables heat conservation by reducing surface cooling. In addition to thermal receptors, other sensory receptors are located within the skin. These are mechanoreceptors which detect touch, pressure and vibration, and nociceptors which detect painful mechanical, thermal or chemical stimuli.

Several biochemical reactions take place in the skin. As an example, vitamin D synthesis begins with activation of a precursor molecule when skin is exposed to ultraviolet light. In addition, the skin supports the metabolism of steroid hormones.

The external environment can compromise these functional roles as skin is exposed to a range of insults, which can be mechanical, biological and chemical in nature. These insults can affect the skin and lead to pathologies in the form of dermatological conditions or chronic wounds, impairing the functional and psychological well-being of the individuals affected (Spilsbury et al. 2007, Kapp et al. 2018).

1.3 Microcirculation of the skin

The network of vascular vessels ensures the supply of blood flow and the resulting transport of oxygen and nutrients required for cell metabolism. The associated lymphatic vessels are critical

for the removal of waste products from the skin and subcutaneous tissues. Oxygenated blood is transported by arteries before arriving at the capillaries, where cellular exchange occurs. The capillary loops drain into venules and subsequently veins, which carry deoxygenated blood back to the systemic circulation, where exchange of gasses occurs in a continuous cycle. However, blood flow to the capillary bed is not constant. Indeed, an important characteristic of the vascular system is the ability to proportionally control local blood flow, relying on the tissue demands resulting from, for example, changing temperature and metabolic activity. As an example hyperaemia, namely the increase in blood flow, may occur with increasing tissue demands, such as an increased exercise demand in muscles, or following a period of restricted oxygenation (ischemia), leading to reactive hyperaemia.

Interstitial fluid accumulates as result of normal vascular microcirculation. The combination of osmotic and hydrostatic pressures in plasma and interstitial fluid determines capillary permeability and reabsorption, as well as affecting the process by which lymphatic vessels remove proteins, waste products and excess fluid. Indeed, the high hydrostatic pressure in the arteriolar end of capillaries exceeds plasma osmotic pressure created by large proteins, such as albumin. Fluid filtration occurs as the interstitial fluid exerts an opposing force. This is balanced by the lower hydrostatic pressure at the venule end of the capillary, where plasma osmotic pressure exceeds capillary hydrostatic pressure and reabsorption occurs. Under normal physiological conditions, approximately 10% of the interstitial fluid created as the result of capillary hydrostatic pressure is not reabsorbed and thus enters the lymphatic capillaries.

Lymphatic capillaries, which have closed ends, consist of a structure that permits the unidirectional flow of interstitial fluid. This ensures that excess fluid and larger particles unable to be reabsorbed by the vascular microcirculation, are drained from the interstitial space. The resulting lymph fluid is transported into larger lymphatic vessels towards lymph nodes followed by lymph trunks, prior to returning to the venous circulation via lymphatic ducts. The interplay between the local vascular and lymphatic systems in the skin and underlying soft tissues ensure homeostasis is maintained.

1.4 Biomechanical considerations

Similar to all soft tissues of the body, the skin is a viscoelastic material, whose biomechanical properties reflect the characteristics of the network of collagen and elastic fibres embedded in a proteoglycan gel that support mechanical loads. These properties play a fundamental role in its protective function, particularly in response to prolonged external mechanical stimuli.

Skin and subcutaneous tissues are commonly subjected to direct mechanical deformations, as result of prolonged and/or cyclic loading during daily life activities, such as in lying or sitting, and during gait. Their biomechanical properties can adapt and tolerate these loads. As an example, when tissues are exposed to loading there is an increased capacity of subcutaneous vessels to dilate, thereby maintaining blood flow. This phenomenon is referred to as pressure –

induced vasodilatation and is regarded as a protective mechanism to minimize the damaging effect of external mechanical loads by delaying the occurrence of ischemia.

However, there may be many situations that lead to changes in the structure and composition of skin and soft tissues, which result in associated changes in mechanical function. As an example, ageing results in numerous changes within skin and soft tissues, such as a flattening of the epidermal-dermal junction. In addition, in the process of ageing, the overall thickness of the skin layers declines with an associated reduction in cell numbers (Farage et al. 2013). This leads to an increased rigidity and a diminished skin elasticity. Ageing further affects the microcirculation, leading a reduction of both the diameter and number of lymphatic capillaries, and the vascular capillary loops in the papillary dermis. Underneath the skin, the density of subcutaneous tissue alters and a loss of both muscle mass and strength occurs with advancing age.

In addition to age-related tissue changes, conditions such as spinal cord injury (SCI) can lead to adaptations in soft tissues behaviour. Following immobilization, which is typical for SCI individuals, there are changes in both geometric and mechanical muscle properties, such as in the gluteus muscles and the fat layer enveloping the muscles. This will result in an increase in the lipid content and a decrease in muscle tone, which will lead to decrease in tissue stiffness. Indeed, the muscle mass of SCI individuals has been found to be 44 % lower and the fat mass 35 - 100 % higher when compared to healthy individuals (Gefen 2007 a). In addition, the circulation in the SCI is impaired by a loss of muscle mass and capillary networks (Gefen 2007 a).

Therefore, changes in the biomechanical and physiological properties of the skin and underlying tissues may contribute to increased vulnerability, leading to an impaired ability to tolerate mechanical loads. Nonetheless, the response of the tissues is highly dependent upon the magnitude, duration and frequency of loading. In many individuals, the prolonged mechanical loading in combination with a decrease in tissue tolerance can result in the breakdown of the soft tissues, leading to the development of chronic wounds, termed pressure ulcers (PUs).

1.5 Pressure ulcers

Pressure ulcers are defined as an area of localized injury of the skin and/or the subcutaneous tissues as a result of a pressure, or pressure in combination with shear forces (NPUAP/EPUAP/PPPIA 2019). PUs represent chronic wounds, which generally affect individuals who have reduced mobility often associated with impaired sensation. These include the elderly, individuals with spinal cord injury (SCI) and those who are bed- or chair- bound following trauma or surgery. By contrast, when able-bodied individuals assume prolonged lying or seated postures, regular postural movements, involving both small- and large-scale movements, relieve pressures from the local tissue sites. This results from a natural sensorimotor function, where sensory feedback provides the stimulus for movement.

An international consensus concluded that reduced mobility/activity, skin condition and/or existing pressure ulcers status, and perfusion represented the most important risk factors for PU development (Coleman et al. 2014 a).

PUs generally develop adjacent to bony prominences, where tissue deformations are highest, for example the sacrum (28-36%), ischium (17-20%) and heels (23-30%) (Ferris et al. 2019). However, any tissue sites are at high risk when exposed to prolonged loading due to the application of functional medical devices (Black et al. 2010). As an example, intensive care patients requiring respiratory masks for prolonged therapy often develop damage, termed medical device-related pressure ulcers (MDRPUs), in vulnerable sites on the face, e.g. bridge of the nose.

1.6 Classification

PUs vary in size and severity and have been numerically staged (i.e. Stage 1, 2, 3, 4) depending on the depth of the damaged tissue. The most recent guidelines updated the staging system, to include the following definitions, as summarised in Table 1-1.

Table 1-1: PU classification system according to NPUAP and EPUAP (2019)

Stages		Description
Stage 1 - Non-blanchable erythema of intact skin		Intact skin with a localized area of non-blanchable erythema, which may appear differently in darkly pigmented skin. Presence of blanchable erythema or changes in sensation, temperature, or firmness may precede visual changes. Colour changes do not include purple or maroon discoloration.
Stage 2 - Partial-thickness skin loss with exposed dermis		Partial-thickness loss of skin with exposed dermis. The wound bed is viable, pink or red, moist, and may also present as an intact or ruptured serum-filled blister. Adipose (fat) is not visible and deeper tissues are not visible. Granulation tissue, slough and eschar are not present. These injuries commonly result from adverse microclimate and shear in the skin over the pelvis and shear in the heel.
Stage 3 - Full-thickness skin loss		Full-thickness loss of skin, in which adipose (fat) is visible in the ulcer and granulation tissue and epibole (rolled wound edges) are often present. Slough and/or eschar may be visible. The depth of tissue damage varies by anatomical location; areas of significant adiposity can develop deep wounds.
Stage 4 - Full-thickness skin and tissue loss		Full-thickness skin and tissue loss with exposed or directly palpable fascia, muscle, tendon, ligament, cartilage or bone in the ulcer. Slough and/or eschar may be visible. Epibole (rolled edges), undermining and/or tunnelling often occur. Depth varies by anatomical location.

The majority of PUs originate in the superficial skin layers and may progress downwards to the deeper tissues. However, it also possible that damage can originate in the deeper tissue adjacent to a bony prominence and project upwards towards the skin surface. The latter case is termed a deep tissue injury (DTI) where, in its early stage, the skin remains intact. DTI damage progresses rapidly and is often categorised as a stage 3 or 4 following skin breakdown. These ulcers are often associated with spinal cord injured individuals who have reduced mobility, impaired sensation and accordingly their vulnerable soft tissues are exposed to prolonged mechanical loading. The prognosis following a DTI is variable, with rates of infection known to be high. Figure 1-3 shows the different initiation sites and progression of PU damage.

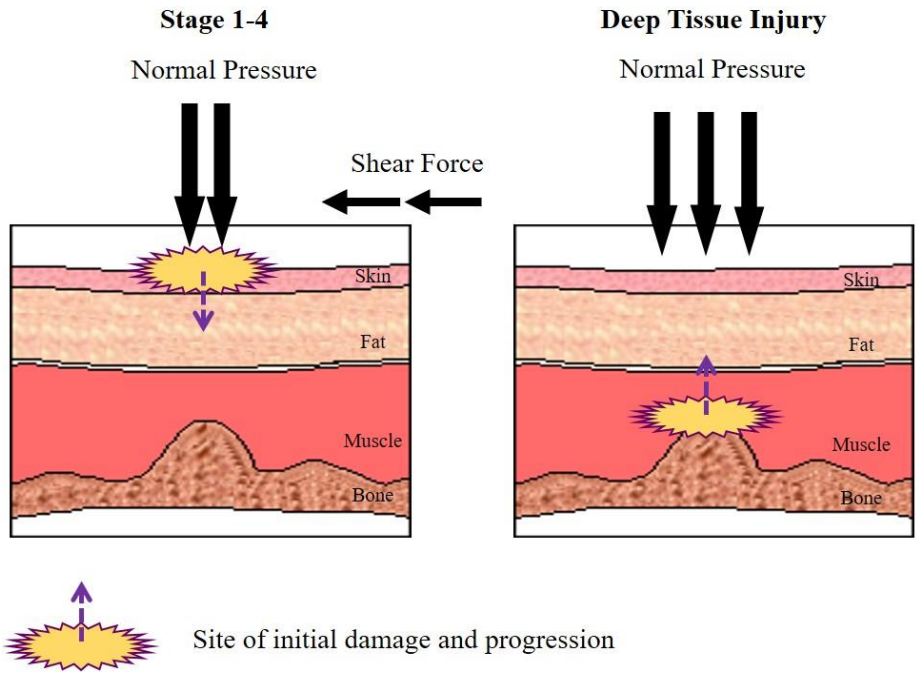

Figure 1-3: Representation of the different initiation sites and progression of PU development. On the left, PUs originate in the superficial skin layers and can progress downwards to the deeper tissues, referred to as PU stages 1-4. On the right, damage in initiated in the deeper tissues near a bony prominence while the skin remains intact and projects upwards to the skin surface (Figure kindly provided by Bader).

1.7 Aetiology of pressure ulcers

Over the years, the aetiology of pressure ulcers has been investigated by seminal research, identifying the main physiological mechanisms involved in tissue breakdown. PU development has traditionally been attributed to pressure, which causes localised tissue ischaemia and capillary closure. Indeed, it is well established that sustained tissue deformation, resulting from pressure alone can create an internal mechanical environment that causes the partial or total occlusion of blood vessels, thereby depriving the tissue of oxygen and nutrients supply, leading to a localized ischemic event (Daniel et al. 1981, Herrman et al. 1999).

Much of the early investigations (Husain 1953, Kosiak 1961, Reswick and Rogers 1976, Daniel et al. 1981) involving animal models, focused on determining the magnitude of loading that lead to the onset of tissue damage. In most cases, the damaging effects of compression of soft tissues were examined via a prescribed indenter applied to the skin for various time periods, with histology used to assess the resulting structural changes in the soft tissues. These studies established threshold values for pressure magnitude and duration above which tissue damage will occur. As an example, Daniel and colleagues (Daniel et al. 1981) indicates that tissue from a porcine model could withstand significant loads of between 150-200mmHg for 15 hours without causing skin necrosis. However, other animal models e.g. rat model (Kosiak 1961), revealed a considerably lower tissue tolerance to damage with respect to the magnitude and time of applied pressure. Thus, although these seminal studies all yielded an inverse relationship between magnitude and time, a large variability was evident (Figure 1-4). This variation might be predicated given the considerable differences between studies in terms of experimental conditions, animal models and the location and application of mechanical loading.

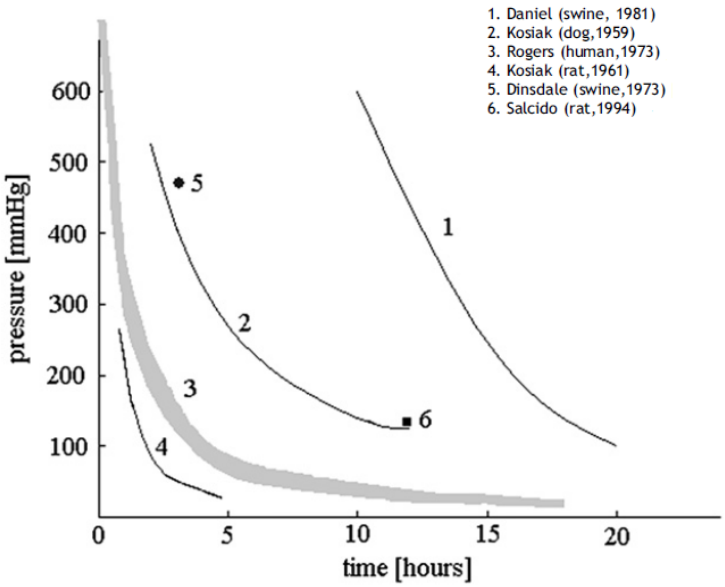

Figure 1-4: Inverse relationship between pressure and time from different studies investigating the aetiology of PUs (Oomens et al. 2010).

Of particular interest is the parabolic curve (curve 3 in Figure 1-4) based on the pressures measured at the body-seat interface in human patients in a US rehabilitation centre (Reswick and Rogers 1976). This trend was well accepted by both the clinical and scientific communities, and was subsequently adopted as a risk curve of applied pressure against time. It strongly implies that low pressures can be tolerated for a long time period, whereas high pressures are only tolerable for relatively short time periods. However, more recently a few researchers have questioned this relationship, based on its validity at both extremes of the time scale and the use

of the interface pressure as the single measure for which tissue compromise was assessed (Gefen 2009 a, Gefen 2009 b). In particular, interface pressures are not generally representative of the internal mechanical conditions, in terms of the states of stress and strain within the tissues, where breakdown will occur. Indeed, the initial phase of damage development can be a local event that will occur inside the tissue and not necessarily at the skin surface (Bosboom et al. 2001, Bouten et al. 2001).

Accordingly to understand the aetiology of pressure ulcers, it is important to consider the internal mechanical conditions of tissues which are not homogenous in nature (Oomens et al. 2003). Due to the complex geometry of the different tissue layers, involving soft tissues down to bone, the stress and strain state within the individual tissue layers for a specific mechanical load will lead to a heterogeneous distribution. This is illustrated in Figure 1-5, which reveals an inhomogeneous stress distribution in buttock tissues, as predicted by a Finite Element (FE) model of an individual sitting on a cushion.

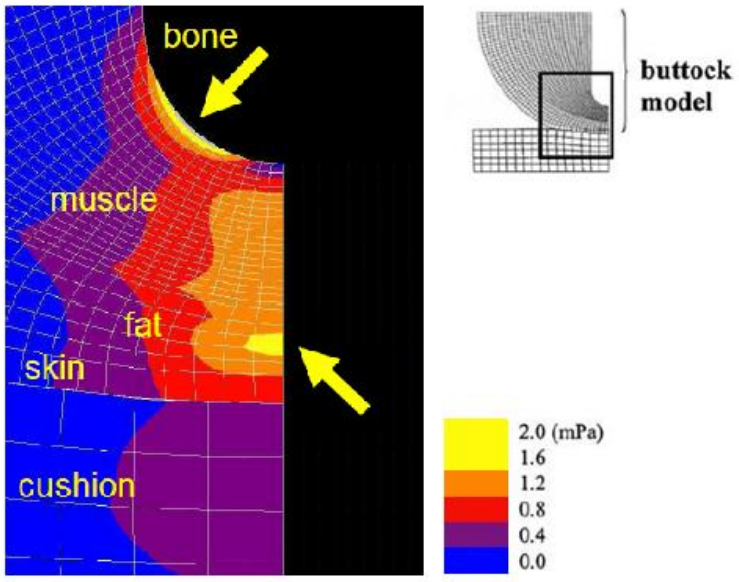

Figure 1-5: Internal stresses in the different tissue layers, involving skin, fat, muscle and bone during a simulation of sitting. The arrows represent the high stresses that occur in both the muscle and fat layers (This figure has been readapted in colour from Bouten et al. (2003)).

It is clear that the highest stresses (and strains) were estimated in the deeper muscle layer near to the body prominence and subcutaneous fat, particularly when compared to the interface regions between skin and supporting cushion (Oomens et al. 2010).

Although it is well acknowledged that sustained mechanical loading of the soft tissues is the primary cause in the development of pressure ulcers, the pathways to tissue breakdown involve several mechanisms (Bouten et al. 2003). These include;

1. direct deformation of cells,
2. localized ischemia,
3. ischemia/reperfusion injury and
4. impaired lymphatic drainage and interstitial fluid flow.

These mechanisms focus on different functional units of the soft tissues involving cells, interstitial space including the extracellular matrix, blood and lymph vessels. Over the years, many studies utilising bioengineering technologies have examined the response of various functional units to mechanical loading to evaluate their contributions to the aetiology of PUs. These have involved single cells (Bouten et al. 2001), in-vitro models of cultured cells (Breuls et al. 2003, Peeters et al. 2003) and engineered tissues models (Gawlitta et al. 2007 a, Gawlitta et al. 2007 b, Gefen et al. 2008). One such study evaluated the cell deformation when subjected to different compressive strains. The results showed that sustained compressive strain of 20% up to 24 h resulted in a significant increase in cell damage with its membrane sensitive to buckling (Bouten et al. 2001). Another study employed models of cultured cells to investigate direct cell damage or death under compressive and/or shear loading. The findings revealed that cells death was possible as a result of moderate but sustained deformation, in the presence of normal oxygen and nutrient supply (Breuls et al. 2003). Moreover, the number of dead cells increased when loading was prolonged for between 1 and 4 hours, remaining fairly constant thereafter. A further study employed tissue engineered muscle constructs to examine the effects of both deformation and oxygen deprivation on cell death, as assessed using fluorescent markers (Gawlitta et al. 2007 a). Their findings revealed that compression alone led to immediate cell death that increased with time. By contrast, the deprivation of oxygen supply did not result in significant cell death within a 22 hour period, although its effect was evident if the compression was sustained over longer time periods i.e. 2-4 days.

A number of animal models have also been used to understand PU aetiology with reference to the temporal effects of loading and offloading. A Dutch research group led by Oomens demonstrated that local tissue damage can occur following short loading periods (up to 2h) if a distinct local deformation threshold was exceeded, in which case the degree of damage depended on the exposure time (Loerakker et al. 2010, Loerakker et al. 2011). For longer periods, ischemia and reperfusion significantly contributed to the damage process more than the deformation (Figure 1-6). The role of ischemia – reperfusion injury in the aetiology of PUs has been investigated in animal models (Peirce et al. 2000). This mechanism was examined by creating a number of ischemic/reperfusion (I/R) load cycles of variable duration applied over the dorsal skin of rats. Its findings suggested that necrotic damage was correlated with both the duration of ischemia and the number and the frequency of I/R cycles (Peirce et al. 2000). The microcirculatory injury due to the cyclic ischaemia/reperfusion was found to be significantly higher than that observed due to a single ischaemic event.

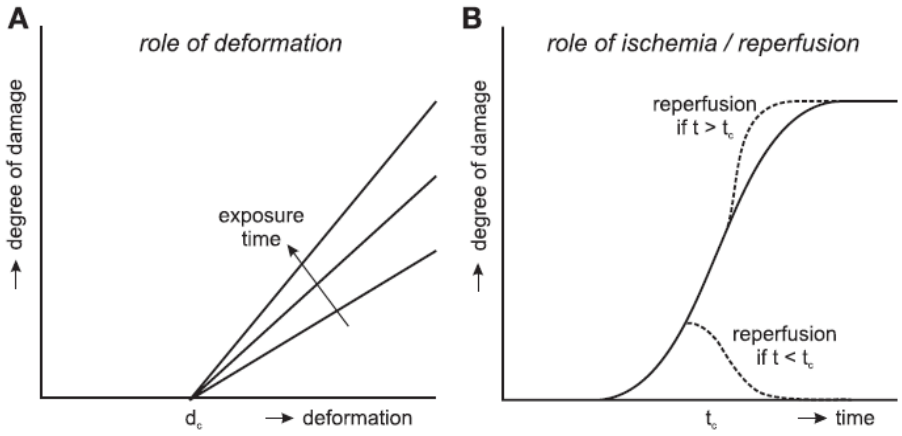

Figure 1-6: Schematic representation of damage caused by deformation and ischemia/reperfusion. A: deformations exceeding a specific threshold (d_c) cause tissue damage, where the degree of the damage depends on the magnitude of the deformation and its exposure time. B: Ischemia increase with exposure time; reperfusion reduce the degree of damage for a limited period of ischemia ($t < t_c$), although above that time ($t > t_c$) tissue damage is enhanced (Loerakker et al. 2011).

Mechanical loading can also lead to the occlusion of lymphatic vessels, affecting the transport of metabolic waste products from cell metabolism, thereby leading to their accumulation in the cell niche. This is supported by seminal animal studies by Miller and Seale (1981), who demonstrated impaired lymphatic clearance at a critical uniaxial pressure of between 60 mmHg and 75 mmHg (8.0-10.0 kPa). The same authors demonstrated that recovery of lymphatic clearance was found to be highly dependent on the magnitude of the post-occlusive pressure (Miller and Seale 1981). With the recent advent of non – invasive imaging modalities, mechanical – induced impairment of lymphatics has been examined in human subjects in the host laboratory (Gray et al. 2016). The study confirmed that an applied pressure of 60 mmHg can compromise dermal lymphatic vessels.

The hierarchical approach involving functional units ranging from cell models to human studies, has demonstrated that the tolerance of the tissues to mechanical load is a product of both the magnitude and duration of deformation. In addition, the tissue tolerance is an inherent property of the biological material. Specifically, the differences in structure, composition and material properties influence the different tissue layers (skin, fat and muscle) in their vulnerability to mechanical – induced damage. The traditional form of the pressure-time relationship proposed by Reswick and Rogers was adapted to take the form of a sigmoidal curve (Linder-Ganz et al. 2006). Both curves are illustrated in Figure 1-7, with the latter now considered to provide a more accurate representation of the acceptable limits in terms of magnitude and exposure time to cell and tissue deformation. The sigmoidal curve clearly demonstrates both a threshold level above which muscle damage can occur even at short times and a threshold level that the tissue can tolerate without damage over extended time periods.

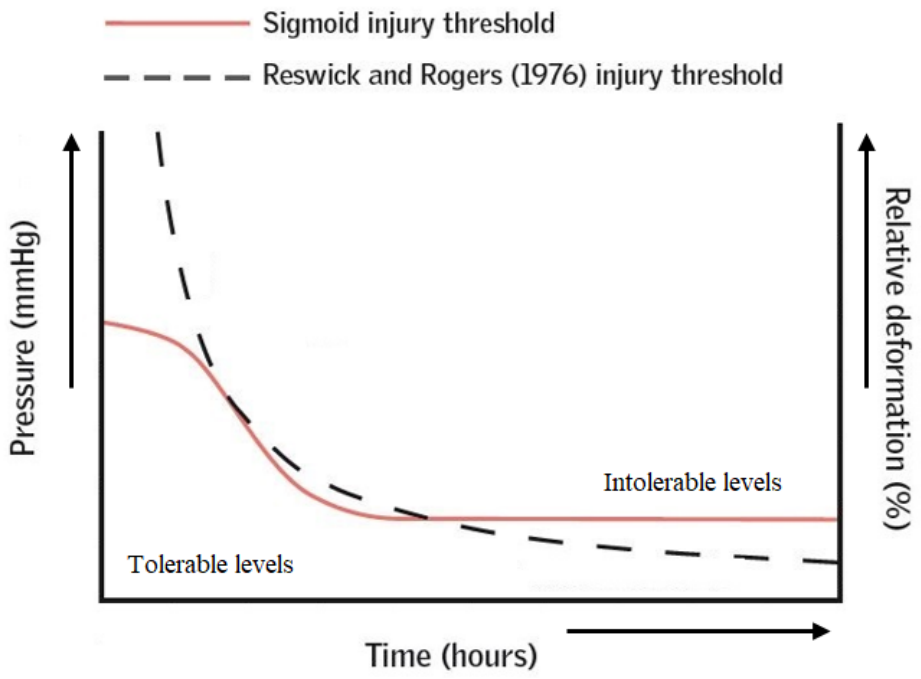

Figure 1-7: Time – pressure relationship including exponential curve, dashed line, by Reswick and Rogers (1976), and sigmoid time – pressure relationship, solid red line, by Linder-Ganz et al. (2006). The left vertical axis represents the direct pressure on muscle tissue (Linder-Ganz et al. 2006) and the right vertical axis the relative deformations in the tissues (Gefen et al. 2008).

Determining a damage threshold that is specific for muscle, fat and skin necessitates the use of multi-scale bioengineering research methods, to determine the internal mechanical conditions in loaded soft tissues. Imaging techniques, such as magnetic resonance imaging (MRI), have been used to assess damage parameters as a result of the direct compression on the skin. From these MRI images, dedicated FE models have been created to predict internal stresses and strains (Oomens et al. 2003, Loerakker et al. 2013, Brienza et al. 2018, Nelissen et al. 2018, Traa et al. 2019). This combined imaging and modelling approach demonstrated that the internal strains in the muscle tissue, fat and skin layers are highly dependent on their relative properties i.e. mechanical stiffness of the individual tissues. However, in these analyses material parameters are often selected based on animal models, assuming that their values approximate to those in human tissues. For skeletal muscles, data from in vivo animal experiments have been used (Nelissen et al. 2018), while skin properties data acquired from humans is available (Loerakker et al. 2013). By contrast, there is very little data describing the biomechanical behaviour of fat or adipose tissue (Oomens et al. 2010). Nevertheless, this modelling approach confirmed that the soft tissues response to loading is non – homogeneous and time dependent in nature. FE models have also been used to perform sensitivity analyses on parameters, which simulate pathophysiological changes associated with conditions, such as muscle atrophy (Shaked and Gefen 2013). However, the clinical translation of these models is still limited due to their complexity, reliance on single imaging data sets and lack of robust material properties.

1.7.1 Influence of shear forces

Although a number of studies have investigated the effects of the pressure on the tissues, relatively few have examined the role of the external shear forces (Dinsdale 1974, Ming and Roberts 1993, Goossens et al. 1994, Linder-Ganz and Gefen 2007). This is predominantly due to the complexity of measuring interface shear forces independent of pressure. Nonetheless, the few studies have generally reported that the presence of shear significantly decreases the tissue tolerance threshold caused by normal pressure alone (Dinsdale 1974).

It is worthy of note that when tissues are subjected to compression alone, internal shear will be induced in the heterogeneous soft tissue layers. This is illustrated in the schematic in Figure 1-8, when the skin and soft tissues are subjected to a load applied perpendicular to a bony prominence. The different tissue layers experience a combination of compressive stresses, tensile stresses reflecting a stretching of the tissues, and shear stresses. This results in an overall distortion of the tissues. If the bone also moves as result of changes in posture, frictional forces pulling at the skin surface will further elevate the magnitude of internal shear stresses/strain in the soft tissues. Shear forces within the tissues can cause the closure of the blood vessels and potential delamination of the tissue layers under higher internal stress and strains. Furthermore, these forces evoke a damaging effect in terms of deformation of the superficial layers of the skin, due to their inherent anisotropy.

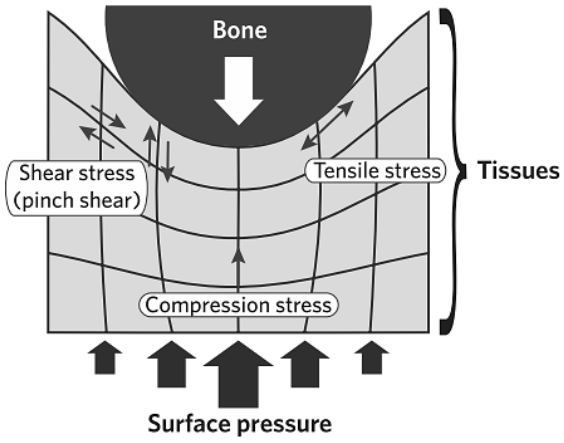

Figure 1-8: Stresses generated within skin and soft tissues overlying a bony prominence upon application of compression (Figure adapted from an international review (2010)). While the skin and soft tissues are presented as a homogenous mass in this figure, these stresses vary between individual tissue layers due to the specific mechanical properties of tissues (Oomens et al. 2010).

In summary, all the four major mechanisms have a role in the development of PUs, although their relative contributions vary depending on the nature (pressure or pressure combined with shear), magnitude and duration of the mechanical insult, and the inherent characteristics of the tissue layers.

1.8 Economic impact, prevalence and incidence of pressure ulcers

PUs lead to a significant decline in the quality of life (Spilsbury et al. 2007, Gorecki et al. 2012), with a physical, emotional and social impact on the life of the individuals affected. Common symptoms include pain frequently associated with a loss of mobility and social isolation. Their treatment costs represent a significant burden on healthcare providers (Guest et al. 2017). Indeed, PUs contribute to an annual cost of treating wounds which was estimated to be ~£5 billion per annum in the UK, in the period 2012 to 2013, approximately 66% of which was incurred in the community with the remainder occurring in secondary care (Guest et al. 2015, Guest et al. 2017). However, in a latter period (2015/2016), cost associated with treating PUs was reported to depend on their severity (Guest et al. 2018), from £1,382 per patient with a stage 1 PU to £ 10,065 for a stage 4 PU. A recent systematic review reported costs associated with PU treatment to be higher than those associated with their prevention (Demarré et al. 2015). These values reinforce the fact that pressure ulcers represent a major problem to healthcare services with a significant socio-economic impact.

The prevalence and incidence of PUs have been examined in many studies involving a variety of clinical settings. Prevalence values of PUs among patients in hospital settings were estimated to be 11%, 8.9%, 10.2 %, 12.1% and 11.6% in Germany, France, UK, Belgium and Sweden, respectively (Lahmann et al. 2006, Barrois et al. 2008, Phillips and Buttery 2009, Gunningberg et al. 2011, Vanderwee et al. 2011). In community settings, high prevalence rates have been reported in long-term care settings, such as nursing homes, with values ranging between 0.4 – 0.77 per thousand of the adult population (Stevenson et al. 2013). Prevalence of community and hospital acquired pressure ulcers in old population were reported at 2.7% and 3.0% respectively (Worsley et al. 2016). A recent systematic review reported worldwide prevalence rate ranging between 6-18.5% (Tubaishat et al. 2017). Incidence rate was reported at 12.8% (Al Mutairi and Hendrie 2018). Moreover, the prevalence and incidence of individuals at their end life were estimated to be 12.4% (range 9.9% - 54.7%) and 11.3% (range 0% - 37.5%), the wide range attributed to type of care setting and patient demographics (Ferris et al. 2019).

With respect to PU classification, the majority of the lesions were reported to be stage 1 PUs (Gunningberg et al. 2011), with a significant proportion of PUs affecting the heels and sacrum (Tubaishat et al. 2017). A separate study (Stockton et al. 2009) reported that the highest percentage of patients that develop pressure ulcers were associated with a cohort of permanent wheelchair users, which include SCI population, totally dependent on either self-propulsion or on carers for mobilisation (24.8%). By contrast, the corresponding value among the bed-bound was 18.6%. The permanent wheelchair group also exhibited the highest percentage of the most severe form of pressure ulcers (4% with stage 4 PUs), with associated poor healing and high recurrence rates.

1.9 Risk Factors

The causation of PUs involves several interacting factors that influence the susceptibility for their development (Figure 1-9). As observed in the previous sections, prolonged mechanical loading represents the most critical issue, the effect of which is highly dependent on the individual ability of the tissues to tolerate the magnitude and nature of the mechanical loading, termed ‘susceptibility or tissue tolerance’.

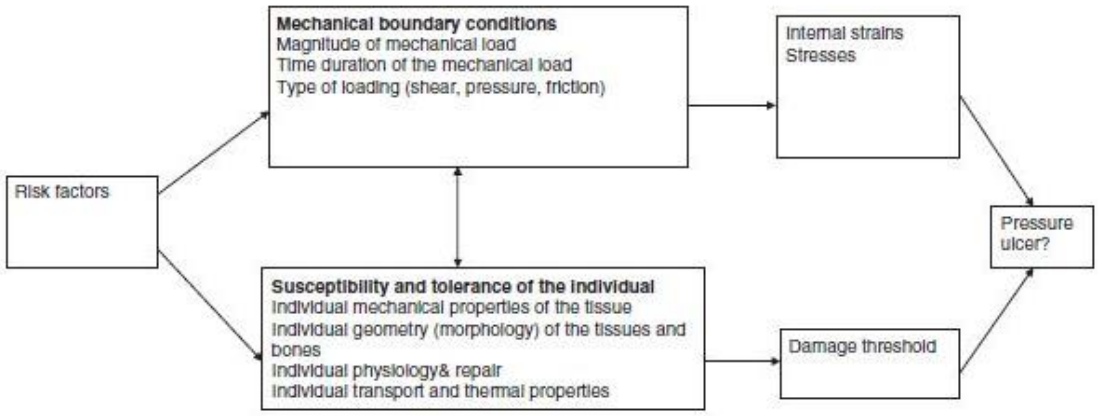

Figure 1-9: Factors that influence susceptibility for pressure ulcer development (Coleman et al. 2014 a).

Risk factors are typically classified as *extrinsic*, denoting factors that directly affect the surface of the skin, or *intrinsic*, indicating factors such as health and soft tissue integrity. An international consensus panel (Coleman et al. 2014 a, Coleman et al. 2014 b) developed a conceptual framework of risk factors, classifying direct, indirect and other potential indirect risk factors. Direct factors included immobility, skin/pressure ulcer status and poor perfusion, including diabetes. Indirect factors were skin microclimate (temperature and moisture), sensory perception and poor nutrition. Other potential indirect factors included ageing, medications, pitting oedema and those that relate to general health status, including infection, acute illness, raised body temperature and chronic wounds.

The levels of mobility, activity and sensory perception will influence the exposure to pressure, and skin microclimate such as temperature and moisture arising from sweat, urinary and faecal incontinence. In turn, microclimate can influence skin structure, physiology and mechanical properties (Figure 1-10) and, as consequence, affects the tolerance of the soft tissues to mechanical loads (Kottner et al. 2018).

In addition, the health status of the individual, in terms of nutritional and hydration status, age, and co-morbidities, such as diabetes, cardiovascular diseases, spinal cord injury etc., will each affect the tissues tolerance to prolonged pressures.

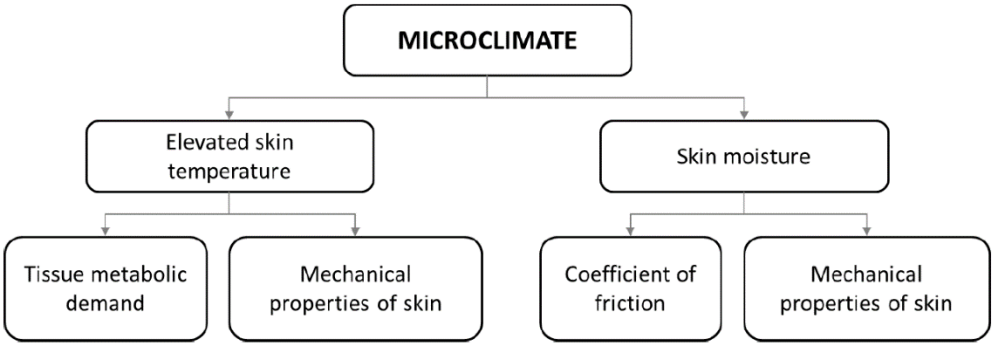

Figure 1-10: The effect of microclimate on the properties of the skin (Kottner et al. 2018).

1.10 Managing pressure ulcers

The management of individuals who have restricted mobility involves risk assessment, careful and regular inspection of skin, and appropriate intervention strategies which includes reducing/relieving interface pressure through adequate support surfaces and repositioning strategies. Each of these strategies have been included in national and international guidelines for the prevention of PUs, although PUs prevalence and incidence still remains unacceptably high (Mervis and Phillips 2019).

1.10.1 Risk Assessment

The purpose of risk assessment is to identify individuals at most risk of developing PUs and thereby implement effective preventative measures. A systemic risk assessment is performed in a clinical setting by means of scales (RASs), recommended by seminal international guidelines (NPUAP/EPUAP/PPPIA 2019). A PU RAS can be defined as tool which estimates a score according to a series of parameters based on risk factors. Several studies have examined the reliability and predictive validity of the RASs between different populations and in different settings. Specifically, sensitivity and specificity analyses were performed at different cut-off scores, namely the score at which PUs are considered likely to occur. A review (Torra i Bou et al. 2006) reported that both sensitivity and specificity vary widely, a finding which can be attributed to the differences in patient groups and settings, in addition to methodological differences, such as the length of the observation (Papanikolaou et al. 2007). Another confounding factor is that preventative strategies actually decrease the predictive capability of the RASs (Defloor and Grypdonck 2005). Despite limited evidence of clinical effectiveness, it has been suggested that RASs are perceived as semi-objective measures of risk, as their prediction is considered preferable to clinical judgment alone (Defloor and Grypdonck 2005). However, a systematic review reported that the regular implementation of standard RASs in clinical practice did not correlate with a reduction in PU incidence (Pancorbo-Hidalgo et al. 2006).

Although more than 40 RASs have been identified in the literature, the three most commonly used in a variety of healthcare settings are the Norton Scale (Norton et al. 1962), Waterlow Scale (Waterlow 1985) and the Braden Scale, devised by Bergstrom et al. (1987). The characteristics of these scales, incorporating the specific factors to assess PU risk, are summarised in Table 1-2. It is noted that both the Norton and Braden scales are based on a low cut-off score, as opposed to Waterlow scale.

Table 1-2: Risk factors incorporated in the most commonly used Risk Assessment Scales.

	Norton scale (Norton et al. 1962)	**Waterlow scale (Waterlow 1985)**	**Braden scale (Bergstrom et al. 1987)**
Setting	Elderly/Generic	Orthopaedic/generic	Generic
Cut off score	≤14	≥10	≤16
Risk factors	Activity Mental status Mobility Moisture Physical conditions	Age Gender Major surgery or trauma Medication Mobility Continence Nutrition Skin condition Weight	Activity Friction and Shear Mobility Moisture Nutrition Sensory perception

Limitations of the RASs involve an inadequate methodological development (Coleman et al. 2014 a, Coleman et al. 2014 b), which includes clinical opinion and/or out – dated literature reviews or adaptations of original instruments. In addition, there is limited evidence of the involvement of target population in their development. Indeed, many scales were designed to identify risk status in patients without PUs, but in practice are often used for all patients including those with PUs, thereby failing to distinguish between these two groups. Moreover, an inconsistent inclusion of risk factors has been highlighted. As an example, the most frequently incorporated risk factors are continence/moisture, nutrition/appetite and mobility and only five scales report skin status, which has been identified as a key predictor of PU development (Coleman et al. 2014 a).

To address the limitations of the current RASs, a Pressure Ulcer Programme of Research (Purpose) developed a new evidence-based tool – Pressure Ulcer Risk Primary or Secondary Evaluation Tool (PURPOSE T) – which has been recently clinically evaluated (Coleman et al. 2018). The important feature introduced by this tool is the skin status assessment. Despite these

recent advances, there remains a need for objective tools to monitor individual risk status in a range of clinical settings.

1.10.2 Prevention strategies involving support surfaces

In both lying and seated postures, the magnitude of pressure exerted on the individual is typically managed using mattresses and seat cushions, respectively. Both strategies are designed to redistribute pressure over maximum tissue contact areas, minimising peak pressures and shear, and in some cases, controlling the local microclimate. The terms *reactive* and *active* are commonly used to categorise the different modes of operation of support surfaces (NPUAP 2007).

The common feature of reactive support surfaces is their ability to conform to the body shape in response to applied loading, thereby increasing the contact area and resulting in a reduced magnitude of pressure. They may be comprised of foam, or a combination of foam and air or gel. Given their low technical specification, they represent so called “low – tech” constant low pressure (CLP) devices. By comparison, air fluidised mattresses and low air loss systems are also classified as reactive support surfaces. The former incorporate beads contained within the mattress through forced pressurised air, thus providing the surface with fluid-like properties. The latter incorporate air flow features that also enable skin microclimate management. Given their technical specifications, they are defined as “high – tech” CLP devices (McInnes et al. 2015).

By contrast, active support surfaces have the capability of changing their load distribution characteristics independent of the applied load, thereby periodically redistributing support pressures. Support surfaces in this category are referred to as alternating pressure air mattresses (APAMs) and are characterised by the cyclical inflation and deflation of air cells, distributed within the devices. Other advanced support surfaces such as lateral turning beds and turning systems, are particularly prescribed for immobile individuals, who are unable to turn on their sides. They are designed to periodically relieve pressure from tissue sites associated with supine lying i.e. over the sacrum.

Despite the advances in support surface technology, there is insufficient evidence that demonstrate the benefits of the high – specification reactive mattresses over low-tech support surfaces (McInnes et al. 2015). Moreover, the benefits of APAM devices over more economical foam mattresses have also not been fully demonstrated (McInnes et al. 2015, Nixon et al. 2019). Indeed, it could be argued that there is an over-reliance on the use of support surfaces technologies to periodically redistribute/relieve the distribution of pressure. Most evidence suggests that these technologies should not be used in isolation but in combination with education and standard repositioning strategies typically adopted by health carers i.e. 30 degree tilt position (NPUAP/EPUAP/PPPIA 2019).

1.10.3 Prevention strategies involving repositioning

In order to both reduce the magnitude and the time during which pressures are applied to vulnerable sites adjacent to bony prominences, frequent repositioning of individuals is advised in both national and international guidelines (NPUAP/EPUAP/PPPIA 2019). Generally, 2 – 4 hourly repositioning strategy has been recommended in lying (Vanderwee et al. 2007), while more frequent repositioning (15 – 30 minutes) is often recommended for sitting postures in at risk groups e.g. SCI (Stockton et al. 2009). In lying, the repositioning strategy is typically achieved through self-evoked movements or, where mobility is limited, by clinicians and carers who manually adjust individual posture. A variety of manoeuvres to shift the body weight by leaning either forward or to the side or lift-off from the support surface are often recommended for wheelchair – bound individuals. However, the effectiveness of these manoeuvres in preventing PUs is strongly dependent on both the ability and the compliance of the individual to perform these manoeuvres (Coggrave and Rose 2012).

Carer-supported repositioning strategies can be time consuming and labour intensive, and has been estimated to cost between €200 and €250 per patient over a four week period (Moore et al. 2013). Nonetheless, these authors reported that repositioning using a 30° tilt, in the sequence left side, back, right side, back, every 3 hours during the night was cost-effective compared to repositioning every 6 hours using 90° lateral rotation. This was attributed to the fact that the smaller turns required less time and fewer staff, while also proving more effective in preventing PUs (Moore et al. 2013). It is well recognised that, in many healthcare settings where resources are limited, the frequency and magnitude of movements recommended for PU prevention are not regularly followed (Defloor et al. 2005). Indeed, a number of studies have suggested that PU incidence does not correlate to the frequency of repositioning (Vanderwee et al. 2007, Peterson et al. 2013). In addition, a recent study in the host laboratory in Southampton demonstrated that even experienced practitioners perform repositioning manoeuvres inconsistently and, in some cases, pressure relief at critical sites such as the sacrum is inadequate (Woodhouse et al. 2019). This indicates that although repositioning strategies are adhered to by many clinicians, ineffective movements are being performed and PU risk is not diminished (Woodhouse et al. 2019).

To date, there is limited evidence supporting the relationship between frequency of movements and reduction in PU incidence, which may be highly dependent on the individual susceptibility (Vanderwee et al. 2007). Indeed, recent guidelines have recognised the limitations of the evidence for manual repositioning, recommending a personalised frequency strategy based on individual characteristics, such as mobility and general medical conditions (Rich et al. 2011, Stephens et al. 2018).

The traditional clinical practice involves a 30^{o} side-lying position (Figure 1-11) and semi-recumbent positions with a 30^{o} to 45^{o} backrest elevation, generally recommended for bed-bound

individuals (Moore et al. 2011). Modifying the lying angle orientation adjusted via a head of bed (HOB) angle can redistribute interface pressures, thereby improving patient comfort and facilitating critical functions associated with eating and respiratory care.

Figure 1-11: 30º side-lying posture, achieved by rolling the patient to a slightly tilted position with pillow support at the back and legs (Moore et al. 2011).

1.10.4 Evaluation of the performance of prevention strategies

The performance of both support surfaces and repositioning strategies have been evaluated using a range of measurement techniques. One of the most common approaches, adopted in both clinical and lab – based studies, involves the measurement of pressures at the individual support surface interface. These studies have demonstrated that postural changes can have a significant effect on interface pressure distribution acting at the skin surface (Defloor and Grypdonck 1999). As an example, elevation of the HOB exposes the sacral area not only to an increase in the magnitude of the pressure, but also increases the tendency of the individual to slide down the support surface (Hermans and Call 2015). In addition, this will inevitably result in the increase in both shear and frictional forces, and a spatial change in peak pressures, which contribute to a decrease in local skin blood flow (Gilsdorf et al. 1990, Hobson 1992).

From a clinical prospective, commercially – available systems are currently used to measure interface pressure distributions at the support surface. These are often employed in settings, such as specialised seating clinics. Clinicians typically use a coloured contour map, which depicts the magnitude and area in which pressures are spatially distributed. This data allows the clinician to view key regions of interest (ROIs), associated with the sacrum, heels or ischial

tuberosities. These parameters are generally observed either at a single time point, or averaged over a short time period, at most tens of minutes in duration. However, this approach can lead to ambiguity in the interpretation of pressure mapping data, which often involves the traditional exponential risk curve (Reswick and Rogers 1976). The so-called safe interface pressure often uses a threshold of 32 mmHg, a value measured as a closing pressure estimated at the nail fold capillaries (Landis 1930). Such a measure clearly does not represent the internal stresses and strains within soft tissues associated with pressure ulcers at areas such as the heels, sacrum and buttocks. Nonetheless, this threshold value is still adopted in some pressure monitoring systems to provide an early warning for tissue damage and as a risk criteria for determining the effectiveness of support surfaces.

There is a wealth of evidence to suggest that the measure of interface pressures alone do not provide clinicians with an effective indication of pressure ulcer development (Reenalda et al. 2009). In addition, pressure relief of any kind could potential lead to reperfusion damage. This has motivated a number of studies to examine the effects of applied pressures on a range of measures indicative of physiological tissue status (Kim et al. 2012, Chai and Bader 2013, Woodhouse et al. 2015, Worsley et al. 2016, Chai et al. 2017). These have indicated that changes in transcutaneous gas tensions (T_cPO_2 and T_cPCO_2) can reflect the vascular status of dermal tissues to different postures (Woodhouse et al. 2015) and support surface configurations (Worsley et al. 2016, Chai et al. 2017). These approaches will be further evaluated in the next chapter.

Moreover, no absolute values can be derived from pressure mapping alone to quantify the exposure and detrimental effects of shear forces. In addition, there are very few reports, which propose devices/sensors sensitive to shear measurements. Of the few, one recent study reported the development of a capacitance-based sensor, which is capable of measuring uncoupled values of interface pressures and shear forces in two directions for use at the stump lower limb prosthetic socket interface of amputees (Laszczak et al. 2016). However, the operating range of this system (designed for standing and gait) is far higher than the values expected at the interfaces associated with sitting or lying postures.

1.11 Summary

This chapter has detailed the normal anatomy and physiology of the skin and soft tissues. There are many biomechanical aspects, which can lead to changes in the tissue structure and accordingly increasing their vulnerability when subjected to mechanical stimuli. In particular, the chronic condition of PUs which represent a debilitating condition for many individuals, was highlighted. Although significant advances have been made in the recent decades in understanding PU aetiology and corresponding risk factors, data from prevalence and incidence studies indicate that such ulcers remain relatively common across many healthcare settings in the hospital and community. Risk assessment scales have been designed to identify individuals

at high risk of developing PUs, thus enabling the targeted use of prevention strategies and, ultimately, reducing their incidence. However, their effectiveness appears to be limited. Prevention strategies, incorporating both reactive and active support surfaces and repositioning, are typically evaluated by measuring interface pressures over a relatively short time period. These measures, however, are characterised by several limitations in informing healthcare professionals of early signs of tissue damage. A critical analysis of the array of bioengineering techniques to provide an objective measure will be provided in Chapter 2.

Chapter 2: Overview of the bioengineering measurements: critical analysis of the current algorithm of a continuous pressure mapping system

The current chapter aims to provide an overview of the bioengineering measurement systems currently used for assessing the effectiveness of the prevention strategies in PU prevention. Systems providing both measures of interface pressures to assess the biomechanical interactions at the body – support interface and the corresponding physiological responses to monitor tissue viability will be described.

2.1 Measures of interface pressures and its assessments

Monitoring the distribution of pressures has become a fairly common practice in both clinical and lab – based settings. Commercial sensor arrays have been developed to estimate these distributions at the interface between the individual and the support surface. The sensors have adopted a range of principles, including electronic, which involve capacitive and resistive sensors, pneumatic and electro – pneumatic (Gyi et al. 1998). The former detects the electronic signal resulting from the proportional variation of either their capacitance or resistance with respect to the applied pressure. Such sensors are typically embedded within large arrays and provide real-time display, thereby enabling visualization of temporal data. Pneumatic sensors consist of an air cell connected to an air reservoir. On inflation the sudden increase in system volume, which occurs when internal pressure in the air cell exceeds the externally applied pressure, causes an abrupt reduction in the rate of pressure increase, which is recorded as the applied interface pressure. Electro-pneumatic sensors are equipped with metallic elements on the opposing inner surfaces of an air cell. By inflating the system, the elements lose contact at the applied pressure, which is then recorded. Due to the differing principles by which pressure is measured, these commercial systems have a range of operating performances (Table 2-1).

In a historical review, Ferguson-Pell and Cardi (1993) compared the performance of pressure measuring systems incorporating both electronic resistive sensors (Tekscan system, Tekscan Inc., South Boston, USA) and pneumatic sensors (Talley Pressure Monitor 3, TPM3, Talley Medical, Romsey, UK). The authors reported that the TPM3 proved the most accurate, stable and reproducible pressure values, but was limited in terms of acquisition speed and data presentation. The latter two features in the Tekscan system was generally preferred by clinicians. Commercial companies have since developed different configurations of these systems, also involving different technical specifications. In typical configurations, resistive and capacitive sensors are typically embedded within large sensor arrays designed to measure pressure distributions under the individual in bed (Wong et al. 2015), wheelchairs or leisure chairs (Worsley et al. 2017). Table 2-1 indicates that both capacitive and resistive – based

systems exhibit similar technical specifications in terms of sampling frequency and spatial resolution (~12–17 mm). By contrast, systems based on pneumatic sensors consist of fewer sensors within an array with a spatial resolution approximately twofold greater than that of equivalent of electric systems. In addition, the corresponding sampling frequencies are 60 fold slower (0.017 Hz) than the electrical equivalent (1 Hz).

Table 2-1: Specification of different commercial pressure monitoring systems**.**

Type of sensors	**Resistive** (i.e. Tekscan systems, Boston MA)	**Capacitive** (i.e. XSensor systems, Canada)	**Pneumatic** (i.e. OPM Mark II, Talley Medical Group, Romsey, UK – *only used in the host lab in Southampton*)
SPECIFICATIONS	**Sensor Number**: Seat configuration: 1024 in 32x32 array Full body configuration: 5034 in 52x34 array **Sensing Area**: Seat configuration: 471.4x471.4mm^2 Full body configuration: 883.9x578.1mm^2 **Sampling frequency**: 8Hz **Spatial Resolution**: Seat configuration: 14.7mm Full body configuration: 16.9mm **Thickness**: 0.1mm **Pressure range**: Typical operating range: 1 – 34kPa (7.5 - 255mmHg)	**Sensor Number**: Seat configuration: 2090 in 36x36 array Full body configuration: 5664 in 118x48 array **Sensing Area**: Seat configuration: 457x457mm^2 Full body configuration: 1880x726mm^2 **Sampling frequency**: Seat configuration: 5Hz Full body configuration: 1Hz **Spatial Resolution**: Seat configuration: 12.7mm Full body configuration: 15.9mm **Thickness**: 0.1mm **Pressure range**: Seat configuration: 1.4 – 26.7kPa (10–200mmHg) Full body configuration: 0.6 – 33kPa (5–250mmHg)	**Sensors Number**: 96 sensors **Configurations**: 12-sensor array+84 sensors 12 -sensor array+12-sensor array+72 sensors **Spatial Resolution**: 30mm in both directions for 12-sensor array 50mm across the width and 12mm along the length **Pressure range**: Typical operating range: 2 – 32.8kPa (15–246mm Hg) **Sampling frequency**: 0.016Hz (1 sample every 60 seconds)

These systems has been employed in a large number of studies to assess the effects of positioning and the performance of support surfaces. As indicated in a selection of studies in Table 2-2, the outcome parameters generally involved peak pressures, peak pressure index (PPI), defined as the peak pressure values averaged over a limited number of sensors, mean or median pressure values and contact area in specific regions of interest (ROIs). These parameters are typically evaluated either at single time points or averaged over relatively short periods of time, for example, tens of minutes.

Table 2-2: Summary of a selection of studies which have employed different pressure measuring systems and outcome parameters to evaluate the performance of repositioning strategies or support surfaces.

Study	Aim		Pressure measuring systems				Outcome parameters			
	Positioning evaluation	Support surface evaluation	Mark III, Talley Medical Group, Romsey, UK	MAP™ System, Wellsense USA, Inc, Nashville, TN	XSensor system, Canada	Tekscan Inc, Boston, MA	Peak pressure	Peak pressure index	Average pressure	Contact Area
Kim et al. (2012)	X					X			X	
Chai and Bader (2013)		X	X				X			
Peterson et al. (2013)	X				X		X			X
Lippoldt et al. (2014)	X				X		X			X
Woodhouse et al. (2015)	X		X					X		
Worsley et al. (2016)		X	X				X	X		
Gunningberg and Carli (2016)	X			X			X	X		
Chai et al. (2017)		X	X				X			

Results from these studies have shown that the recorded values depend on the posture of the individual cohort and the type of support surface (Table 2-3). For example, when lying supine on a continuous low pressure (CLP) mattress incorporating rows of air cells, the median values of peak interface pressure for a healthy cohort (n=10) over the sacrum were estimated at 66 mmHg (Woodhouse et al. 2015). By contrast, on a different support surface referred to as a reactive therapy system, equivalent pressures over the sacrum area were considerably lower with values of approximately 22 mmHg (Worsley et al. 2016). On a viscoelastic foam mattress, the mean interface pressure values over the sacrum rarely exceeded 50 mmHg (Kim et al. 2012).

Table 2-3: Summary of the pressure data in a selection of studies.

	Pressure measurements [mmHg] – sacrum area		
Study	**Supine**	**High sitting**	**Lateral turning**
Kim et al. (2012)*	36	/	/
Chai and Bader (2013)**	37	46	/
Peterson et al. (2013)***	66	/	65
Woodhouse et al. (2015)****	66	/	52
Worsley et al. (2016)*****	70	75	48

* values based on the mean pressure over a 20 minutes period

** maximum interface pressure value corresponding to 1 subject

*** mean value of the peak pressures over 14 subjects

**** median value of the peak pressures over 10 subjects

***** maximum value of the peak pressures over 17 subjects

It is clear that the existing measurements are difficult to compare due to the different pressure sensing technologies and methods of interpretation i.e. median and maximum peak pressure over different cohorts. In addition, the same measures were estimated over different time intervals. For example, Kim et al. (2012) estimated the mean interface pressure over a 20 min period in 5 min intervals. By contrast, Woodhouse et al. (2015) and Worsley et al. (2016) estimated median and maximum values of the peak pressures, respectively, for a static posture over three 1-min cycles of interface pressures after a period of 10 minutes. Thus, findings clearly show that pressure measuring systems are often used over relatively short time periods offering only a "snap shot" of the interface conditions, although capable of recording data over prolong time periods (>48 hours). This clearly provides a limited overview of the long-term performance of support surfaces and the effects of prolonged postures, which are commonly adopted over prolonged time periods. Indeed, long-term monitoring would provide a more effective means of evaluation of pressure conditions over extended periods (Scott and Thurman 2014, Wong et al. 2015). Furthermore, findings are also difficult to compare as the sensing area dimensions, the sensors number and resolution of the different systems all influence the sensitivity and repeatability of the pressure measures (Harstall 1996). In some cases, system manufacturers (i.e. XSensor, Canada) supply calibration and specifications, defining sensitivity and accuracy data, although standards for these features such as spatial resolution and sampling frequency need to be established (Gefen 2007 b). Indeed, a "gold standard" sensor system has yet to be defined (Bogie et al. 2008).

Commercial systems (e.g. XSensor system) provides real-time images of the pressure distribution whose display is in the form of a colour map. This is typically used by healthcare professionals to evaluate intervention strategies as it provides feedback on “at risk” sites where low pressures are represented by cold (or blue) tones and higher pressure values by warm (or red) tones. The colour gradient is associated with a scale bar, which represents the pressure range (Figure 2-1). The nature of the colour map is inevitably influenced by the bar scale indicating absolute pressure values. This is illustrated in Figure 2-1, for an identical pressure distribution which employs two distinct scales of 0 – 100 mmHg and 0 – 50 mmHg, representing the left and right maps, respectively. The features, such as peak pressure gradient, appear to be distinctively different.

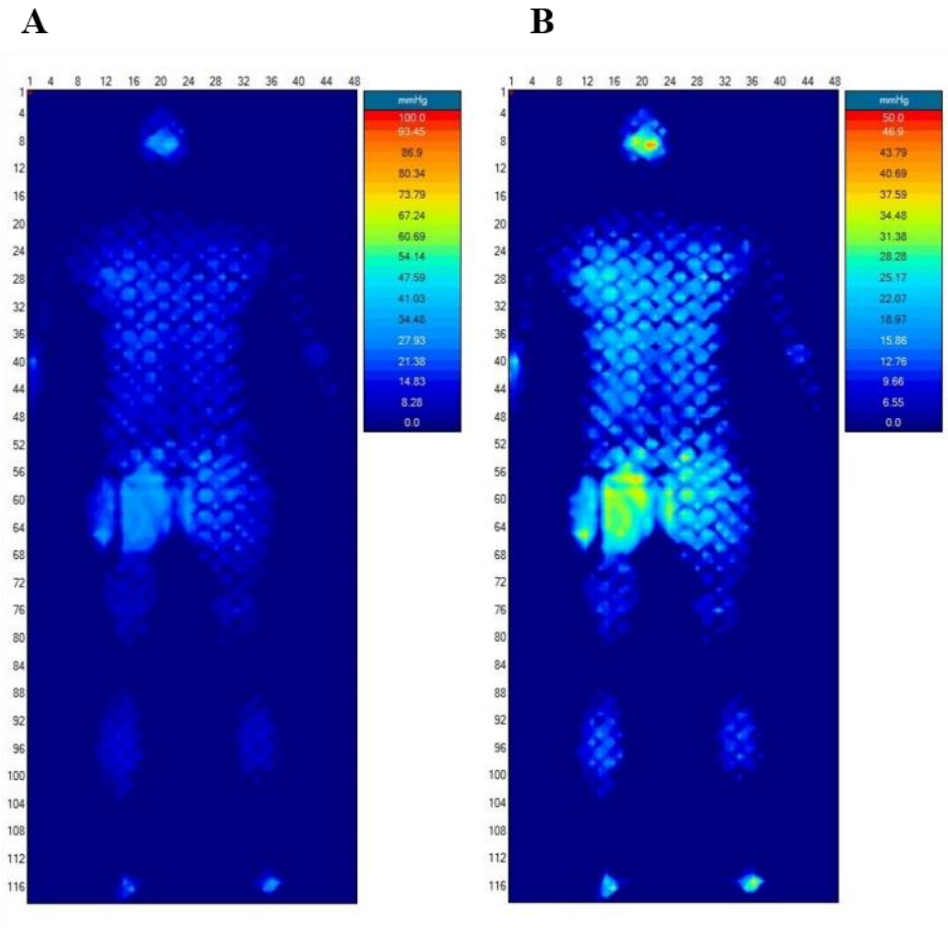

Figure 2-1: Full body pressure distribution, colour mapping and scale bar, with different pressure range. In Figure (A), the distribution of the pressures ranges from 0 – 100 mmHg, (B) between 0 – 50 mmHg. Both images have been exported from the analyser software of a continuous pressure mapping system (ForeSite PT, XSENSOR Technology, Canada).

A few recent studies demonstrated the effectiveness of using continuous pressure mapping technologies when compared to situations which do not involve monitoring devices, as they can alert healthcare providers regarding the exposure to prolonged loads, thereby facilitating timely interventions (Walia et al. 2016, Gunningberg et al. 2018). However, it has been recently

demonstrated a limited impact of these technologies in reducing both prevalence and incidence of PUs (Gunningberg et al. 2017).

As previously described, some of these commercial systems rely on arbitrary threshold values to denote PU risk, typically the closing pressure of 32 mmHg measured at the nail fold capillaries (Landis 1930). Indeed, some lab – based and clinical studies (Peterson et al. 2008, Peterson et al. 2013, Lippoldt et al. 2014) have included the definition of an "at-risk area" based on this unrealistic threshold value. Critical external pressure values capable of damaging skin and soft tissues, have not been identified. As a result, the predictive capability of continuous pressure mapping systems has been questioned.

The present analysis highlighted the fact that in both research and clinical applications of interface pressure measurement there is not an established methodological approach for the estimation of clinically relevant data, resulting in limited translation to clinical advances (Bogie et al. 2008). Parameters such as average pressure are often used to characterise the effectiveness of prevention strategies as reported in Table 2-2, although they are clearly not representative of the visual gradients within the pressure distribution (Stinson et al. 2003). Moreover, single frame or mean values of peak pressures and peak pressure index are limited in representing the temporal changes in the pressure distribution. By contrast, pressure gradient, which potentially represents the most meaningful pressure parameter, is rarely investigated. In addition, these pressure parameters measured at the external skin surface do not reflect the mechanical conditions, typically the stress – strain states within the tissues. Indeed, state of the art research adopting an hierarchical approach (Section 1.7) have identified that the tolerance to mechanical loads in tissues sites is a product of both the magnitude of stress/strain and the duration in which this is sustained (Linder-Ganz et al. 2006). This threshold is largely dependent on the tolerance of the different tissue layers which itself is influenced on intrinsic factors such as co – morbidities, nutritional status and previous incidence of skin damage (Figure 1-9) (Coleman et al. 2014 a). Thus, the clinical use of pressure monitoring is necessarily limited in predicting PUs development (Reenalda et al. 2009), as it does not assess the status and/or viability of loaded tissues and hence provide clinicians with clear predictor of skin and soft tissue risk (Chai and Bader 2013, Woodhouse et al. 2015).

2.2 Measures of shear and friction

By contrast to pressure mapping, only a few studies have monitored shear forces at the individual – support surface interface. These measures are dependent on the friction between two opposing materials at the interface and commonly occur as consequence of involuntary i.e. sliding or voluntary movements i.e. repositioning. The coefficient of friction of materials against skin is particularly exacerbated by moisture, for example, in the form of sweat or urine (Shaked and Gefen 2013).

The paucity of studies is due to technical challenges inherent in the development of compliant, thin and flexible sensors able to distinguish between signals associated with normal forces and those with forces acting parallel to the skin surface (Bader and Worsley 2018). A recent study (Laszczak et al. 2015) has described the development of 3D-printed sensors made of an elastomeric material, which are capable of measuring pressure and shear simultaneously, for the specific application at the stump – socket interface of lower limb amputees. This sensor, however, still has to be adapted for the measurement of shear forces at interfaces associated with sitting or lying postures. The measurement of shear forces in sitting postures have been investigated in a few studies (Akins et al. 2011, Cho et al. 2014) involving the design and validation of strain – gauge – based shear sensors. However, the applicability of these sensors in clinical settings still needs to be verified. Due to the paucity of available measurement technology, the assessment of shear forces is beyond the scope of the current thesis.

2.3 Measures of tissue viability

Mechanical loading in the form of pressure and shear affects tissue viability, by occluding capillaries thereby reducing blood and lymph flow, as discussed in Section 1.7. Localized ischemia, reperfusion injury and impaired lymphatic drainage represent three of the four mechanisms associated with mechanical – induced tissue damage. The measurement of blood and lymph flow represent a means of determining the viability of the soft tissues.

Different techniques has been proposed to evaluate the vascular status of the skin and subcutaneous tissues subjected to different loading regimens. These include Laser Doppler Fluxmetry (LDF) and transcutaneous gas tension monitoring. LDF provides a measure of tissue perfusion, generated as a result of a laser light source and the Doppler shift induced by moving erythrocytes in the blood. This measure is assessed at an approximate depth of 1 – 2mm from the skin surface, and the output signal, referred to as flux, is expressed in arbitrary units (Rajan et al. 2009). Studies have revealed LDF measures vary widely between sites and are sensitive to artefact noise, which can occur as a result of subject movement, producing erroneously high readings (Worsley and Voegeli 2013). In a recent study, LDF has been used to evaluate the perfusion when different designs of clamps were applied to penile tissues (Lemmens et al. 2019).

By contrast, transcutaneous gas tension monitors tissue oxygenation (T_cPO_2) and carbon dioxide (T_cPCO_2) tensions, and the output signal is a measure of local variations of the gas delivery in the blood capillary loops. In particular, T_cPO_2 and T_cPCO_2 are monitored by a small sensor, attached to the skin by a fixation ring. Some contact gel is placed in the wall of the fixation ring to provide good thermal contact with the skin. The heating element in the sensor warms the skin to 43-45°C, which causes vasodilatation of the capillary loops, producing an increase in local skin blood flow. Normal unloaded values of T_cPO_2 at these elevated temperatures are generally

considered to range between 51 and 90 mmHg with corresponding T_cPCO_2 values ranging from 36 to 44 mm Hg (Knight et al. 2001).

Many studies incorporating gas tension measures have been conducted (Rithalia 2004, Chai and Bader 2013, Woodhouse et al. 2015, Worsley et al. 2016). One such study (Chai and Bader 2013) examined the gas tensions at the sacrum of able – bodied individuals lying in different supine postures on an APAM system. The authors compared the gas tension levels relative to unloaded baseline and identified three categories of response as indicated in Figure 2-2, namely:

- Category 1, characterised by minimal changes in both T_cPO_2 and T_cPCO_2 values
- Category 2, characterised by >25% decrease in T_cPO_2 with minimal change in T_cPCO_2
- Category 3, characterised by >25% decrease in T_cPO_2 associated with an >25% increase in T_cPCO_2

The perturbation in each of the three categories represent the nature of cyclic support pressures provided by the APAM.

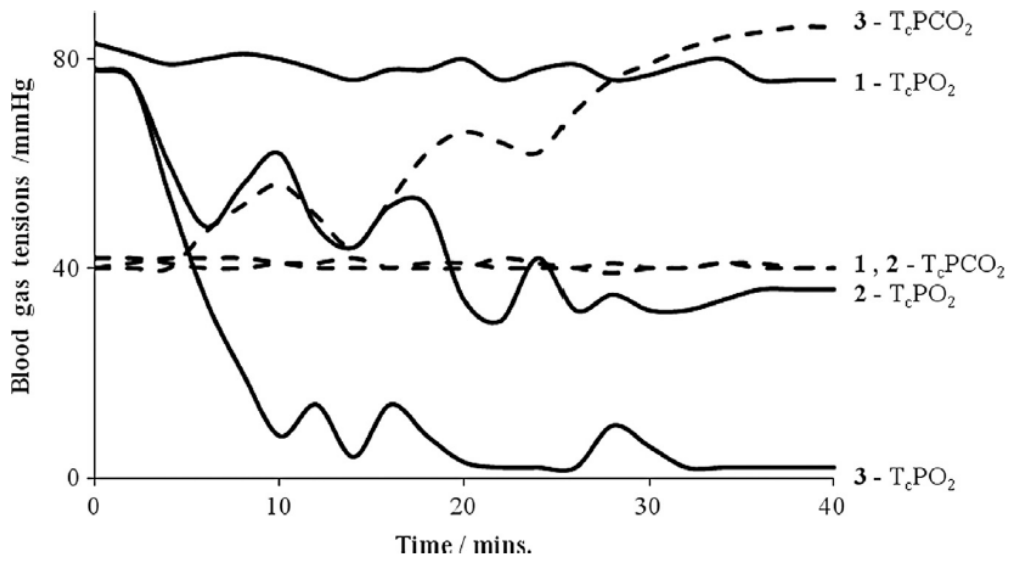

Figure 2-2*:* Three categories of response for oxygen (T_cPO_2) and carbon dioxide tensions (T_cPCO_2) due to cyclic loading at the sacrum of able-bodied volunteers (Chai and Bader 2013).

Further studies by the host group have observed category responses for a range of support surfaces and postural changes (Woodhouse et al. 2015, Worsley et al. 2016, Chai et al. 2017, Worsley et al. 2017). The studies have revealed that movements between postures clearly influence the transcutaneous gas response. In some selected number of individuals, typically 10 – 20% of cases, a Category 3 response has been observed. In the majority of conditions following a change in posture, this response returned to either Category 1 or 2. In one study involving able – bodied cohort of various ages i.e. 18 to 85 years, there was a weak correlation between peak interface pressures and changes in T_cPO_2 and T_cPCO_2 values (Worsley et al.

2017). This finding supports the proposition that increased interface pressures are associated with restriction in the oxygen supply to the loaded tissues.

A combination of transcutaneous gas tensions and interface pressure measurements have also been employed to assess tissue viability in at-risk immobilized subjects, for example, SCI individuals (Bogie et al. 1995). In this study, transcutaneous oxygen values of 30 mmHg, representing an approximate 60% reduction from unloaded baseline, were defined as the upper threshold values below which tissue viability can be compromised. The 60% threshold value was supported in a subsequent study (Knight et al. 2001). This reported some relationship between parameters reflecting tissue viability and specific biomarkers, reflective of anaerobic cell metabolism. Both lactate and urea concentration were collected in sweat and their concentrations were indicative of soft tissues in an ischaemic state. As applied pressure was increased, there was a reduction in oxygen levels with a corresponding increase in both lactate and urea concentration. A threshold value was identified, equivalent to a reduction of approximately 60% from unloaded values in T_cPO_2 levels, above which there was a significant increase in both sweat lactate and T_cPCO_2. Indeed, the latter parameter exceeded 50 mmHg for a significant proportion of the loading period, further indicating compromise to tissue health.

2.3.1 Limitations of transcutaneous gas tension measures

Many studies have established that transcutaneous gas tensions provide a measure of the relative change in oxygen and carbon dioxide tensions in localized regions by applying an electrode to the skin, and inducing maximum vasodilatation by heating the skin up to 45^o. This experimental procedure yields measurements which are relatively simple, reliable, reproducible and sensitive to local changes in microclimate (Dowd et al. 1983, Bader 1990). However, the heating component clearly affects the normal physiological response of the skin microcirculation and the finite size of the sensor may cause high pressure gradient at the loaded interface (Rithalia 2004). Indeed, it is worthy of note that the technique is only appropriate for assessing the loaded interface if at least one of the materials i.e. support surface, are relatively compliant, to ensure that the electrode will not affect interface conditions.

2.4 Measures of postures and mobility

As discussed in Section 2.1, several studies have focussed on the effects of repositioning strategies on interface pressures. However, relatively few have examined the temporal relationship between individuals postural movements, in terms of magnitude and frequency, and their propensity to PU development. This is particularly surprising given that immobility represents one of the primary factors in the development of PUs and individuals are encouraged to move regularly as a primary prevention strategy.

Both frequency and magnitude of postural movements are typically estimated by measurements of tilt angles at specific body sites derived from actimetry systems. A large range of actimetry

sensors have been developed for different applications. These include uni-axial or tri-axial accelerometers and a combination of accelerometers and gyroscopes. These actimetry systems have been shown to be an appropriate means of determining movements (Grant et al. 2006) and have been reported to accurately discriminate between postural changes in different anatomical planes (Edwardson et al. 2016, Lyden et al. 2016, Worsley et al. 2017). Nonetheless, these studies have revealed the importance of the location of the actimetry systems in discriminating between postures. As an example, one study revealed that by locating a tri-axial actimetry system on the thigh it was not able to discriminate between sitting and lying (Lyden et al. 2016), although this classification proved accurate when it was located on the trunk (Culhane et al. 2004).

The use of actimetry systems is established in both research and clinical settings to evaluate the effectiveness of relief strategies in individuals at risk of developing PUs (Stinson et al. 2013, Stinson et al. 2018). In addition, recent actimetry-based studies reported that the provision of optimal turning and repositioning was enhanced with a use of wearable patient sensor in clinical settings (Källman et al. 2016, Ifedili et al. 2018, Pickham et al. 2018). Actimetry has also been used to identify that the majority of seated individuals at risk of developing PUs do not comply with the recommended frequency for pressure relief (Stinson et al. 2018).

A few studies have combined interface pressure measurements with actimetry to assess the efficacy of the postural changes in sitting (Worsley et al. 2017, Stinson et al. 2018). Both reported that the magnitude of movements in off-loading vulnerable soft tissue areas, estimated as a relative change in the tilt angle at the target body site (i.e. trunk), was typically not achieved with traditional repositioning strategies. In addition, the ability of the trunk tilt in predicting changes in interface pressure parameters was investigated (Stinson et al. 2013). Findings from this study reported a weak relationship between the two measures, with a 1% increase in tilt angle associated with a minimal change in interface pressure parameters.

Although actimetry systems provide a reference for position and movement detection, they cannot characterise the biomechanical conditions at the patient – support interface. A further study of note (Fenety et al. 2000) reported that the trunk movements in sitting postures are correlated with evaluating the displacements of the centroid of the pressure distribution (COP) at the body-seated interface. Thus, its estimation could provide information about postural adjustments (Karatas et al. 2008). However, limitations in these studies were related to the short-term assessment of the pressure distributions and accordingly to the evolution of the COP during postures.

With the advent of intelligent methods to process data i.e. artificial intelligence and machine-learning, algorithms have been developed for the detection of a range of lying and sitting postures from the distribution of pressure at the subject-support interface (Wai et al. 2010, Yousefi et al. 2011, Foubert et al. 2012, Zemp et al. 2016, Rus et al. 2017, Kim et al. 2018,

Matar et al. 2019). A limited number of these studies have also detected the transition phases between static postures (Foubert et al. 2012, Duvall et al. 2019). However, many of these studies included the short-term estimation of the pressure distribution (up to tens of seconds) and a limited range of lying postures (i.e. supine, prone, left and right turn), not fully representative of those typically adopted in clinical settings over long periods. Limitations also involved the nature of the pressure parameters and features utilised to detect both postures and corresponding transitions. Indeed, their capability in detecting movements and their clinically relevance have not been investigated to date.

2.5 Motivation for the present research

This chapter has considered the role of distinct bioengineering technologies in the assessment of support surface interactions (pressure, shear), the physiological response to tissue loading and techniques to assess mobility. Although there are limitations in the individual measurements, a combined approach could provide a comprehensive view of the effects of mechanical loading on tissue viability. Long-term monitoring of pressures has the potential to estimate biomechanical parameters, such as centre of pressure, contact area and pressure gradients, from distributions, thereby creating an opportunity to track individual posture and mobility over prolonged periods. Such an approach has not been investigated to date. Indeed, there is a lack of studies to quantify movements relative to pressure-related variables and their temporal profiles. It will be inevitable that long term pressure monitoring will result in large sets of data (Bogie et al. 2008) and thus there is a need to identify minimum data sets using appropriate algorithms. There is the potential for machine learning to facilitate this process and translate this data into meaningful clinical information.

Accordingly, the present work is focussed on assessing the use of technologies to monitor interface pressure, where the effectiveness of repositioning strategies can be assessed in a robust objective manner. A commercially available continuous pressure mapping system, the ForeSite PT Patient Turn system (XSENSOR Technology, Canada), subsequently referred as to ForeSite PT system, whose specification are detailed in Table 2-1, was used throughout the current work. ForeSite PT is marketed as a “patient repositioning reminder” system and its effectiveness has been demonstrated for optimising repositioning interventions within at risk hospitalised patients (Wong et al. 2015) and those in the community (Aylward-Wotton and Kent 2017). It is current used in conjunction with an algorithm, whose characteristics are integrated in the next section.

2.6 Critical appraisal of current algorithms used in continuous pressure mapping systems

ForeSite PT system (XSENSOR Technology, Canada), incorporates a warning algorithm, detailed in Appendix A, which provides some identification of vulnerable areas based on the pressure – time integral and defined threshold values. It informs clinicians of potentially damage to risk areas (Figure 2-3).

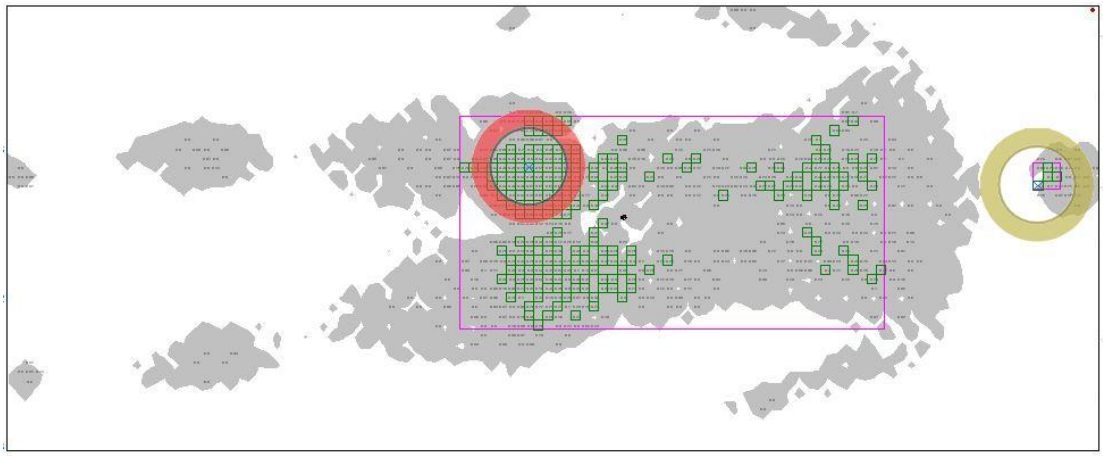

Figure 2-3: Red and yellow indicators highlight body areas associated with risk, when the pressure – time values, in the form of normalised exposure, exceed arbitrary exposure thresholds. This image is derived from the analyser software of the ForeSite PT system.

The algorithm is based on the pressure values, which are recorded continuously at each sensor of the array, at a sampling frequency of 1Hz (Table 2-1). For each sensor cell, the accumulated sum of pressure is normalised with respect to the product of the maximum calibrated pressure and the turn timer interval to calculate an "exposure reading" (Figure A-1). The turn timer interval represents the expected time interval at which the subject is supposed to be turned for pressure relief or skin inspection. This value is arbitrary and it can be managed from the system settings. The default value is 900 seconds (15 minutes).

The yellow and red indicators, illustrated in Figure 2-3, correspond to normalised exposure readings, which have exceeded exposure thresholds. Their values are arbitrary and adjustable by the user within the system settings. Thus, if the exposure reading exceeds the exposure threshold either yellow or red indicators will appear on the system readout. These indicators are designed to alert the carers as to the areas exposed to high pressure values, promoting the need for repositioning. After repositioning, they are encouraged to reset the turn timer button to restart the accumulation of the exposure of pressure. This relies on an understanding of the exposure metric in the software and on the manual re-setting of the turn timer. Clearly, the system is not programmed to automatically detect when individuals are repositioned.

Moreover, there are clear limitations in the estimation of the pressure exposure with respect to the normalisation in both maximum pressure value and turn timer interval. The former is based on the calibration which, as stated in Section 2.1, is performed by the manufacturer prior to distribution and therefore does not account for any change in system performance. In addition, the fact that the cells exposure are normalised with respect the maximum pressure reading creates a non – absolute reference as this value may change from system to system or from different configurations (Table 2-1). The other parameter used to calculate the cells exposure is

the turn timer interval. The default value does not reflect the 2 – 4 hourly repositioning interval time typically advised in the clinical guidelines (NPUAP/EPUAP/PPPIA 2019), and is more based on short term pressure monitoring. In addition, the system does not account for the specific anatomical region and their relative tissue tolerance.

Clearly, the current algorithm of the ForeSite PT system limits the possibility to establish appropriate intervention strategies for pressure ulcer prevention and limitations have been observed with respect to the:

1) Calibration is provided by manufacturers in their facility. This limits the opportunity for researchers and clinicians to perform sensors calibration and sensitivity analyses, with particularly emphasis on examining any changes with time and usage;
2) Measurements are obtained at the skin – support surface interface and, as such, the values do not reflect the stress/strain status within the skin and soft tissues, (Section 1.7). Accordingly interface pressure values cannot be used as a direct warning for tissue damage;
3) The algorithm does not provide indication of posture and mobility.

Thus, there is a need to define temporal objective parameters as indicator of movements. This implies the assessment of the system performance and the development of a novel data analysis to identify the most clinical relevant parameters.

2.7 Aims and objectives

The PhD project aims to develop an intelligent algorithm designed to detect and classify posture and mobility by using a range of biomechanical parameters. It will incorporate parameters estimated from selected bioengineering sensing technologies to discriminate between a range of evoked postural movements in lying. A series of separate experimental phases have been designed to accomplish this global aim of the project, as detailed in separate phases and summarised in Figure 2-4.

Phase 1

This initial phase is designed to evaluate the capability of a number of different biomechanical parameters derived from the continuous pressure mapping and actimetry systems in detecting changes in defined lying postures. In particular, the sensitivity and specificity of each parameter were estimated in a cohort of able-bodied individuals. A ranking of the most accurate parameters was established for the findings as reported in Chapter 3.

The objectives of this phase are:

- To examine a range of different lying postures, evoked in a pre – defined order, by utilising series of biomechanical measures;

- To estimate a range of parameters and selection of appropriate threshold ranges for each, to perform a comprehensive sensitivity and specificity analyses;
- To quantify the capability of all parameters in detecting postural changes by performing a Receiver Operating Characteristics (ROC) analysis;
- To establish a ranking of the most accurate parameters using area under the curve (AUC) analysis.

Phase 2

This phase was designed to examine the potential of machine learning approaches, in the form of well-established classifiers, by considering the biomechanical parameters selected from Phase 1. It aims to investigate these signals ability to train classifying models, which were tested and validated using a range of "unknown" postures.

The objectives of this phase incorporated in Chapter 4 are:

- To perform data reduction and feature extraction of the raw signals in accordance with the previous ranking of selected parameters;
- To create a methodology for the automatically detection of postural changes from the set of data;
- To apply different machine learning algorithms in the form of classifiers, cross – validated with leave one out testing, and evaluate their accuracy in identifying the range of postures adopted.

Phase 3

This third phase was designed to validate the automatic methodology developed in Phase 2 for range of postures adopted in a random sequence on different support surfaces. For this purpose, a set of pressure data from able – bodied subjects, previously acquired in a research project in collaboration with a healthcare company, was utilised.

The objectives of this phase incorporated in Chapter 5 are:

- To detect the frequency of postural changes from the biomechanical pressure parameters;
- To investigate the accuracy of machine learning classifiers in identifying the range of postures adopted.

Phase 4

This final phase was designed to evaluate clinical data of interface pressure, recorded with patients from spinal cord injured population based in a specialised hospital unit. It utilised the methodology developed to determine frequency and magnitudes of postural movements. This was examined in the light of the recording of skin integrity collected from each patient.

The objectives of this phase incorporated in Chapter 6 are:

- To apply the methodology developed for the detection of frequency and magnitude of postural changes;
- To compare the methodology to the exposure algorithm of the ForeSite PT system, which promoted postural changes and skin integrity. This will be assessed in the light of skin examination provided by specialised healthcare professionals.

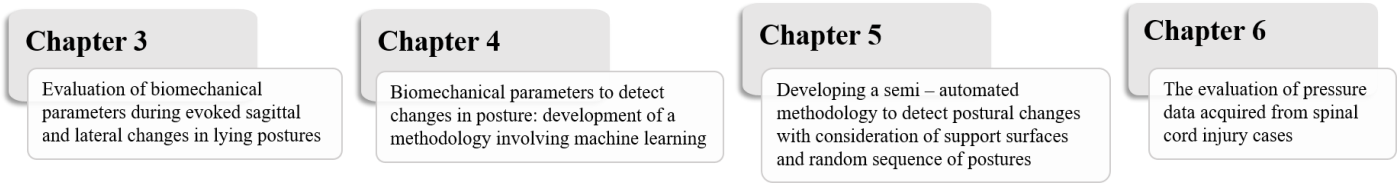

Figure 2-4: Flow diagram summarising the progression of the phases included in the experimental chapters of the thesis.

Chapter 3: Evaluation of biomechanical parameters during evoked sagittal and lateral changes in lying posture

Pressure monitoring technology provides an opportunity to estimate time – related biomechanical parameters from the pressure distributions which have the potential to evaluate postural changes, natural in origin and/or evoked. Thus, these data have the potential to act as surrogate for movements . However, it has not been examined whether these parameters are sensitive and specific in detecting specific lying postures.

The present chapter was designed to evaluate the performance of the pressure monitoring technology in conjunction with an established commercial actimetry system. In particular, it investigated the response of a range of distinct sagittal and lateral lying postures using biomechanical parameters estimated from the pressure distribution and kinematic data derived from actimetry systems. Sensitivity and specificity analyses were conducted to investigate the accuracy of these parameters in detecting the temporal profiles of a range of different static lying postures with a cohort of healthy subjects.

3.1 Materials and methods

3.1.1 Interface pressure measurements

Interface pressure measurements were recorded using a full body pressure monitoring system (ForeSite PT, XSENSOR Technology Corporation, Canada), in the form of a fitted mattress cover. It incorporates 5664 pressure measuring sensor cells, with a spatial resolution of 15.9 mm, covering a sensing area of 762 mm x 1880 mm. Each sensor operates within a pressure range of 5 – 200 mmHg (0.7 – 26.6kPa), with an accuracy ± 2 mmHg and an acquisition rate of 1 Hz. Calibration was performed by the manufacturer prior to acquisition of the system. A touch screen monitor connected to the pressure mat saved the acquired data.

The system provides a series of parameters which are exported using a dedicated software (ForeSite PT Analyser and ProV7, Xsensor, Canada), incorporating a matrix (48 x 118) of pressure values. For each frame of the acquisition, specific parameters included the mean and peak pressures, contact area and coordinates of the centre of pressure (COP), with respect to a direction both parallel and perpendicular to the long axis of the mat (Figure 3-1).

Figure 3-1: ForeSite PT system placed as mattress cover and the monitor which displays the distributions of the pressures. Schematic representation of the system reference axes are indicated in orange.

The manufacturer supplied the calibration and specifications, defining sensitivity, resolution and accuracy. As detailed in Section 2.1, system performance could change with usage. Accordingly, a static and quasi – static test were designed to evaluate the performance of selected pressure cells within the sensing array in response to different temporal loading regimens. These tests and their results are detailed in full in the Appendix B.

To review briefly, during the static testing the pressure map was located on top of a foam mattress and a “buttock shaped” indenter was used to load the surface for prolonged periods (24h), as illustrated in Figure B-1. During the quasi-static testing, a spherical wooden indenter integrated into an Instron loading machine was used to provide ramped displacements, as illustrated in Figures B-4 and B-5 (Appendix B). During the static tests, the results indicated no systematic changes in the pressure values for a period of constant loading for 24 hours (Figure B-2 and B-3). The quasi – static test involved a series of five increments of displacement, each held for 5 minutes, up to a maximum of 60mm, equivalent to approximately 50% compression of the foam surface. These increments were then reversed in the unloading cycle. Results of two pressure parameters namely, peak pressure index and contact area, estimated above two threshold pressures, were compared with the contact pressure estimated at the interface between the indenter and foam support. Typical result for the temporal profile of the peak pressure index above a threshold of 10 mmHg is illustrated in Figure 3-2 (curve in red). The trend reveals differences with respect to the increments in the loading and unloading phases. Moreover, there are clearly differences between the absolute value of the peak pressure index and the predicted contact pressure (curve in green) particularly at high increments of deformation (Figure 3-2). This suggests that the contact area of indenter has been over – estimated at the higher increments of the loading cycle.

The static test confirmed that long – term monitoring would not result in significant drift. The quasi – static test demonstrated that the system was sensitive to small increments of pressure

changes, up to clinical relevant peak pressure of 60mmHg. Although the absolute output is dependent on whether the changes correspond to either the loading or unloading phases, the system is clearly sensitive to relative changes in displacement, as will be further observed in postural repositioning. Therefore, ForeSite PT was accepted for usage in the current study.

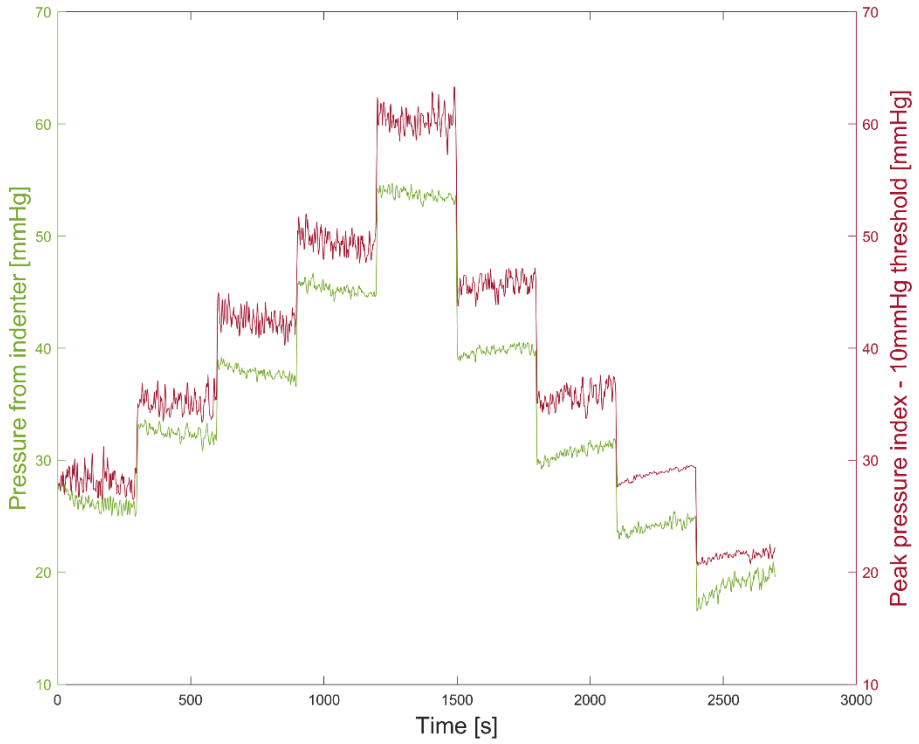

Figure 3-2: Typical comparison between peak pressure index, signal in red, estimated at 10mmHg and the contact pressure between the indenter and the pressure map (signal in green).

3.1.2 Accelerometer measurements

Three wearable sensors (Shimmer Platform, Realtime Technologies Ltd, Dublin), integrating a tri – axial accelerometer, gyroscope and magnetometer, were used in the present work to measure trunk and waist movements, with respect to the standard anatomical planes. Shimmer sensor provides a high range of parameters compared to other commercial systems and, accordingly, was used in the current study.

Individual sensors were attached to the sternum and to the right and left anterior iliac crest in the coronal plane, using Velcro straps (Figure 3-3). Each device represents a small wireless sensor (51mm x 34mm x 14mm) that records calibrated real-time kinematic data at 1-51 Hz (range ± 2g). A frequency rate of 51 Hz was used for the actimetry data recording. Calibrated Euler angles, namely, tilt angles, with respect to the sagittal and transverse planes were estimated from all sensors at the different body locations.

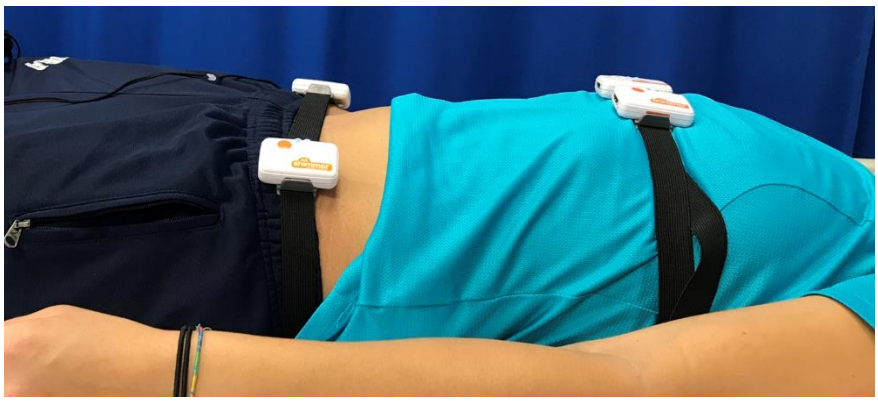

Figure 3-3: The location of the individual sensors, specifically in the anatomical coronal plane to the sternum and to the right and left anterior iliac crest.

Tri-axial accelerometers and gyroscope for each sensor were calibrated using a dedicated application (Shimmer 9DoF Calibration v2.10) provided by the manufacturer. This calibration ensured the devices were working at a pre-determined accuracy prior to each data collection period. No drift was visible in the data after calibration (data not shown).

3.1.3 Study protocol

The study was approved by the local Faculty Ethics committee of the University of Southampton (FoHS - Ethics - 26379). Participant recruitment was conducted by means of poster advertisements and word of mouth. Each potential participant was given an information sheet and allowed at least 48 hours to decide whether to take part or not. The participant inclusion criteria were as follows:

- Healthy volunteers;
- Age between 18-80 years;
- No participation in another research study;
- Ability to lie in the supine position for a period of in excess of 120 minutes.

Potential subjects were excluded if they met any of the following criteria, each of which could potentially affect the biomechanical and physiological responses:

- Medical history of any dermatological condition, including pressure ulcers;
- History of neurological and vascular conditions e.g. diabetes.

Following written consent, the height and weight of each participant were recorded.

The test protocol was performed in the Biomechanics Testing Laboratory in the Clinical Academic Facility in Southampton General Hospital, where room temperature was maintained at $24^{o} \pm 2^{o}$. Participants were requested to wear loose fitting clothing and adopt a series of postures on a standard mattress with a castellated foam surface (Solace Foam Mattress, Invacare UK) located on a standard hospital bed frame (AvantGuard^{TM}, Hill-Rom, US). Prescribed

sagittal changes in posture from the initial supine posture involved the raising of the head of bed (HOB) by 10° increments to a maximum of 60°, the latter representing a high cardiac sitting posture (Figure 3-4). The HOB was then lowered in 10° increments until the supine posture was re-established. Each posture was evoked by the researcher using the bed frame control and held for a period of 10 minutes. The subsequent movements involved 20-25° tilting of the mattress in the transverse plane on an automated 10 minute cycle time (Figure 3-5) using a continuous lateral rotational system (CLRS) (Vikta Komfitilt®). An overview of the test protocol is shown in Figure 3-6.

Figure 3-4: Sagittal increments of the HOB every 10° from supine posture to 60°.

Figure 3-5: Left and right lateral turning.

Interface pressure distributions and actimetry data were continuously recorded throughout the entire test period of 140 minutes. Participants were instructed to remain as still as possible on the mattress, so that the changes in posture were evoked either through the bed frame or the CLRS device.

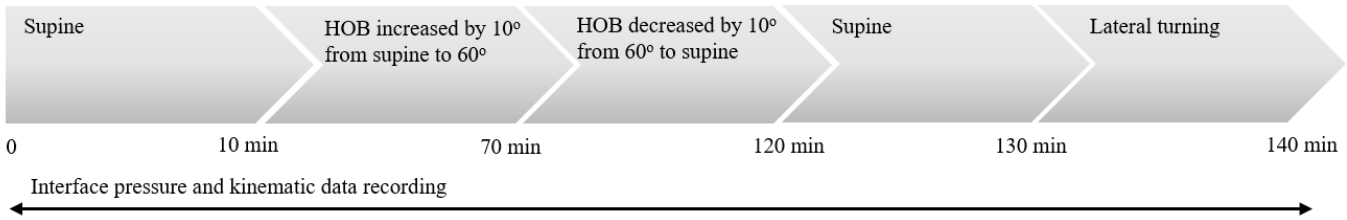

Figure 3-6: Schematic of the testing protocol and data collection process.

3.1.4 Outcome parameters

Pressure distributions and actimetry signals were processed and analysed using a custom software developed in Matlab (Mathworks, US).

The post-processing of the pressure data involved the estimation of temporal – related parameters, namely:

- Centre of pressure (COP), in the directions parallel and perpendicular to the long axis of the mat, defined as the centroid of the distribution (units = mm);
- Peak pressures (PP) (units = mmHg);
- Peak pressure gradient (PPG) in the directions parallel and perpendicular to the long axis of the mat, which describes the maximum change in pressure between adjacent sensing cells (units = mmHg/mm);
- Contact area (CA) between the mattress and the individual sensors recording a pressure above separate cut-off values, namely 5 mmHg, 10 mmHg, 20 mmHg, 30 mmHg and 40 mmHg (units = mm^2).

These parameters were estimated from distinct regions of interest (ROIs), namely the whole body (WB), upper body and head (UB), buttock area (B), lower body including the heels (LB), as depicted in Figure 3-7.

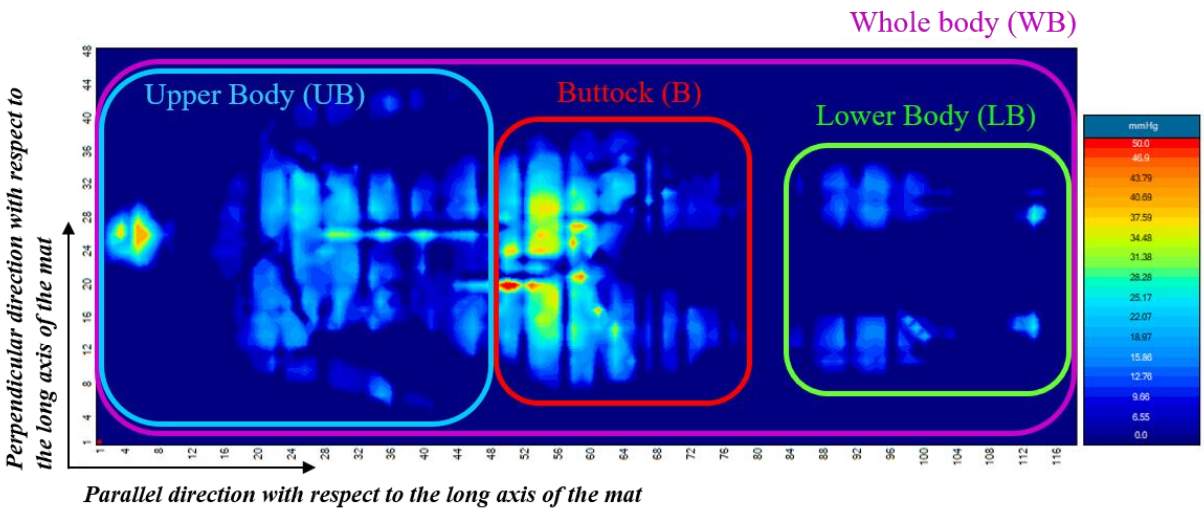

Figure 3-7: ROIs selection from the distributions of the pressure. The colour gradient of the pressure distribution is associated with a scale bar (scale on the right) which, in this case, was set at a pressure range between 5 mmHg, which represent the lower limit of the system, and 50 mmHg. All the pressure values below 5mmHg were reported to 0.

It was found in the early part of the study that parameters for both upper body and lower body ROIs did not achieve an acceptable level of accuracy in detecting changes in posture. Hence, this chapter only details findings for the parameters estimated at the whole body and buttock ROIs.

3.1.5 Post processing and analysis of the data

A series of distinct processes were performed to optimise the biomechanical signals for analysis. Contact area was estimated following an initial stage of normalisation expressed as percentage variation with respect to the first supine frame of acquisition. Actimetry signals were resampled at 1Hz prior to filtering. To remove high frequency noise, all signals were filtered using a moving average filter with a window length of 15 samples, as indicated in Figure 3-8. Subsequently, they were manually labelled denoting each posture, by manually selecting the beginning and the end of each posture within a Matlab Graphical User Interface (GUI). The signals were then normalised with respect the first frame i.e. initial supine posture, of the acquisition. Both the amplitude of the signal changes between the postures and the deviations during each posture were estimated for all parameters from both measurement systems.

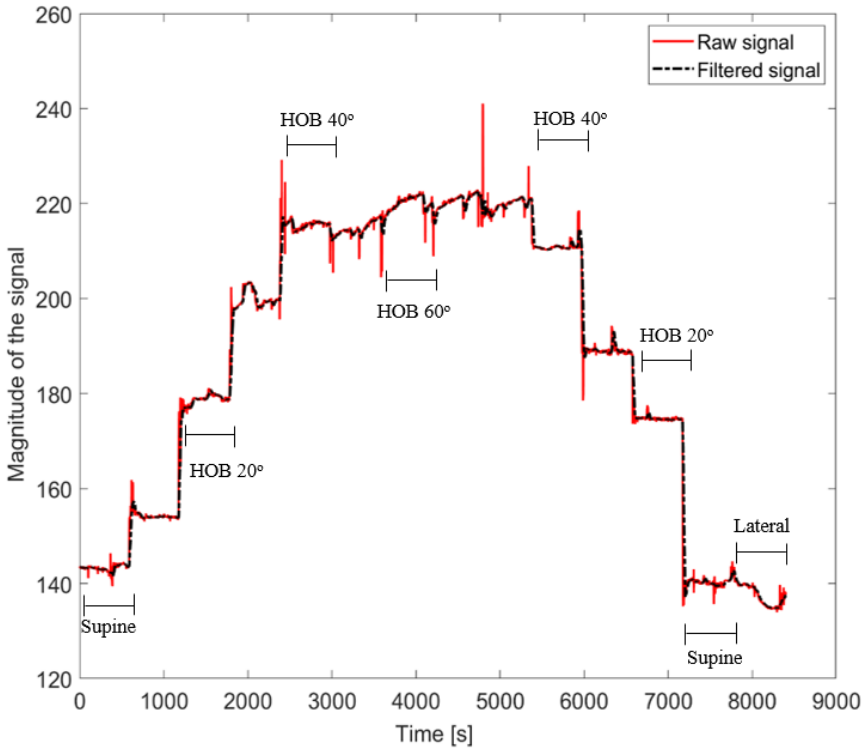

Figure 3-8: The effect of filtering on a signal. The acquired signal (red line) was filtered using an average moving filter, which result is remove the high frequency variations of the signal (black dotted line). All the spikes visible in the raw signals were removed after filtering

3.1.6 Amplitude of the movements in the sagittal plane

Figure 3-9 exemplifies the procedure used to determine the amplitude of the signal changes between the sagittal postures. The movements performed in this direction were characterized by incremental steps, coincident with prescribed changes in the HOB angles, as depicted in Figure 3-8. Pressure parameters estimated in the parallel direction with respect to the long axis of the mat and tilt angles estimated in the sagittal plane were representative of sagittal movements.

The assessment of the amplitude of these changes involved:

- The selection of the extremes of each postures as identified by their x/y coordinates. As some perturbation in the signals characterised each of the changes due to the transition from one posture to the following posture, the selection involved a number of data points within each static posture which do not comprise these perturbations;
- The difference was calculated between the average of the last 50 samples of a selected posture and the average of the first 50 samples of the subsequent posture. This represents the amplitude of the movement performed during a prescribed change in posture, as denoted by the black dashed arrows in Figure 3-9.

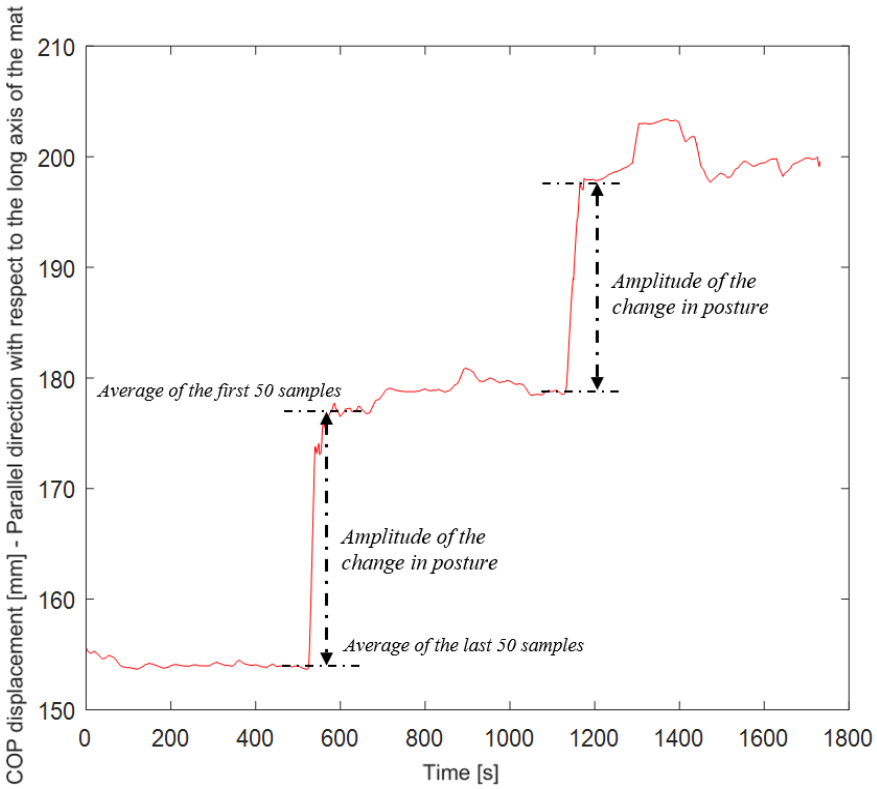

Figure 3-9: Determination of the amplitude of the sagittal changes in posture. The amplitude (black dashed arrows) is calculated as the difference between the average of the last 50 samples of a posture and the average of the first 50 samples of the next posture.

3.1.7 Amplitude of movements in the transverse plane

Figure 3-10 illustrates the procedure to determine the amplitude of the signal changes in the two lateral postures. The movements performed during the lateral turning were visible as a displacement in the signal magnitude. Pressure parameters estimated in the perpendicular direction with respect to the long axis of the mat and tilt angles estimated in the transverse plane were representative of lateral movements. The assessment of the amplitude of these changes involved:

- The selection of the end of the final supine posture;
- The range of the movement during each turning phase, calculated as the signal displacement with respect to the data point depicting the end of the supine posture. This is denoted by the black dashed arrows in Figure 3-10.

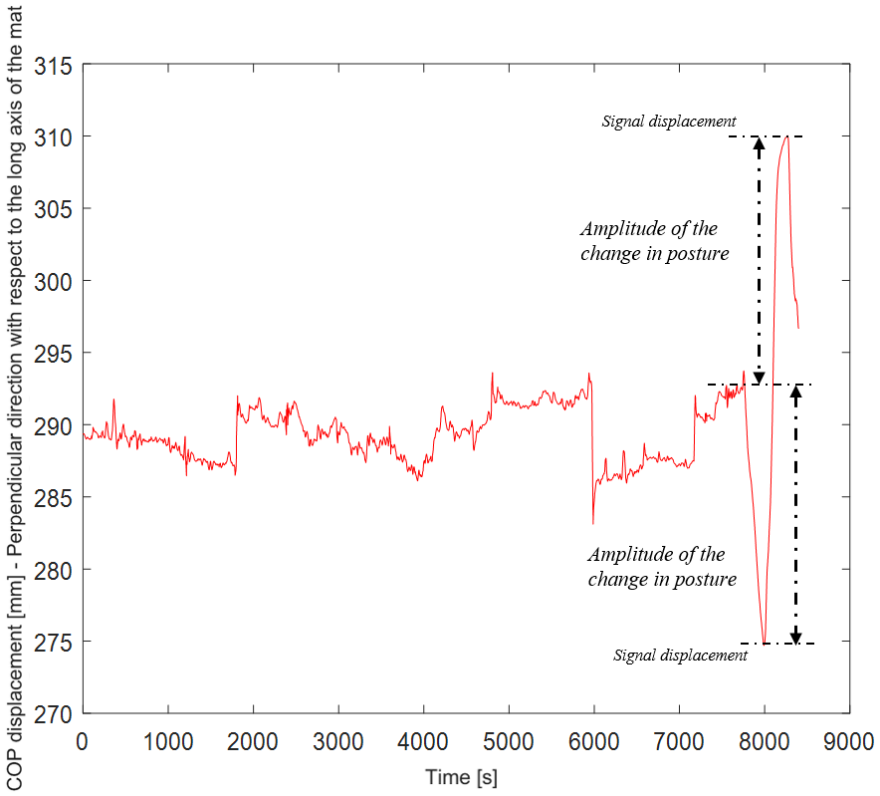

Figure 3-10: Evaluation of the amplitude of the changes in posture performed during lateral turning. The amplitude (black dashed arrows) is calculated as the displacement of the signal with reference to the end of the final supine posture.

3.1.8 Amplitude of the movements performed during static postures

The evaluation of the amplitude of the movements performed during each static posture was assessed for sagittal movements alone. Minimal signal perturbations resulting from natural postural movements for each participant were evident during lateral turning. Indeed, the continuous nature of the lateral turning made these perturbations difficult to estimate.

Figure 3-11 illustrates the procedure used to determine the amplitude of the movements performed during each sagittal posture. The difference between the maximum and the minimum values of the signal, calculated over the entire period of each static posture, defines a “range of motion” for all the static postures.

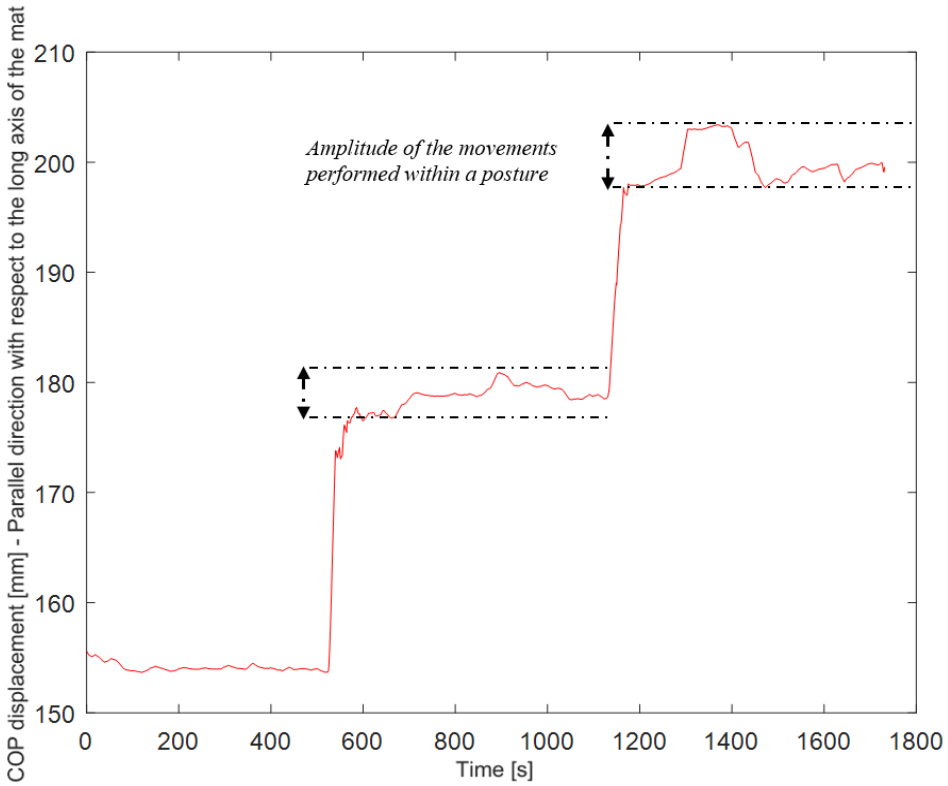

Figure 3-11: Amplitude of the movements performed during sagittal static postures, calculated as the difference between the maximum and the minimum values of the signal.

3.1.9 Sensitivity and specificity analyses in detecting changes in posture

Appropriate threshold values, detailed in Table 3-1, were selected for each of the biomechanical parameters to distinguish between postural changes. These provided the means to assess the sensitivity and specificity of the pressure monitor and actimetry signals (tilt angles) to discriminate the changes in the adopted postures during the test protocol.

Table 3-1: Summary of the threshold values for each of the biomechanical parameters.

Biomechanical parameters	Threshold value				
COP [mm]	1	5	10	20	30
PP [mmHg]	2	4	6	8	10
PPG [mmHg/mm]	0.1	0.2	0.4	0.5	1.0
CA [% variation]	5	10	15	20	25
Tilt angles [degree]	2	4	6	8	10

Sensitivity represents the true positive rate, namely the movement from one posture to the next, which is classified as a distinct change in posture based on the specific threshold value. Thus, a

posture was classified as a true change if the amplitude of the movement performed exceeded the prescribed threshold value as depicted in Figure 3-12.

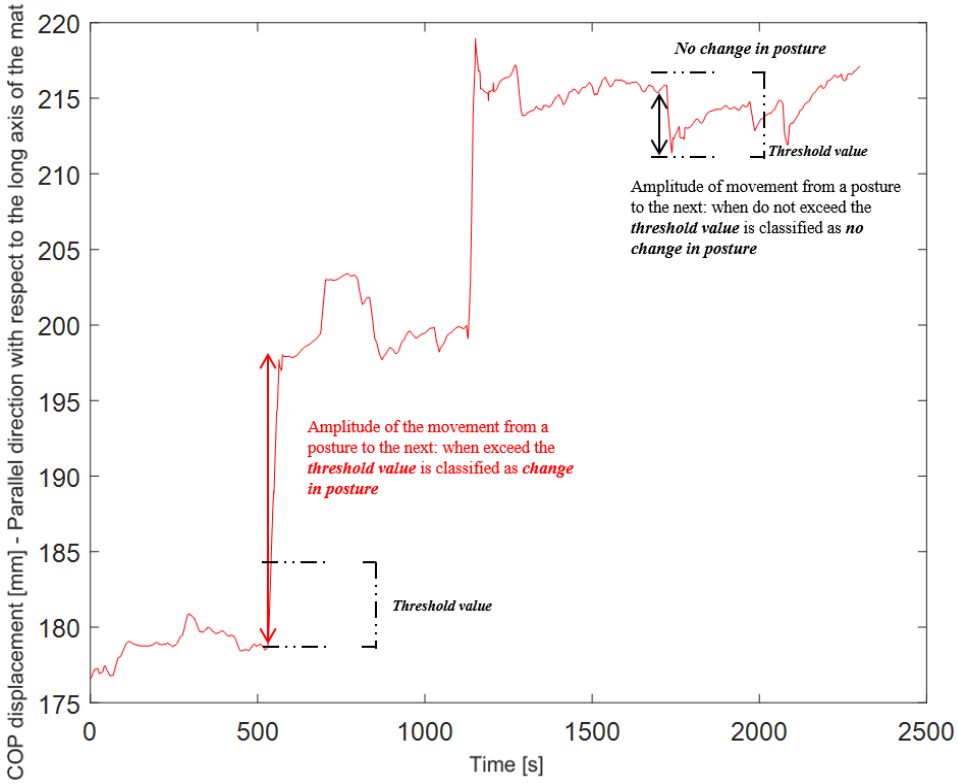

Figure 3-12: Characteristic features of four postures. A pre – determined threshold value, represented by the dotted lines, has been selected to denote the sensitivity analysis. A specific change in posture (true positive) was identified where the amplitude of the movement performed in the change in posture was greater than the selected threshold value (red arrow).

Specificity represents the true negative rate, namely the amplitude of the movements during the 10 minutes static postures, which do not exceed the prescribed threshold value. If the amplitude of the movements within a posture did exceed the threshold, a false positive was observed, as depicted in Figure 3-13.

It should be noted that specificity during the lateral turning was not evaluated, as participants did not adopt a static posture during lateral postures.

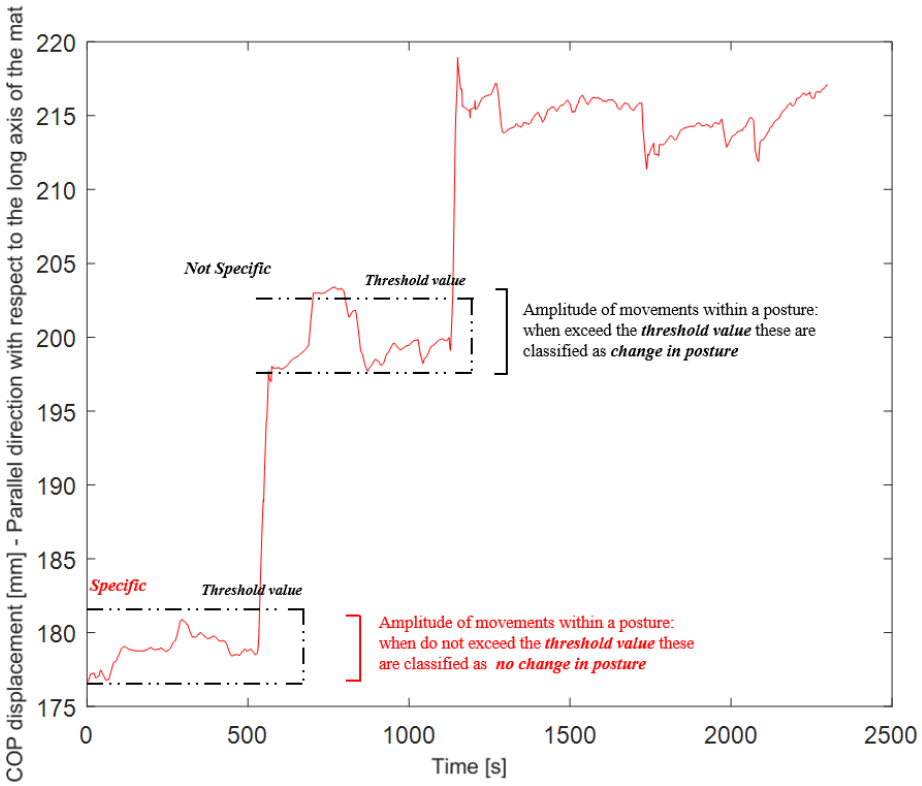

Figure 3-13: Characteristic features of four postures. A pre – determined threshold value, represented by the dotted lines, has been selected to denote the specificity analysis. A true negative (specific posture) was identified where the amplitude of the movements within a posture did not exceed the threshold value.

Both sensitivity and specificity to detect postural changes for each threshold value were estimated for all biomechanical signals and presented as a percentage of the cohort (n = 11). It is inevitable that higher threshold values will result in a lower sensitivity and a corresponding higher specificity. To accommodate this, Receiver Operating Characteristic (ROC) analysis was performed, which represents a combined integral of sensitivity and specificity.

ROC curves were created within Matlab (MathWorks, US), and used to determine the optimal range of parameters and thresholds, which discriminated between the presence and absence of postural changes (Alhassan and Robinson 2010). Each of the biomechanical signals and the range of threshold values were examined to identify the combination with the optimal sensitivity and specificity for all evoked movements. The area under the ROC curve (AUC), defined by sensitivity plotted against 100 – specificity, was calculated to rank each parameter and threshold. The trend, exemplified in Figure 3-14, shows that an increase in sensitivity results in a decrease in specificity. AUC quantifies the probability that the test correctly discriminates the presence or absence of a postural movement, ranging from 0 to 1. An AUC of 0.5 suggests no discrimination between true positive and true negative condition, while a value of 1 indicates an optimum discrimination between the two.

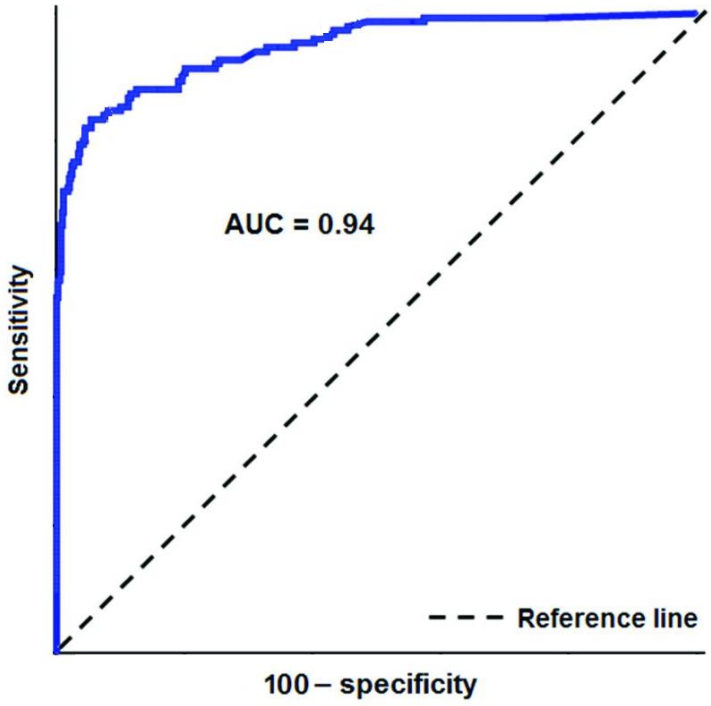

Figure 3-14: Example of a ROC curve and associated AUC value.

3.2 Results

3.2.1 Participants

Demographics of the subject cohort are summarised in Table 3-2. They represent a group of young able – bodied individuals with a range of body types and body mass indexes (19 – 30 kg/m^2).

Table 3-2: Demographics of the subjects cohort.

Subject	Age	Sex	Height [cm]	Weight [kg]	BMI [kg/m^2]
1	36	M	176	87	28
2	31	F	152	50	22
3	37	M	183	73	22
4	27	F	168	58	21
5	31	M	185	84	25
6	25	F	177	64	20
7	28	M	172	78	26
8	35	F	153	44	19
9	32	M	173	90	30
10	34	M	182	76	23
11	32	F	174	80	26
Mean (SD)	32 (4)		172 (11.0)	71 (15.2)	24 (3.5)

3.2.2 Temporal trends of biomechanical parameters

The temporal trends of both interface pressure parameters and tilt angles signals were in most cases characterized by incremental steps coinciding with the evoked movements in the HOB angles. This is exemplified in Figures 3-15A and B, which show the filtered signals of COP estimated in the parallel direction with respect to the long axis of the mat and trunk tilt angles in the sagittal plane, respectively. It was evident that the changes in HOB angles were clearly reflected in the tilt angles in the sagittal plane with similar increments between each posture (Figure 3-15B). By contrast, the increments in some pressure related signal e.g. COP at the buttock ROI, revealed only small increments between postures for angles exceeding 40° HOB (Figure 3-15A). In addition, differences were observed in the increments on whether the HOB was increasing or decreasing, as exemplified for HOB angles less than 40^o (Figure 3-15A). It also occurred that the magnitude of movements within some static postures was greater than the corresponding increments to the following posture, as exemplified in Figure 3-15A for postures involving HOB angles >40^o.

Figures 3-15C and D show the temporal trends of COP in the perpendicular direction and trunk tilt angles in the transverse plane, respectively. Relatively small changes for the evoked movements in the HOB angles were visible in both signals. By contrast, consistent changes in the magnitude were observed during lateral turning.

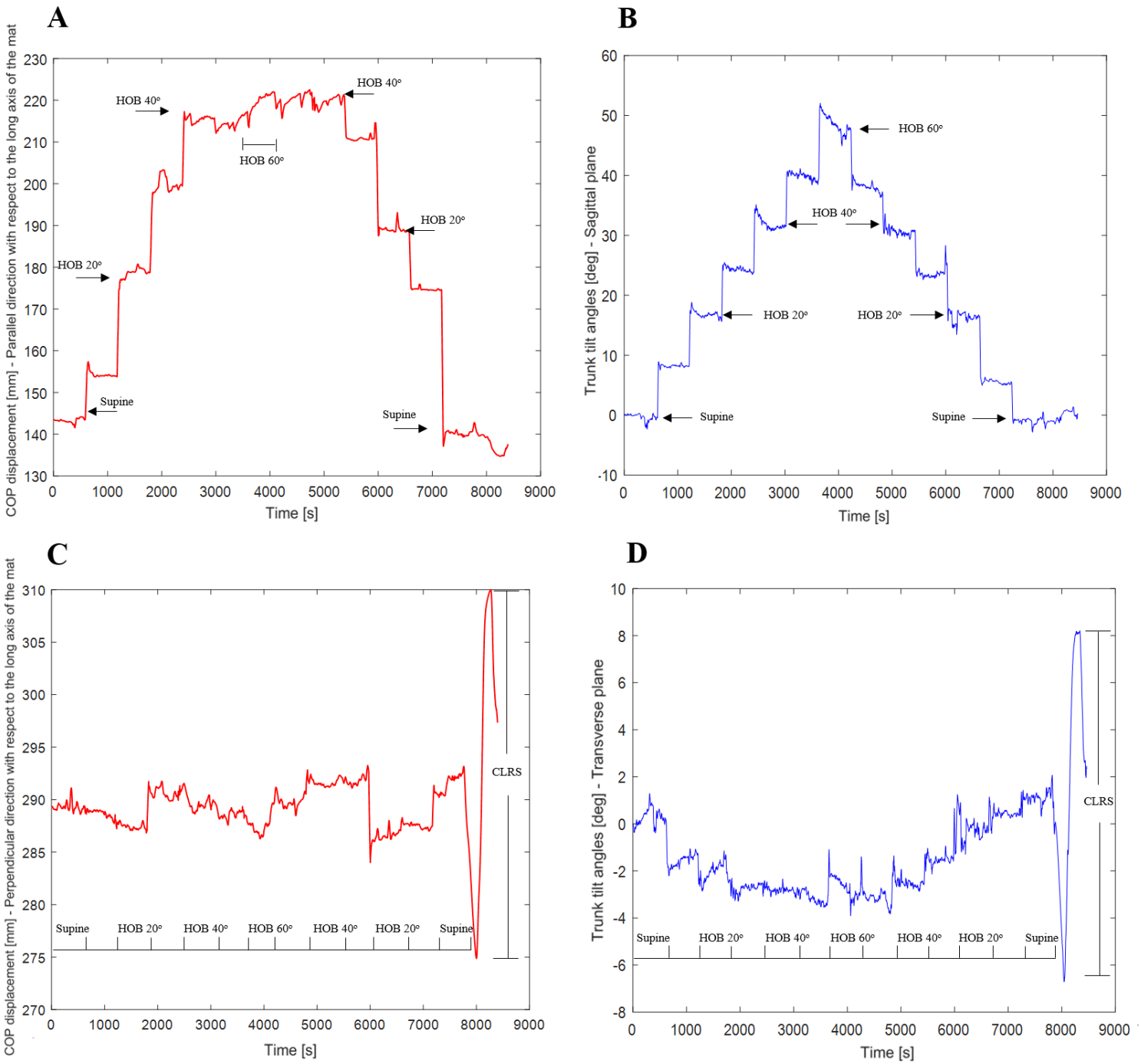

Figure 3-15: Temporal trends of the displacement of the COP at the buttock ROI and trunk tilt angles for prescribed movements in the HOB angles (A and B) and CLRS system (C and D).

3.2.3 Sensitivity and specificity of contact area signals estimated from different threshold values

As contact area at both whole body and buttock ROIs was estimated for pressure readings above separate cut-off values, a preliminary step was conducted to identify the most indicative signal in detecting postural changes. Sensitivity and specificity were evaluated for the threshold value reported in Table 3-1.

To review briefly, contact area between the mattress and the individual sensors were estimated for pressure values above 5 mmHg, which represent the default lower limit of the system. In addition, it was also estimated for values exceeding 10 mmHg, 20 mmHg, 30 mmHg and 40 mmHg. Signals were particularly influenced by the cut-off values. Indeed, increase in the cut-off values exacerbates the changes between postures in the signals. For example, contact area estimated at high cut-off values e.g. 30 and 40 mmHg, revealed high deviations between postures when compared with signals estimated at lower cut-off values, as such high pressure values are gradually observed during elevation of the HOB. Perturbations in the signals during static postures were observed high for high cut-off values.

Sensitivity and specificity of the contact area signals were influenced by both the posture and the threshold values used for the discrimination (Table 3-1). As an example, sensitivity is reported in Figure 3-16A for change in posture from supine to 10^{o} HOB and specificity in Figure 3-16B for the corresponding supine posture. It is observed that the range of sensitivities increased for higher cut-off values as only small increments in the change in posture from supine to 10^{o} HOB were observed. By contrast, the corresponding specificity decreased.

A cut-off value of 20 mmHg provided the optimum ratio between sensitivity and specificity for all postural changes in all subjects. Thus, contact area signal of pressure values ≥20 mmHg was most conveniently used in the following analyses.

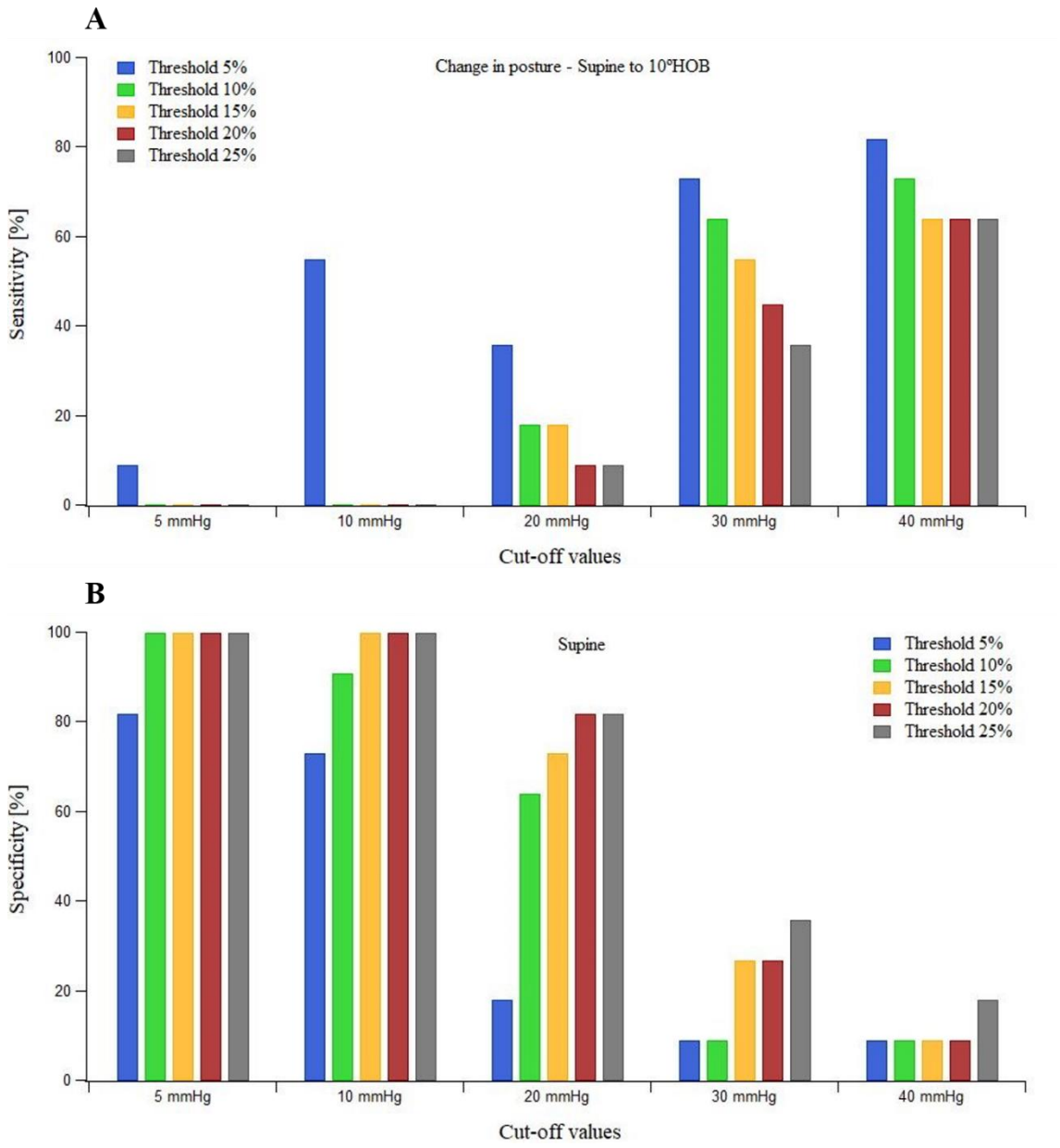

Figure 3-16: Sensitivity (A) and specificity (B) of **contact area signals estimated at the whole body ROI** for pressure readings above different cut-off values (5 mmHg – 40 mmHg), in detecting change in posture from supine to 10º HOB. For each of the signals, the sensitivity and specificity have been calculated with respect to different threshold values (5%, 10%, 15%, 20% and 25%). A cut-off value of 20 mmHg showed the best ratio between sensitivity and specificity.

3.2.4 Inter – subject variability

The interface pressure data revealed a high inter-subject variability specifically for some parameters such as peak pressure and peak pressure gradients. In order to examine the nature of the distribution of pressure parameters, a cumulative frequency approach was produced for each biomechanical parameter.

The cumulative frequency trends, indicated by the blue lines, are shown in Figures 3-17A and B for contact area at the whole body ROI and the trunk tilt angle, respectively. It is clear that the

relationship for the contact area (20mmHg) during the postural changes with respect to both planes and within each static posture, was non – linear in distribution. This was also the case for other pressure parameters (data not shown). By contrast, the corresponding distribution for the tilt angle was fairly linear in form (Figure 3-17B). These findings strongly suggested the use of non – parametric descriptors for pressure-related data and parametric descriptors for actimetry data.

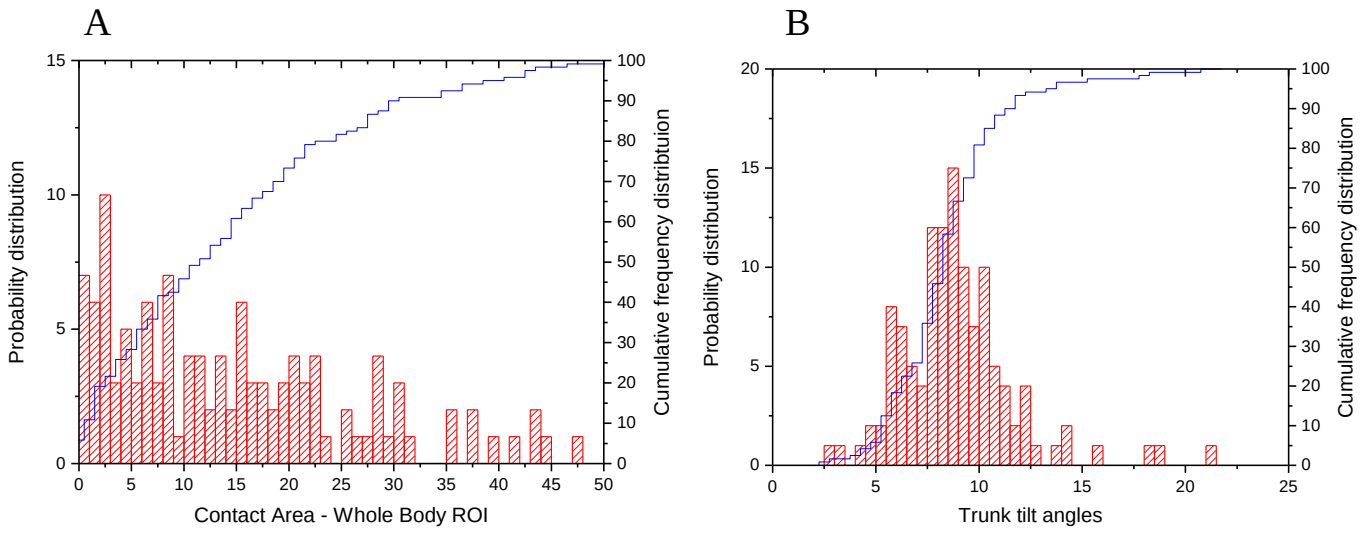

Figure 3-17: Graphical representation of the distribution of the data with reference to the amplitude of the changes in posture of A) the contact area estimated at the whole body ROI, B) the trunk tilt angles. The histogram represents the probability distribution, while the blue curve represents the corresponding cumulative frequency distribution.

3.2.5 Amplitude of movements in the sagittal plane

Tables 3-3 and 3-4 summarises the median and interquartile range (IQR) for changes in five pressure parameters during each of the evoked sagittal movements, for the whole body and buttock ROIs. These values were estimated from the changes relative to the previous posture. The corresponding mean values and standard deviation (SD) for the tilt angles at the two body segments, namely trunk and waist, are shown in Table 3-5.

COP displacement values varied considerably across all the postures. It was evident that from supine to 10° HOB there were small magnitude changes (<5 mm) for both ROIs. Subsequent magnitudes up to 60^{o} HOB revealed greater values at the whole body ROI, ranging between 12 - 21 mm. When the HOB was lowered, the displacements were relatively small, until the bed reached angles <20°, where the values increased (>19mm). By contrast, signal changes at the buttock ROI were smaller for HOB angles >30°.

A few trends were evident in the peak pressure changes at both ROIs. For example, the signal changes from supine up to 40^{o} were small in magnitude with median values of 3.2 - 7.1 mmHg

and 1.0 - 4.4 mmHg, for whole body and buttock ROI, respectively. Subsequent signal changes at the highest HOB were larger (>10 mmHg). When the HOB was lowered back to supine, there was a decrease in the magnitude of the peak pressure changes. There was considerable variability in values across the cohort, as demonstrated by the high interquartile (IQR) range. This was evident for both peak pressures and peak pressure gradients for each of the ROIs.

Changes in contact area (20mmHg) were relatively low in both ROIs at HOB angles <30^o, with median values <6% and <20%, respectively. For higher angles of HOB the percentage values increased by approximately 2 – 4 fold, with the maximum amplitude evident when HOB was lowered from 60^o to 50^o HOB. Sagittal tilt angles at the trunk and waist revealed similar changes for each incremental HOB angle with mean angles between 5.7 - 9.4° and 2.2 – 7.6°, respectively (Table 3-5). However, in the final postural change from 10^o HOB to supine these changes were noticeably smaller at both body sites.

Table 3-3: Summary of median (IQR) values of the parameters estimated from the pressure distributions at the **whole body** ROI in **sagittal plane**.

Changes in posture	COP [mm]	PP [mmHg]	PPG – parallel direction [mmHg/mm]	PPG – perpendicular direction [mmHg/mm]	CA (20mmHg) [% variation]
`Supine – 10^o	3.4 (0.5)	7.1 (7.1)	0.8 (9.4)	0.8 (9.4)	3.2 (6.1)
10^o - 20^o	17.5 (0.6)	3.2 (6.7)	1.2 (14.2)	1.0 (8.2)	4.6 (6.8)
20^o - 30^o	13.4 (0.5)	5.5 (9.0)	0.9 (10.6)	0.5 (8.0)	5.6 (9.8)
30^o - 40^o	20.6 (2.1)	6.6 (12.9)	0.8 (15.5)	0.3 (6.3)	13.6 (9.9)
40^o - 50^o	15.1 (1.4)	9.8 (12.2)	0.3 (9.1)	0.5 (14.3)	15.4 (20.6)
50^o - 60^o	12.7 (1.8)	12.2 (10.5)	0.6 (4.7)	0.6 (7.9)	22.8 (21.8)
60^o - 50^o	7.3 (0.2)	10.3 (9.9)	0.4 (13.9)	0.5 (9.0)	35.1 (21.0)
50^o - 40^o	6.0 (1.4)	6.8 (8.5)	0.9 (16.0)	0.8 (5.3)	20.7 (9.7)
40^o - 30^o	4.3 (0.4)	5.2 (9.7)	0.8 (7.1)	0.4 (9.1)	19.4 (15.2)
30^o - 20^o	11.4 (1.3)	4.2 (5.9)	0.6 (9.5)	0.4 (15.2)	16.5 (6.3)
20^o - 10^o	16.7 (1.4)	4.4 (3.2)	0.5 (2.9)	0.6 (7.1)	10.5 (10.6)
10^o - Supine	19.2 (1.0)	3.1 (6.5)	0.5 (6.3)	0.2 (5.9)	6.6 (5.7)

Table 3-4: Summary of median (IQR) values of the parameters estimated from the pressure distributions at the **buttock** ROI in **sagittal plane**.

Changes in posture	COP [mm]	PP [mmHg]	PPG – parallel direction [mmHg/mm]	PPG – perpendicular direction [mmHg/mm]	CA (20mmHg) [% variation]
Supine – 10º	4.8 (0.6)	1.0 (6.0)	0.2 (5.0)	0.1 (3.5)	11.1 (9.4)
10º - 20º	13.4 (0.8)	2.6 (3.6)	0.4 (7.2)	0.2 (1.8)	5.5 (15.3)
20º - 30º	11.7 (0.5)	3.2 (4.4)	0.3 (4.2)	0.4 (3.9)	17.7 (16.7)
30º - 40º	12.6 (0.5)	6.5 (6.5)	0.6 (6.1)	0.2 (1.6)	30.2 (21.9)
40º - 50º	3.9 (0.8)	4.4 (11.8)	0.5 (6.4)	0.4 (8.5)	31.1 (12.4)
50º - 60º	2.3 (0.3)	12.2 (10.5)	0.6 (2.7)	0.6 (8.1)	37.1 (14.6)
60º - 50º	2.9 (0.4)	9.1 (11.9)	0.4 (9.2)	0.3 (7.7)	41.9 (21.0)
50º - 40º	2.0 (0.3)	7.4 (5.8)	0.3 (4.0)	0.3 (3.8)	32.8 (8.7)
40º - 30º	5.0 (0.4)	5.5 (6.7)	0.3 (3.2)	0.3 (6.7)	33.4 (11.6)
30º - 20º	9.0 (0.7)	3.2 (2.4)	0.2 (1.6)	0.1 (2.5)	23.5 (8.0)
20º - 10º	14.3 (0.4)	3.2 (3.5)	0.2 (4.6)	0.2 (4.1)	19.6 (9.8)
10º - Supine	24.4 (1.0)	2.1 (2.6)	0.3 (1.7)	0.3 (2.4)	9.3 (15.7)

Table 3-5: Summary of mean (SD) values of the tilt angles estimated from the accelerometer signals at the **trunk and waist** locations in sagittal plane.

Changes in posture	Trunk tilt angles [deg]	Waist tilt angles [deg]
Supine – 10º	8.2 (1.5)	5.4 (3.6)
10º - 20º	8.3 (1.1)	5.6 (3.5)
20º - 30º	7.6 (4.3)	6.8 (3.3)
30º - 40º	9.1 (2.5)	5.2 (1.7)
40º - 50º	8.7 (3.8)	4.2 (2.6)
50º - 60º	9.4 (3.7)	5.4 (2.6)
60º - 50º	7.5 (2.4)	6.1 (3.5)
50º - 40º	7.2 (2.7)	6.7 (3.5)
40º - 30º	8.7 (1.9)	7.6 (2.7)
30º - 20º	8.4 (2.7)	6.3 (2.3)
20º - 10º	8.8 (2.4)	6.2 (3.0)
10º - Supine	5.7 (0.8)	2.2 (1.9)

3.2.6 Amplitude of movements performed during static postures

Tables 3-6 and 3-7 indicate the amplitude of each interface parameter for all the static postures. These values are presented as the median (IQR) changes in all participants. The corresponding tilt angles at the trunk and waist are summarised in Table 3-8 and presented as mean (SD) changes across all participants.

No trends in COP values were evident at the whole body (Table 3-6). By contrast, COP displacements at the buttock ROI were relatively low at static postures involving HOB $\geq 30^{o}$, with median values ranging between 2.5 and 7 mm (Table 3-7). Peak pressure and peak pressure gradients revealed a considerable variability across the cohort, as reflected in the high IQ values. The median values showed changes in peak pressures ranging between 5 and 20 mmHg at the whole body. By contrast, lower changes, with median values ranging between 2 and 9 mmHg were observed at the buttock ROI. Percentage variations of contact area were low (<15%) in both ROIs during each of the static postures. Tilt angles changes were more consistent, with trunk and waist values ranging between 2.2 – 4.1° and 3.1 – 5.9°, respectively (Table 3-8).

It emerged that median values of pressure parameters during specific static postures were in some cases higher than the amplitude of the corresponding changes in posture (Tables 3-3 and 3-4). This was particularly the case for peak pressure and peak pressure gradients at both ROIs. COP and contact area at both ROIs revealed only a few higher values during static postures. By contrast, this was not observed for tilt angles at both locations.

Table 3-6: Summary of median (IQR) values of the parameters estimated from the pressure distributions at the **whole body** ROI during each static posture.

Postures	COP [mm]	PP [mmHg]	PPG – parallel direction [mmHg/mm]	PPG – perpendicular direction [mmHg/mm]	CA (20mmHg) [% variation]
Supine	10.1 (1.0)	13.8 (13.4)	1.1 (13.1)	1.3 (16.1)	9.6 (7.3)
10º	7.7 (0.7)	10.4 (7.7)	1.0 (4.4)	1.2 (5.5)	7.9 (6.6)
20º	12.7 (1.0)	9.3 (7.0)	0.9 (11.2)	0.5 (10.3)	6.8 (15.2)
30º	11.7 (1.3)	5.9 (11.6)	1.2 (13.9)	0.6 (10.9)	8.5 (7.0)
40º	9.9 (1.5)	12.3 (17.3)	1.2 (17.8)	1.5 (12.0)	8.4 (7.0)
50º	14.2 (1.0)	19.0 (11.6)	0.9 (10.0)	1.5 (12.4)	9.9 (6.7)
60º	12.0 (0.7)	9.0 (14.1)	0.8 (17.0)	0.7 (15.6)	9.2 (7.8)
50º	9.8 (1.1)	9.3 (10.1)	0.7 (15.1)	0.6 (6.2)	13.8 (10.0)
40º	12.5 (0.7)	13.0 (14.5)	0.6 (18.4)	0.9 (10.3)	11.5 (10.6)
30º	11.4 (0.9)	7.5 (5.7)	0.7 (7.2)	0.3 (4.7)	10.0 (13.2)
20º	16.5 (0.6)	9.2 (11.0)	0.8 (12.2)	0.5 (16.6)	13.5 (11.0)
10º	16.5 (1.3)	8.6 (8.5)	1.2 (5.6)	0.7 (6.9)	9.6 (15.8)
Supine	9.6 (0.5)	10.3 (9.7)	1.1 (9.9)	0.6 (7.0)	11.9 (11.5)

Table 3-7: Summary of median (IQR) values of the parameters estimated from the pressure distributions at the **buttock** ROI during each static sagittal posture.

Postures	COP [mm]	PP [mmHg]	PPG – parallel direction [mmHg/mm]	PPG – perpendicular direction [mmHg/mm]	CA (20mmHg) [% variation]
Supine	7.9 (0.9)	3.5 (7.5)	0.5 (9.1)	0.4 (4.7)	11.5 (6.1)
10º	8.7 (1.4)	4.2 (8.3)	0.5 (6.3)	0.4 (9.3)	7.6 (5.1)
20º	11.7 (0.80	3.7 (4.9)	0.4 (5.0)	0.4 (5.4)	14.3 (15.9)
30º	6.7 (0.8)	2.5 (6.4)	0.2 (6.5)	0.3 (4.9)	9.6 (11.9)
40º	5.8 (0.9)	5.2 (6.7)	0.3 (5.1)	0.4 (7.2)	7.5 (11.3)
50º	4.5 (0.8)	2.7 (11.5)	1.0 (3.9)	0.9 (10.3)	7.6 (16.8)
60º	2.5 (0.3)	8.5 (15.2)	0.7 (6.0)	0.6 (7.3)	9.9 (7.7)
50ºº	3.2 (0.6)	8.1 (6.5)	0.4 (4.9)	0.3 (5.7)	10.3 (9.5)
40º	4.4 (0.7)	3.2 (9.2)	0.3 (3.3)	0.2 (2.6)	12.3 (9.6)
30º	3.9 (1.1)	2.8 (1.9)	0.2 (2.4)	0.3 (2.0)	7.0 (10.2)
20º	12.9 (1.1)	2.9 (5.8)	0.2 (2.7)	0.4 (3.4)	8.3 (14.8)
10º	17.7 (1.1)	3.5 (2.5)	0.3 (4.3)	0.3 (1.7)	6.9 (13.7)
Supine	8.0 (0.6)	2.4 (4.1)	0.3 (2.8)	0.3 (2.3)	10.4 (8.1)

Table 3-8: Summary of the mean (SD) values of the tilt angles estimated from the accelerometer signals at the **trunk and waist** locations during each static sagittal posture.

Postures	Trunk tilt angles [deg]	Waist tilt angles [deg]
Supine	4.1 (4.5)	3.1 (2.2)
10^{o}	2.3 (1.7)	2.9 (2.2)
20^{o}	3.2 (2.3)	3.9 (2.8)
30^{o}	3.5 (2.5)	4.0 (1.9)
40^{o}	3.7 (2.4)	5.6 (3.6)
50^{o}	3.6 (2.6)	4.6 (2.5)
60^{o}	3.7 (2.6)	5.6 (2.4)
50^{oo}	3.7 (3.2)	5.9 (3.6)
40^{o}	3.5 (2.4)	4.0 (2.1)
30^{o}	2.7 (2.1)	4.5 (2.8)
20^{o}	2.8 (2.2)	4.5 (2.9)
10^{o}	2.2 (2.3)	4.3 (2.3)
Supine	2.6 (1.7)	3.5 (2.5)

Figure 3-18 illustrates the differences for each subject in the contact area signal (20mmHg) at the buttock ROI for three different postures, namely supine, 10^{o} and 20^{o} HOB. Differences were evident in the magnitude of the signal for both postural changes and static postures. As an example, subject #8 (dark red curve) showed a percentage decrease in contact area when the HOB was elevated at 10^{o} and 20^{o}. By contrast, subject #1 (dark blue curve) showed an increase for changes in the corresponding postures. Movements within postures varied between subjects. As an example, subject #3 and #6 showed high perturbations during specific static postures i.e. 20^{o} HOB. In some cases, as for example for subject #3 (yellow curve), the range of movement during the static posture at 20^{o} HOB was higher than the amplitude in the change in posture from 10^{o} to 20^{o} HOB. This was observed for some pressure parameters at both ROIs, whose amplitude of movement during specific static postures (Tables 3-6 and 3-7) was higher than the amplitude between the corresponding changes in postures (Tables 3-3 and 3-3). Inevitably, this had a substantive effect on the signals sensitivity and specificity to detect postural changes.

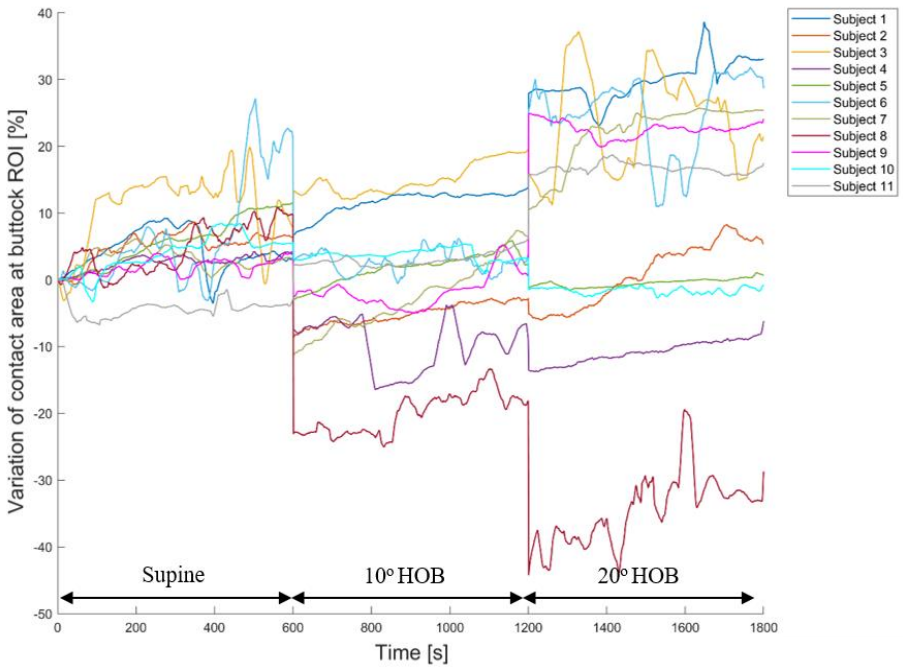

Figure 3-18: Contact area signals estimated at the buttock ROI of three postures, namely supine, HOB at 10^{o} and HOB at 20^{o}, for all subjects. A considerably variability was evident in the magnitude of both the changes between postures and within each static posture.

3.2.7 Amplitude of movements in the transverse plane

Table 3-9 summarises the median and IQR values for changes in the pressure parameters during lateral turning for both ROIs. These were estimated as relative changes with respect to the previous posture (supine). The relative changes in the tilt angles at the two body segments, namely, trunk and waist, are presented as mean (SD) and shown in Table 3-10.

COP displacement values varied considerably. It was evident that the displacement increased more than a twofold when turning to the right compared to the left in both ROIs (Table 3-9). This was associated with a corresponding decrease in the contact area. No evident trend were visible for peak pressure and peak pressure gradients.

The tilt angles measured at the trunk and waist (Table 3-10) indicated only moderate lateral turns were achieved with mean values of less than 10°, with values approximately 25% higher in the trunk.

Table 3-9: Summary of the median (IQ) values of the parameters estimated from the pressure distribution at all ROIs during the changes in posture in the transverse plane.

Postures	COP [mm]	PP [mmHg]	PPG – parallel direction [mmHg/mm]	PPG – perpendicular direction [mmHg/mm]	CA (20mmHg) [% variation]
			Whole body		
Left turning	11.4 (0.8)	8.7 (4.7)	0.5 (0.9)	0.7 (3.9)	9.6 (7.3)
Right turning	24.0 (1.0)	10.6 (9.9)	0.6 (1.4)	0.9 (2.5)	7.9 (6.6)
			Buttock		
Left turning	11.4 (0.5)	6.3 (6.6).	0.3 (0.7)	0.4 (4.2)	11.5 (6.1)
Right turning	18.3 (0.7)	2.6 (2.8)	0.2 (1.3)	0.3 (0.1)	7.6 (5.1)

Table 3-10: Summary of the mean (SD) values of the tilt angles estimated from the accelerometer signals at the trunk and waist locations during the changes in posture in the transverse plane.

Postures	Trunk tilt angles [deg]	Waist tilt angles [deg]
Left turning	8.2 (1.8)	5.3 (1.9)
Right turning	8.3 (2.5)	5.6 (3.5)

An example of the changes in the COP displacements in the perpendicular direction during the two turning phases is shown for all subjects in Figure 3-19. A higher displacement was clearly evident when turning to the right. Moreover, the relative magnitudes of the displacements varied between subjects, as confirmed by the high interquartile range in some pressure parameters, e.g. peak pressure (Table 3-9).

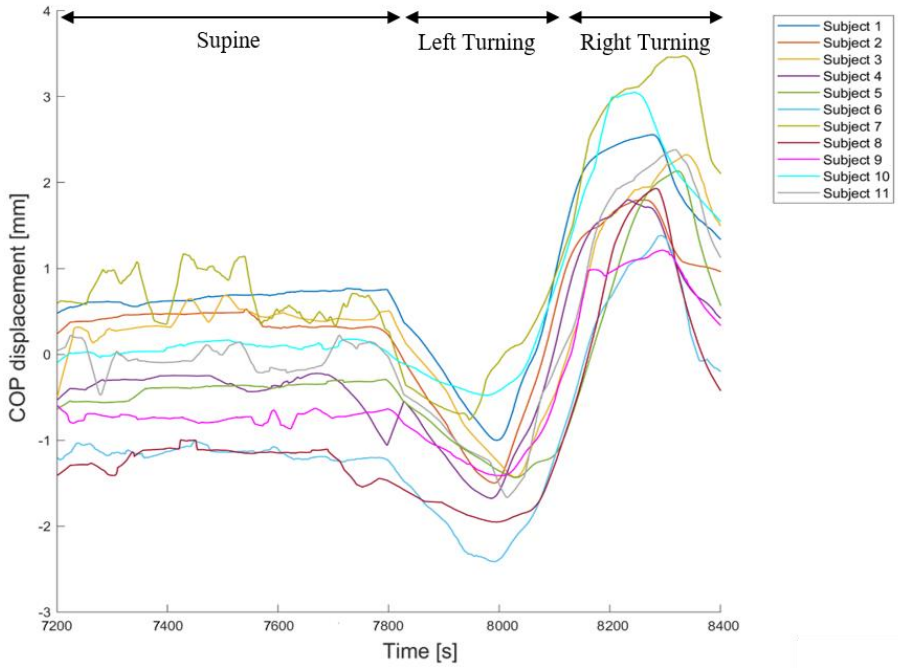

Figure 3-19: COP displacement signals estimated at the buttock ROI in the perpendicular direction with respect to the long axis of the map during lateral turning, for all the subjects. For the majority of subjects, the magnitude was considerably greater when turning to the right.

3.2.8 Sensitivity and specificity

Sensitivity and specificity to detect evoked postural changes for each of the parameters were assessed at each of the defined threshold values (Table 3-1). These are presented as percentage values derived from the individual values from the cohort.

3.2.8.1 Postural changes in the sagittal plane

The relative inclination of the bed angle had a significant effect on amplitude of the movements performed (Tables 3-3 and 3-4) and accordingly on the sensitivity in detecting postural changes. As an example, the sensitivity of the COP estimated from the buttock ROI at each threshold is presented in Figure 3-20. It revealed marked differences at different HOB angles. For example, at HOB < 30^{o} the threshold values significantly influenced the range of sensitivities. By contrast, when the HOB exceeded 40^{o} the values of sensitivity were reduced, most significantly at the lower threshold values of 5-10 mm. A reverse trend was evident when the HOB was reduced back down to the supine posture. The sensitivity of the whole body COP revealed a similar trend (Figure D-1 – Appendix D).

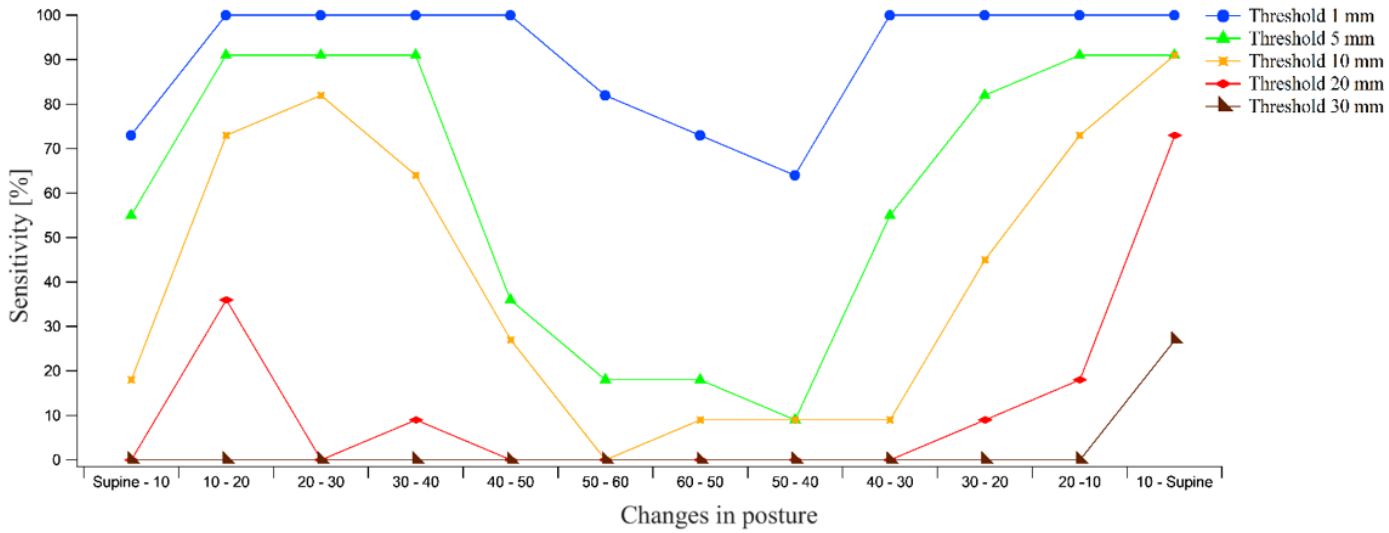

Figure 3-20: Sensitivity trend in evaluating changes in posture in **buttock ROI** for **COP displacements**. Each curve represents the trend with respect to a specific threshold value, ranging between 1 mm and 30 mm. Each data point represents the sensitivity value [%], across all participants, for a specific threshold value.

Peak pressures revealed high sensitivity values when HOB angles exceeded 40^{o} at each of the threshold values (2 - 10 mmHg) for both ROIs (Figures D-2 and D-3 – Appendix D). This supported earlier findings according to which amplitudes of postural changes at the highest HOB were high (Tables 3-3 and 3-4). By contrast, peak pressure gradients in both directions revealed no particular trends for both ROIs, with high sensitivity values at low thresholds i.e. 0.1 and 0.2 mmHg/mm (Figures D-4, D-5, D-6 and D-7– Appendix D) and compromised sensitivity at higher thresholds. Contact area at both ROIs revealed high sensitivity values at elevated HOB angles (>30^{o}). By contrast, when the HOB <30^{o}, the sensitivity values varied depending on the threshold (Figures D-8 and D-9 – Appendix D).

Tilt angles at the trunk, illustrated in Figure 3-21, revealed high sensitivity values at low thresholds i.e. 2^{o} - 4^{o}, although there was some variability during changes in posture. Of particular note was the decrease in sensitivity in the final transition from a 10^{o} HOB to supine posture. A similar trend was observed in the tilt angles at the waist (Figure D-10 – Appendix D)

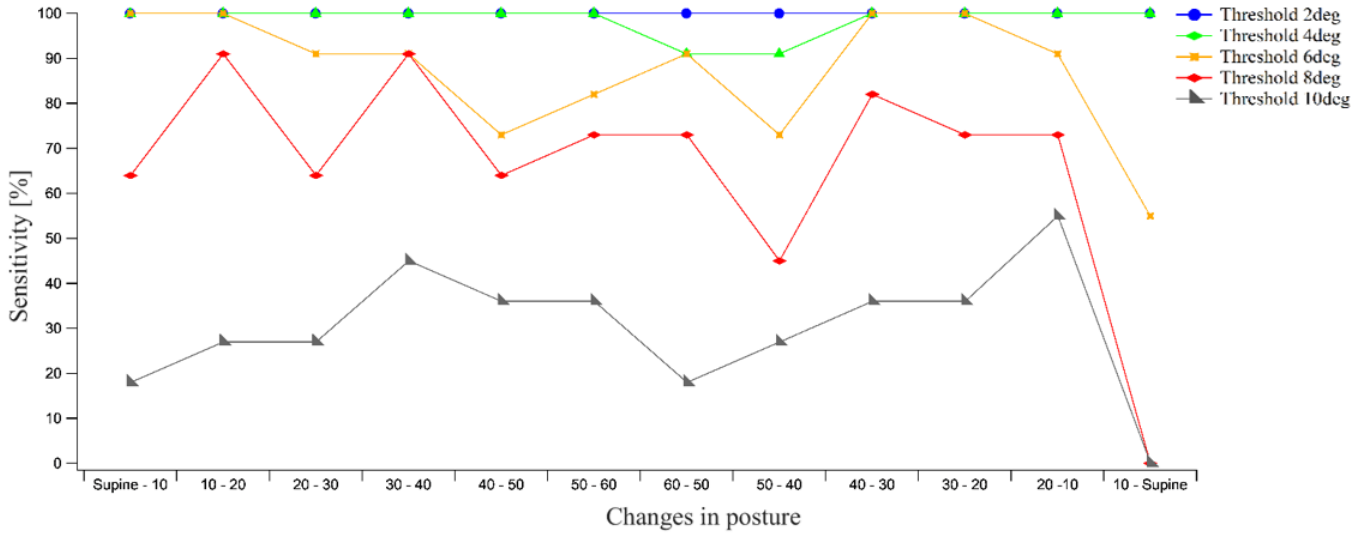

Figure 3-21: Sensitivity trend in evaluating changes in posture for **tilt angles of the trunk**. Each curve represents the trend with respect to a specific threshold value, ranging between 2 and 10°. Each data point represents the sensitivity value [%], across all participants, for a specific threshold value.

The movements performed during each of the static postures had a significant effect on the false positive rate i.e. 100 – Specificity [%]. As an example, the specificity of the buttock COP for each threshold is presented in Figure 3-22. In this case, the specificity was high for the large thresholds i.e. >20 mm. By contrast, the specificity was <10% for threshold of 1 mm for all the changes in posture. Whole body COP displacements revealed a considerable range of specificity values across the thresholds (Figure E-1– Appendix E).

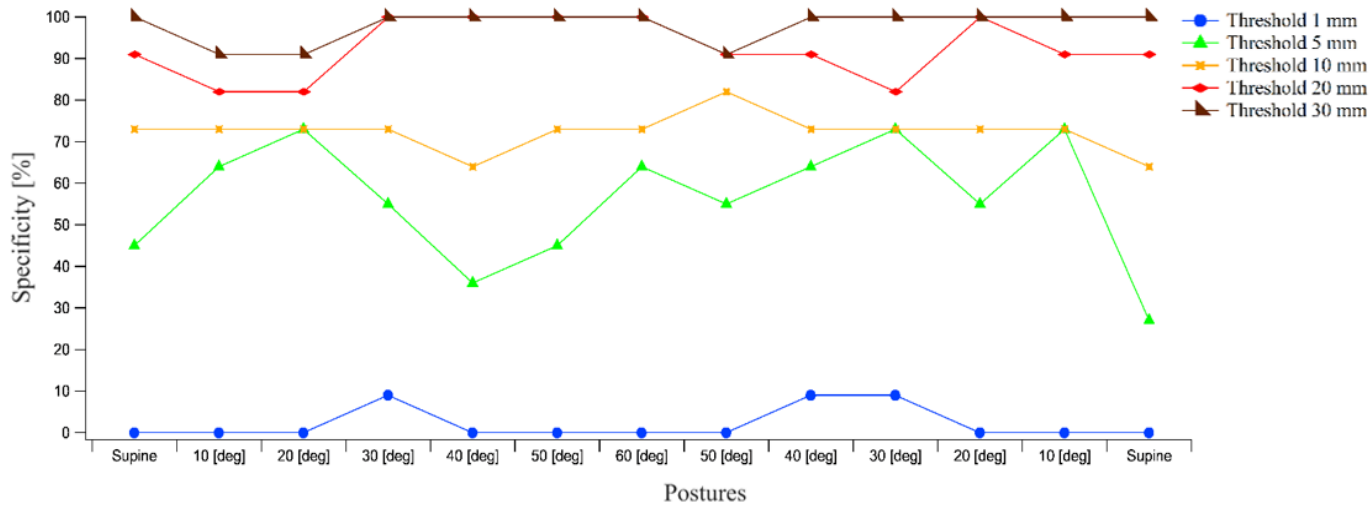

Figure 3-22: Specificity trend in evaluating the movements within each postures in b**uttock ROI for COP displacements**. Each curve represents the trend with respect to a specific threshold value, ranging between 1 mm and 30 mm. Each data point represents the specificity value [%], across all participants, for a specific threshold value.

The specificity of peak pressure values and peak pressure gradients was also highly dependent on the threshold values and the two ROIs. As an example, peak pressures at the buttock ROI (Figure E-3 – Appendix E) revealed high specificity values for HOB < 40°. By contrast, when HOB was lowered, the specificity decreased. Peak pressures at whole body revealed specificity values <70% for all the static postures at the highest threshold i.e. 10mmHg (Figure E-2– Appendix E). Peak pressure gradients in both directions revealed for whole body ROI specificity values below 70% for most of the static postures at the highest threshold i.e. 1.0mmHg/mm (Figures E-4 and E6 – Appendix E). By contrast, at the buttock ROIs the accuracy was higher when HOB <40° (Figures E-5 and E-7– Appendix E). Contact areas showed a considerable variability in specificity with values ranging from 0 - 100% with no evident trends across the thresholds (5% - 25%) in both whole body and buttock ROIs (Figures E-8 and E-9 in Appendix E).

In a similar manner, tilt angles at the waist showed a wide-range of specificity values across the threshold range, with no evident trends (Figure E-10 - Appendix E). By contrast, tilt angles at the trunk showed high specificity (>60%) for threshold values ≥4° (Figure 3-23). Moreover, at 2° threshold accuracy was found >30% for HOB ≤ 30°.

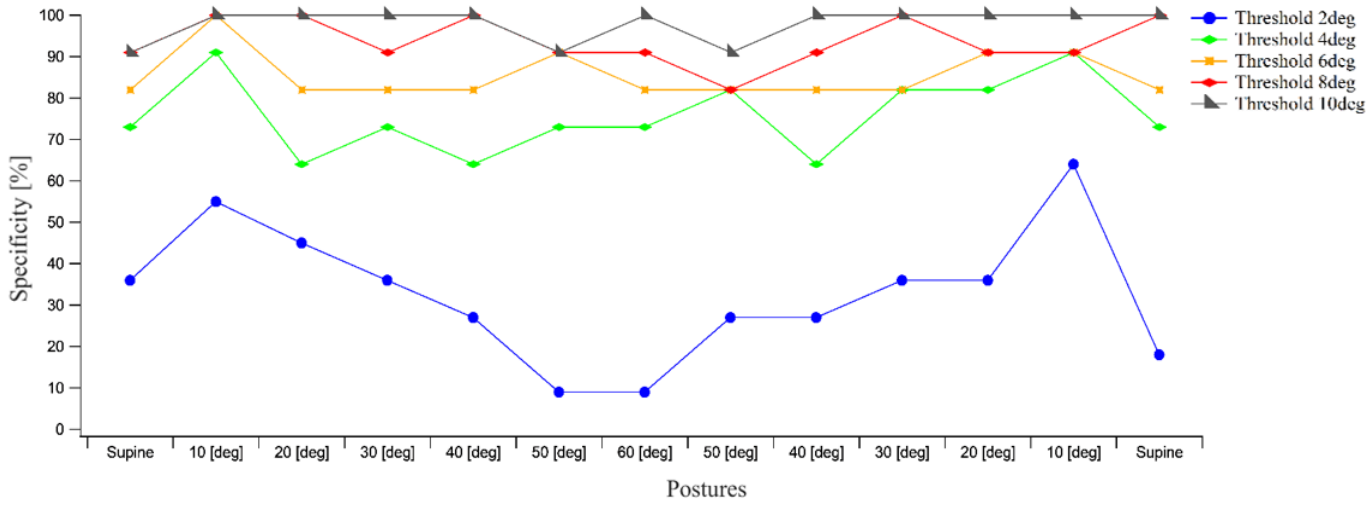

Figure 3-23: Specificity trend in evaluating the **trunk tilt angles** within each postures. Each curve represents the trend with respect to a specific threshold value, ranging between 2° and 10°. Each data point represents the specificity value [%], across all participants, for a specific threshold value.

3.2.8.2 Postural changes in the transverse plane

The sensitivity of movements in the transverse plane decreased for all parameters with an increased in threshold values. This is exemplified in Figure 3-24 with the values estimated for the buttock COP. There were also differences during the left and right lateral turning protocols at both ROIs, suggesting considerable asymmetry, thus supporting earlier findings with respect

raw biomechanical values for both ROIs (Table 3-9). Sensitivity of contact area at both ROIs are shown in Figures F-8 and F-9 in the Appendix F. Peak pressures (Figures F-2 and F-3 – Appendix F) and peak pressure gradients (Figures F-4 to F-7 - Appendix F) revealed some differences in the sensitivity between the turning protocols with few specific trends to highlight. In a similar manner, tilt angles at both trunk and waist showed asymmetries in sensitivity between the turning protocols for all the threshold values, presented in Figure 3-25 for the trunk and in Figure F-10 (Appendix F) for the waist.

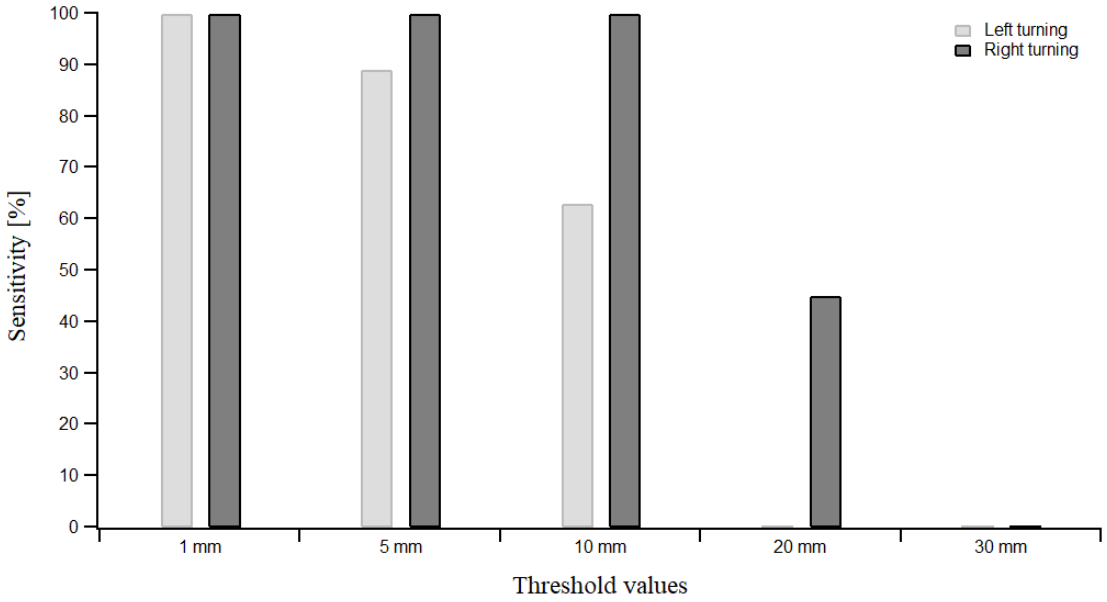

Figure 3-24: Sensitivity values in detecting the lateral changes in posture during left and right turning for the **buttock COP** at four threshold values, ranging between 1 mm and 30 mm.

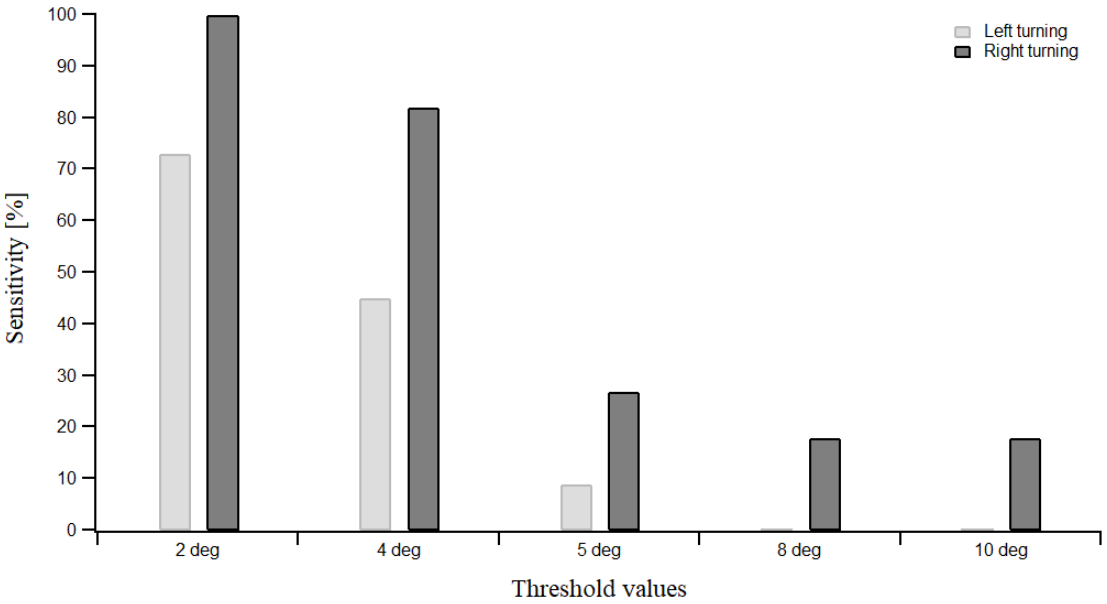

Figure 3-25: Sensitivity values in detecting the lateral changes in posture during left and right turning for the **trunk tilt angles** at four threshold values, ranging between 2º and 10º.

3.2.9 ROC analyses

Examples of the resulting ROC curves for each of the postural changes for the buttock COP displacements, contact area at the whole body ROI and the trunk tilt angles are presented in Figures 3-26, 3-27 and 3-28, respectively. There are clear differences in the trends for each of these parameters. As an example, the curves with respect to COP displacement revealed that the values associated with higher HOB angles i.e. >30° HOB, fell below the reference line denoting an AUC = 0.5 (Figure 3-26). This suggests a limited ability for these signals to detect the prescribed postural changes within the threshold range. Similar curves below the reference line were observed with respect to the whole body contact area (Figure 3-27), although these cases were generally associated with low HOB angles i.e. <20^{o} HOB. By contrast, the ROC curves associated with the tilt angle at the trunk were all above the reference line (Figure 3-28). However, many curves did not encompass the full range of specificities and this inevitably led to relatively low AUC values. A similar behaviour characterised waist tilt angles (Figure G-9).

Curves above the reference line which did not encompass the full range of sensitivity were observed for the contact area estimated at the buttock ROI for postures corresponding to elevated HOB angles (>30^{o}) (Figure G-8). In these particular cases, as the curves encompassed the full range of specificity, the estimation of the AUC values was not compromised (Table 3-11). The ROC curves for all the remaining parameters are included in Appendix G.

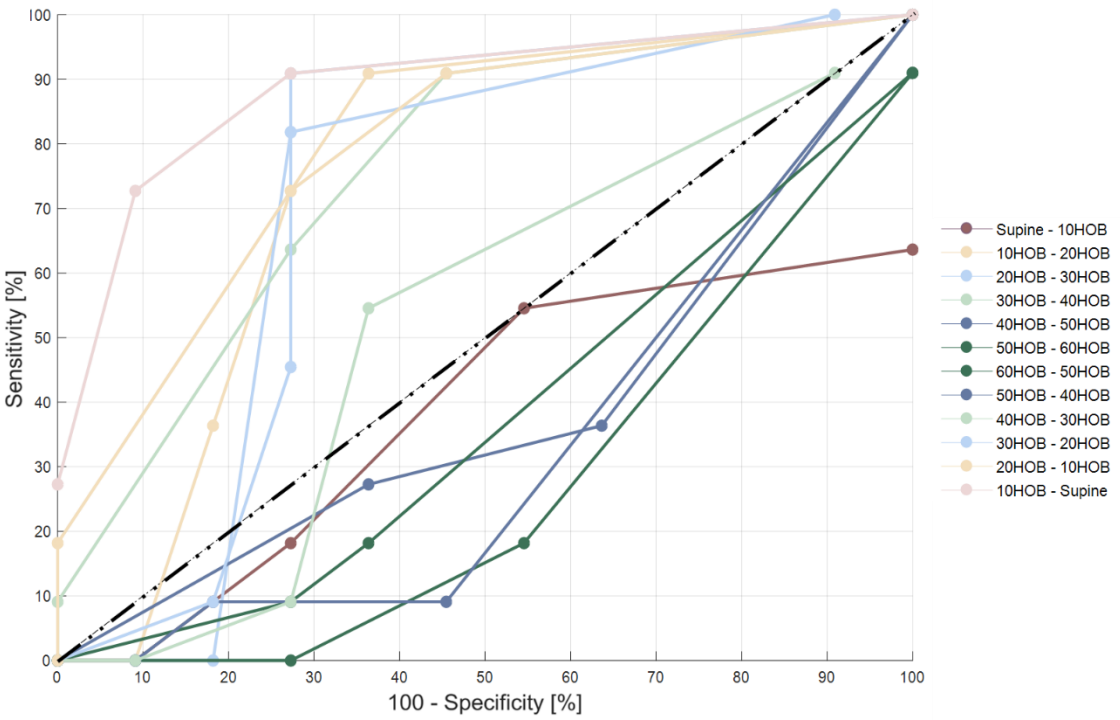

Figure 3-26: ROC curves across all changes in posture **f**or **COP displacements at the buttock ROI**. Each data point represents a sensitivity/specificity pair corresponding to a specific decision threshold (1mm, 5mm, 10 mm, 20 mm, 30mm). The threshold values increase from the right side to the left side of the curves. Curves in the darkest shades denotes a compromised sensitivity/specificity pair, falling below the reference line.

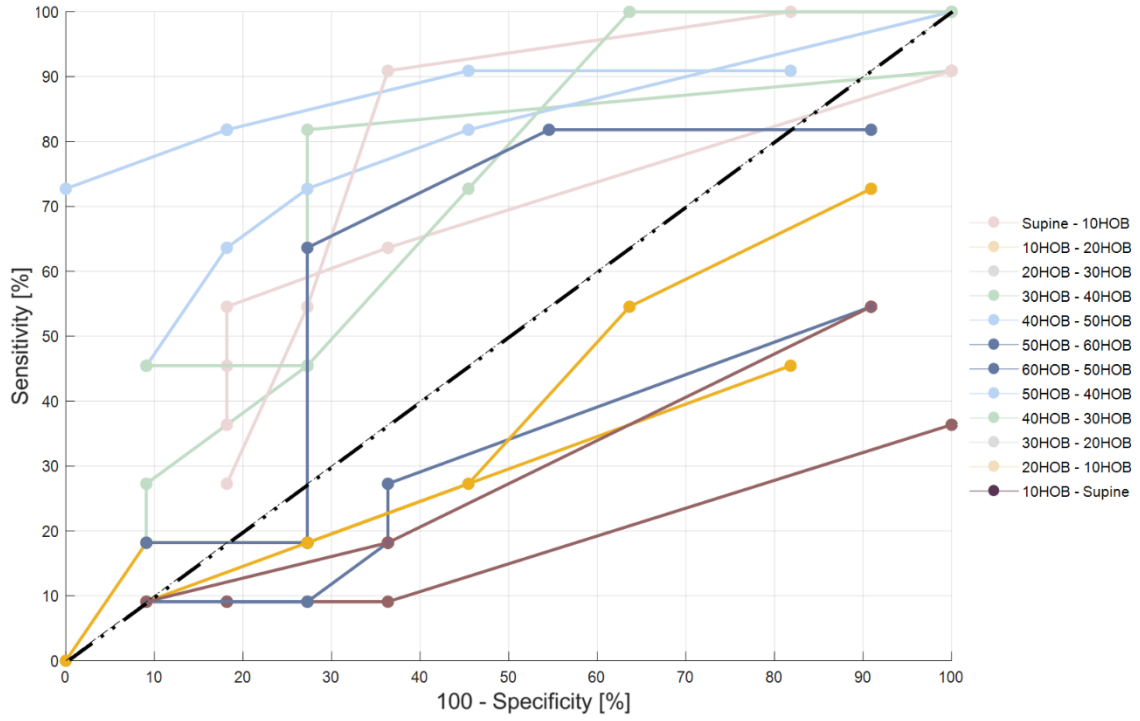

Figure 3-27: ROC curves across all changes in posture for **contact area at the whole body ROI**. Each data point represents a sensitivity/specificity pair corresponding to a specific decision threshold (5%, 10%, 15%, 20%, 25%). The threshold values increase from the right side to the left side of the curve. Curves in the darkest shades denotes a compromised sensitivity/specificity pair, falling below the reference line.

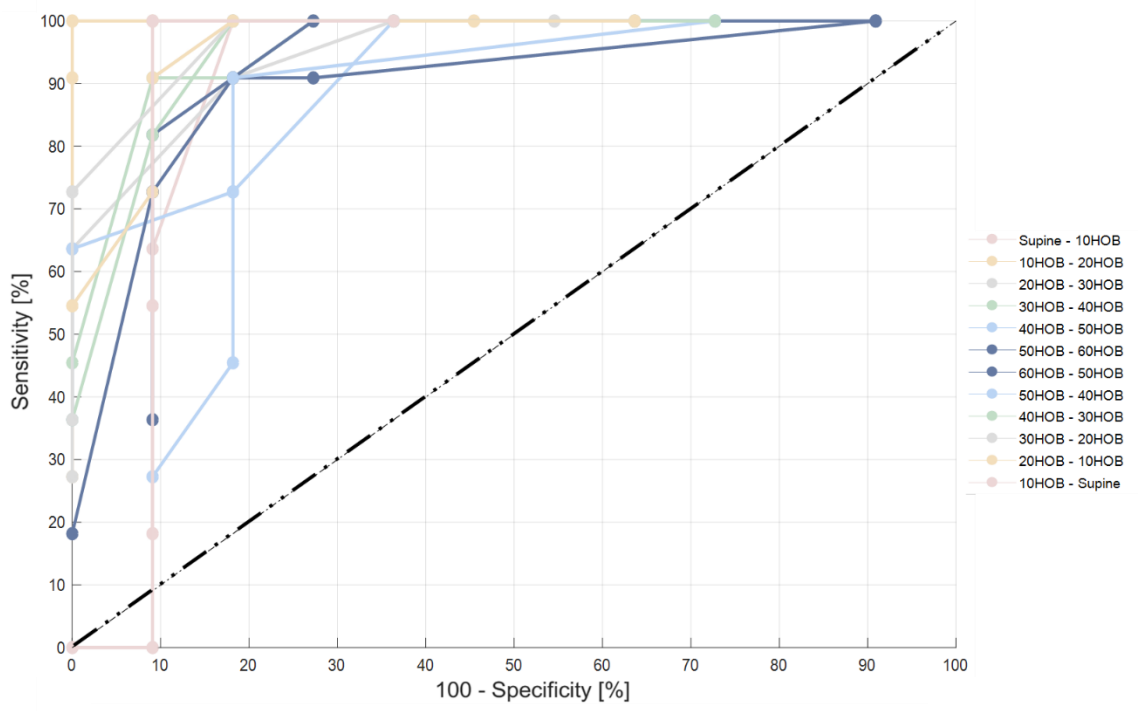

Figure 3-28: ROC curves across all changes in posture for **tilt angles evaluated at the trunk**. Each data point represents a sensitivity/specificity pair corresponding to a specific decision threshold (2deg, 4deg, 6deg, 8deg, 10deg). The threshold values increase from the right side to the left side of the curve. Some curves did not encompass the full range of specificity.

Table 3-11 summarises the AUC values estimated from all the ROC curves of the interface pressure parameters. The corresponding AUC values associated with the trunk and waist tilt angles are summarised in Table 3-12. For both series of parameters, AUC values revealed considerable variability between postures. Peak pressure and peak pressure gradients at both ROIs revealed AUC values not exceeding the threshold value of 0.5 for all the postures, as the result of the compromised sensitivity and specificity ratio. COP at both ROIs revealed AUC values exceeding 0.5 for some postures associated to HOB angles <40°. By contrast, the AUC values estimated from the contact area at the whole body ROI did exceed this threshold in 7/12 postures, indicating a good predictive capacity in detecting the changes in posture associated with HOB angles >20°. The same trend was observed for contact area at the buttock ROI, where values exceeding 0.5 were associated to ROC curves which did not encompass the full range of sensitivity. However, this did not affect the estimation of the corresponding AUC values. The majority of AUC values estimated from the tilt angles also exceeded 0.5 (Table 3-12). As observed from the ROC curves (Figure 3-28), the majority of these values were not estimated across the full range of specificity, showing relatively low values. These are reported in Table 3-12.

Table 3-11: AUC of the interface pressure parameters evaluated at the whole body and buttock ROIs calculated from the ROC curves for all the changes in posture.

	COP		**PEAK**		**PPG – parallel direction**		**PPG – perpendicular direction**		**CA**	
	Whole Body	**Buttock**	**Whole Body**	**Buttock**	**Whole Body**	**Buttock**	**Whole Body**	**Buttock**	**Whole Body**	**Buttock**
Supine – 10°	0.09	0.38	0.09	0.21	0.20	0.27	0.33	0.27	0.16	0.31
10° - 20°	0.72*	0.75*	0.13	0.07	0.38	0.38	0.21	0.29	0.21	0.41
20° - 30°	0.63*	0.73*	0.24	0.23	0.21	0.28	0.32	0.33	0.25	0.36
30° - 40°	0.74*	0.67*	0.29	0.26	0.30	0.55	0.41	0.40	0.69*	0.53*
40° - 50°	0.61*	0.38	0.24	0.31	0.17	0.36	0.23	0.35	0.59*	0.54*
50° - 60°	0.45	0.27	0.15	0.28	0.30	0.19	0.26	0.31	0.74*	0.61*
60° - 50°	0.11	0.37	0.35	0.43	0.41	0.48	0.28	0.29	0.71*	0.74*
50° - 40°	0.37	0.33	0.31	0.29	0.33	0.29	0.43	0.52*	0.71*	0.72*
40° - 30°	0.23	0.43	0.19	0.32	0.41	0.48	0.24	0.48	0.71*	0.71*
30° - 20°	0.49	0.61*	0.23	0.30	0.39	0.21	0.38	0.24	0.53*	0.55*
20° - 10°	0.60*	0.79*	0.22	0.10	0.32	0.36	0.48	0.36	0.31	0.43
10° - Supine	0.59*	0.89*	0.16	0.16	0.14	0.21	0.27	0.38	0.23	0.19

* indicates AUC values which exceeded 0.5.

Table 3-12: AUC of the tilt angles at the trunk and waist locations calculated from the ROC curves for all the changes in posture.

	Trunk	**Waist**
Supine – 10º	0.53*	0.49*
10º - 20º	0.45*	0.44*
20º - 30º	0.49*	0.47*
30º - 40º	0.59*	0.45*
40º - 50º	0.64*	0.29*
50º - 60º	**0.80**	**0.60**
60º - 50º	**0.81**	**0.56**
50º - 40º	0.55*	0.47*
40º - 30º	0.68*	0.68*
30º - 20º	0.61*	0.50*
20º - 10º	0.59*	**0.51**
10º - Supine	0.27*	0.09*

* indicates AUC values estimated not across the full range of specificity; in bold are indicated AUC values estimated across the total range of specificity.

3.3 Discussion

This chapter has examined the use of biomechanical signals indicative of pressure distribution at the body – support surface interface and angles from body segment movements. It considered the nature of signal changes for a cohort of able – bodied participants adopting a range of different evoked lying postures. To the author's knowledge, this is the first analysis of sensitivity and specificity of both interface pressure and kinematic data and was published in *Medical Engineering and Physics Journal* (Caggiari et al. 2019). Prior to the study, the performance of the commercial interface pressure measuring system was investigated under both static and quasi – static tests (Appendix B). These demonstrated no drift in the system output over 24 hours (Figures B-2 and B-3) and sensitivity to detect clinical relevant pressure increments (Figure 3-2).

Initially the pressure parameters were examined at four separate ROIs. However, it soon became apparent that the ROIs associated with the whole body and buttock were more accurate in detecting postural changes. Indeed, both the upper and lower body ROIs (Figure 3-7) were clearly affected by signal deviations during natural movements in the legs, arms and head of the volunteers, leading to a poor accuracy of the corresponding parameters. Segmental tilt angles estimated from a commercial actimetry system positioned at the trunk and waist were used to

provide a relative comparison of postural movement detection and act as standard of human movement analysis (Pickham et al. 2018, Smits et al. 2018).

The results revealed a high degree of variability between subjects which influenced the perturbations in the signals during both changes in posture and within each static posture. Amplitude of movements during static postures were affected by the postural adjustments of the individual. Indeed, although participants were instructed to remain as still as possible, inevitable perturbations in the signals occurred. In some cases, the magnitude of these movements was greater than the changes during the evoked postural changes (Tables 3-3, 3-4, 3-6 and 3-7). This might be attributed to a sensory feedback reponse of able-bodied individuals to prolong postures over the test period, leading to movements as a natural strategy for preventing the development of pressure ulcers.

During sagittal repositioning, changes between postures in some parameters varied depending on the increasing or decreasing phase associated with the HOB increments (Figure 3-15A). Moreover, some signals at specific body regions e.g. COP at the buttock ROI, were influenced by the immersion of the individual on the support surface. As an example, small changes in the displacement of COP around the buttock area were evident in the majority of the individuals for changes in posture involving HOB angles $>40^{o}$ (Tables 3-4). By contrast, there were corresponding high changes for peak pressures and contact area (Table 3-4). This could be exacerbated on different support surfaces which are more immersive in nature e.g. air mattresses (Worsley et al. 2016).

Contact area signals at both ROIs were examined for pressures exceeding different cut-off values. These included the default lower limit of the system of 5mmHg up to a value of 40mmHg. Results indicated that signals derived from pressure values exceeding 20mmHg were most accurate in detecting postural movements (Section 3.2.3), supported by an optimum ratio between sensitivity and specificity in all subjects (Figure 3-16).

Small changes in the interface pressure parameters during lateral repositioning (Table 3-9) indicated a limited redistribution of pressure, particularly evident with respect to the buttock ROI. Differences between left and right turning protocols were also evident and may be attributed to an asymmetry which occurred in the automated lateral turning system and corresponding position of the individuals in bed. A limited pressure redistribution was recently reported in a study from the host group, where similar peak pressure values at the scrum were recorded for supine and lateral postures (Woodhouse et al. 2015). However, no differences were observed in the median values between left and right evoked turning. By contrast, pressure relief in the sacral area during lateral turning was reported in the study conducted by Do et al. (2016).

The analysis revealed limitations in the sensitivity and specificity of some parameters, dependent on their prescribed threshold and the magnitude of the HOB angles. It should be noted that the threshold values were arbitrary selected. As an example, the COP at the buttock

ROI demonstrated low sensitivity at high HOB angles i.e. >40^{o} (Table 3-4 and Figure 3-20), and high specificity during each static posture, reflecting limited values of COP displacements (Table 3-6 and Figure 3-21). This affected the potential of this parameter to discriminate between specific sagittal postural changes, as revealed by the ROC curves (Figure 3-26) and the corresponding low AUC values (Table 3-11). Peak pressures and peak pressure gradients at both ROIs revealed a relatively poor predictive potential in discriminating different postures as reflected in the compromised sensitivity and specificity ratio (Figures G-2 to G-7 – Appendix G). By contrast, the contact area of sensors recording pressures ≥20mmHg at the whole body and buttock ROIs were able to accurately discriminate between the evoked postures when HOB angle exceeded 20^{o}, as revealed by the corresponding AUC values >0.5 (Figure 3-27 and Table 3-11). Despite incomplete ROC curves across the sensitivity range were observed for contact area at the buttock, AUC values were >0.5.

Findings also revealed that the tilt angles estimated at the trunk were able to detect the majority of the evoked postural changes as depicted by the corresponding ROC curves above the reference line (Figure 3-28 and Table 3-12). However, it was noted that the majority of the AUC values were not estimated across the full range of specificity for the selected threshold range (2^{o}-10^{o}). This is reflected in incomplete curves (Figure 3-28) and in relatively low AUC values (Table 3-12). However, the capacity of the tilt angles in accurately discriminating between the postural changes is fully demonstrated.

The literature reveals a paucity of studies, which have investigated the sensitivity and specificity of a range of temporal pressure parameters for the detection of movements. Previous studies have evaluated the temporal displacement of COP estimated at the feet-ground interface, whose accuracy in detecting postural body sways was examined (Saripalle et al. 2014, Lee et al. 2019). By contrast, a large number of studies have performed ROC analyses to examine the accuracy of actimetry – based signals at different body locations, typically the trunk and waist. However, AUC values obtained in these studies are not directly comparable to the present work involving tilt angles, given the different nature of the movements investigated and the signals used (Mathie et al. 2003, Lee et al. 2019). Nonetheless, their findings do reveal a higher predictive capacity for actimetry signals when compared to COP (Lee et al. 2019). Neither of these studies, however, were related to the detection of movements in either lying or sitting postures for pressure ulcer prevention.

Measurement of tilt angles at specific body sites, estimated from actimetry signals, have been reported to discriminate between postural changes in different anatomical planes with an accuracy dependent on the anatomical placement of the device(s) (Fortune et al. 2014, Lyden et al. 2016). As an example, a thigh-worn actimetry placed in the antomical coronal plane, demonstrated a low accuracy in discriminating between lying and sitting. By contrast, the same study relealed a high accuracy (>95%) in discriminating betewen lying supine and lateral

postures (Lyden et al. 2016). Generally, it emerged that signals representive of trunk tilt angles are more accurate in detecting movements, as the trunk represents the major part of body mass and moves with many physical activities (Yang and Hsu 2010). As an example, Pickham and colleagues utilised a threshold value of 20^{o} for the detection of lateral lying postures from trunk movements in hospitalised individuals. By contrast, the present study found lateral movements of less than 10^{o} (Table 3-5). This can be attributed to the different nature of lateral postures, which occurred with an automated lateral turning system in the present study, as opposed to manual lateral repositioning (30° pelvic tilt). However, no sensitivity analyses were performed in this context to evaluate the accuracy of actimetry systems in detecting a range of different postures in the same anatomical planes.

The present study revealed that long-term pressure monitoring had the potential to provide objective measures that can act as surrogate for postural movements. This approach demonstrated that some of the interface pressure parameters (e.g. contact area) at specific regions of interest e.g. whole body and buttock area ROIs, proved good predictors in detecting incremental changes in posture, although there was some variations with respect to the magnitudes of the HOB angles. Furthermore, the potential of detecting postural changes was also influenced by the corresponding specific threshold values. In some cases, although the selected thresholds could encompass the full range of sensitivities and specificities, they did not reflect the magnitudes of the movements performed e.g. 10^{o} HOB increments. This is exemplified by the threshold of 1 mm to detect changes in posture with COP displacements (Figure 3-26).

In the light of the results, a series of signals estimated from both pressure mapping and actimetry system has the potential to track lying postures and mobility. However, pressure signals in isolation demonstrated a limited sensitivity and specificity. Moreover, these temporal signals will inevitably result in the acquisition of large data sets, which would benefit from intelligent processing. Many studies have utilised intelligent processing from machine learning algorithms to predict range of postures from pressure distributions recorded at the subjects interface (Wai et al. 2010, Yousefi et al. 2011, Kim et al. 2018, Duvall et al. 2019). However, limitations of these studies involved snap shots of pressure distribution and a limited range of individual positioning, which mainly involved supine and lateral postures. Furthermore, the potential of temporal pressure parameters and kinematic data in predicting ranges of postures has not been explored. Accordingly, second phase of data collection and analysis was conducted (Chapter 4) examining the accuracy of different machine learning algorithms for the prediction of lying postures from signals estimated from both pressure mapping and actimetry systems.

Chapter 4: Biomechanical parameters to detect changes in posture: development of a methodology involving machine learning

Systems capable of automatically classifying patterns of movement performed by a human subject are widely used in many clinical and research applications in the field of healthcare monitoring and in developing advanced human – machine interfaces.

The literature reveals a significant number of studies using wearable sensors, incorporating inertial measurement units (IMU) and actimetry systems, to predict and classify individual movements and activities, optimised through signal processing and machine learning algorithms (Manini and Sabatini 2010, Mohammed et al. 2016, Hu et al. 2018). A few studies have been proposed their use in pressure ulcer research, where commercial actimetry monitoring systems have been shown to improve the provision of optimal repositioning (Ifedili et al. 2018, Pickham et al. 2018). Nonetheless, the information gleamed from actimetry does not correspond to interface pressure measurements (Stinson et al. 2018), which currently represent one of the primary means to assess PU risk. In recent years, interface pressure measurements estimated at the subject – support surface interface have been used to predict and classify a range of postures (Wai et al. 2010, Yousefi et al. 2011, Kim et al. 2018, Duvall et al. 2019). However, the predictive power of these algorithms is largely dependent on the magnitude of the applied pressure in pre-determined areas of the sensing mat. In addition, approaches to date have relied on arbitrary thresholds for the assessment of postures related to early PU risk. Only a few studies have combined interface pressure measurements and actimetry monitoring (Zemp et al. 2016) for classifying postures, although the focus of this research was not related to pressure ulcers. While it is well known that actimetry systems provide a reference for position and movement detection (Edwardson et al. 2016, Lyden et al. 2016), there is no evidence in the current literature that parameters estimated from pressure distribution could predict postures and movements with a similar degree of accuracy.

Findings of Chapter 3 identified a collection of signals estimated from both continuous pressure mapping and actimetry systems, inevitably resulting in large data sets, which would benefit from intelligent data processing. However, the signals, in isolation demonstrated limitations in sensitivity and specificity. Therefore, a combined signal approach was needed to improve the predictive ability (Lee et al. 2019). Thus, the present chapter was designed to subject two sets of experimental data to three conventional machine learning algorithms, namely *k*-Nearest Neighbors (KNN), Naïve – Bayes (NB) and Support Vector Machine (SVM) classifier, each of which have been adopted in research studies to classify postures (Chi-Chun et al. 2008, Foubert et al. 2012, Duvall et al. 2019). The analysis involved a combination of signals estimated from

pressure monitoring and actimetry systems, and interface pressure signals in isolation. The global aims were to:

1. Detect the occurrence of postural changes;
2. Classify the range of postures, established with training data and validated with new test data sets;
3. Evaluate the predictive performance of the three classifiers using cross-validation techniques.

4.1 Materials and Methods

A number of processes were developed, including data reduction and features estimation. Optimal parameters were then selected to detect the occurrence of postural changes and an evaluation process detailed to estimate the accuracy of the classification algorithms. These processes are illustrated in Figure 4-1, in conjunction with their corresponding sections.

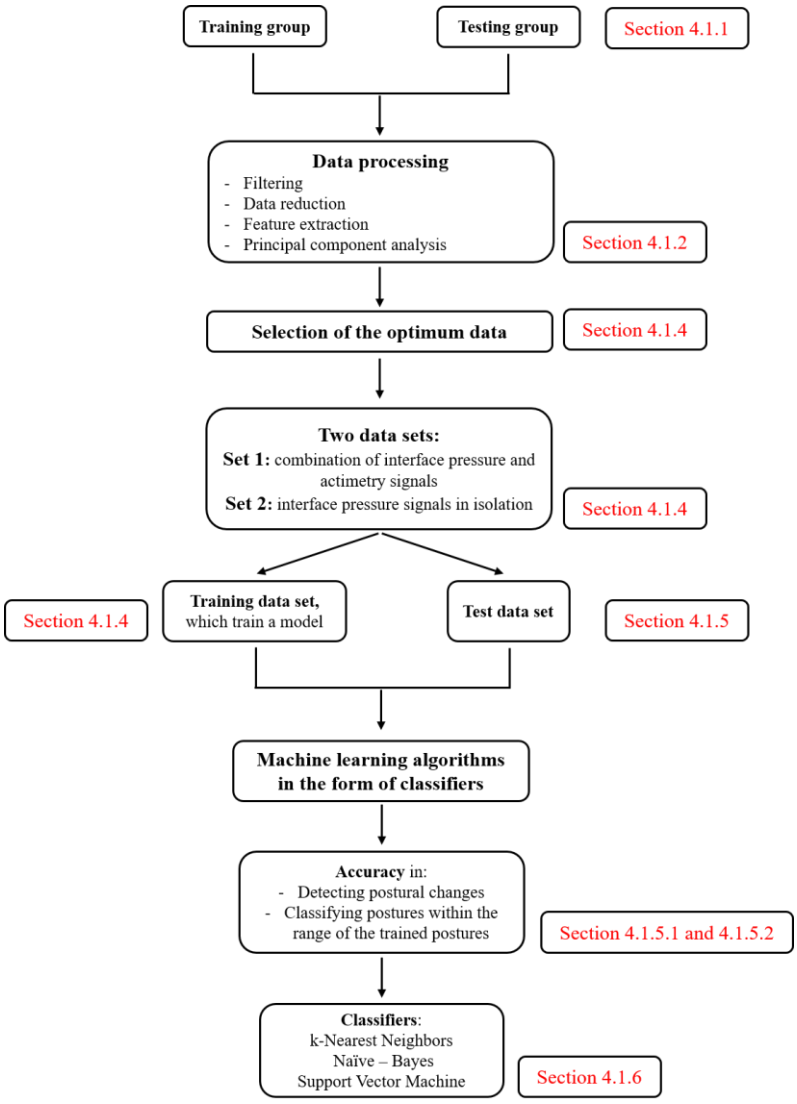

Figure 4-1: Flow chart depicting the different processes and the corresponding sections in which they are described in the chapter.

4.1.1 Data prior to processing

For analysis, it was important to select the most appropriate participant data from the previous study. Accordingly, any participant who yielded a high number of false positives due to the postural adjustments during the static postures were excluded from the present analysis. This left 9 of the 11 subjects (Table 3-2), who had been involved in the assessment of the biomechanical responses and were allocated to the **training group**. It was interesting to note that these two subjects presented relatively low BMIs.

To review briefly, each of this group adopted a series of sagittal and lateral postures held for 10 minutes, achieved by adjusting the HOB in 10° increments to a maximum of 60^{o} and then lowering the HOB by 10^{o} to supine, and through a continuous lateral system, respectively (Section 3.1.3). To evaluate the performance of the classifiers, a further cohort of participants were recruited utilising a modified protocol. Specifically, they were asked to adopt prescribed sagittal and lateral postures starting in the supine posture followed by raising the HOB by 20° increments to a maximum of 60°. The HOB was then lowered in 20° increments until the supine posture was re-established. It is worth mentioning that increments in 20^{o} HOB were used to better reflect the resolution of changes in the biomechanical signals. Each posture was evoked by the researcher using the bed frame control and held for a period of 20 minutes. The lateral postures involved the use of the same automated lateral rotational system as previously described (Section 3.1.3). These subjects were allocated to the **test group**.

The results detailed in Section 3.2.9 involving a comprehensive ROC analysis revealed a number of parameters able to detect specific changes in posture with different degrees of accuracy, namely:

1. Tilt angles of the trunk with respect to the sagittal and the transverse planes;
2. Contact areas (>20mmHg) estimated at the whole body and buttock ROIs;
3. Tilt angles of the waist with respect to the sagittal and the transverse planes;
4. Centre of pressure of the whole body and buttock ROIs estimated in the parallel and perpendicular directions with respect to the long axis of the mat;
5. Peak pressure gradient of the whole body and buttock ROIs estimated in the parallel and perpendicular directions with respect to the long axis of the mat.

Accordingly, these parameters were estimated for both the training and test groups, whose processing and analysis are most conveniently described separately.

4.1.2 Post – processing of the signals from training group

Both pressure and actimetry signals from the training group were processed, as previously described in Section 3.1.5. However, a moving average filter with a window length of 30 samples was applied in the present analysis, compared with the 15 samples length used in the previous analysis. Indeed, this revealed some cases where the magnitude of movements during

static postures was greater than the magnitude of postural changes (Tables 3-3, 3-4, 3-6 and 3-7). Thus, an increased filter window length was considered more appropriate for the present analysis, in order to limit a high number of false positive in the detection of both magnitude and frequency of postural changes.

After normalisation and manual labelling of each posture, all signals were interpolated to include signals and hence postures of equivalent length, encompassing 600 data points. Moreover, the lateral postural movements, which lasted approximately 10 minutes in total, were conjointly interpolated to 600 data points. The transitions between postures were not included in the processing of signals from the training group, as they contained noise due to natural adjustments in posture observed in all subjects.

The signals were then subjected to a two-level approach, as indicated in Figure 4-2. The first level was represented by a fixed – width sliding window of 60 samples to down sample the data. Distinct features were then calculated within each sliding window for each signal, namely values of the mean, median, range, standard deviation and derivative. This resulted in a reduced number of points for each signal, from 8400 to 140 data points. Subsequently, a principal component analysis (PCA) was performed and the resulting Eigen – values and vectors were estimated.

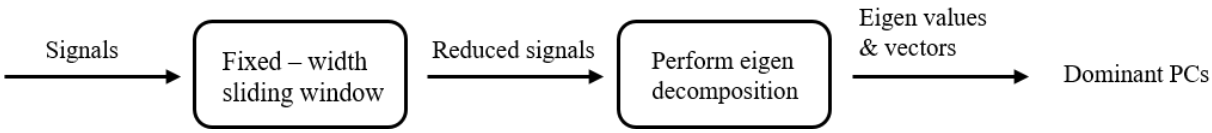

Figure 4-2: Two-level approach applied to the signals of training group, which involved the reduction of the raw data and the estimation of Eigen values and vectors, performing PCA.

4.1.3 Principal component analysis

Principal component analysis (PCA) represents a statistical approach for extracting patterns by reducing the dimensionality of data set. It is widely used in the field of image processing, feature reduction, feature extraction, anomaly detection, classification and pattern recognition (Shlens 2014). It is also widely used with biomechanical signals. PCA represents an approach that uses an orthogonal transformation to project a set of observations into a set of orthogonal linear variables, called principal components (PCs) (Figure 4-3). The greatest percentage of the variance is represented by the first principal component.

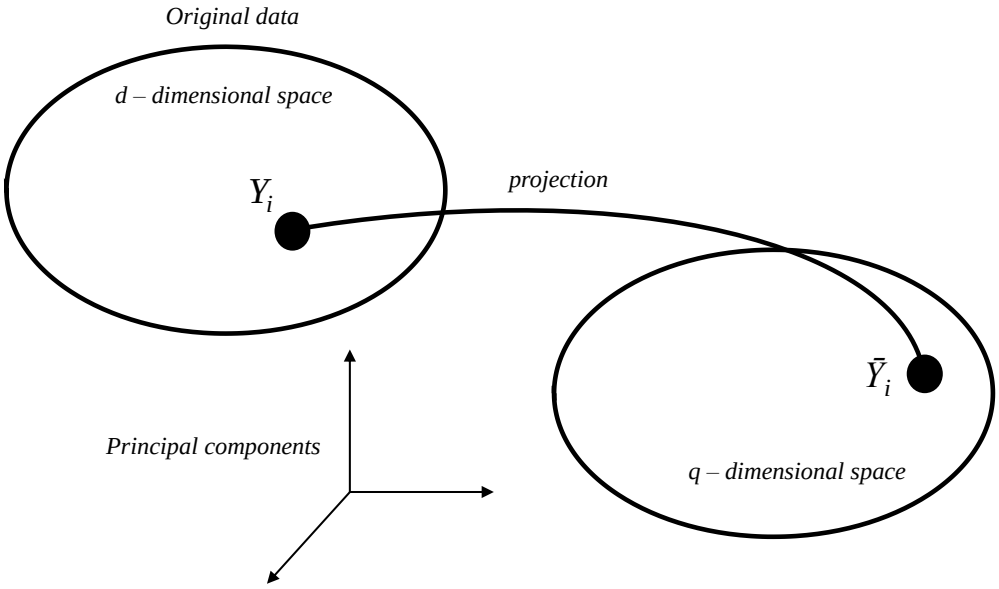

Figure 4-3: Action of PCA, where a data point of the original data is projected to a new dimensional space.

PCA is performed through Eigen decomposition (Eigen values and vectors) of a data covariance matrix, after a normalisation step, which consists of "mean centering" of the original data, equivalent to subtracting each of the data values from their mean value.

4.1.4 Analysis of the data to create a training data set

Eigen decomposition of the reduced signals included in the training group was performed, which resulted in a number of principal components, and a cumulative variance graph as indicated in Figure 4-4. The first two PCs were selected as they were associated with the highest percentage of variance in the signals, which, in this case, represented 89% and 6%, respectively.

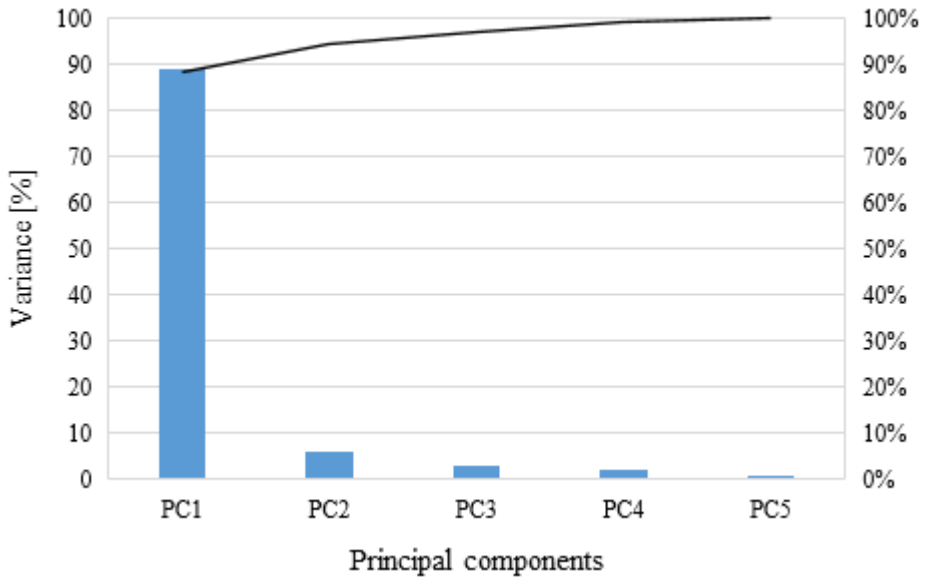

Figure 4-4: Variance and cumulative variance graph of the principal components.

Accordingly, the first two Eigenvectors corresponding to the highest Eigenvalues were examined in detail to perform a reduction of the set of data. An arbitrary cut – off value of 0.3 was considered to identify the most robust parameters and their corresponding features from the Eigenvectors. These were:

- Mean, median, maximum and minimum values of contact area at the whole body and buttock ROIs;
- Mean, median, maximum and minimum values of trunk tilt angles in both sagittal and transverse planes:
- Mean, median, maximum and minimum values of waist tilt angles in both sagittal and transverse planes;

The relationship between the selected parameters and features was then assessed to identify any redundancy. As an example, Figure 4-5 shows the relationship between two features, mean and median of contact area at the whole body ROI. The equation of the linear regression (4.1), was evaluated.

$$y = mx + b \tag{4.1}$$

where m: slope or gradient, b: intercept. The corresponding R and p values were also investigated.

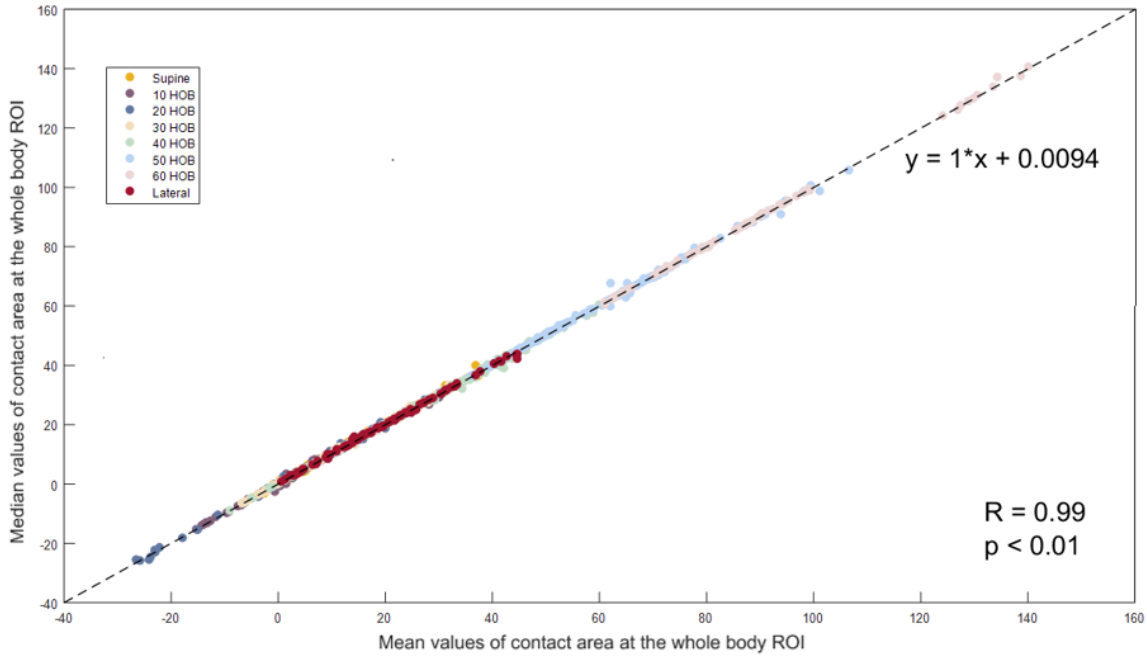

Figure 4-5: An example of the linear relationship between the mean and median values of the contact area at the whole body ROI.

These results revealed that mean, median, maximum and minimum signals of each of the parameters correlate in a linear relationship, with the slope *m* of the linear regression equivalent to approximately 1.0. These findings imply that the relationship between the features of each parameter follow a normal distribution. Accordingly the mean of each signal previously identified was used for subsequent evaluation.

The discrimination with the Eigenvectors confirmed the findings from the sensitivity and specificity analyses described in Chapter 3, where contact area estimated at both whole body and buttock ROIs resulted in the most accurate of the interface pressure parameters in detecting postural changes. In addition, both trunk and waist tilt angles proved to discriminate postures, with the former representing the most accurate parameter from the actimetry signals. For this reason, trunk tilt angles signal were considered in the subsequent analysis.

However, as contact area estimated at both ROIs can result in some redundancy, the signals were divided in two distinct data sets to evaluate their performance, namely:

i. **Data set A**: Contact area estimated at the whole body ROI, sagittal and lateral trunk tilt angles;
ii. **Data set B**: Contact area estimated at the buttock ROI, sagittal and lateral trunk tilt angles.

The two combined data sets, estimated from both measurement systems, were subsequently used as training data sets to predict the range of sagittal and lateral postures. Data from both the whole body and buttock ROIs were compared.

PCA was performed for each of the data sets, defining two distinct **training models** in the principal component space. As an example, the PC1 and PC2 corresponding to the data set incorporating the contact area from the whole body and trunk tilt angles (data set A) for all subjects (n=9) is illustrated in Figure 4-6. With appropriate labelling, each posture is represented by clusters of points spatially distributed. The data clearly reveals some overlapping of data points between distinct postures e.g. between 30^{o} and 40^{o} HOB angle. It also shows that the discrimination between postures is primarily achieved through the first PC (x-axis).

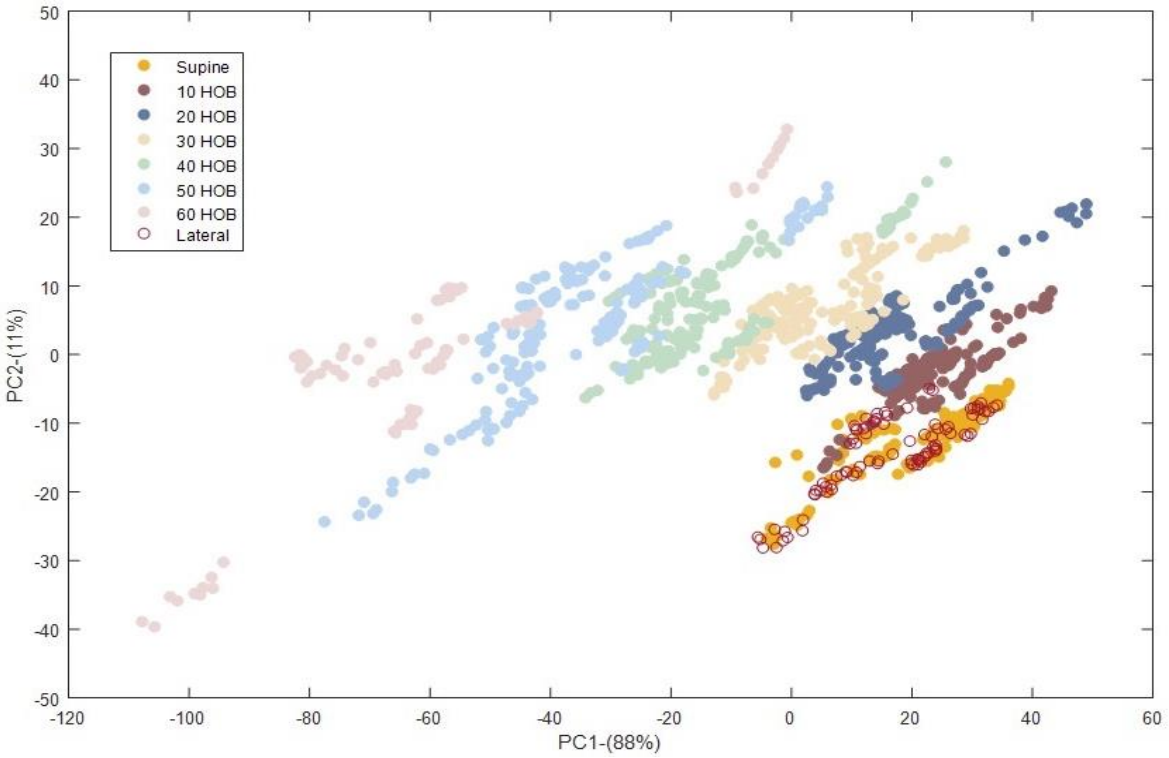

Figure 4-6. Data set involving contact area at the whole body ROI and trunk tilt angles of 9 subjects projected onto the first two principal components, PC1 and PC2, with their corresponding variance in brackets. Each posture is represented by a spatially distributed coloured cluster.

4.1.4.1 Evaluation of pressure parameters in isolation

It is recognised that actimetry signals generally represent the reference for movement detection, with limited evidence supporting the potential for interface pressure signals to detect movements. However, in many clinical situations pressure monitoring alone are used and thus it was important to extend the analysis to investigate selected pressure parameters in the absence of actimetry data.

Pressure signals were subjected to filtering, interpolation and down sampling as detailed in Section 4.1.2. For each of the two ROIs, distinct data sets were then established, incorporating:

- **Data set 1**: Contact area (>20mmHg) and centre of pressure estimated in the parallel and perpendicular directions with respect to the long axis of the pressure sensing mat;
- **Data set 2**: Contact area (>20mmHg) and peak pressure gradient estimated in the parallel direction with respect to the long axis of the pressure sensing mat;
- **Data set 3**: Contact area (>20mmHg) and peak pressure gradient estimated in the perpendicular direction with respect to the long axis of the pressure sensing mat.

Subsequently, PCA was performed for each of the data sets (data not shown), defining three distinct training models to predict the range of postures.

4.1.5 Test data sets

Data from testing group were subjected to filtering as described in Section 4.1.2. All testing signals were then interpolated to encompass 9000 data points (2.5 hours of recording), including both static postures and the transition between postures. This matched the aims of the chapter, namely, to detect when a change in posture occurs and identify static postures utilising machine learning approaches in the form of classifiers. Distinct data sets were evaluated for each subject, including:

i. Combination of pressure and actimetry signals, namely contact area estimated at the whole body and buttock ROIs, sagittal and lateral trunk tilt angles to validate the combined models;
ii. Data sets of pressure parameters, to validate the training models of data set 1, 2 and 3;

Each of the test data sets was subjected to a two-level approach, as illustrated in Figure 4-7. A 60-second sliding window was used for data reduction and mean and derivative values were estimated within each window prior to detecting postural changes and classifying postures.

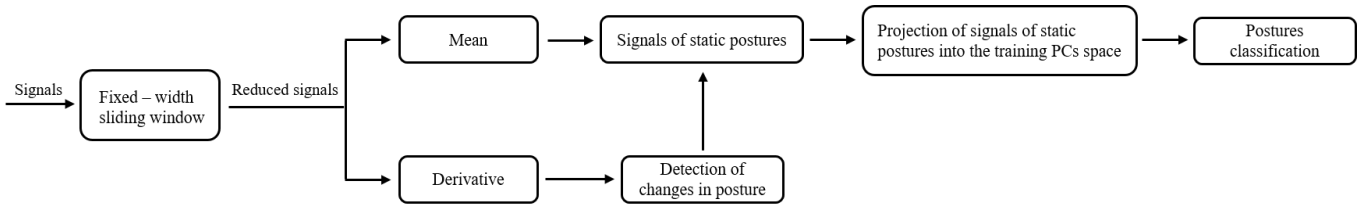

Figure 4-7: The two level approach applied to the data sets derived from the testing group

4.1.5.1 Detecting changes in posture

The derivative values of the signals were selected as they represent the rate of change of a function with respect to an independent variable (Merino et al. 2010, Taborri et al. 2016). The derivative was subjected to processing. This involved the rectification of the signals which were then assessed through a range of specific thresholds to identify where the variations in the

derivative signals occurred. Accuracy values were estimated to identify the optimum threshold values for all subjects. Once the postural changes were identified, the signals were subjected to posture classification.

4.1.5.2 Postures classification

Set of data corresponding to the static postures were projected into the corresponding training PCs dimensional space, multiplying the test signals with the training Eigenvectors. PCA enables data points from both training and test data sets to be viewed in the same dimensional space, as illustrated in Figure 4-8.

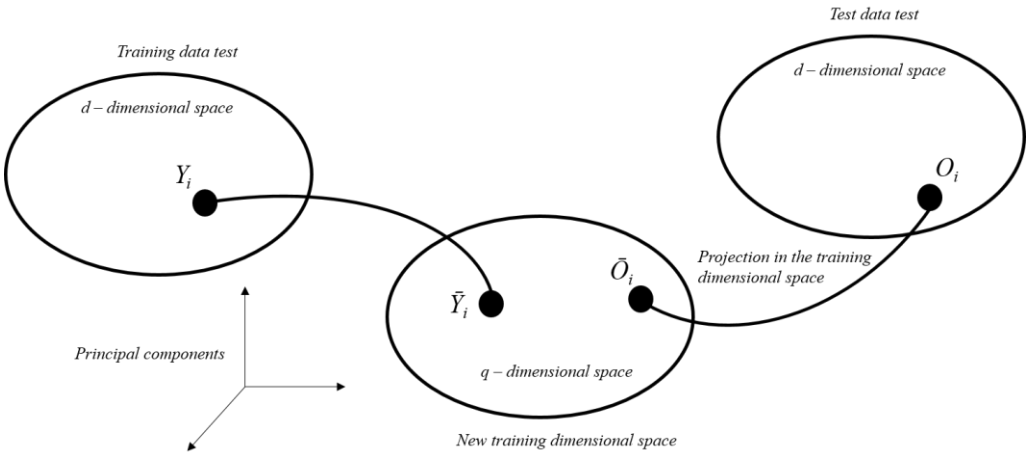

Figure 4-8: Action of PCA to project new input data (testdata points) into the training PCs space.

As an example, Figure 4-9 illustrates the signals corresponding to the static postures of one subject, represented by the test data points in red, projected onto the training PCs space of Figure 4-6. It should be noted that the test data involved postural changes with 20^o HOB increments.

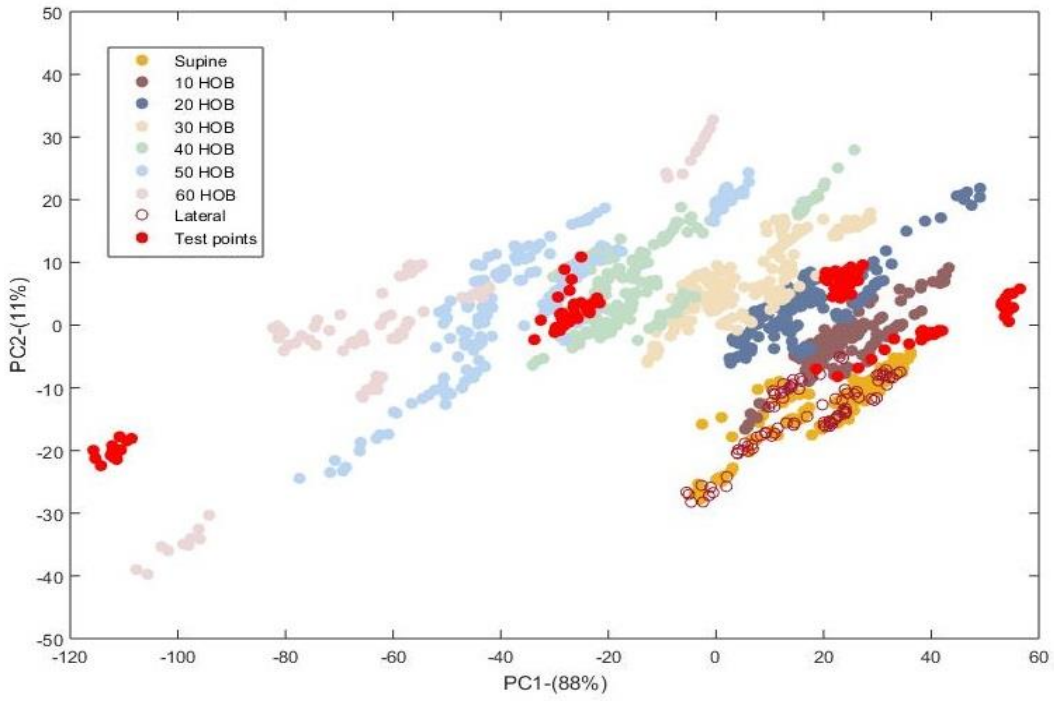

Figure 4-9: Signals from one subject (Subject #1, test data points in red) projected onto the PCs dimensional space of contact area at the whole body and trunk tilt angles.

Different classifiers were applied to identify the range of postures to which new data points in the test set could be attributed, based on the training models. Initially, the capability of the algorithms in detecting postures was investigated via a leave-one-subject-out cross – validation. Accordingly, the training models were established with data from 8 of the 9 subjects in the training cohort (Table 4-1), selected at random. The data from the excluded subject were then tested and the accuracy in the classification was assessed. This process was repeated for each of the test individuals to provide a robust accuracy assessment. Subsequently, a training model was developed with the data from all 9 training subjects. The accuracy of the classifiers in detecting the range of postures from the test cohort was then investigated.

4.1.6 Classification using machine learning algorithms

The algorithm of three different classifiers was developed in Matlab (Mathworks, US). Each of the three, the *k*-Nearest Neighbors (KNN), the Naïve Bayes classifiers and the Support Vector Machine (SVM), will be described separately.

4.1.6.1 KNN classifier

The KNN classification rule, first described by Cover and Hart (1967), is defined as a non-parametric, instance-based classifier, used in a supervised learning setting. It is based on the fact that:

- No explicit assumptions are made about the functional form of new observations to test, hence, it is non – parametric in nature;
- It is an instance – based model, where predictions are made based on training instances only;
- There is a labelled data set containing training observation as an input.

Given a new observation, its classification depends on the distance metric between the new observation point and *k* nearest data point(s) (Short and Fukunaga 1981). Given the nature of the data, the Euclidean distance is used as the distance metric, as described:

$$d\left(P_{1,}P_2\right) = \sqrt{(x_1 - x_2)^2 - (y_1 - y_2)^2} \tag{4.2}$$

The parameter *k* determines how many neighbors will be chosen (Figure 4-10). The choice of *k* has significant impact on the diagnostic performance of KNN algorithm. A large *k* reduces the impact of variance caused by random errors, although it may ignore small patterns or trends. Accordingly, the accuracy of the algorithm in identifying the range of postures was assessed for different *k* values, ranging between 1 and 45 in intervals of 5, with the highest value representing the maximum number of points which accommodates both left and right lateral postures. *k* value for leave – one – out cross validation was prescribed as 1.

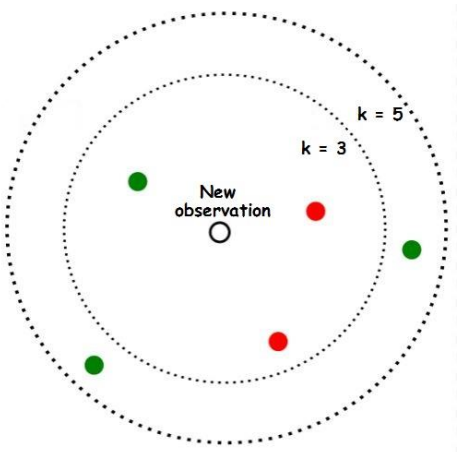

Figure 4-10: Example of the KNN classifier. The new observation (open circle) should be classified either to the first class of green markers or to the second class of red markers. If *k* = 3 i.e. 3 nearest neighbours, it is assigned to the second class because there are 2 red markers and only 1 green marker in the inner circle. If *k* = 5 it is assigned to the first class (3 green vs. 2 red markers) in the outer circle.

4.1.6.2 Naïve – Bayes classifier

Bayes classifier (Efron 2013) represents a probabilistic strategy used in a supervised learning setting. It is based on Bayes' theorem, which describes the probability of an event based on the prior knowledge that some other events have already occurred i.e. conditional probability.

Specifically, if ***H*** represents a new event and ***E*** represent some observed event, the conditional probability can be written as:

$$P(H \mid E) = \frac{P(E \mid H) * P(H)}{P(E)} \qquad (5.3)$$

It is based on the assumptions that:

1. The data from each observation is derived from a Gaussian distribution;
2. The features derive from a multinomial distribution i.e. the Poisson distribution.

Given the time – dependent nature of signals in the present study, a continuous distribution (Gaussian) was considered the most appropriate approach. Thus, the conditional probability can be written as:

$$\mathrm{P(H \mid E)} = \frac{1}{\sqrt{\det(2\pi\sigma_E)}} \exp\left(-\frac{1}{2}(h-\mu_E)^T \sigma_E^{-1}(h-\mu_E)\right) \qquad (5.4)$$

where μ_E represents the mean and σ_E the covariance matrix.

4.1.6.3 Support vector machine (SVM) classifier

SVM represents a supervised classifier based on defining a hyperplane that divides the clusters of data (Burges 1998). The optimal hyperplane is the one representing the largest distance to the nearest element of each cluster (support vectors). SVM projects the data into a higher dimension from the original space where the hyperplane can be derived from kernel functions, as illustrated in Figure 4-11, with no additional computational cost.

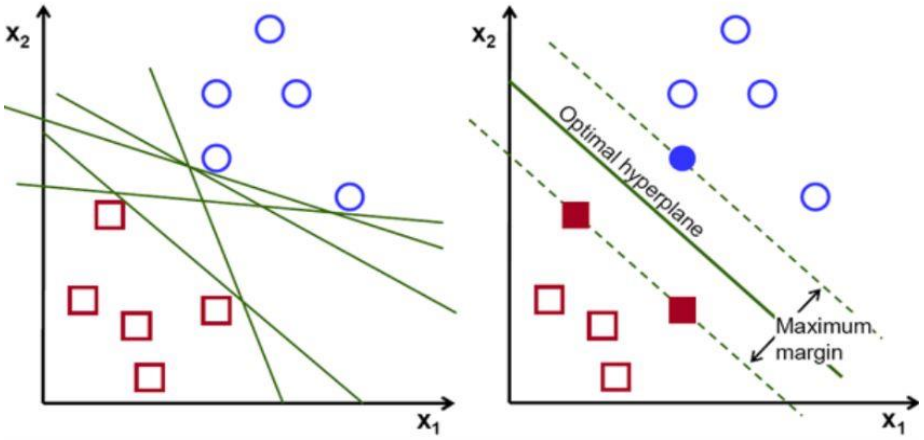

Figure 4-11: Action of SVM where possible hyperplanes can divide the two clusters (left)..From these, the optimal hyperplane represents the one characterised by the maximum distance to the nearest elements of the clusters (right).

Different SVM algorithms use different kernel functions. Give the spatial distribution of the data points in the present study, a linear and a Gaussian kernel function were used for classifying postures.

4.2 Results

The results of the processes used to detect the postural changes and classify the static postures for each data set are reported, as indicated in Figure 4-12.

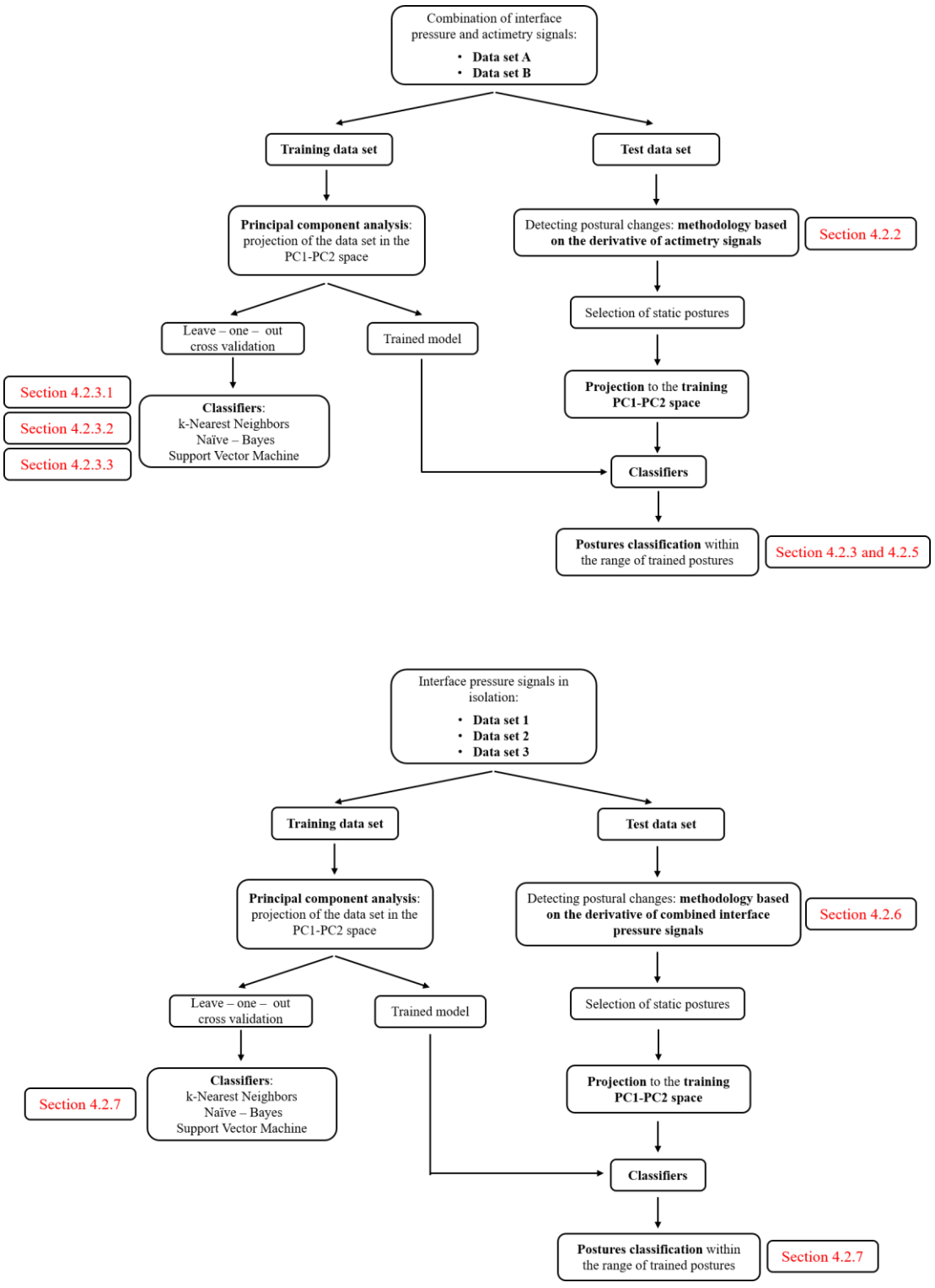

Figure 4-12: Flow chart summarising the sequence of analyses performed on both training and test data sets and the corresponding sub-sections in which they arise in the results section.

4.2.1 Participants

Demographics of subjects allocated in the training and test groups are summarised in Tables 4-1 and 4-2, respectively. The training group involved 5 male and 4 female of age ranging between 27 and 36 years. Height and weight ranged between 1.50 – 1.85 m and 50 – 90 kg, respectively. The corresponding BMI ranged between 19 – 30 kg/m^2. Subjects allocated in the test group included 5 male and 5 female, of age between 27 and 56 year. Similar demographics to the training group were evident (Table 4-2). Four of the participants were included in both training and test groups. Both protocols were conducted under the same University ethics FoHS - Ethics - 26379), which occurred 12 months apart.

Table 4-1: Demographics of the training group of subjects.

Subject	Age	Sex	Height [cm]	Weight [kg]	BMI [kg/m^2]
1	36	M	176	87	28
2	31	F	152	50	22
3	27	F	168	58	21
4	31	M	185	84	25
5	28	M	172	78	26
6	35	F	153	44	19
7	32	M	173	90	30
8	34	M	182	76	23
9	32	F	174	80	26
Mean (SD)	32 (3.0)		170 (11.4)	72 (17.0)	24 (3.5)

Table 4-2: Demographics of the test group of subjects.

Subject	Age	Sex	Height [cm]	Weight [kg]	BMI [kg/m^2]
1	28	M	190	67	19
2	23	M	180	80	25
3	33	M	173	89	30
4	56	F	160	52	20
5	36	M	176	88	28
6	36	F	153	46	20
7	37	M	183	76	23
8	32	F	152	52	22
9	33	F	178	80	25
10	27	F	168	58	21
Mean (SD)	34 (8.9)		171 (12.8)	69 (15.9)	23 (3.8)

4.2.2 Detecting changes in posture – combined data sets

Consistent variations in the derivative magnitude of the trunk tilt angles were identified in association with the postural changes for all subjects. Smaller variations in the derivative were also evident when lateral postures were adopted. The derivative profile of trunk tilt angles in both sagittal and transverse planes were rectified, as described in section 4.1.5.1, and summed to obtain a single signal, as illustrated in Figure 4-13.

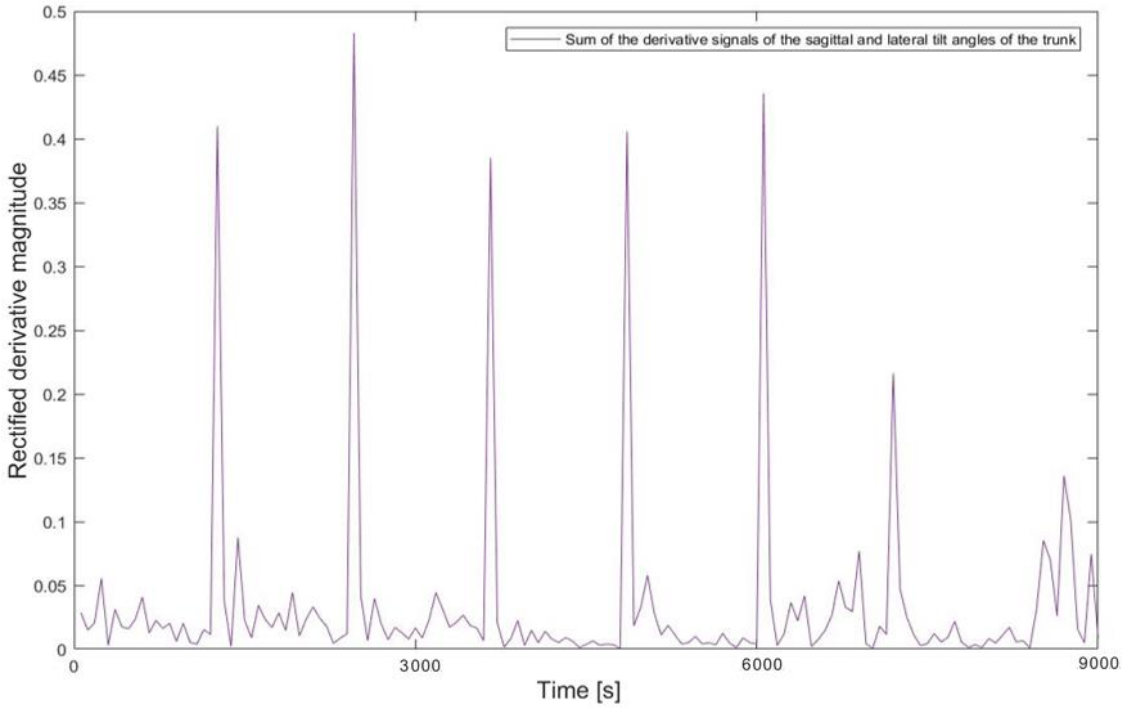

Figure 4-13: Rectified derivative profile of the sum of **trunk tilt angles in both sagittal and transverse planes** for subject #1. Each data point corresponds to a derivative value calculated within a 60-sec moving window.

The corresponding rectified derivative of the contact area at both ROIs for one subject is illustrated in Figure 4-14. It is characterised by variations in magnitude in association with some postural changes, which were evident for all subjects. However, variations in magnitude were also apparent during static postures. These variations were observed in postures involving low HOB angles, i.e. < 20^{o}, limiting the discriminatory power to detect the corresponding changes in posture. Accordingly, only the derivative of the trunk tilt angles was used for subsequent detection of postural changes. This finding reaffirms that reported in Chapter 3, where contact area signals for lower HOB angles revealed low AUC values i.e. <0.5 estimated from the ROC curves (Table 3-11).

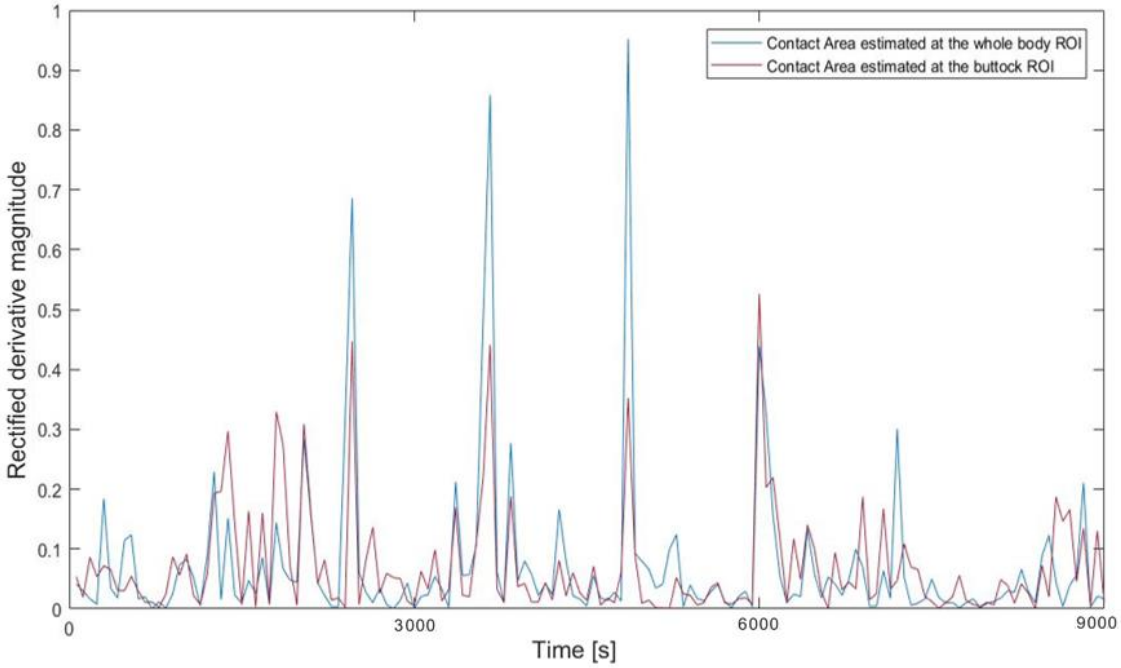

Figure 4-14: Rectified derivative profiles of **the contact area estimated at whole body (blue curve) and at the buttock (red curve) ROIs** for subject #1. Each data point corresponds to a derivative value calculated within a 60-sec moving window.

Thus, the derivative of the trunk tilt angles was examined and the ability of four discriminant thresholds, ranging from 0.05 – 0.20, were assessed to detect the correct number of events. In this case, events detected in intervals incorporating 10 data points were combined to represent a single event. This approach clearly limits the possibility to discriminate between changes in the right lateral posture and those in the left lateral posture, as the total number of points corresponding to these two postures was 10. Accordingly, only one event was identified, which corresponded with the change in posture from the last supine to lateral, with no discrimination between right and left lateral posture. The findings for each subject are summarised in Table 4-3. It is clear that at higher threshold values there was a reduced number of detected events. For all subjects, a threshold value of 0.10 was able to detect 7 events, corresponding to 6 occurring in the sagittal plane and 1 in the transverse plane with a 100% accuracy.

Table 4-3: The influence of threshold values in identifying the number of events corresponding to changes in posture in both sagittal and transverse planes for all subjects, based on the derivative of **tilt angles**.

	Threshold values - Number of events			
Subjects	**0.05**	**0.10**	**0.15**	**0.20**
1	7	7	6	6
2	7	7	6	6
3	7	7	6	6
4	7	7	7	5
5	7	7	6	4
6	8	7	6	6
7	8	7	7	5
8	8	7	7	6
9	7	7	6	4
10	8	7	7	6
Accuracy [%]	95%	100%	91%	77%

Following the identification of the postural change events, the signals corresponding to the static postures were subjected to classification.

4.2.3 Postures classification – combined data sets

The accuracy of the three classifiers was evaluated for each subject as defined by the percentage number of data points correctly classified using the test data. The data sets involving trunk tilt angles and the contact area at both ROIs, namely **data set A** and **data set B**, were used for comparison.

4.2.3.1 KNN classifier

The leave – one – out cross – validation demonstrated an accuracy ranging between 57% - 83% and between 55% - 91% in classifying the range of postures from data set A and B, respectively.

The algorithm accuracy was then investigated for the 10 subjects in the test cohort for the different *k* values. The accuracy values of each test subject for data set A is illustrated in Figure 4-15. It is evident that for all *k* values the variability of the accuracy ranged considerably between subjects from less than 10% (subject #1) to 30% (subject #3). In general, the higher *k* values yielded an increased accuracy, although the maximum values ranged considerably from approximately 40% to 80%. It was also evident that accuracy for the subjects varied for the same *k* value. A similar trend was observed for data set B, at different *k* values (data not shown).

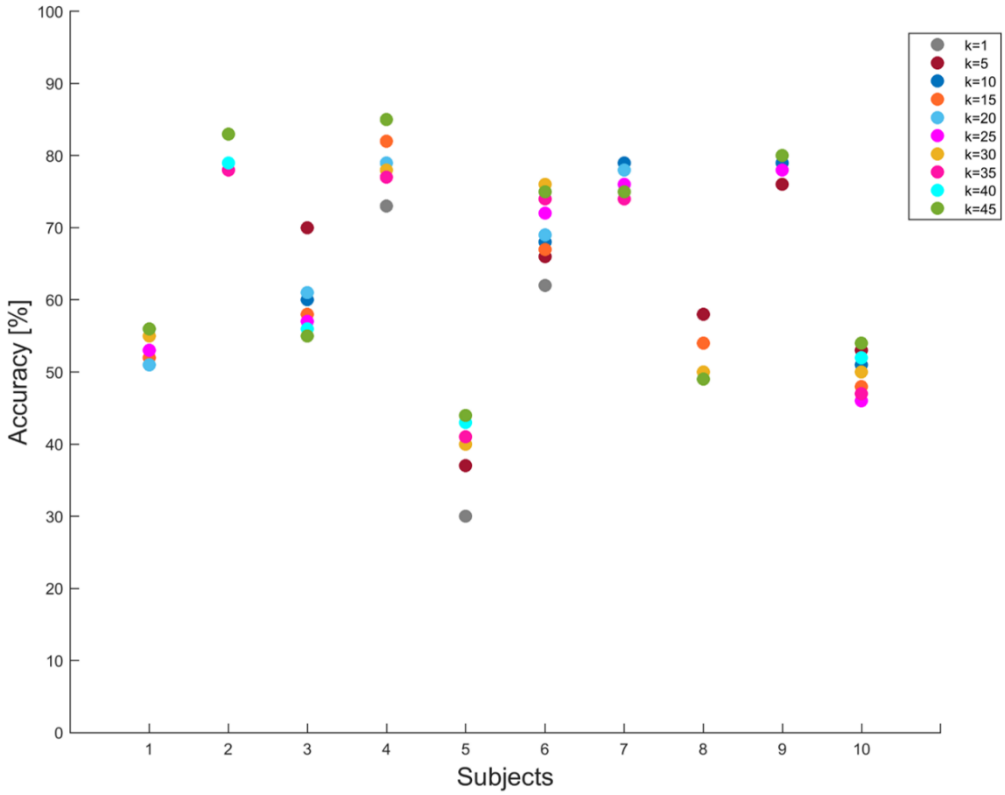

Figure 4-15: Percentage accuracy in correctly identifying postures of each test subjects from data set A, using the KNN classifier and different *k* values.

4.2.3.2 Naïve – Bayes classifier

The leave – one– out cross – validation demonstrated an accuracy ranging between 63% - 88% and between 54% - 86% in classifying the range of postures from the combined data sets A and B, respectively.

The accuracy in classifying postures of the 10 test subjects was investigated with Naïve – Bayes classifier for the combined test data sets (Table 4-4). Accuracy ranged between 67% to 98% and 67% to 94%, for data sets A and B, respectively. For each subject, the accuracy values were fairly similar for both ROIs, with the exception of subject #3 who yielded a 20% difference.

Table 4-4: Percentage accuracy in classifying the range of postures with Naïve-Bayes classifier for data set A and B.

	Naïve – Bayes – Accuracy [%]	
Subjects	**Data set A**	**Data set B**
1	60	59
2	87	83
3	74	94
4	79	81
5	76	71
6	66	70
7	88	92
8	90	82
9	98	90
10	67	67

4.2.3.3 Support Vector Machine

The leave-one-out cross validation using the SVM approach with linear kernel demonstrated an accuracy ranging between 74% - 100% and 71% - 100% in classifying data sets A and B, respectively. The corresponding accuracy using the Gaussian kernel ranged between 56% - 99% and 73% - 99%. The accuracy in postures classification for all the 10 test subjects with SVM with linear and Gaussian kernels was investigated for combined test data sets (Table 4-5). Both linear and Gaussian kernels revealed accuracy values ranging between 62% and 100%.

Table 4-5: Percentage accuracy in classifying the range of postures for data set A and B with the SVM classifier.

	SVM – Accuracy [%]			
	Linear kernel		SVM – Gaussian kernel	
Subjects	**Data set A**	**Data set B**	**Data set A**	**Data set B**
1	97	91	80	98
2	97	99	80	87
3	86	99	83	97
4	90	88	87	87
5	72	79	79	97
6	77	83	74	78
7	91	89	95	94
8	69	69	66	78
9	100	99	100	100
10	70	70	62	76

4.2.4 Considerations of the results in postures classification

The high variability in the percentage accuracy for KNN (Figure 4-15), Naïve – Bayes (Table 4-4) and SVM (Table 4-5) classifiers could be attributed to the comprehensive range of postures, including 10^{o} HOB increments and left/right lateral postures. It has been shown that with this increment of movement i.e. 10^{o} HOB, there was substantive overlapping between clusters of data points (Figure 4-6). Accordingly, to minimise this effect, further analysis was conducted on training data sets, which involved a coarser resolution of 20^{o} HOB increments. This necessitated the re-evaluation of the accuracy for all classifiers in detecting static postures.

4.2.5 Postures classification involving 20^{o} HOB increments

The accuracy of the KNN algorithm is detailed in Figure 4-16 for the full range of *k* values, corresponding to the data set A. It is clear that the accuracy of this data is higher and the variability between *k* values is considerably reduced, when compared with the data set involving the 10^{o} HOB increments (Figure 4-15). This trend was also evident in the data set B (data not shown). A *k* value of 10 was chosen to perform the KNN algorithm as its associated accuracy resulted in the lowest variability between subjects and the highest values in the majority of test subjects.

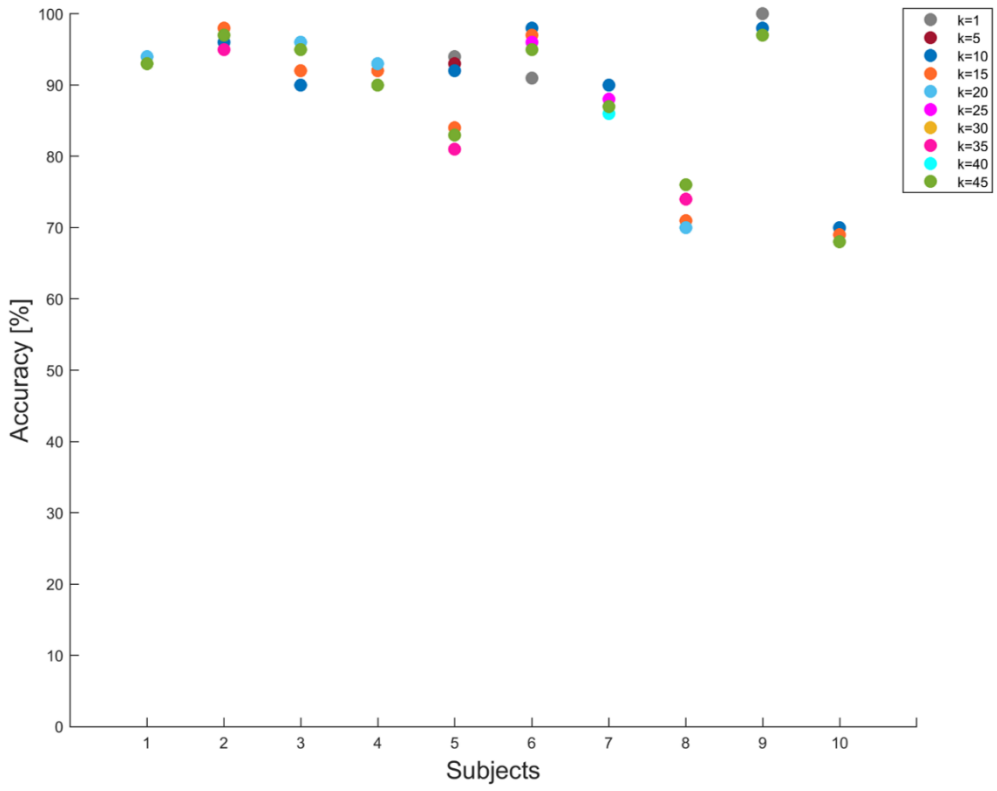

Figure 4-16: Percentage accuracy in correctly classifying postures of each test subjects from data set A, using the KNN classifier and different *k* values.

The accuracy for each of the three classifiers was assessed, involving the data sets A and B (Table 4-6). It is evident from Table 4-6 that increments in 20^{o} of the HOB angles resulted in an increased accuracy for each subject and all classifiers. In particular, the accuracy in identifying postures using the KNN classifier for data set A was ≥ 90% in 8/10 subjects, with the remaining two subjects showing accuracy values of 70% and 74%. The corresponding values for data set B were ≥80% in all subjects. The Naïve – Bayes classifier resulted in an accuracy >80% for both data sets. SVM with both linear and Gaussian kernels resulted in accuracy values of >80% in the majority of the subjects for both data sets. The other subjects (subject #8 and #10) showed a lower accuracy, which was of 72% and 78% for data sets A and B, respectively. In addition, subjects #10 showed an accuracy of 69% for classification of data set A performed with the linear kernel.

Table 4-6: Percentage accuracy in classifying the range of postures for KNN (k = 10), Naïve – Bayes and SVM classifiers. Combined data sets included contact areas for whole body and buttock ROIs for all subjects.

	Accuracy [%]							
	KNN (*k*=10)		**Naïve – Bayes**		**SVM– Linear kernel**		**SVM– Gaussian kernel**	
Subjects	**Data set A**	**Data set B**	**Data set A**	**Data set B**	**Data set A**	**Data set B**	**Data set A**	**Data set B**
1	94	94	90	90	88	85	97	96
2	97	97	95	89	92	93	91	90
3	90	96	98	94	99	98	86	95
4	92	93	89	87	89	85	90	90
5	93	95	97	95	86	84	97	98
6	97	91	83	79	89	86	82	79
7	90	97	93	94	87	87	97	97
8	74	85	98	91	83	82	71	81
9	98	97	100	97	98	95	100	97
10	70	80	82	80	72	77	69	82
Mean value	90	93	92	90	88	87	88	91
Range	70 – 97	80 – 97	82 – 100	80 – 97	72 – 99	77 – 98	69 – 100	79 – 98

4.2.6 Detecting changes in posture – interface pressure data only

Derivative of the interface pressure parameters estimated at both the whole body and buttock ROIs were characterized by variations in magnitude, which did not enable detection of all sagittal postural changes (Figure 4-14). Thus, composite derivative signals calculated by the product of contact area with either COP or peak pressure gradients signals, estimated with

respect to the parallel and perpendicular directions, were assessed for detecting the postural changes for both ROIs. As described in 4.1.5.1, the derivative were rectified and subjected to discriminant thresholds to identify variations in the signals. Figure 4-17 shows a typical composite derivative, obtained from the product of contact area with COP and peak pressure gradient in both directions. The scale of the combined derivative of contact area and COP (top figure - Figure 4-17) is an order of magnitude lower (order of thousandths) than the combined derivatives of contact area and peak pressure gradients (order of hundredths).

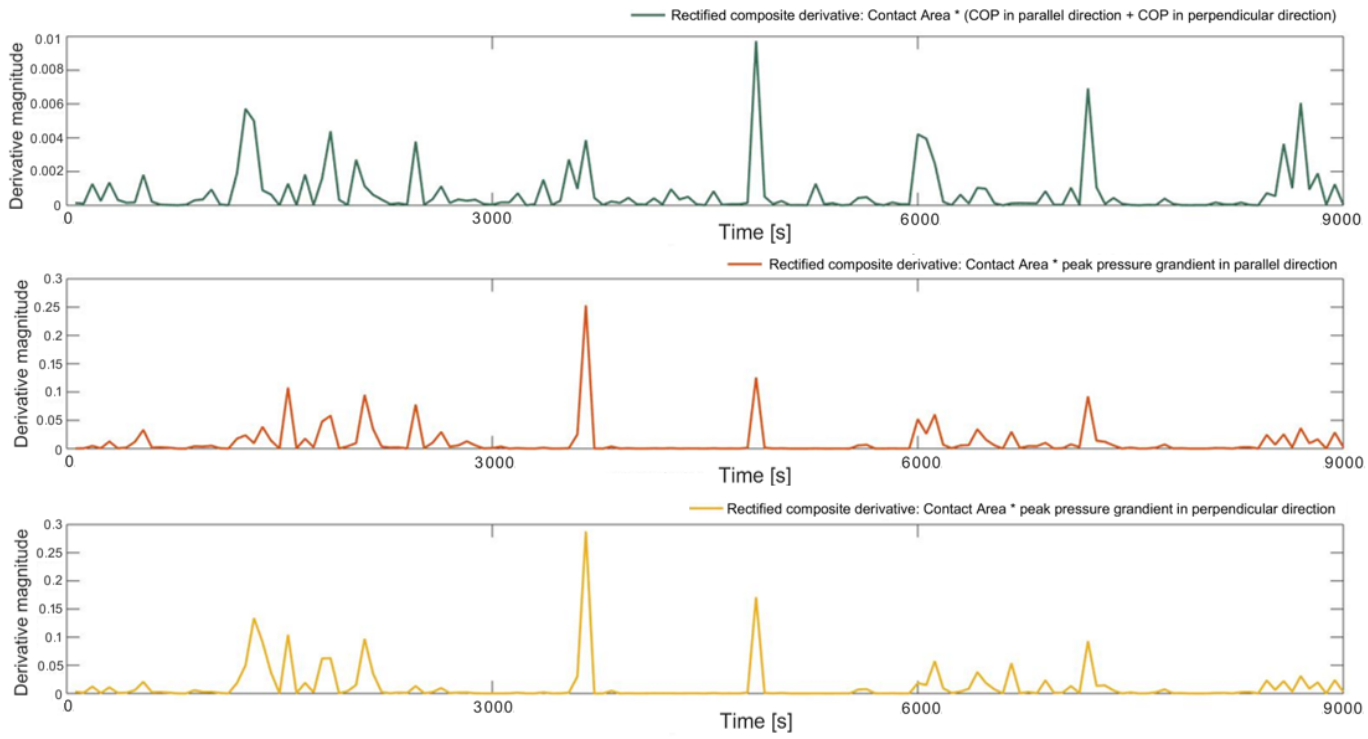

Figure 4-17: Composite derivative profiles at the whole body ROI for subject #1 obtained as result of the product of the derivative signal of contact area with the derivative of, (upper signal) COP estimated for both parallel and perpendicular directions with respect to the long axis of the sensing mat; (middle signal) peak pressure gradient estimated at the parallel direction with respect to the long axis of the sensing mat; (lower signal) peak pressure gradient estimated at the perpendicular direction. Each data point corresponds to a derivative value calculated within a 60-sec moving window.

Small perturbations in the magnitude were observed in the composite derivative signals of contact area and peak pressure gradients for changes in lateral postures (Figure 4-17– middle and lower signals). It is evident that these signals have a reduced potential to detect the corresponding changes in posture. By contrast, the composite derivative of contact area and COP (upper signal) showed significant variations corresponding with both changes in supine and lateral postures. Thus, it was selected to detect changes in posture at both ROIs.

The signals were subjected to discriminant threshold values and their ability to detect the correct number of events was assessed. The number of detected events are summarised in Table 4-7, for

threshold values ranging from 0.0005 to 0.005. These threshold values were lower than those used for the tilt angles derivative (Table 4-3). Derivative signals showed some variations in magnitude during static postures. Thus, events detected in intervals including 10 data points were combined to represent a single event. As discussed in Section 4.2.3, only one event corresponding with the change in posture from the last supine to lateral posture was identified.

Table 4-7: The influence of threshold values in identifying the number of events associated with changes in posture for all subjects, based on the **composite derivative of interface pressure signals** estimated from the whole body and buttock ROIs.

	Threshold values - Number of events							
	Whole body ROI				**Buttock ROI**			
Subjects	**0.0005**	**0.001**	**0.002**	**0.005**	**0.0005**	**0.001**	**0.002**	**0.005**
1	7	7	7	4	6	6	6	6
2	7	7	7	6	7	7	6	6
3	7	7	7	7	7	7	7	4
4	7	7	7	4	7	7	7	5
5	7	7	7	6	7	7	7	6
6	6	6	6	6	5	5	5	5
7	5	5	5	5	7	7	7	5
8	6	5	4	2	7	6	5	1
9	7	7	7	5	6	6	5	4
10	7	6	5	5	7	6	6	4
Accuracy [%]	91	90	87	71	94	91	87	66

The number of events detected depended on the specific threshold values. The findings revealed that the threshold value of 0.0005 was the most accurate in detecting the events corresponding with sagittal and lateral changes in posture at both ROIs. All 7 events corresponding to postural changes were detected in 7/10 subjects (Table 4-7). For the remaining subjects, some of events corresponding to the postural changes were not identified. On further examination, it emerged that for subject #8 a number of false positives, namely postural movements within static postures classified as events corresponding to changes in posture, were detected at the whole body ROI.

Once postural change events were identified, the signals corresponding to the static postures were subjected to classification. As the static postures were recognised depending on two subsequent postural change events, their misdetection inevitably affected the classification of the corresponding static postures. Some misclassifications were observed in those subjects

where misdetection of the changes in posture occurred (Table 4-7). These are indicated in red in Tables 4-8 and 4-9 for whole body and buttock ROIs, respectively.

4.2.7 Postures classification – interface pressure data sets

Subsequently 20^{o} HOB increments were considered for interface pressure data sets, using KNN, Naïve – Bayes and SVM with Gaussian kernel classifiers. k = 10 was chosen for KNN as it provided the highest accuracy. Linear kernel was excluded from the current analysis as it produced lower accuracy values in the previous analysis.

To review briefly, three distinct data sets involving interface pressure parameters estimated at the whole body and buttock ROIs were evaluated, involving:

Data set 1: Contact area and centre of pressure estimated in the parallel and perpendicular directions with respect to the long axis of the mat;

Data set 2: Contact area and peak pressure gradient estimated in the parallel direction with respect to the long axis of the mat;

Data set 3: Contact area and peak pressure gradient estimated in the perpendicular direction with respect to the long axis of the mat.

The cross validation demonstrated an accuracy ranging between 26% - 94% and between 15% - 91% in classifying the range of postures for all subjects corresponding to the three data sets at whole body and buttock ROIs, respectively.

The accuracy of the classifiers was then investigated for the 10 test subjects and a summary of these results are presented in Tables 4-8 and 4-9. The data for the whole body ROI revealed that subjects #6, #7 and #8 were subjected to a misclassification due to the fact that some events corresponding to a change in posture were not detected (Table 4-8). As a result, it compromised the classification accuracy values, which were in most cases the lower of the accuracy range. This was also evident for the buttock ROI, where events were not detected in the derivative signal (Table 4-9). This was the case for subjects #6 and #9. By contrast, subject #1 showed a high accuracy, with particular reference to data set 1, despite incurred in a misdetection of the change in posture from the last supine to lateral.

Data set 1 revealed the highest accuracy values for both classifiers when compared with data sets 2 and 3. A comparison of the two ROIs revealed that data set 1 at both whole body resulted in highest accuracy values when the classification was performed with SVM. By contrast, the corresponding accuracy values at the buttock ROI were comparable when the classification was performed with Naïve – Bayes and SVM (Tables 4-8 and 4-9).

Table 4-8: Percentage accuracy in classifying the range of postures with KNN (k = 10), Naïve – Bayes and SVM classifiers, using data sets of interface pressure parameters estimated at the **whole body ROI**. The subjects highlighted in red are those whose classification was compromised due to misdetection of some changes in posture.

	Accuracy [%]								
	KNN			**Naïve Bayes**			**SVM– Gaussian kernel**		
Subjects	**Data set 1**	**Data set 2**	**Data set 3**	**Data set 1**	**Data set 2**	**Data set 3**	**Data set 1**	**Data set 2**	**Data set 3**
1	77	30	57	79	46	52	97	49	64
2	75	43	72	73	86	75	76	81	86
3	64	61	46	70	62	58	84	71	73
4	68	48	54	78	74	62	68	90	80
5	63	44	21	64	48	54	67	44	54
6	47	23	27	22	13	16	25	37	45
7	63	60	48	55	67	60	66	71	54
8	40	29	28	45	38	31	46	36	35
9	77	79	43	79	67	52	83	96	60
10	71	64	36	56	47	41	71	60	45

Table 4-9: Percentage accuracy in classifying the range of postures with KNN (k = 10), Naïve – Bayes and SVM classifiers, using data sets of interface pressure parameters estimated at the **buttock ROI**. The subjects highlighted in red are those whose classification was compromised due to misdetection of some changes in posture.

	Accuracy [%]								
	KNN			**Naïve Bayes**			**SVM– Gaussian kernel**		
Subjects	**Data set 1**	**Data set 2**	**Data set 3**	**Data set 1**	**Data set 2**	**Data set 3**	**Data set 1**	**Data set 2**	**Data set 3**
1	89	51	75	88	63	64	98	65	70
2	87	55	79	98	53	67	99	97	98
3	86	51	77	85	55	54	99	94	86
4	76	68	66	93	76	74	80	90	79
5	83	67	71	91	53	53	99	61	79
6	40	45	45	25	53	42	24	55	56
7	81	67	71	94	53	61	88	70	62
8	67	43	52	63	54	50	66	75	60
9	61	66	42	36	68	40	58	71	66
10	53	52	27	57	62	27	71	41	29

4.3 Discussion

This study has detailed the application of intelligent data processing of biomechanical signals depicting changes in lying posture from angles of body segments (actimetry) and pressures measured at the interface between the body and support surface. These signals were both combined and considered in isolation for detecting the postural changes in both sagittal and transverse planes and classifying the range of static postures. The derivative of signals was assessed to identify changes in posture. A series of established machine learning algorithms in the form of Naïve - Bayes, KNN and SVM classifiers were applied to data sets estimated from two distinct ROIs of the body. A cross – validation technique was applied to each algorithm. This reveals that the training data sets, involving both combination of actimetry and pressure signals and pressure – related signals alone, could provide a robust means for classifying the data. Subsequently, an adapted protocol was used evaluate the models with new test data.

Findings revealed that the derivative of the signal representing the trunk tilt angles correctly identified the changes in posture for all subjects, as characterised by a transient increase in the magnitude of the derivative at each of the evoked movements (Figure 4-13, Table 4-3). By contrast, the derivatives for each of the interface pressure signals were less distinctive and thus it proved more difficult to identify changes in posture e.g. Figure 4-14. This motivated a further approach involving the combination of derivative signals obtained from the product of the derivative of different pressure – related parameters i.e. contact area and COP, with data sets of interface pressure alone (Figure 4-17). This approach proved successful in most test subjects (Table 4-7). However, for a few subjects, incorrect detection of changes in posture was evident. The approach based on the derivative of biomechanical parameters has been applied in several other areas of the biomedical field, for example, for the detection of the different gait phases (Taborri et al. 2016).

Machine learning algorithms were chosen based on the models of the training data, which were labelled. This inevitably resulted in the domain of supervised learning. Moreover, as the nature of the posture detection involved classification and clustering, Naïve - Bayes, KNN and SVM were considered the most appropriate approaches. In addition, the principles underpinning each of these algorithms makes them easy-to-implement and perform at low computational costs, when used to reduce data dimensionality. Accordingly, they have commonly been used in previous relevant studies (Wai et al. 2010, Yousefi et al. 2011, Foubert et al. 2012, Zemp et al. 2016, Rus et al. 2017, Kim et al. 2018, Duvall et al. 2019, Matar et al. 2019). A few other algorithms were considered for the present analysis but excluded as their principles were not appropriate. As an example, linear regression was excluded from the analysis as modelling the relationship between variables was not the primary goal of the classifiers. In addition, Decision Trees were considered, but were excluded due to their inherent instability. Indeed, a small change in the data can lead to a large change in the structure of the optimal decision tree.

Accordingly, calculations can result very complex, particularly if many values are uncertain and/or many outcomes are linked.

When projected into the training model, the test signals resulting from combined actimetry and pressure signals were observed to correspond with the clusters derived from the training phase (Figure 4-9). However, the approach revealed that by increasing the increments of HOB from 10^{o} to 20^{o} the accuracy in classification improved, resulting in an increased spatial distance between clusters. Indeed, the resulting classification accuracy of the test data from 20^{o} HOB increments was >80% for the vast majority of data from participants when applying each of the classifiers (Table 4-6).

It was interesting to note that models of pressure parameters alone were able to identify the range of postures (Table 4-8 and 4-9). In particular, the model involving contact area and COP revealed the highest accuracy in the majority of subjects when compared with data sets involving peak pressure gradients.

Previous research have utilised intelligent data processing from machine learning algorithms to classify a range of lying and sitting postures and their changes from the distribution of pressure at the subject – support interface (Wai et al. 2010, Yousefi et al. 2011, Foubert et al. 2012, Zemp et al. 2016, Rus et al. 2017, Kim et al. 2018, Duvall et al. 2019, Matar et al. 2019). Their approaches and results are summarised in Table 4-10.

Table 4-10: Summary of relevant studies classifying postures in lying and sitting.

Study	Feature used for classification	Classifier(s)	Accuracy	Changes in posture
Wai et al. (2010) – *Lying postures*	i) Raw pressure values	SVM	i) > 70%	✗
	ii) Eigen vectors		ii) > 50%	
	iii) Mean, variance, standard deviation, root mean square estimated in 9 ROIs		iii) > 60%	
Yousefi et al. (2011) – *Lying postures*	Binary pressure images projected in PCA space	KNN	> 97%	✗
Kim et al. (2018) – *Sitting postures*	Heat map of pressure distribution	Naïve – Bayes	> 85%	✗
		SVM	>90%	
Duvall et al. (2019) *Lying postures*	Weight measured by four cells placed under the legs of the bed	KNN	> 95%	✓
Zemp et al. (2016) – *Sitting postures*	Median of the force data divided by the subject's body weight and backrest angles	SVM	> 70%	✗
Foubert et al. (2012) – *Lying to sitting*	i) Weighted number of active sensors	SVM and KNN	> 90%	✓
	ii) COP displacements		> 75%	
Matar et al. (2019) – *Lying postures*	Oriented gradient and local binary patterns estimated from pressure distribution	Artificial neural network	> 97%	✗
Present study – *Lying postures*	i) Eigen vectors estimated from combined data set of actimetry and interface pressure signals	Naïve – Bayes	i) 80 – 97% ii) 56 – 98%	✓
		KNN	i) 70 – 97% ii) 53 – 89%	
	ii) Eigen vectors estimated from a data set of interface pressure signals (contact area and COP)	SVM	i) 69 – 100% ii) 66 – 99%	

It is clear that the present results are comparable with those from previous studies, with high accuracy values in posture classification for the detection of a range of postures. This was in particular the case of data sets involving combination of actimetry and pressure signals at a movement increment of 20° HOB. In the case of pressure parameters evaluated in isolation, some subjects resulted in an accuracy of below 70%. Some of the reduced values was determined by the inaccuracy of the derivative in the detection of the postural changes (Table 4-7). It was observed that only two studies have detected the transition phases between static postures, prior their classification. Foubert et al. (2012) used a metric involving lateral and longitudinal displacements of the centre of pressure, estimated from pressure distribution, to detect postural changes corresponding to transitions from lying to sitting, reporting an accuracy of >90%. Certainly, the high resolution of this transition decreased the difficulties in detecting such movement. A separate study utilised the total weight on the bed measured by using a

system involving four load cells for the detection of changes in lateral postures (Duvall et al. 2019). Their results reported that a change of 7lb (3.2kg) in the measured weight within a temporal window of 7secs was able to detect postural changes with an accuracy ranging between 90 – 98%. It could be questioned whether changes in the body weight could accurately detect sagittal changes in postures.

Furthermore, limitations of many previous studies included the short – term estimation of the pressure distribution (up to tens of seconds) and a limited range of supine postures i.e. supine, prone, left and right turn, which decreased the difficulties in detecting static postures (Wai et al. 2010, Foubert et al. 2012, Matar et al. 2019). There are, however, some studies which have evaluated a range of postures involving the elevation of the HOB angle (Yousefi et al. 2011) and data derived from a longer period i.e. 5 minutes of pressure monitoring (Kim et al. 2018). In addition, Zemp et al. (2016) utilised a composite data set involving force values acquired at the support surface, normalised to individual body weight, and the corresponding backrest tilt angle estimated with actimetry positioned on the backrest, for the detection of sitting postures. However, both parameters were acquired at a single time point.

Another limitation of the previous studies involved the sequence of postures, which occurred either in different anatomical planes, e.g. supine to lateral, or in the same plane with a wide range of movement e.g. supine to 60^{o} HOB. This represented a relatively simple challenge in detecting the changes between the postures. Results from Foubert et al. (2012) showed that the displacement of COP accurately detected changes from supine to sitting posture. By contrast, the current study has involved postures with a lower resolution of movements in the same anatomical plane (20^{o} HOB increments), which resulted in a low discriminative power from the majority of the pressure parameters in detecting postural changes. For this reason, a combination of signals was evaluated and the approach proved successful in detecting postural changes in the majority of the test subjects (Table 4-7).

The present study has applied an automated method involving biomechanical parameters to identify the occurrence and magnitude of changes in posture based on signal derivatives and machine learning algorithms. This could be achieved using either actimetry or pressure parameters. To date, these temporal data are not typically evaluated in many care settings. Therefore, any clinical data sets which only include pressure monitoring would still provide an opportunity to detect changes in posture and identify specific postures with some degree of accuracy.

The study protocol was limited in selecting a pre–determined order of relatively small postural changes (20^{o} HOB increments) maintained for a relative short period of 10-20 minutes. Thus the current method would require further validation to account for random lying postures associated with pressure parameters alone and testing with both healthy subjects and patients whose frequency and magnitude of movements are support by clinical or carer support (Defloor et al.

2005, Woodhouse et al. 2019). It is also critical to evaluate the effects of different support surfaces on the detection and classification of postural changes. This forms the basis of the approach adopted in Chapters 5 and 6.

Chapter 5: Developing a semi – automated methodology to detect postural changes with consideration of support surfaces and random sequence of postures

The analysis detailed in Chapter 4 were restricted to a relatively small range of evoked postural changes, involving 20^{o} HOB increments and 20^{o} –25^{o} of automatic lateral turning, prescribed in a pre-determined order on a foam support surface. This provided a limited representation of the postures typically adopted in clinical settings. Indeed in many cases, repositioning involves semi-recumbent positions using either a 30^{o} to 45^{o} HOB elevation or a 30^{o} side-lying position, typically delivered by rolling the patient with pillow support at the back and legs (Moore et al. 2011). In addition, more advanced support surfaces including alternating pressure air mattresses (APAM) are designed to periodically relieve support pressures at vulnerable body sites particularly for immobile individuals.

Therefore, there is a clear need to assess the developed methodology associated with the pressure parameters when adopting randomly allocated clinical postures on different support surfaces. In addition, further validation is required for testing with patients in real clinical care settings. Thus, the present chapter examined whether the automated posture detection and machine learning approaches can be translated to data sets represented by those routinely collected in the clinic. As an example, postures adopted in random order on different support surfaces were subjected to two distinct analysis. Initially, the **data set 1** from Chapter 4, including signals of contact area and centre of pressure at the whole body ROI, was considered as the training data set. Subsequently, new test data was acquired from a cohort of healthy subjects lying supine on both a commercial air cell mattress system and a conventional foam mattress. Figure 5-1 details the different methods of analysis involved in this study.

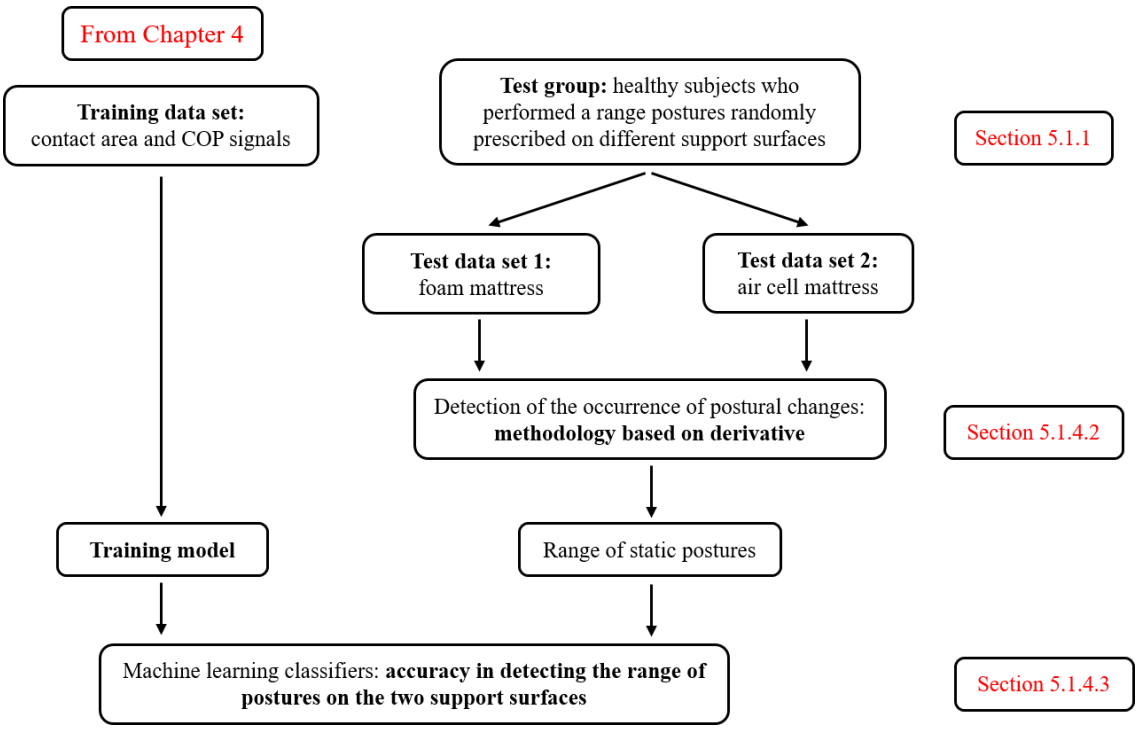

Figure 5-1: Flow chart depicting the methods of analysis involved in the chapter.

5.1 Detection of a range of postural changes randomly prescribed on different support surfaces

5.1.1 Experimental protocol

The set of experimental data from healthy individuals used for the present analysis involved a separate study associated with a healthcare company performed with institutional ethics approval (FoHS-ETHICS-2011-978), conducted in the host laboratory. The test protocol, schematically represented in Figure 5-2, involved 14 able – bodied volunteers encompassing a wide demographic range, detailed in Table 5-1. Each test subject was asked to adopt three distinct postures, prescribed in a random order to one of two mattresses, namely an air cell mattress functioning in alternating mode (AS-M001 Nagomi, Japan), and a castellated foam mattress (Medstrom, Ashby de la Zouche, UK). The three postures involved supine, lateral lying (pelvis titled to 30° as judged by a hand held inclinometer (SOAR, Digital Level meter 1700)) and high sitting (HS) with the head of bed (HOB) set at 45° (Figure 5-3). Lateral postures were achieved by placing pillows under the back and legs, in a similar manner to that in clinical settings to off – load the sacrum. Each posture was maintained for a period of 20 minutes, during which the interface pressure distributions were continuously recorded using the ForeSite PT system, throughout the test period of 60 minutes.

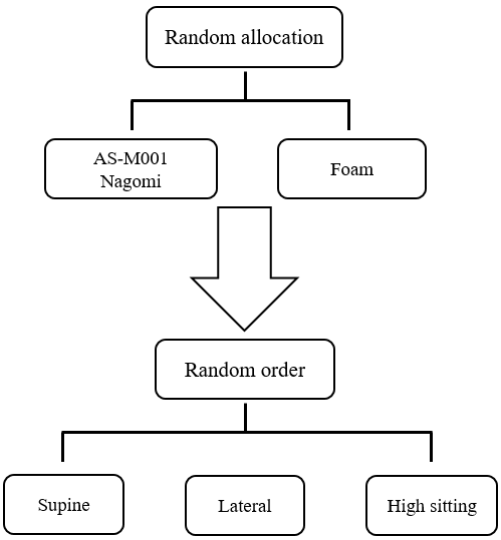

Figure 5-2: Test protocol involving the randomisation of both the mattress allocation and postures adopted on the support surfaces.

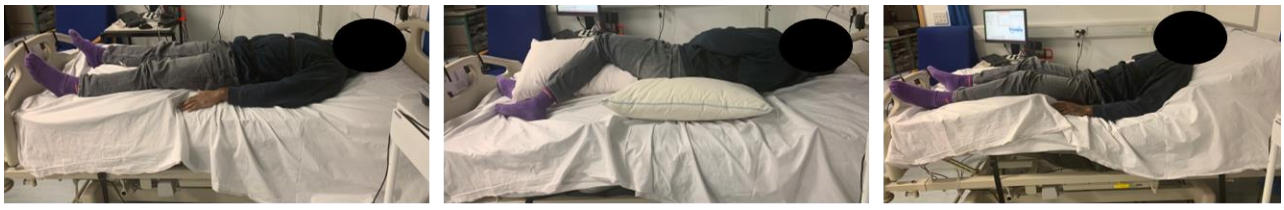

Supine Lateral High sitting

Figure 5-3: Images of the three postures adopted on each support surface, namely, supine, lateral and high sitting.

The pressure distributions were acquired for all subjects on each support surface and allocated to two separate **test groups** (air cell and foam mattress). Both the contact area, involving all sensors recording a pressure above a threshold of 20 mmHg and the centre of pressure (COP) in the parallel and perpendicular directions with respect to the long axis of the mat, were estimated from the whole body for both groups. Signals corresponding to each subject represented a distinct test data set to validate the training model.

5.1.2 Test data set

The signals corresponding to all subjects allocated to both test groups were subjected to processing following the approach described in Section 4.1.5. In this case, a 30-second sliding window was considered more appropriate for data reduction, given the reduced length of the testing protocol and the parameters estimated from the pressure distribution, accordingly. The composite derivative signal for each subject was subjected to discriminant threshold values to identify the postural changes. After these were identified, the corresponding static postures were projected into the training PC dimensional space.

5.1.3 Training model

To review briefly, the training model corresponded to the set of data (**data set 1**) estimated from whole body pressure distribution from an able – bodied cohort (n=9). This included signals of contact area (>20mmHg) and COP corresponding to postures prescribed in a pre – determined order on a foam mattress, involving 20^{o} HOB increments and 20^{o} – 25^{o} of automatic lateral turning. Signals processing was previously detailed in Section 4.1.2.

Figure 5-4 illustrates the PC1 and PC2 where static postures corresponding to the signals of contact area and COP were projected. With appropriate labelling, each posture is represented by a cluster of points spatially distributed. The clusters clearly revealed overlapping between a number of data points derived from distinct postures. In addition, it was evident that the spatial distribution of some clusters was characterised by a high dispersion, particularly when considering the supine and lateral postures. This high spatial distribution observed in the clusters might be attributed to the fact that there were differences in the signals for some subjects, with particular reference to COP, dependent on whether the HOB increments were increasing or decreasing (Section 3.2.2 - Figure 3-15A). This is depicted by the closed and open symbols (raised and lowered HOB, respectively), and indicated as “first” and “second” in the legend. This was the case for supine, 20^{o} HOB and 40^{o} HOB postures.

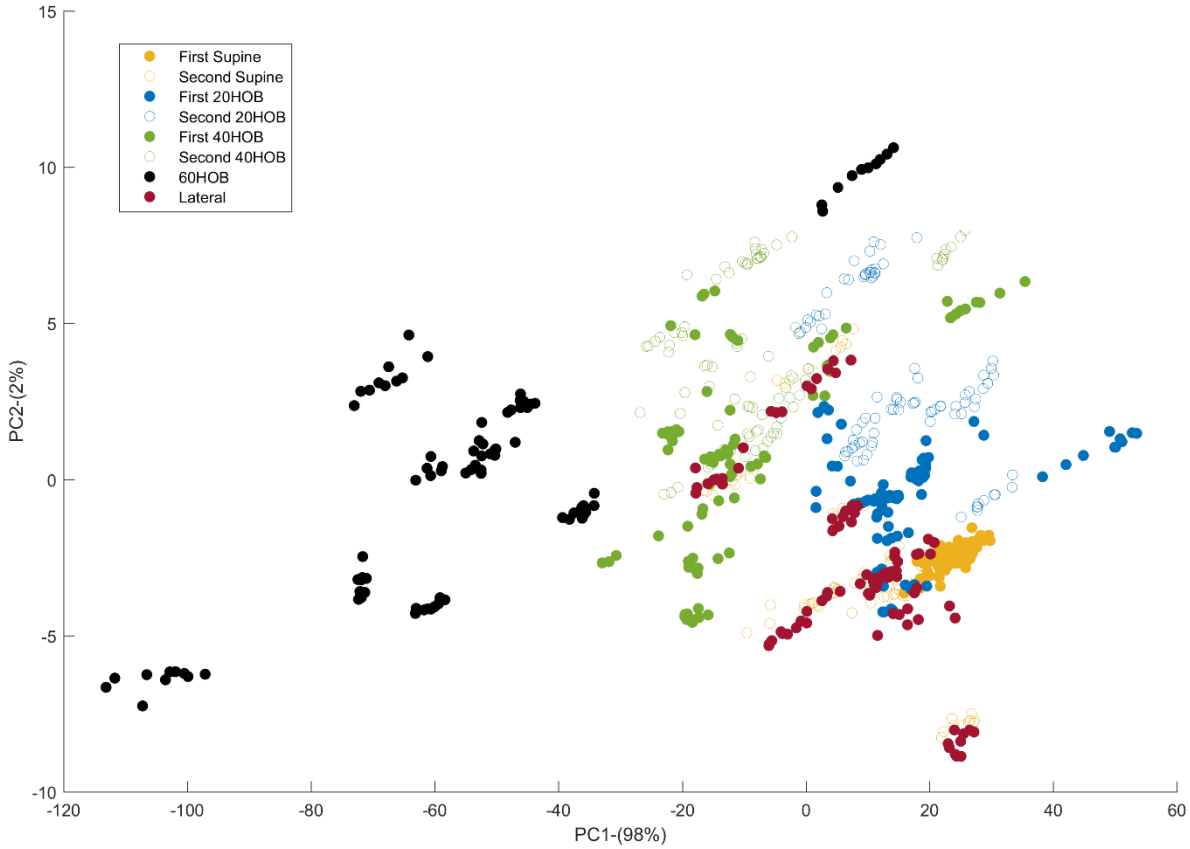

Figure 5-4: Data set involving contact area and COP at the whole body of 9 subjects (data set 1) projected onto the first two principal components, PC1 and PC2, with their corresponding variance in brackets. Each posture is represented by a coloured cluster of closed and open symbols, depending on whether the HOB was in the increasing or decreasing phase, respectively.

5.1.4 Results

5.1.4.1 Participants

Demographics of subjects from the new test group are summarised in Tables 5-1. Compared to the subjects in the previous training group which included relatively young individuals (Table 4-1), this cohort involves 4 male and 10 female of age ranging between 25 and 77 years. Nonetheless, the height, weight and BMI were similar between groups.

Table 5-1: Demographics of the training group of subjects.

Subject	Age	Sex	Height [cm]	Weight [kg]	BMI [kg/m^2]
1	44	F	176	79	26
2	25	F	171	80	27
3	77	M	191	108	30
4	36	F	160	55	21
5	30	F	156	64	26
6	35	M	167	62	22
7	34	M	185	117	34
8	54	F	160	90	35
9	35	M	181	90	27
10	61	F	164	63	23
11	60	F	161	67	26
12	28	F	164	60	22
13	61	F	147	63	29
14	40	F	172	65	22
Mean (SD)	44 (15.6)		168 (12.0)	75.9 (19.0)	27 (4.3)

5.1.4.2 Detecting changes in posture

To automate the detection of the changes in postures, a range of threshold values were examined for each subject, namely, 12%, 16%, 20% and 25% of the maximum derivatives for each subject. Accordingly, the number of detected events was determined for each threshold. Events detected in intervals including 10 data points were combined to represent a single event. The number of the detected events and the corresponding threshold values are detailed in Table 5-2 for all subjects supported on both the foam and the air cell mattresses.

Table 5-2: The influence of threshold values, derived from a percentage of the maximum corresponding derivative, identifying the number of events corresponding to the changes in posture performed on both foam and air cell mattress. The columns in red represent the threshold values and the corresponding number of detected events associated with the highest accuracy value.

	Foam mattress								Air cell mattress							
Subjects	**12%**	**Events**	**16%**	**Events**	**20%**	**Events**	**25%**	**Events**	**12%**	**Events**	**16%**	**Events**	**20%**	**Events**	**25%**	**Events**
1	0.013	4	0.017	3	0.021	3	0.027	2	0.006	2	0.008	2	0.010	2	0.013	2
2	0.007	2	0.009	2	0.011	1	0.014	1	0.104	4	0.138	3	0.173	3	0.216	2
3	0.018	2	0.023	2	0.029	2	0.037	1	0.066	6	0.088	3	0.110	2	0.138	1
4	0.018	4	0.024	4	0.030	4	0.038	4	0.005	3	0.007	3	0.008	3	0.010	3
5	0.019	2	0.025	2	0.032	2	0.039	2	0.037	2	0.049	2	0.061	2	0.077	1
6	0.007	2	0.010	2	0.012	2	0.015	2	0.014	3	0.018	3	0.023	3	0.028	3
7	0.026	2	0.035	2	0.044	2	0.055	2	0.015	2	0.019	2	0.024	2	0.030	2
8	0.030	2	0.040	2	0.050	2	0.062	2	0.037	2	0.049	2	0.062	2	0.077	2
9	0.017	2	0.022	2	0.028	1	0.035	1	0.012	5	0.016	4	0.020	4	0.024	2
10	0.007	2	0.009	2	0.012	2	0.015	2	0.018	2	0.025	2	0.031	2	0.038	2
11	0.020	2	0.026	2	0.033	2	0.041	2	0.030	2	0.040	2	0.050	2	0.063	2
12	0.007	2	0.009	1	0.011	1	0.014	1	0.063	2	0.084	2	0.105	2	0.131	1
13	0.030	2	0.039	2	0.049	2	0.062	2	0.019	2	0.025	2	0.032	2	0.040	2
14	0.033	2	0.044	2	0.055	2	0.069	2	0.037	2	0.049	2	0.060	2	0.077	1
Accuracy	93%		88%		81%		79%		83%		87%		86%		81%	

It is clear that the number of events was dependent on the threshold value for each subject on both mattresses. For example, with a threshold of 12% of the maximum derivative 2 events were detected in 12/14 subjects, corresponding with sagittal and lateral postural changes on the foam mattress. For the remaining two subjects, #1 and #4, 4 events were detected, as revealed for the latter subject in Figure 5-5. This showed consistent variations in magnitude, indicating other movements occurring during the static postures, representing a false positive result. When the threshold was increased, a reduced number of events was detected on the foam mattress, for some of the subjects, namely, #2, #9 and #12.

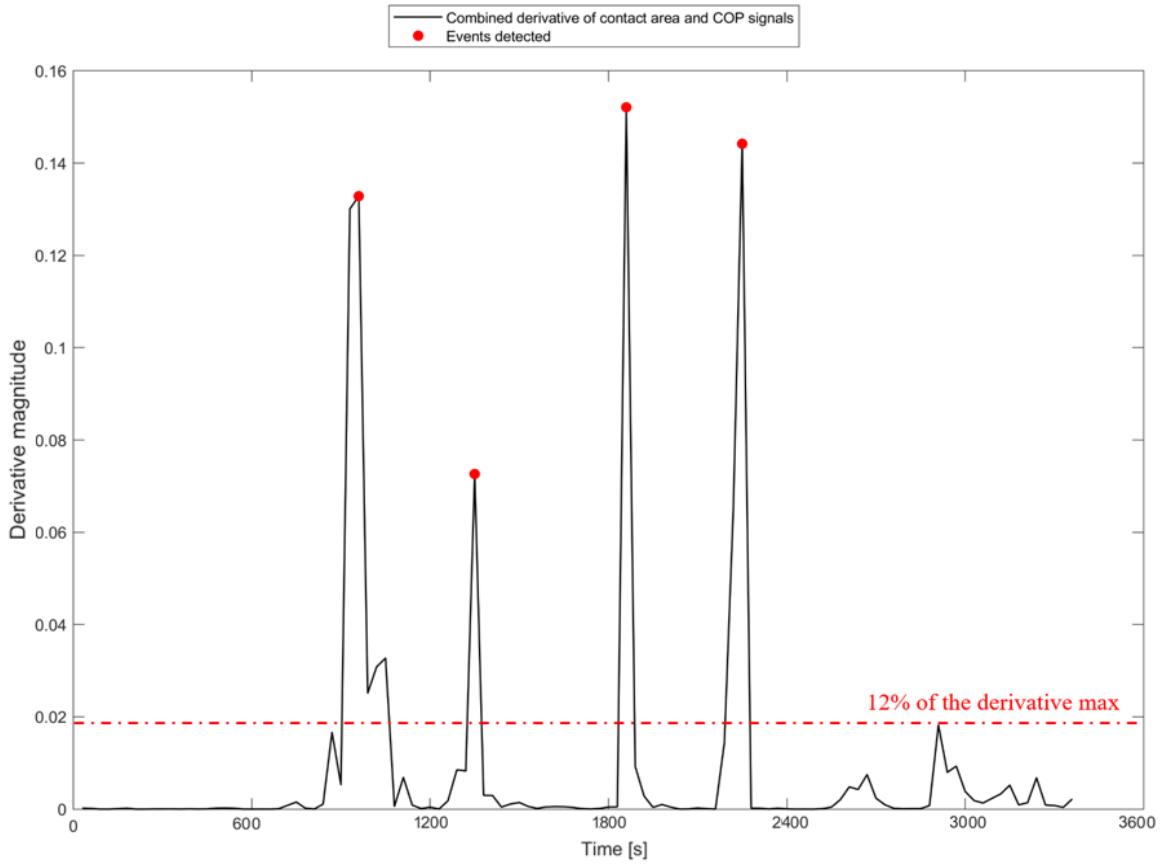

Figure 5-5: Composite derivative profile of subject #4 lying on the foam mattress, obtained by multiplying derivative signals of contact area and COP estimated for both parallel and perpendicular directions with respect to the axis of the sensing mat. The red markers represent the events detected when the derivative magnitude exceeded a threshold value estimated as the 12% of its maximum value.

For the air cell mattress, a higher threshold of 16% of the maximum derivative detected 2 events for 9/14 subjects. By contrast, 3 events were detected for subjects #2, #3, #4 and #6, corresponding to some other movements occurring during the static postures, representing a false positive. Four events were detected for subject #9, which are indicated as red dots in Figure 5-6, where consistent variations in derivative magnitude were observed during the static postures. It should be also be noted that immediately after the fourth event, a further event could

be detected as exceeding the threshold value (Figure 5-6). However, this event was not recognised due to the criteria adopted in which 10 data points were combined to represent a single event.

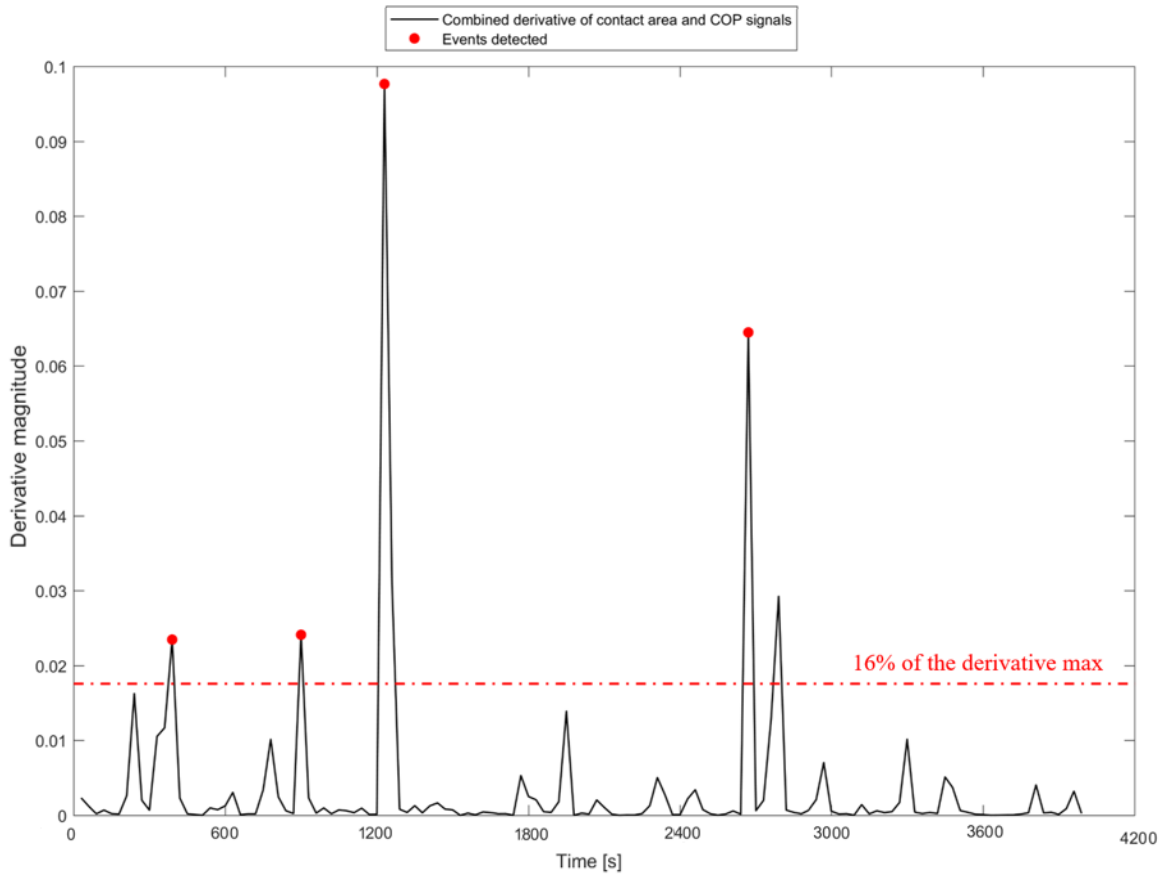

Figure 5-6: Composite derivative profile of subject #9 lying on the air cell mattress, obtained by multiplying derivative signals of contact area and COP estimated for both parallel and perpendicular directions with respect to the axis of the sensing mat. The red markers represent the events detected when the derivative magnitude exceeded a threshold value estimated as the 16% of its maximum value.

Following the identification of the postural change events with a threshold value of 12% and 16% for the foam and air cell mattresses respectively, the relevant signals from static postures were subjected to classification with the algorithms described in Section 4.1.6. The accuracy in correctly classifying the range of postures adopted on the two mattresses was assessed for each of the subjects.

5.1.4.3 Postures classification

When projected into the training PCs space (Figure 5-4), the test data points of all subjects showed three separate clusters, which were spatially distributed. These are shown for subject #1 in Figure 5-7, during the foam mattress test protocol. It is evident that there is overlapping of clusters for the 20^{o} HOB and 40^{o} HOB postures.

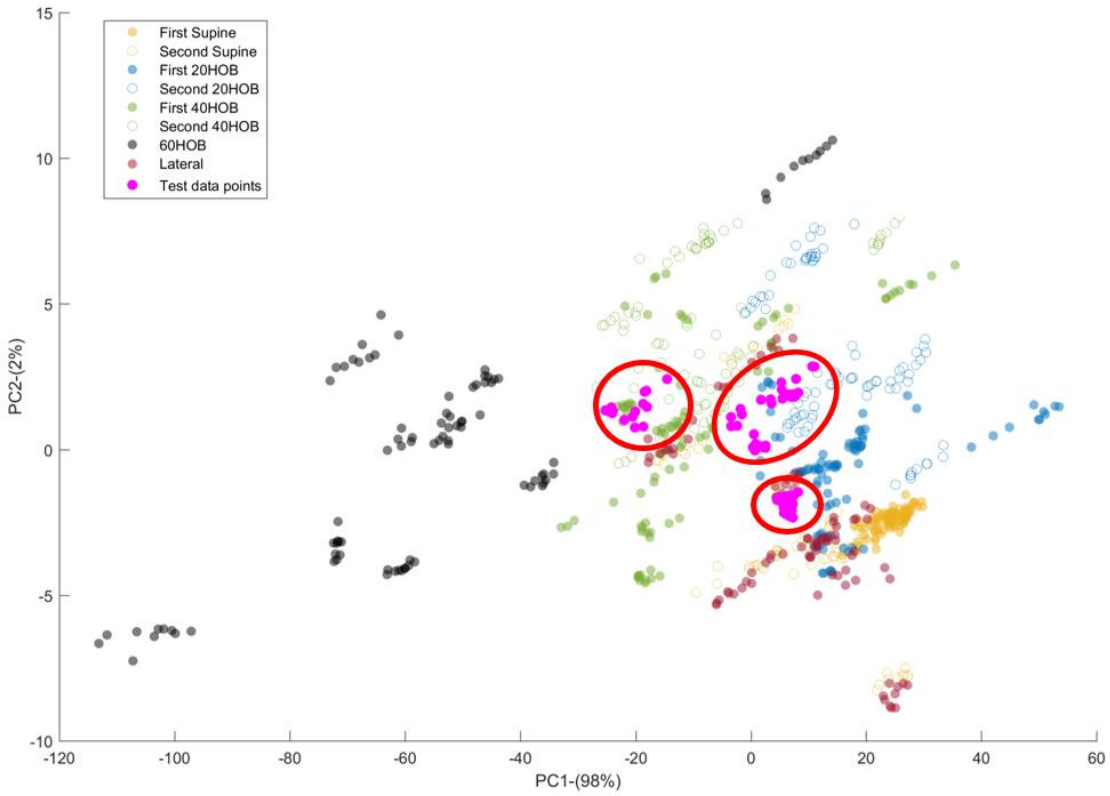

Figure 5-7: Signals of subject #1 (test data points in pink) projected onto the training PCs dimensional space. The test data points showed three separate clusters, circled in red, corresponding to the supine, lateral and high sitting postures.

The accuracy in postures classification was assessed for KNN with k=10, Naïve – Bayes and SVM with Gaussian kernel classifiers. The findings from the KNN classifier are summarised in Tables 5-3 and 5-4 for all subjects who adopted the postures on the foam and air cell mattresses, respectively. The corresponding accuracy with the Naïve – Bayes and SVM classifiers is detailed in Tables I-1 to I-3 in Appendix I. It is worth mentioning that the correct classification of high sitting posture, reported as HS in the tables, is associated with 40^{o} HOB. The relative accuracy in classifying each single posture was examined for all classifiers, although this was limited for SVM, due to its binary nature. It was evident that the total accuracy for all the three classifiers was characterised by a high variability between subjects. As an example, only 2 subjects revealed an accuracy >70% with the KNN classifier, for postures adopted on both mattresses. Lower accuracy values were evident when the classification was performed with both Naïve – Bayes and SVM classifiers on both support surfaces. The difference in performance between the classifiers was particularly marked when identifying the supine and high sitting postures. Indeed, these were generally classified as the lateral posture by both Naïve – Bayes and SVM classifiers (Tables I-1 to I-3 – Appendix I). By contrast, KNN detected high sitting with a reasonable level of accuracy. For each of the three classifiers, the lateral posture was detected for the majority of the individuals with a higher level of accuracy e.g. Table 5-3 and Table 5-4.

Table 5-3: Percentage accuracy for KNN classifier in classifying the range of postures on the foam mattress. For each subject the total accuracy is reported in addition with the accuracy in correctly classifying each static posture (in bold). It also includes the complementary percentage values which were misclassified for each of the static posture in bold.

		Accuracy [%] – Foam mattress														
		KNN (*k* = 10)														
Subjects	**Postures sequence**	**Supine**	20HOB	40HOB	60HOB	Lateral	Supine	20HOB	**HS**	60HOB	Lateral	Supine	20HOB	40HOB	60HOB	**Lateral**	**Total**
1	HS, Sup, Lat	**42**	30	3	18	6	0	0	**81**	0	19	0	0	0	32	**68**	**60**
2	Lat, Sup, HS	**0**	0	55	45	0	0	100	**0**	0	0	0	0	0	0	**100**	**29**
3	HS, Lat, Sup	**6**	0	0	0	94	0	0	**0**	33	67	0	0	100	0	**0**	**2**
4	Lat, HS, Sup	**0**	3	0	0	97	10	66	**14**	10	0	0	0	100	0	**0**	**4**
5	Lat, HS, Sup	**0**	0	0	0	100	0	0	**55**	0	25	0	0	0	0	**100**	**52**
6	HS, Sup, Lat	**0**	0	0	11	89	0	0	**100**	0	0	0	0	100	0	**0**	**34**
7	Lat, HS, Sup	**0**	0	0	0	100	0	0	**0**	0	100	0	97	3	0	**0**	**0**
8	Lat, HS, Sup	**82**	3	6	9	0	0	3	**36**	0	61	0	0	5	0	**95**	**68**
9	HS, Sup, Lat	**0**	0	0	0	100	0	0	**86**	0	14	0	0	0	0	**100**	**63**
10	Lat, Sup, HS	**0**	52	0	25	23	0	0	**53**	0	47	0	0	0	7	**93**	**44**
11	HS, Sup, Lat	**0**	0	0	64	36	0	13	**87**	0	0	0	0	0	30	**70**	**49**
12	Lat, Sup, HS	**0**	0	0	96	4	0	21	**79**	0	0	0	0	0	0	**100**	**65**
13	Lat, HS, Sup	**100**	0	0	0	0	0	0	**86**	0	14	0	0	0	0	**100**	**95**
14	Lat, HS, Sup	**26**	32	10	22	10	0	0	**100**	0	0	0	0	0	0	**100**	**78**

Table 5-4: Percentage accuracy for KNN classifier in classifying the range of postures on the air cell mattress. For each subject the total accuracy is reported in addition with the accuracy in correctly classifying each static posture (in bold). It also includes the complementary percentage values which were misclassified for each of the static posture in bold.

		Accuracy [%] – Air cell mattress															
		KNN (*k* = 10)															
Subjects	**Postures sequence**	**Supine**	20HOB	40HOB	60HOB	Lateral	Supine	20HOB	**HS**	60HOB	Lateral	Supine	20HOB	40HOB	60HOB	**Lateral**	**Total**
1	Sup, HS, Lat	**0**	34	53	13	0	0	15	**85**	0	0	0	0	0	0	**100**	**77**
2	Lat, Sup, HS	**17**	3	10	17	53	0	10	**90**	0	0	31	13	12	22	**22**	**43**
3	Lat, HS, Sup	**8**	31	25	33	3	0	47	**14**	33	6	50	9	0	9	**32**	**18**
4	HS, Lat, Sup	**0**	63	21	0	16	0	4	**0**	74	22	32	65	0	3	**0**	**0**
5	Sup, Lat, HS	**15**	0	3	15	68	0	6	**47**	0	47	36	0	64	0	**0**	**19**
6	HS, Sup, Lat	**14**	28	27	3	28	0	50	**31**	0	19	0	0	0	21	**79**	**44**
7	Lat, HS, Sup	**0**	0	0	0	100	0	0	**61**	0	39	0	0	100	0	**0**	**24**
8	Sup, Lat, HS	**3**	0	75	15	6	0	0	**75**	0	25	0	0	57	0	**43**	**42**
9	HS, Sup, Lat	**7**	29	12	32	20	0	0	**84**	16	0	0	0	0	70	**30**	**31**
10	Sup, Lat, HS	**65**	0	0	0	35	0	32	**53**	0	15	15	0	85	0	**0**	**38**
11	Sup, HS, Lat	**0**	10	0	42	48	0	11	**89**	0	0	0	0	0	0	**100**	**65**
12	Sup, HS, Lat	**0**	0	0	0	100	0	35	**55**	0	35	0	10	24	61	**15**	**25**
13	HS, Lat, Sup	**0**	0	0	0	100	0	0	**48**	0	52	26	0	56	0	**18**	**22**
14	Sup, Lat, HS	**58**	0	6	0	36	0	0	**50**	0	50	0	0	0	0	**100**	**70**

5.1.5 Appraisal of the classifier performance

The present analysis incorporated the methodology based on combined derivatives of interface pressure signals and three distinct machine learning algorithms to identify postural changes and classify static postures, respectively. To test the machine learning algorithms, a new test data set from 14 individuals was applied to the training model, which involved lying postures adopted on two different support surfaces in a random sequence.

The combined derivative of contact area and COP resulted in accurate detection of events associated with postural changes on foam and air cell support surfaces for 12 and 9 subjects, respectively. This was supported by a subject – specific threshold approach from the composite derivative. There were some differences between surfaces, with a higher threshold necessary to accurately detect the change in posture events on the air cell mattress. However, results were also dependent on the sequence of the postures performed.

The accuracy in classifying the range of postures for each classifier was characterised by a high inter-subject variability, regardless of support surface, which was influenced by the following factors:

i) The differences in the signals, particularly associated with COP, was dependent on whether the increment of the HOB angles was in the increasing or decreasing phase. This resulted in clusters in the training model (Figure 5-4) characterised by a considerable spatial distribution;
ii) The principles underpinning the individual classifiers i.e. probability or Euclidean distance (Section 4.1.6);
iii) The variability in the magnitude of the test signals which, associated with the above two factors, contributed to a high proportion of misclassified postures.

The variability in signal changes is exemplified in Figure 5-8, which illustrates the magnitude of the COP signals estimated in both directions with two subjects (#9 and #11) performing an identical sequence of postures on the foam mattress. It is clear that the COP signals in the parallel direction showed significant differences in magnitude during the high sitting posture. By contrast, COP in the perpendicular direction demonstrated either negative or positive magnitudes in the lateral posture for the two subjects. When two subjects (#9 and #10) performed a different sequence of postures on the foam mattress, the changes in the signals magnitude are illustrated in Figure 5-9. It reveals a considerable variability in the change of COP displacements. In a similar manner, a considerable variability was evident with the contact area signals (data not shown).

These findings highlight the importance of the order of adopted postures when estimating the predictive potential of the classifiers. Although lateral posture was achieved differently between training and test data sets, a high number of points were classified as lateral, resulting in some

misclassifications. This may be explained by the fact that the cluster of lateral posture is characterised by a high distribution in the training PC space (Figure 5-4), with overlapping of the training data points associated with supine and high sitting.

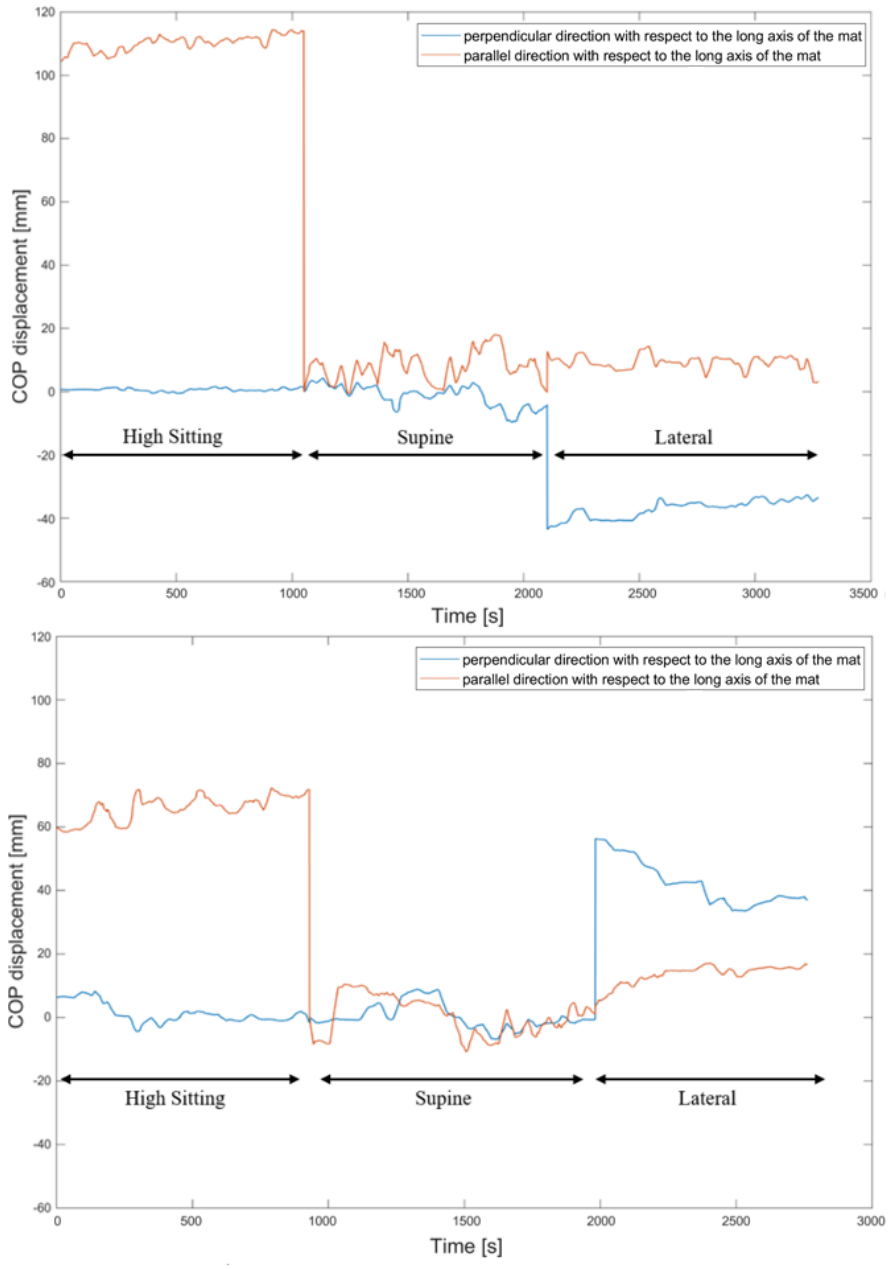

Figure 5-8: COP signals estimated in both parallel (curve in orange) and perpendicular (curve in blue) directions with respect to the long axis of the pressure mat for two subjects (top: Subject #9; bottom: Subject #11). Both subjects performed an identical sequence of postures on the foam mattress.

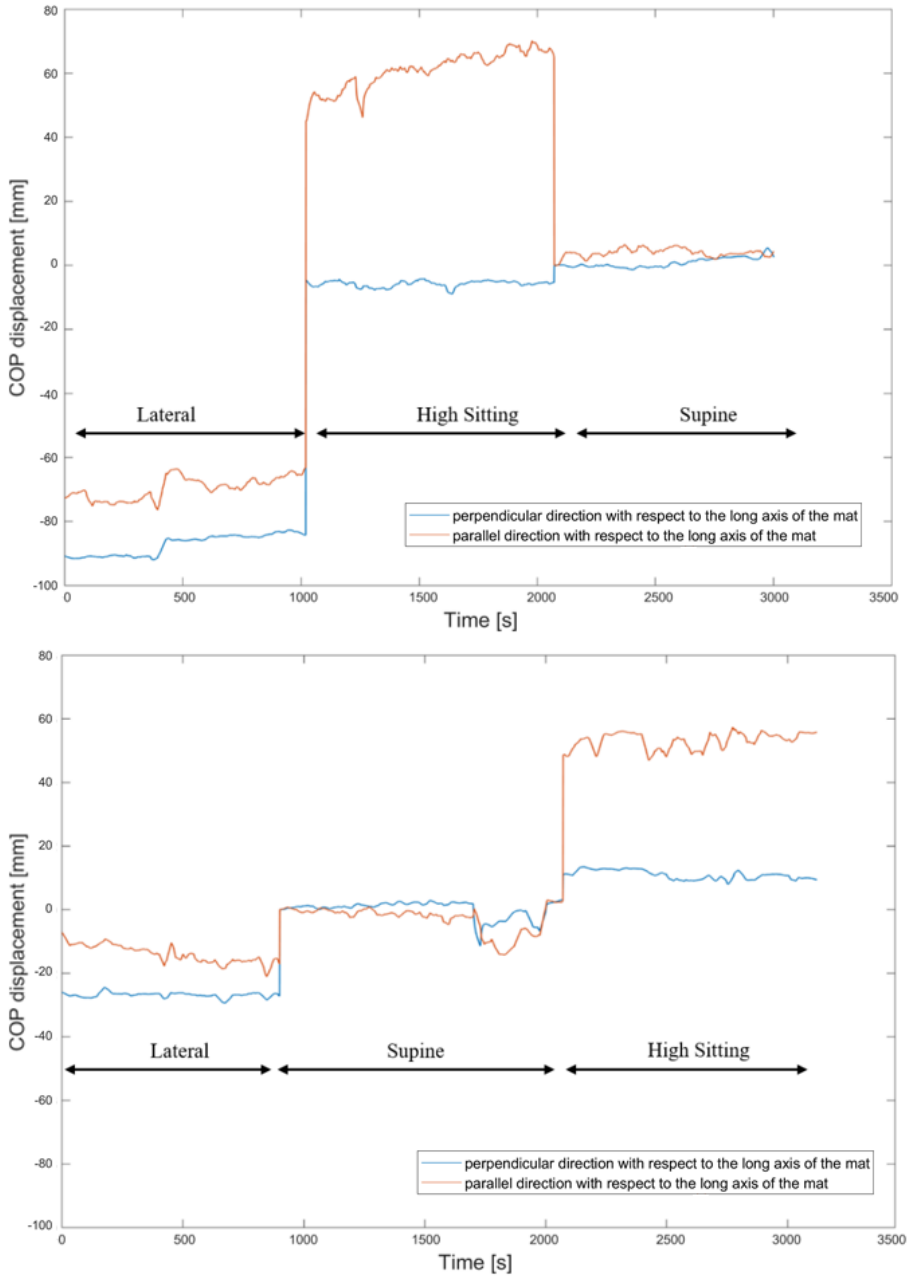

Figure 5-9: COP signals estimated in both parallel (curve in blue) and perpendicular (curve in red) directions with respect to the long axis of the pressure mat for two subjects (top: Subject #9; bottom: Subject #10). Both subjects performed a different sequence of postures on the foam mattress.

Although the posture sequence for all the subjects was randomised, three subjects (#2, #7 and #9) performed an identical order in postures on two mattresses. A direct comparison revealed some differences in identifying postural changes between surfaces. This is illustrated in Figure 5-10 for subject #9. The contact area signal derived from the foam mattress (green curve) revealed distinct changes in magnitude associated with the postural changes. By contrast, the corresponding signal from the air cell mattress (yellow curve) demonstrated a reduced sensitivity during postural changes. The signals were clearly affected by the cyclic nature of the

air mattress. Accordingly, this would affect the spatial distribution of the test data points with a resulting decrease in the accuracy of classification on the air cell mattress.

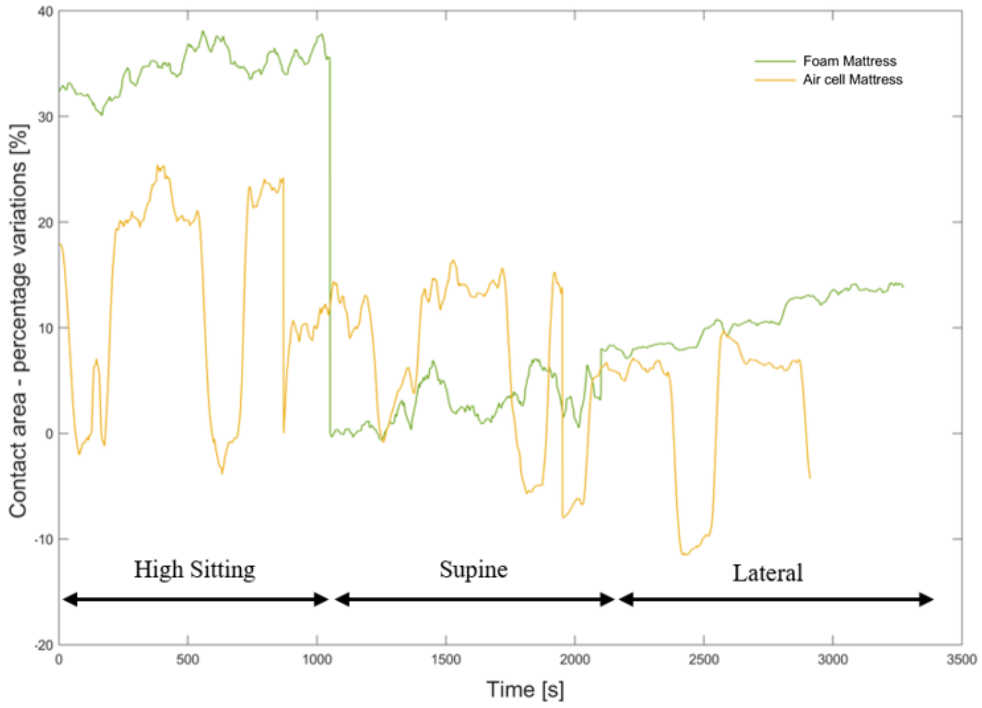

Figure 5-10: Comparison of contact area signals referred to the same subject (#9) who performed an identical sequence of postures on both foam mattress (curve in green) and air cell mattress (curve in yellow).

In the light of these results, there was a need to develop training models with an improved consideration of random postures and support surface selection, which are typically encountered in clinical settings. Thus, the pressure signals from the 14 subjects (Table 5-1), who adopted postures in a random order on both mattresses, were utilised to develop two new training models.

5.2 Evaluation of predictive models based on random sequence of postures

5.2.1 Models derived from signals of postures adopted on different support surfaces

Signals were subjected to analysis and then projected into the PC dimensional space, as illustrated in Figures 5-11 A and B for foam and air cell mattress, respectively.

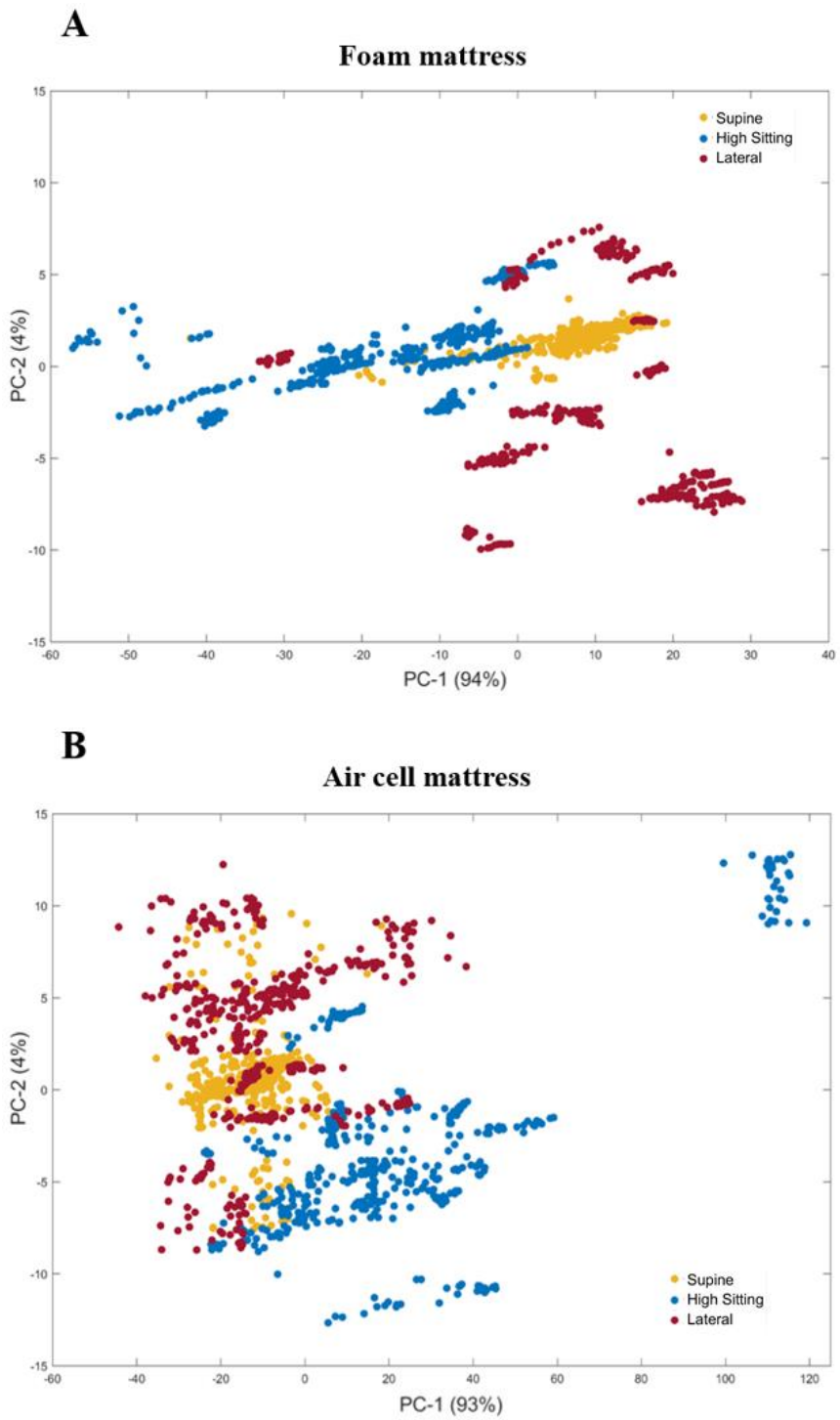

Figure 5-11: Dimensional space of the principal components, PC1 and PC2 with their corresponding variance in brackets, incorporating the signals of contact area and COP corresponding to 14 subjects who performed a range of random postures on a foam mattress (Figure A, top) and air cell mattress (Figure B, bottom) are projected.

Both models clearly reveal clusters of points characterised by high spatial distribution and a degree of overlapping. Both features can be attributed to the random order in which the postures were adopted and variability between subjects. In order to reduce the variability between subjects, the signals of contact area and COP for each subject were normalised with respect to the corresponding root mean square value (RMS) before projecting onto the PC space.

However, by examining the clusters, it was evident that lateral posture magnitudes were strongly influenced by the sequence in which the postures were conducted. Thus, a further normalisation step was introduced, involving the inverse of the absolute value of the signals corresponding to lateral postures. Figures 5-12A and B represents PC1 and PC2 for all subjects (n=14), who adopted the range of postures on foam and air cell mattress, respectively.

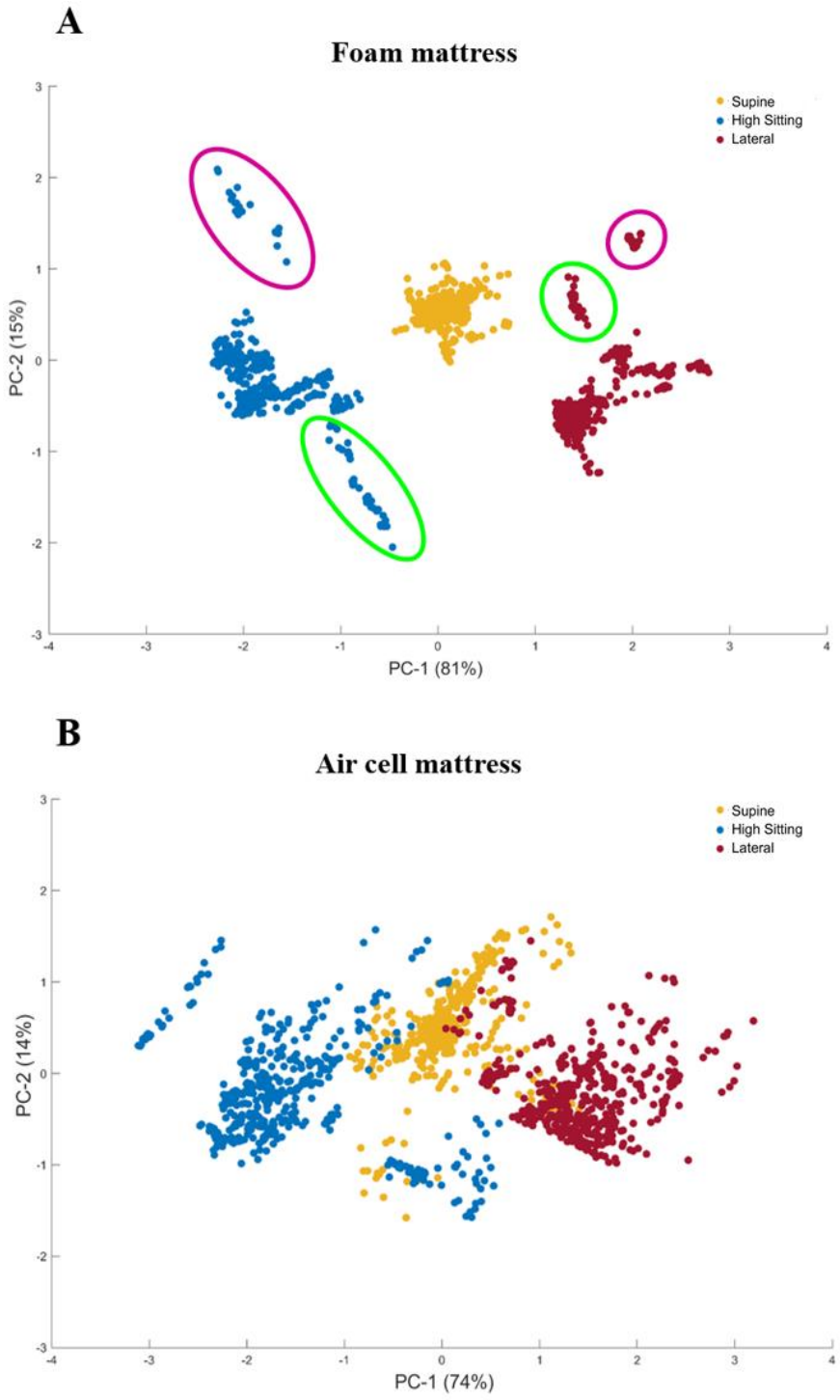

Figure 5-12: Dimensional space of the principal components, PC1 and PC2 with their corresponding variance in brackets, where the normalised signals of contact area and COP corresponding to 14 subjects who performed a range of random postures on a foam mattress (Figure A, top) and air cell mattress (Figure B, bottom) are projected.

It was evident that these normalisation processes resulted in a distinct reduction in the spatial distribution of each cluster, such that each was clearly differentiated in the case of the foam mattress (Figure 5-12A). However, close examination of the individual data for subjects #4 and #14 resulted in points away from the clusters centres, associated with high sitting and lateral posture, as indicated in Figure 5-12A, where are circled in pink and green, respectively.

By contrast, the model involving the air cell mattress still revealed overlapping and high spatial distribution of clusters (Figure 5-12B). Nevertheless, both features were reduced when compared to the pre – normalisation case (Figure 5-11B). Although the model of postures adopted on the air cell mattress demonstrated limitations as a training model, there are many clinical situations in which air cell support surfaces are used, particularly in individuals deemed to be at high risk of developing pressure ulcers. It is therefore important to determine whether the training model of the postures adopted on the foam mattress is also able to accurately classify postures adopted on a different mattress. This was evaluated for the KNN, Naïve Bayes and SVM classifiers.

5.2.2 Classification of postures with the new normalised model

The accuracy of all classifiers was investigated for the 14 subjects, who adopted the range of static postures in a random order on the air cell mattress. The accuracy for the KNN classifier was examined for *k* values from 1 to 450. The results, as illustrated in Figure 5-13, revealed that within subjects there was variation ranging from approximately 10% (subject #4) to 40% (subject #10). It was also evident that the trends in accuracy with the *k* values varied between subjects. Thus, for subject #10 higher *k* values were associated with a higher accuracy, while for subject #6 the reverse trend was observed. A *k* value of 100 was selected to perform the KNN algorithm, as it was generally associated with relatively high accuracy across the cohort of test subjects.

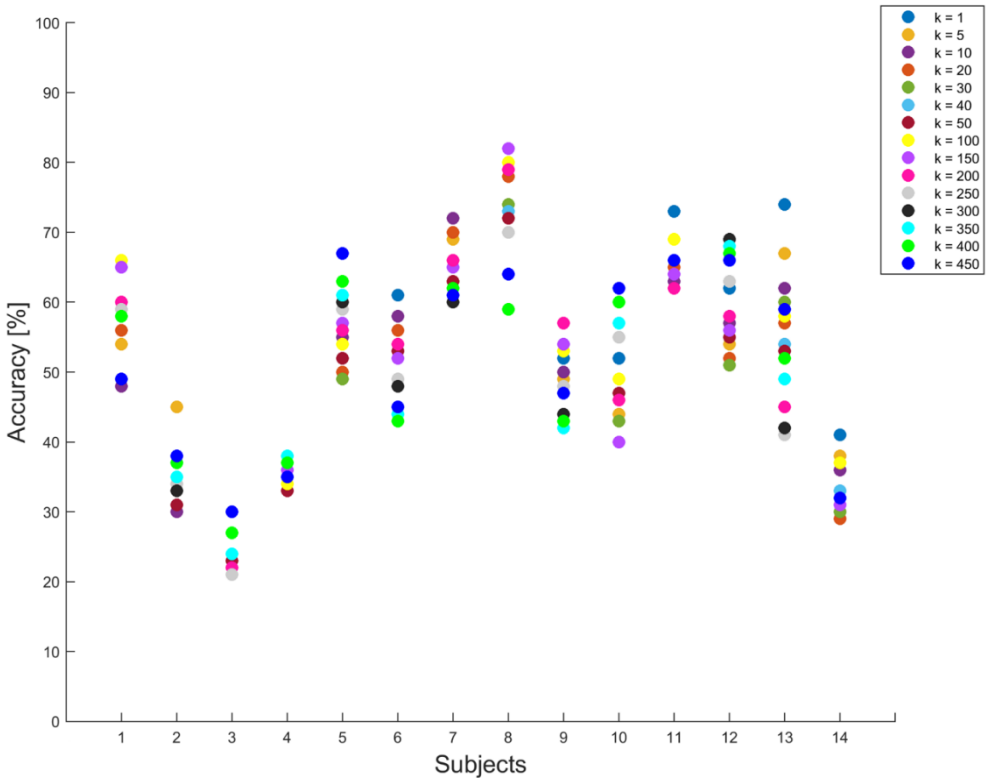

Figure 5-13: Percentage accuracy in classifying postures adopted on the air cell mattress with the KNN classifier for different *k* values for all subjects to test.

The accuracy for the three classifiers is summarised in Table 5-5. It was evident that the accuracy for each subject is higher for both Naïve – Bayes and SVM classifiers compared with KNN. Indeed, with respect to the former two classifiers, the accuracy was 100% for some subjects. By contrast, the accuracy for the KNN classifier ranged between 24% and 88%. Such low values could be attributed to both the spatial distribution of the test points with respect to the corresponding cluster and the principle underpinning the algorithm with k=100.

Table 5-5: Percentage accuracy in correctly identifying the range of postures with KNN (k = 100), Naïve – Bayes and SVM classifiers, adopted on the air cell mattress by using a training model of postures adopted on the foam mattress.

	Accuracy [%]		
Subjects	**KNN (*k* = 100)**	**Naïve – Bayes**	**SVM**
1	73	100	98
2	37	81	84
3	24	89	78
4	38	75	50
5	59	99	100
6	60	91	94
7	69	86	100
8	88	100	96
9	59	96	91
10	57	100	100
11	77	100	100
12	65	100	100
13	65	100	100
14	34	70	100
Average	58	92	92
Range	24 - 88	70 - 100	50 - 100

5.2.3 Translation to data not supported by previous knowledge of postures adopted

The previous analysis demonstrated the success of a normalisation step with respect to the RMS, in reducing the variability in the signals, providing a training model of postures with distinct clusters (Figure 5-12A). This model was also influenced by normalisation with respect to both supine and lateral postures.

However, clinical data are not often supported by prior knowledge of the postures adopted, which increases the difficulties in normalising the corresponding signals. Thus, there is a need for a classification process which precedes the normalisation step, to establish the order of the postures and support their labelling. Accordingly, an algorithm of classification which utilises a more sophisticated form of learning i.e. deep learning, was introduced in the present analysis. This uses the intensity of the pixel values, corresponding to values in the pressure distribution, to perform image classification.

5.2.4 Models for classifying images: introduction to convolutional neural networks

In addition to conventional machine learning algorithms for classification, there are more sophisticated algorithms, namely deep learning, based on artificial neural networks. A class of deep neural networks is represented by the convolutional neural network (CNN) algorithm, which is widely used in various research fields, including image, pattern and speech recognition (Abdel-Hamid et al. 2014, Zhou et al. 2017, Wang et al. 2019), and yields high values of accuracy.

Artificial neural network algorithms are inspired by biological neural networks, simulating the way in which a neuron is connected, perceives input signals from its dendrites and produces output along its axon (Figure 5-14). The frequency of the signal is regulated by an activation function, transmitted to the adjacent neurons through synapsis.

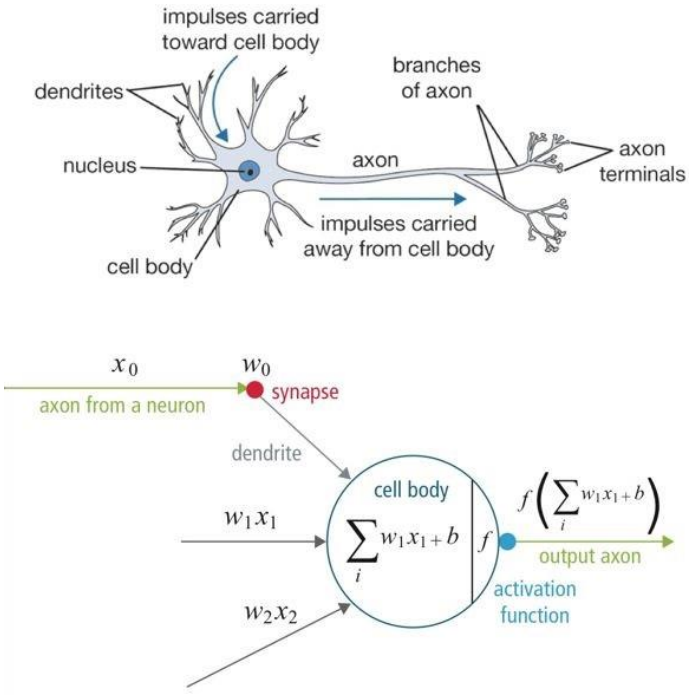

Figure 5-14: Schematic of a biological neuron (top) and the corresponding mathematical model implemented in the Convoluted Neural Network (bottom) (Figure adapted from Hijazi et al. (2015)).

A CNN consists of multiple layers of feature – detecting neurons. In particular, it consists of an input layer, which corresponds with the pixel values which range between 0 and 255, of a series of images, as well as hidden layers. Each of these layers process different combinations of input from the previous layer, gradually extracting higher – level features. The most common four types of layers are termed convolution, pooling, non – linear and fully connected layers.

A number of processes are typically involved in creating the CNN algorithm, namely:

1. The input layer holds the raw pixel values of the series of images. The grey scale images corresponding to pressure distribution were of W x H x D where D is the number of colours channels, which are 3 for RGB images and 1 for grey scale images;
2. The convolution layers extract different features from the input layer. Here, the input images are convoluted with H kernels of k x k x D where D is the number of the colour channels. Starting from the top left corner, each kernel moves from the left to the right, n elements at a time (stride). Once the top right corner is reached, the kernel moves in a downward direction, again moving from left to right. Sometimes it is convenient to pad the dimension of the input image with zeros around the border. After the convolution, each feature in the output will contain (W-k+1) x (H-k+ 1) x H. If the stride >1 each feature will contain ((W-k+1) – stride) x ((H-k+1) – stride) x H;
3. The pooling layers reduce the resolution of the features. The input is divided into two dimensional space (2x2) non-overlapping (stride = 2). There are 2 pooling methods, which consist of calculating either the maximum or the average of the 4 values in the region;
4. The non – linear layer is typically applied after the convolution layer and it is referred to as an activation function, commonly termed the Rectified Linear Unit Layer (ReLU), which is designed to simulate whether the biological neuron is activated or not. ReLU sets any negative pixel values to a value of 0;
5. The fully connected layers are usually used as a final layer of the CNN and connect, through a multiplication and accumulation process, every feature of all layers to determine each element of each class.

The architecture of the CNN used in the present analysis is illustrated in Figure 5-15. The input layer is represented by a grey scale image of 118x48x1, representing the height, width and the number of colour channels, respectively. The first convolution, which typically detects low – level features such as edge, lines or corners, applies 8 kernels of 5x5x1 with a stride of 1, resulting in 8 features maps of 114x44, activated by a ReLu. The following max pooling of size 2x2 and stride of 2 provided a down-sampling to 57x22x8 of the feature maps after convolution. A further convolution was applied, which extracts higher level features such as shape or objects, which was followed by ReLu and max pooling. This is followed by the application of dropout, a technique that randomly ignores units (along with their connections) from the neural network during training to prevent overfitting. In the fully connected layers, all layers were flattened and activated. Another dropout was applied to prevent overfitting. Before prediction, a softmax activation function was used to normalise the output.

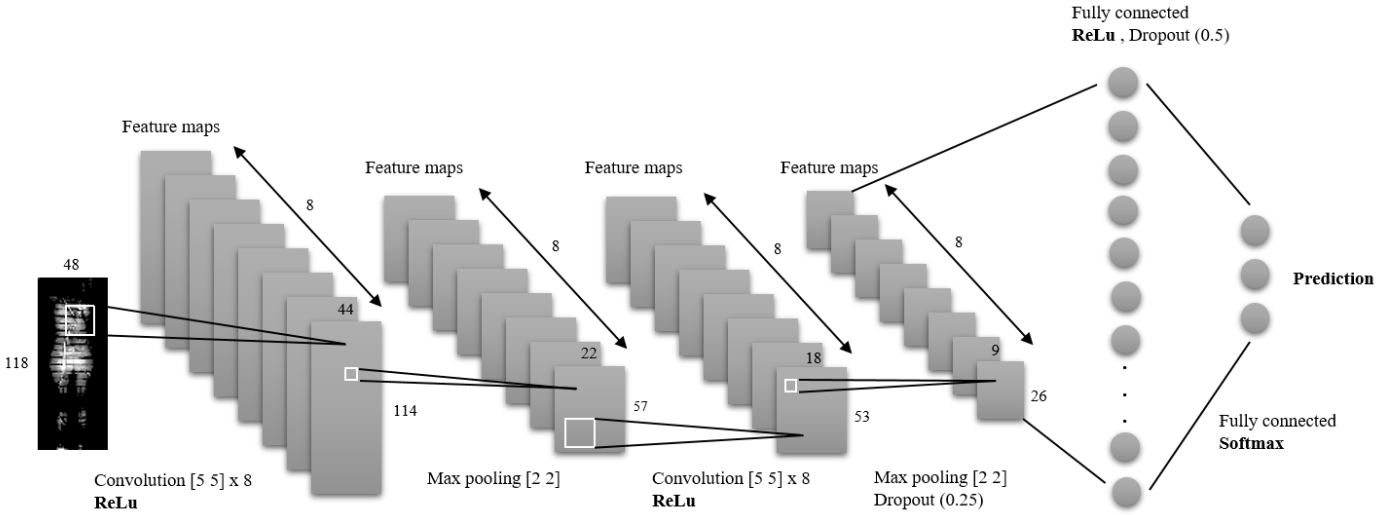

Figure 5-15: Illustration of the architecture of CNN used to predict postures adopted on sagittal and transverse planes.

CNN was implemented to create predictive models based on grey scale images corresponding to the pressure distributions during postures adopted on both the foam and air cell mattress. The accuracy of both models was evaluated via a cross – validation technique. The models were trained with data from 13 of the 14 subjects in the cohort, who were randomly selected. The data of the excluded subject were then tested and the accuracy in the classification was assessed. This process was repeated for each individual who has been used to test the trained models and the accuracy of CNN in classifying their corresponding postures was assessed.

5.2.5 Convolutional neural network algorithm for images classification: cross – validation

Results of the cross – validation showed an accuracy ranging between 40% - 100% and 33% - 97% for postures adopted on the foam (Table 5-6) and air cell mattress (Table 5-7), respectively. Both ranges of accuracy showed a high variability between subjects, with only few of them yielding an accuracy value >70%. The relative accuracy revealed high number of misclassifications in identifying the supine posture on the air cell mattress (Table 5-7). By contrast, both high sitting and lateral postures on this mattress were correctly classified in the vast majority of individuals.

Classification on the foam mattress (Table 5-6) revealed 4 subjects, who showed a high percentage of misclassification i.e. > 40% for supine posture. This was mainly classified as high sitting, with the only exception of subject #13. Moreover, half of the subjects revealed a high percentage of misclassification in detecting both high sitting and lateral postures. In both cases, high sitting was mainly classified as supine, with the exception of subjects #3 and #13, for whom high sitting was classified as lateral (Table 5-6).

Table 5-6: Percentage accuracy in classifying the range of postures adopted on the foam mattress via cross-validation. For each subject, who has been used to test the trained model with 13 of the 14 subjects, total accuracy is reported in addition to the relative accuracy in correctly classifying each static posture (in bold). It also includes the complementary percentage values which were misclassified for each of the static posture.

	Accuracy [%]									
Subjects	**Supine**	HS	Lateral	Supine	**HS**	Lateral	Supine	HS	**Lateral**	**Total**
1	**100**	0	0	0	**100**	0	0	0	**100**	**100**
2	**48**	38	14	37	**47**	16	31	28	**41**	**45**
3	**42**	34	24	9	**19**	72	18	24	**58**	**40**
4	**100**	0	0	22	**78**	0	91	9	**0**	**50**
5	**100**	0	0	19	**81**	0	0	0	**100**	**94**
6	**100**	0	0	0	**100**	0	100	0	**0**	**62**
7	**6**	94	0	0	**100**	0	0	0	**100**	**69**
8	**91**	9	0	0	**86**	14	0	0	**100**	**92**
9	**100**	0	0	95	**5**	0	100	0	**0**	**43**
10	**100**	0	0	100	**0**	0	0	0	**100**	**69**
11	**100**	0	0	0	**100**	0	0	0	**100**	**100**
12	**100**	0	0	0	**100**	0	100	0	**0**	**69**
13	**58**	0	42	0	**0**	100	0	0	**100**	**56**
14	**100**	0	0	88	**12**	0	100	0	**0**	**61**

Table 5-7: Percentage accuracy in classifying the range of postures adopted on the air cell mattress via cross-validation. For each subject, who has been used to test the model trained with 13 over the 14 subjects, total accuracy is reported in addition with the relative accuracy in correctly classifying each static posture (in bold). It is also reported the complementary number of points belonging to the static posture in bold, which were misclassified.

	Accuracy [%]									
Subjects	**Supine**	HS	Lateral	Supine	**HS**	Lateral	Supine	HS	**Lateral**	**Total**
1	**24**	3	73	0	**100**	0	0	0	**100**	**70**
2	**34**	66	0	0	**100**	0	0	0	**100**	**76**
3	**88**	0	12	0	**100**	0	0	0	**100**	**97**
4	**0**	0	100	0	**95**	5	0	100	**0**	**28**
5	**94**	6	0	0	**100**	0	0	0	**100**	**98**
6	**0**	0	100	0	**100**	0	0	0	**100**	**64**
7	**0**	0	100	0	**0**	100	0	0	**100**	**33**
8	**0**	100	0	0	**100**	0	0	0	**100**	**62**
9	**78**	19	3	0	**100**	0	0	0	**100**	**93**
10	**0**	0	100	0	**100**	0	0	0	**100**	**62**
11	**0**	100	0	0	**100**	0	0	0	**100**	**62**
12	**88**	0	13	100	**0**	0	0	0	**100**	**58**
13	**31**	0	69	0	**100**	0	0	0	**100**	**78**
14	**0**	0	100	0	**0**	100	0	0	**100**	**35**

5.3 Discussion

This study has improved the methodology based on the combination of the derivative of pressure signals and machine learning algorithms for the detection of both the frequency and magnitude of a range of postures adopted in a random sequence on two support surfaces. It revealed that the combined derivative of COP and contact area signals was able to accurately detect the frequency of postural changes in the majority of subjects (Table 5-2), regardless of the support surface. However, the training model described in Chapter 4 and illustrated in Figure 5-4, utilising data from postures prescribed in a pre-determined order, was limited in classifying the new data set of postures randomly allocated on two support surfaces (Tables 5-3 and 5-4, Tables I-1 to I-3 Appendix I).

A number of factors could be attributed to these findings, namely,

1. Clusters in the training model characterised by a high dispersion in the spatial distribution, with respect to supine and lateral postures (Figure 5-4). This could be attributed to the difference in the signals based on whether the increments in HOB angles were increasing or decreasing (Figure 3-15A);

2. Differences in achieving lateral posture, which involved automatic lateral turning for the training model and manual repositioning for the test data. Indeed, differences have been revealed between the two manoeuvres in a previous study in the host laboratory (Woodhouse et al. 2015);
3. Variability in the magnitude of the test signals due to the random sequence of postures, which affected their spatial distribution (Figures 5-8 and 5-9), leading to a significant proportion of misclassified postures;
4. Variability in the test signals associated with the two support surfaces (Figure 5-10).

Combining these findings identified a need to modify the algorithm for predicting posture and movements to establish training models which accommodate different support surfaces and random postures (Figures 5-11A and B). To account for this variability, a normalisation process was used to reduce the spatial distribution of the pressure-related signals. The resulting predictive model of signals associated with postures on the foam mattress resulted in a distribution of data points characterised by separate clusters (Figure 5-12A). By contrast, the model of postures adopted on the air cell mattress still revealed a degree of overlapping between the clusters of points (Figure 5-12B). Accordingly, the latter was not considered in subsequent analysis.

Normalisation represents an important step in data processing as it facilitates the comparison between data sets affected by a high variability, by re-scaling their magnitude. Although there are many indicators of variability in the data, there is a lack of guidance in the literature as to a standard means of normalisation. As an example, the range, standard deviation or root mean square (RMS) are all considered reliable indicators of variability and used for normalisation, depending on the nature of the data (Jacobs and Ferris 2015, Ghazwan et al. 2017). Given the non-linearity of the pressure related signals (Section 3.2.4), the RMS proved successful in reducing signal variability, thus providing the means to improve the accuracy in classification. Indeed, RMS normalisation has allowed the re-scaling of the signal magnitude to a specific range, thus emphasizing the differences in the magnitudes between the postures in the different anatomical planes. This resulted in clusters of data points without overlap (Figure 5-12A), as opposed to the model of signals prior to normalisation (Figure 5-11A). The model proved fairly efficient in classifying of a range of postures adopted on the air cell mattress (Table 5-5).

Close examination of the individual data revealed two subjects, namely, subjects #4 and #14, having data points at a distance from the clusters centres, associated with high sitting and lateral postures, as indicated in Figure 5-12A. It was interesting to note that these subjects presented with the lowest BMI of the cohort (Table 5-1). There is no evidence in the current literature that low BMI affects the movement patterns of individuals. However, evidence has been reported of a correlation between low BMI and PU occurrence (Kottner et al. 2011, Tsaousi et al. 2015). It might be hypothesised that a low ratio between weight and height might influence the

magnitude of some pressure related parameters, as an example contact area, whose magnitude is highly dependent on the individuals silhouette.

As discussed in Chapter 4, a number of studies have applied machine learning algorithms to classify both lying and sitting postures, utilising snap shots of features estimated from the pressure distribution (Table 4-10). Moreover, neither of these studies have examined a random sequence of postures adopted on different support surfaces. By contrast, the present study evaluated the ability of the three machine learning algorithms, namely KNN, Naïve – Bayes and SVM, in classifying a range of postures adopted in a random sequence on different mattresses, which more closely align with the data commonly acquired in clinical setting.

However, clinical data are not often supported by the knowledge of the postures adopted. This certainly increases the difficulties in normalising the corresponding signals. Accordingly, an algorithm of classification, namely CNN, was introduced with the aim of supporting the labelling of the postures prior to normalisation. CNN used a series of operations to evaluate the intensity of the pixel values corresponding to values of the pressure distribution, thus extracting higher – level features for classification. The predictive models of postures adopted on the two support surfaces provided encouraging potential in detecting specific postures (Tables 5-6 and 5-7). As an example, lateral and high sitting postures were accurately detected in the majority of the subjects when postures were adopted on the air cell mattress (Table 5-7). By contrast, for 7/14 subjects who adopted lateral and high sitting postures on the foam mattress, a high percentage of misclassification was observed (Table 5-6). Indeed, although the image silhouettes between lateral lying and supine or high sitting are clearly demonstrated, misclassification occurred as the intensities of pressure during these postures might have resulted similar. This is particularly evident on the foam mattress where a high number of lateral postures was classified as supine. Moreover, misclassification occurred when identifying the supine posture on the air cell mattress (Table 5-7). By contrast, supine posture was accurately detected in the majority of the subjects when adopted on the foam mattress (Table 5-6). In the light of these findings, CNN demonstrated a potential to distinguish between postures adopted in the sagittal (supine or high sitting) and transverse plane (side lying), particularly when the subjects were supported on the air cell mattress.

Deep learning algorithms and, in particular, CNN are widely applied in the healthcare field for image recognition, such as medical images for diagnosis, signal recognition for patterns classification, such as speech or gait recognition. However, the application of deep learning algorithms has been rarely reported for postures detection. In addition, CNN has been reported in classifying sitting postures in children (Kim et al. 2018). Results revealed higher accuracy values when compared with other algorithms. However, to the author's knowledge, CNN has not been reported for recognition of lying postures, in either healthy individuals or patients predominantly supported in beds or wheelchairs.

The current study has successfully applied the new approach, based on signals derivative and machine learning algorithms, to postures adopted in a random order on different support surfaces. It demonstrated how the sequence of postures and the support surface influenced the magnitude of the biomechanical signals. A training model of signals based on postures adopted on the foam mattress demonstrated a potential to identify a range of postures performed in a random order on an air cell mattress. The potential of this analytical approach to classify postures could be combined with a more sophisticated algorithm e.g. CNN for test data with no prior knowledge of the adopted postures. Preliminary findings suggest that CNN has the potential to distinguish between postures adopted in both sagittal and transverse planes. Thus, CNN would support the labelling of postures according to different anatomical planes. Accordingly, this would promote the normalisation of the corresponding signals with respect to supine, RMS and lateral posture. The normalised signals could be then projected into the training model (Figure 5-12A) to perform the classification with machine learning algorithms. Thus, the combination of the CNN algorithm, derivative and machine learning methodology could be used in a semi – automated work – flow, which is illustrated in Figure 5-16, to detect both frequency and magnitude of postures.

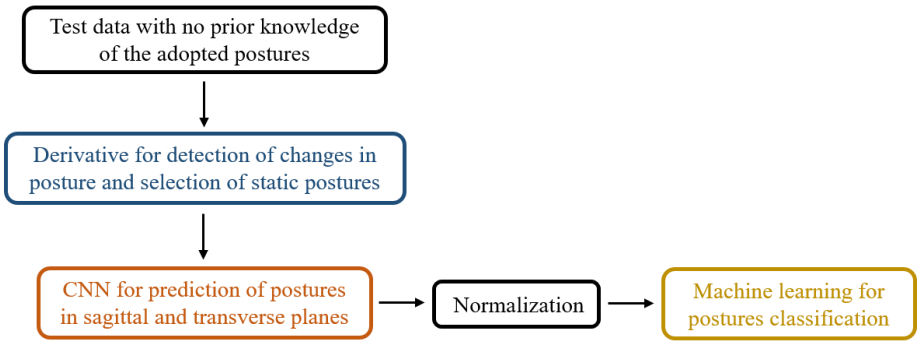

Figure 5-16: Work – flow which involves derivative for detection of postural changes, CNN for prediction of postures in the sagittal and lateral planes, supporting their labelling, normalization of the corresponding signals and postures classification through machine learning algorithms.

Chapter 6: The evaluation of pressure data acquired from spinal cord injury cases

Repositioning represents a primary intervention for PU prevention and is advocated in the current international guidelines (NPUAP/EPUAP/PPPIA 2019), which recommend repositioning at 2 – 4 hour intervals depending on the individual level of risk. As detailed in Section 2.1, recent studies (Walia et al. 2016, Gunningberg et al. 2018) have demonstrated that the use of continuous pressure monitoring systems can promote timely interventions by alerting healthcare providers and carers to periods of prolonged loading over vulnerable bony landmarks. However, there are a number of issues associated with the current algorithm incorporated within these systems (Section 2.6) including the use of arbitrary pressure exposure values, which provide the warning for tissue damage, resulting in inadequate indicators that pressure relief is required.

The present chapter involves clinical data of interface pressure monitoring derived from spinal cord injured (SCI) patients managed in a specialised hospital unit. In particular, it was designed to analyse both the frequency and magnitude of postural movements by these individuals utilising the work – flow detailed in Figure 5-16. The detected postural changes were then examined in the light of the associated risk status identified by the pressure monitoring system, using its arbitrary threshold values. In addition, data of skin integrity pre- and post- pressure measurements were recorded by a specialist SCI nurse.

6.1 Materials and methods

6.1.1 Pressure monitoring of Spinal Cord Injured patients

The data was acquired as part of a clinical academic PhD project, supervised by the host academics, entitled; ‘An evaluation of pressure monitoring technologies to create an “Individualized Pressure Ulcer Prevention Plan” for patients with Spinal Cord Injury (SCI) and Cauda Equina Syndrome’. The project, which is being carried out at the Salisbury District hospital, focuses on the rehabilitation of patients and aims to understand how pressure monitoring technologies can recognise support postures and promote regular repositioning. The protocol for data acquisition received Ethical approval, namely, University of Southampton (FoHS – 41814) and was also approved by NHS ethics, Integrated Research Application System ((IRAS) – 244580). Three convenient SCI cases were identified for inclusion in the present analysis. Patients were continuously monitored during prolonged periods (>10 hours) of lying postures, which are alternated by periods of approximately 5 hours of wheelchair sitting. Only one period, which involves day and night-time activities, was taken into account in the present analysis. This typically occurred prior to the skin check.

6.1.2 Case series data sets

Pressure data were acquired from prolonged time periods (>10 hours), yielding a large amount of data (Gigabytes in size). Signals of contact area and COP at both parallel and perpendicular directions with respect to the long axis of the mat were estimated from the pressure distribution with a sampling frequency of 1Hz. The data was subsequently down sampled 10 fold to 0.1Hz, which was considered adequate to detect large scale postural changes. Subsequently, the data were subjected to analysis to extract the frequency and magnitude of postural changes through the evaluation of the composite derivate, deep learning and machine learning algorithms, respectively.

The distinct postures were assessed by means of the training model detailed in Section 5.2.1 (Figure 5-12A), which was established using a normalisation process based on the prior knowledge of the adopted postures. As there was no prior knowledge of the postures, the CNN algorithm (Section 5.2.4) was used as a normalisation step to perform classification of grey scale images to automatically distinguish between sagittal and lateral postures, before projecting the corresponding signals of postures in the PCA space of the training model. The signals were subjected to classification by using two classifiers, namely Naïve – Bayes and KNN with k = 100 algorithms. The binary nature of SVM algorithm precluded its use with this data.

6.1.2.1 Data processing

Pressure data were subjected to three stages of processing, as detailed schematically in Figure 6-1.

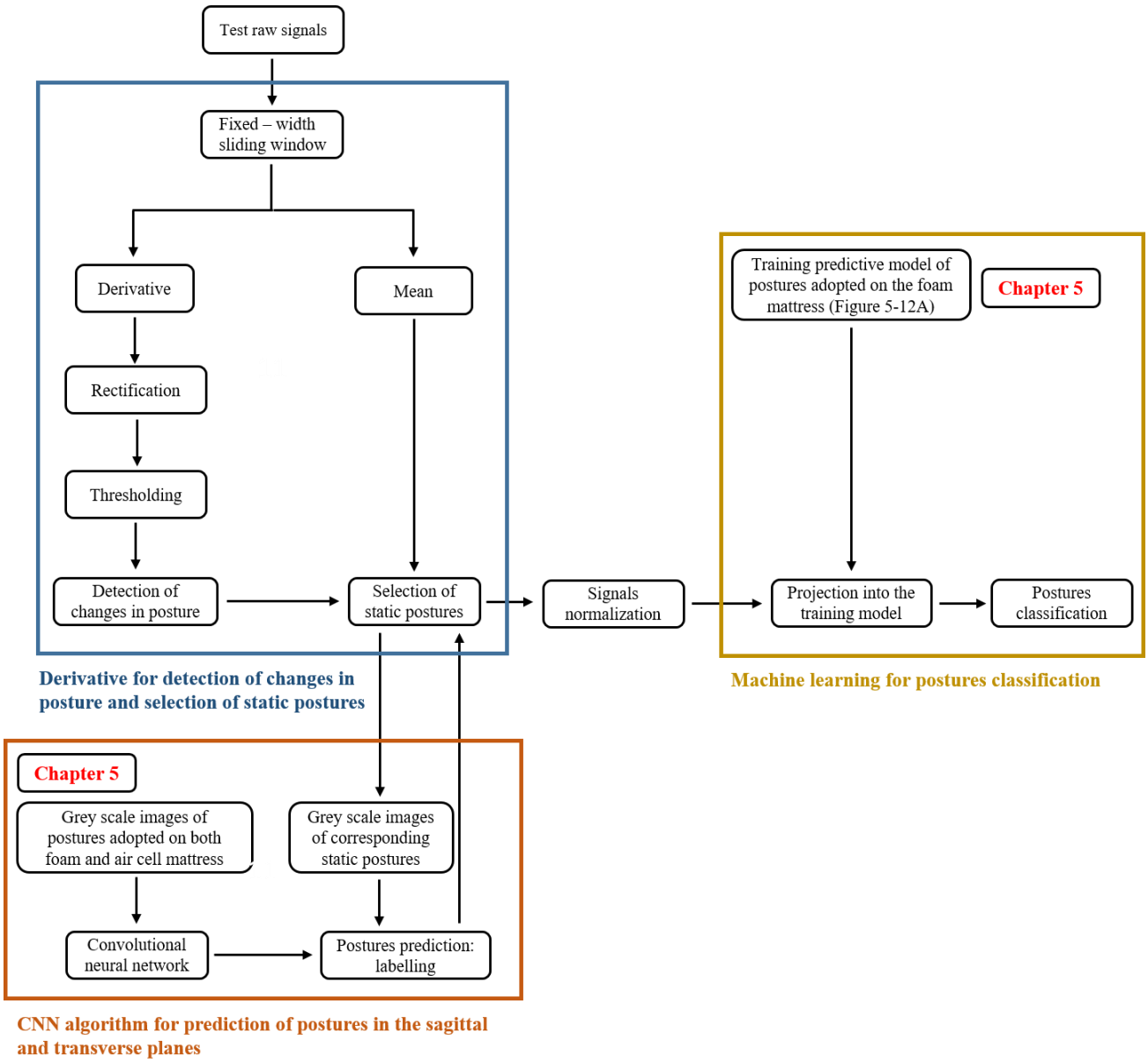

Figure 6-1: Overview of the data processing involving three separate stages. The first involves the use of derivative signal to identify the occurrence of the postural changes. Once the postural changes were identified, the static postures were estimated from the mean signals. The second stage comprises image data processing through the CNN algorithm to distinguish between postures adopted in the sagittal and transverse planes. Signals corresponding to postures were then normalised, projected to the training PC space and subjected to classification through the machine learning algorithms.

The first stage of the data processing comprised the calculation of the combined derivative of contact area and COP signals. This was subjected to the discriminant thresholds of 12% or 16% of the derivative maximum (Table 5-2), depending on the mattress type, to identify the occurrence of changes in posture. Once the postural changes were identified, the mean signal corresponding to static postures in between two postural changes were estimated (Figure 6-1). The subsequent stage involved image classification through the CNN algorithm, which was designed to label the corresponding posture, as either in the sagittal plane (supine or high

sitting) or transverse plane (lateral lying). In particular, two distinct training sets of grey scale images for postures adopted on both foam and air cells mattress were created using the pressure distribution derived from the data allocated in the training group (Table 5-1). Image classification was conducted with consideration of the support surface (foam or air), with each image frame labelled. Thus, the signals corresponding to the postures were normalised with respect to the supine posture, root mean square and lateral posture. After normalisation, signals were projected into the training PC space (Figure 5-12A) and subjected to machine learning algorithms for postures classification.

6.2 Results

6.2.1 Participants

Demographics of the three SCI participants are summarized in Table 6-1.

Table 6-1: Demographics of the three participants, including the grade of the spinal injury (ASIA), Braden score, type of mattress used and previous history of PUs.

Subject	Age	Sex	BMI [kg/m^2]	ASIA	Braden Score	Type of mattress	Previous history of PUs	Monitoring period
SCI 1	64	M	27	A	14	Air cell – alternating working mode	yes	~17 hours
SCI 2	66	F	24.6	D	17	Foam	yes	~11 hours
SCI 3	75	M	28	A	15	Foam	yes	~17 hours

6.2.2 Detecting changes in posture

Changes in posture for each participant were detected by using the combined derivative signal. A threshold value of 12% of the maximum derivative was used for the two participants positioned on the foam mattress, namely SCI 2 and 3, and 16% for the one positioned on the air cell mattress (SCI 1).

In all three cases, distinct changes in the magnitude of the derivative were visible. This is exemplified in Figures 6-2, 6-3 and 6-4 for SCI 1, SCI 2 and SCI 3, respectively. Changes which exceeded the corresponding threshold value were visible in all derivatives and identified as changes in posture. In addition, a number of events characterised by small changes in magnitude were observed. These events were identified as movements associated with postural adjustments performed within the same static posture. However, as prior knowledge of the postures was not available, it is difficult to assess the accuracy of the selected thresholds used to detect changes in posture. Closer examination of the pressure data revealed that there were some false positive and false negative predictions of postural movements in all individuals.

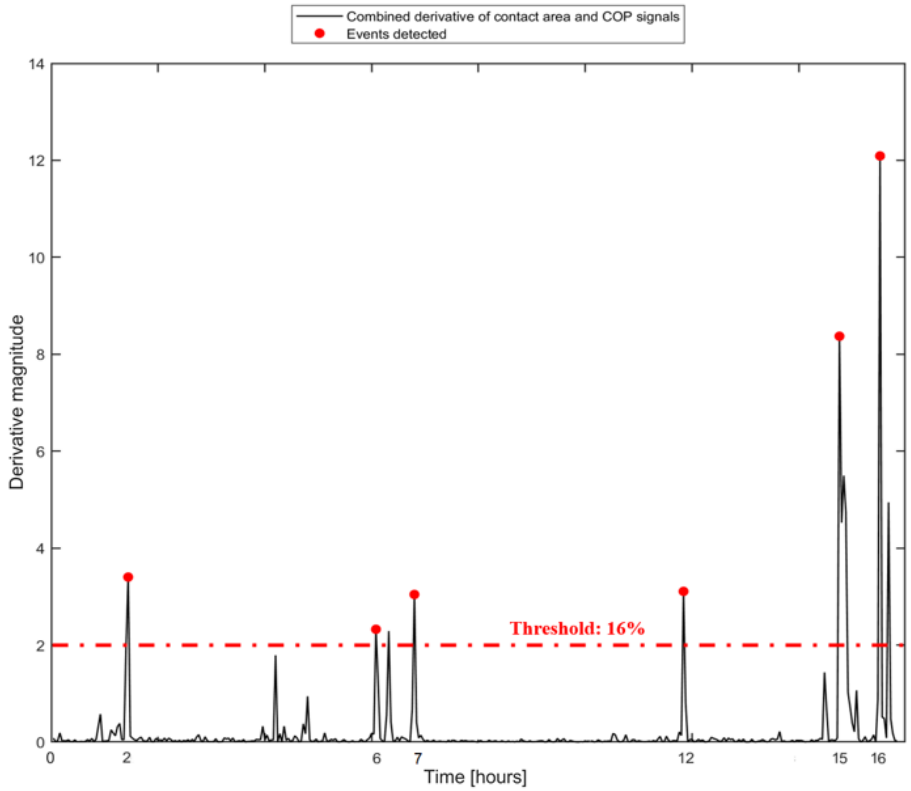

Figure 6-2: Composite derivative profile SCI 1 lying on an air cell mattress over the monitoring period. The red markers represent the events detected when the derivative magnitude exceeded a threshold value estimated as the 16% of its maximum value. Events detected in intervals including 10 data points were combined to represent a single event.

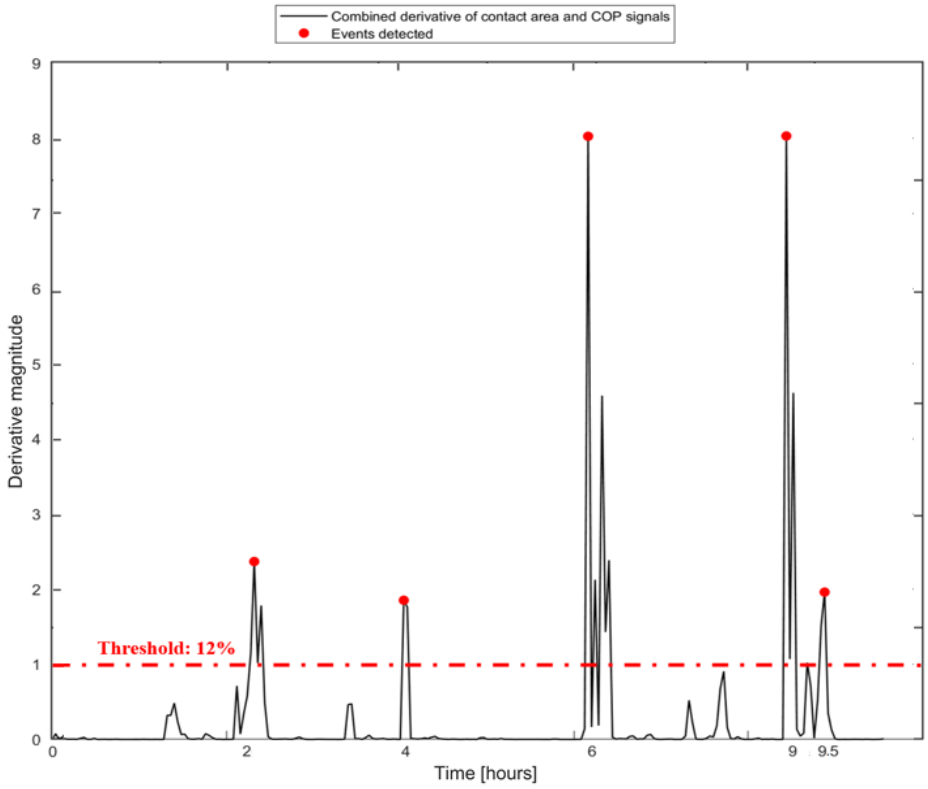

Figure 6-3: Composite derivative profile SCI 2 lying on a foam mattress over the monitoring period. The red markers represent the events detected when the derivative magnitude exceeded a threshold value estimated as the 12% of its maximum value. Events detected in intervals including 10 data points were combined to represent a single event.

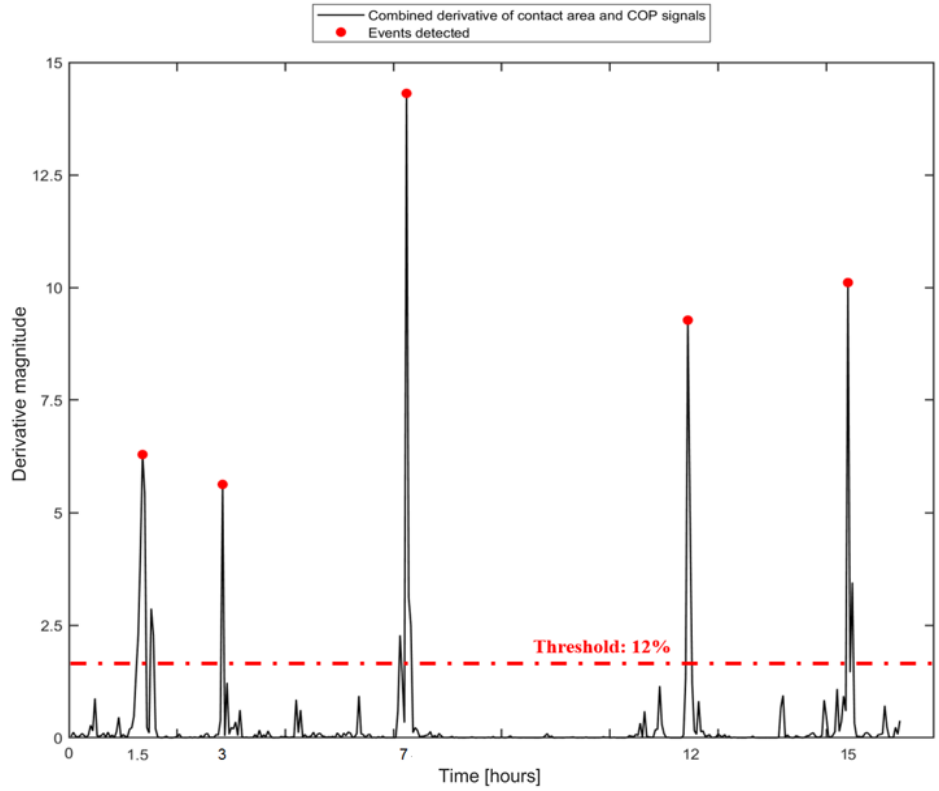

Figure 6-4: Composite derivative profile SCI 3 lying on a foam mattress over the monitoring period. The red markers represent the events detected when the derivative magnitude exceeded a threshold value estimated as the 12% of its maximum value. Events detected in intervals including 10 data points were combined to represent a single event.

It is worth of note that the magnitude of the derivative signals is 10 fold higher than the derivatives of previous chapters. This is due to the fact that the signals were not normalised as prior knowledge of the postures was not available.

Table 6-2 indicates the number of events classified for each individual. In addition, the frequency of repositioning based on the events detected during the monitoring period is reported. Closer examination of the data revealed that SCI 2 was repositioned at regular intervals of approximately 2 hours (Figure 6-3). By contrast, repositioning of SCI 1 and 3 followed different time intervals, which varied from a minimum of 1 and a maximum of 5 hours (Figures 6-2 and 6-4, Table 6-2).

Table 6-2: Number and frequency of the detected postural changes events, performed on the foam and air cell mattress.

Subjects (mattress)	Number of postures detected as changes in posture	Frequency of repositioning	Maximum time in between repositioning
SCI 1 (APAM)	5	~ every 3.5 hours	5 hours
SCI 2 (foam)	5	~ every 2 hours	2 hours
SCI 3 (foam)	5	~ every 3.5 hours	5 hours

6.2.3 Postures classification

As no prior knowledge of posture exists for the three SCI patients, the accuracy of the predictive algorithms (CNN, Naïve – Bayes and KNN) in classifying static postures could not be assessed.

After prediction with CNN, signals of static postures were normalised and then projected into the training PC space. As an example, Figure 6-5 indicates the test data, in green, corresponding to the signals from postures adopted by SCI 2, projected onto the training space. It is evident that the majority of the points in the clusters overlap with the clusters of the three postures, namely supine, high sitting and lateral, derived from the training model.

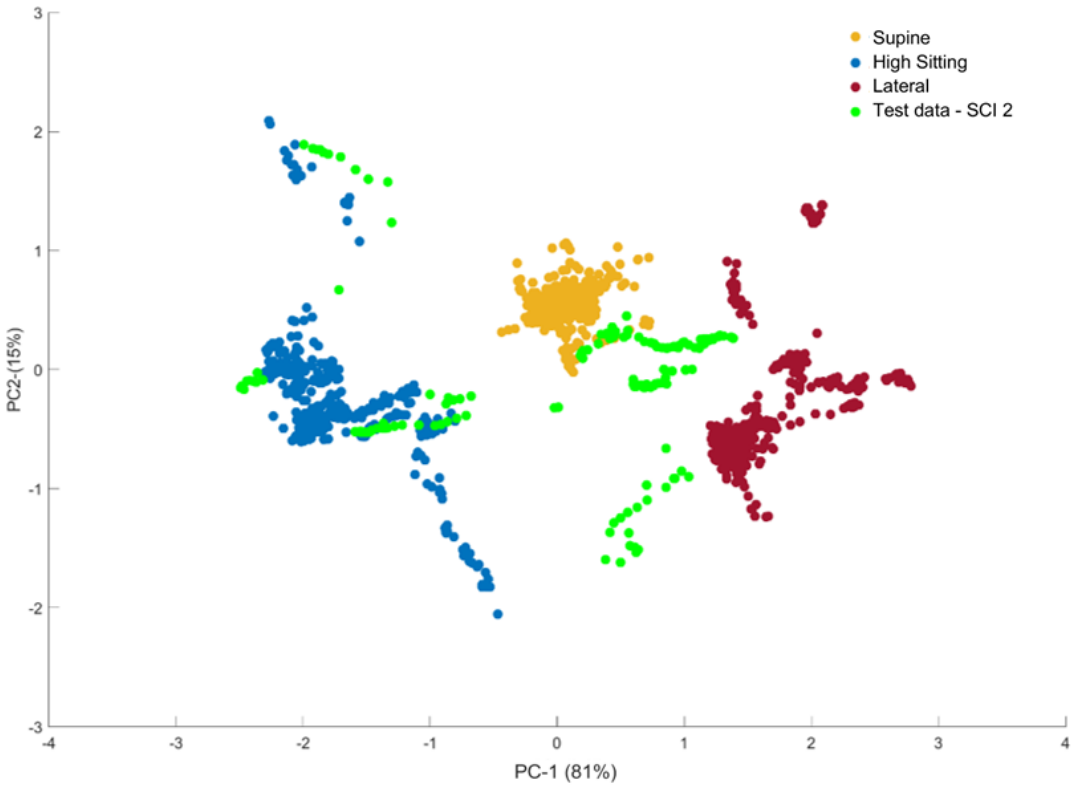

Figure 6-5: Signals of static postures, in green, corresponding to SCI 2 projected onto the training PC1 and PC2 space.

Figure 6-6 and 6-7 illustrate the grey scale images corresponding to representative static postures adopted by SCI 2 on the foam mattress. The corresponding grey scale images in the static postures adopted by SCI 1 and 3 are illustrated in Appendix L. For each image, the caption represents the posture classification with the Naïve – Bayes (Figure 6-6) and KNN (Figure 6-7), respectively. It is evident that there are differences in the predicted postures. This clearly depends on the principles underpinning each classifier.

Close examination of the prediction with Naïve – Bayes revealed that SCI 1 would have spent the majority of the time (>10 hours) in lateral posture and no time in supine. A similar prediction was observed for SCI 2, who would have spent few minutes in supine posture, and prolonged periods in both lateral and high sitting postures. By contrast, SCI 3 would have spent all the monitoring period in supine posture. Moreover, classification with KNN revealed that SCI 1 would have spent most of the time in high sitting (>12 hours) and no time in lateral posture. Equally distributed between the three postures was the classification for SCI 2. By contrast, SCI 3 would have spent all the monitoring period in high sitting posture. It is evident that both Naïve – Bayes and KNN have incurred in some misclassifications.

Figure 6-6: Grey scale images representing some of the static postures adopted by **SCI 2** on the foam mattress. The captions represent the classification performed with the **Naïve – Bayes algorithm**.

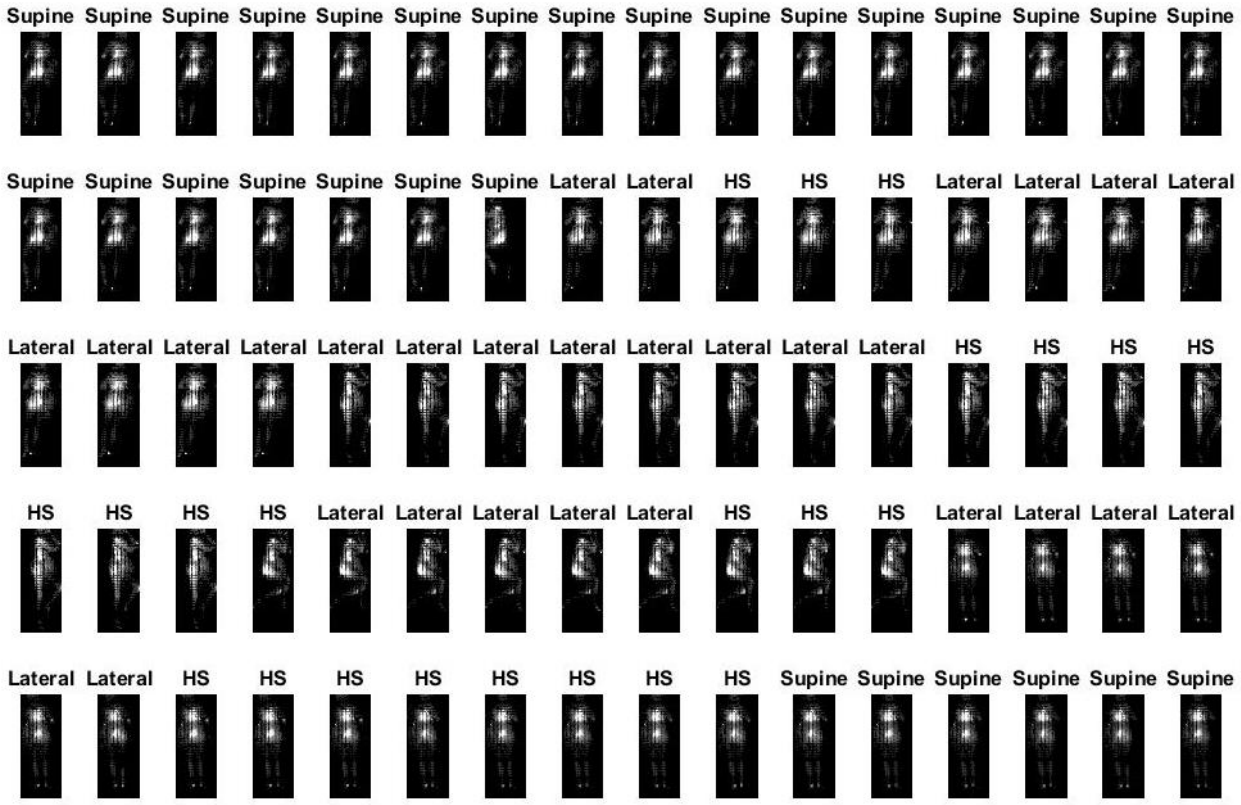

Figure 6-7: Grey scale images representing the static postures adopted by **SCI 2** on the foam mattress. The captions represent the classification performed with the **KNN algorithm**.

6.2.4 Critical appraisal of the warning system to promote repositioning in the light of skin examination

As discussed in Section 2.6, the algorithm of the commercial pressure mapping system is programmed to warn clinicians of potential damage to vulnerable body areas. Indeed, the system provides indicators, which identify areas exposed to prolonged postures (Figure 2-3), thus promoting the need for repositioning. However, these indicators are dictated by the selected exposure thresholds and turn interval timer, which are arbitrarily selected.

Visual examination of the skin integrity provided a direct comparison with the prediction of the skin damage indicated by the various criteria in to the continuous monitoring systems. Findings for each individual are summarised in Table 6-3, which indicates the at risk body areas identified by the software, both prior to and following detected changes in posture. Skin examination pre- and post-monitoring are also reported.

Table 6-3: Postures and the associated at risk areas identified by the indicators from the pressure mapping system. Skin checks prior and after pressure monitoring are reported.

Subjects	Indicator pressure	Postures associated with indicators of risk	At risk after changes in posture	Skin examination
SCI 1	150mmHg (yellow) 200mmHg (red)	No indicators were shown		Post-monitoring: red blanching mark on sacrum
SCI 2	150mmHg (yellow) 200mmHg (red)	Posture 1: no indicators		Pre-monitoring: red circular blanching mark on sacrum Post- monitoring: faded red blanching mark on sacrum
		Posture 2: 1 yellow on great trochanter	✗	
		Posture 3: 1 yellow which became red on the sacrum; 2 yellow on the back	✓	
		Posture 4: 1 yellow on the great trochanter	✓	
		Posture 5: 1 yellow which became red on the sacrum	✓	
		Posture 6: No indicators	✗	
SCI 3	150mmHg (yellow) 200mmHg (red)	No indicators were shown		Pre-monitoring: superficial scuff mark on right hip Post-monitoring: Moisture damage to left buttock and blanching red mark on right hip

As an example, SCI 1 presented with a history of a stage 3 PU on the left shoulder. The pressure mapping system was programmed to identify vulnerable areas at pressure values of 150 mmHg and 200 mmHg. In addition, the turn timer interval, to alert clinicians of a need to reposition, was set at 6 hours. This represents an unacceptable time, given that the individual had a history of pressure ulcers and would have been deemed at high risk and therefore in need of regular repositioning according to the international guidelines. However, detection of movements from the derivative signal (Figure 6-2) revealed a prolonged sustained posture. Although the pressure mapping system did not indicate any sign of risk, close examination of pressure data within this posture revealed a relatively high pressure gradient over the buttock area, as observed in Figure 6-8. Indeed, after pressure monitoring, skin examination revealed a blanching red mark on the sacrum. A similar pattern was identified with SCI 3.

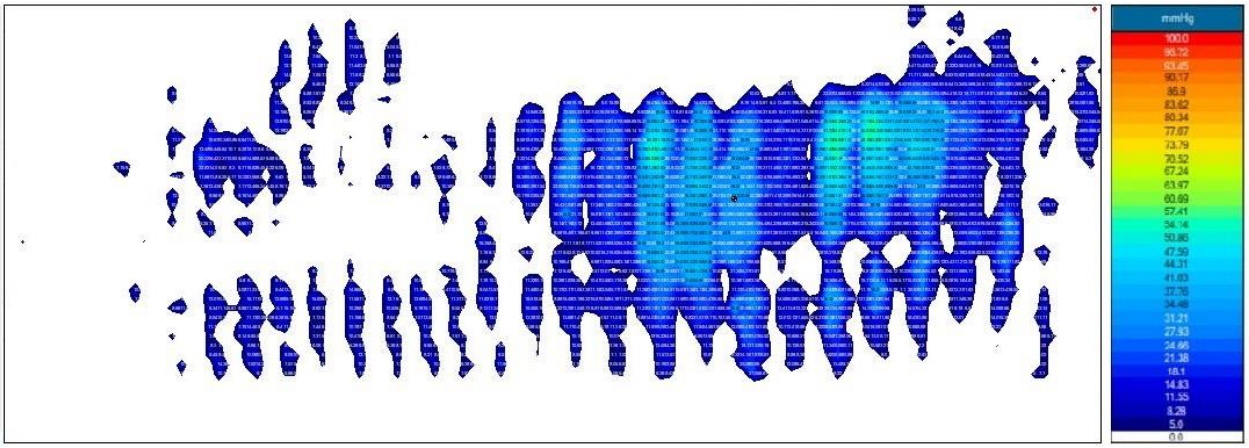

Figure 6-8: Pressure distribution and associated colour mapping and scale bar (5-100mmHg) for SCI 1. A relatively high pressure gradient is evident over the sacrum area, as result of a prolonged sustained postures.

By contrast, pressure monitoring of SCI 2 indicated some areas at risk, on the basis of pressure thresholds of 150 mmHg and 200 mmHg, although regular repositioning of approximately 2 hours was followed. However, it was evident that following a change in posture from lateral to supine, the indicators still identified the same sensors cells recording pressure above the thresholds. This is illustrated in Figure 6-9. Indeed, a close examination of the normalised exposure pressure, which represents the metric used in the algorithm and represented as a red curve (Figure 6-10), revealed a constant increase over the monitoring period. The exposure pressure corresponding to postures indicated in Figure 6-9 did exceed the normalised threshold value of 0.75, which corresponds to the exposure pressure of 150mmHg, thus identifying the at risk area in the same sensor cells.

Subsequent skin examination revealed a faded blanching red mark on the sacrum, which the patient presented prior to the monitoring period.

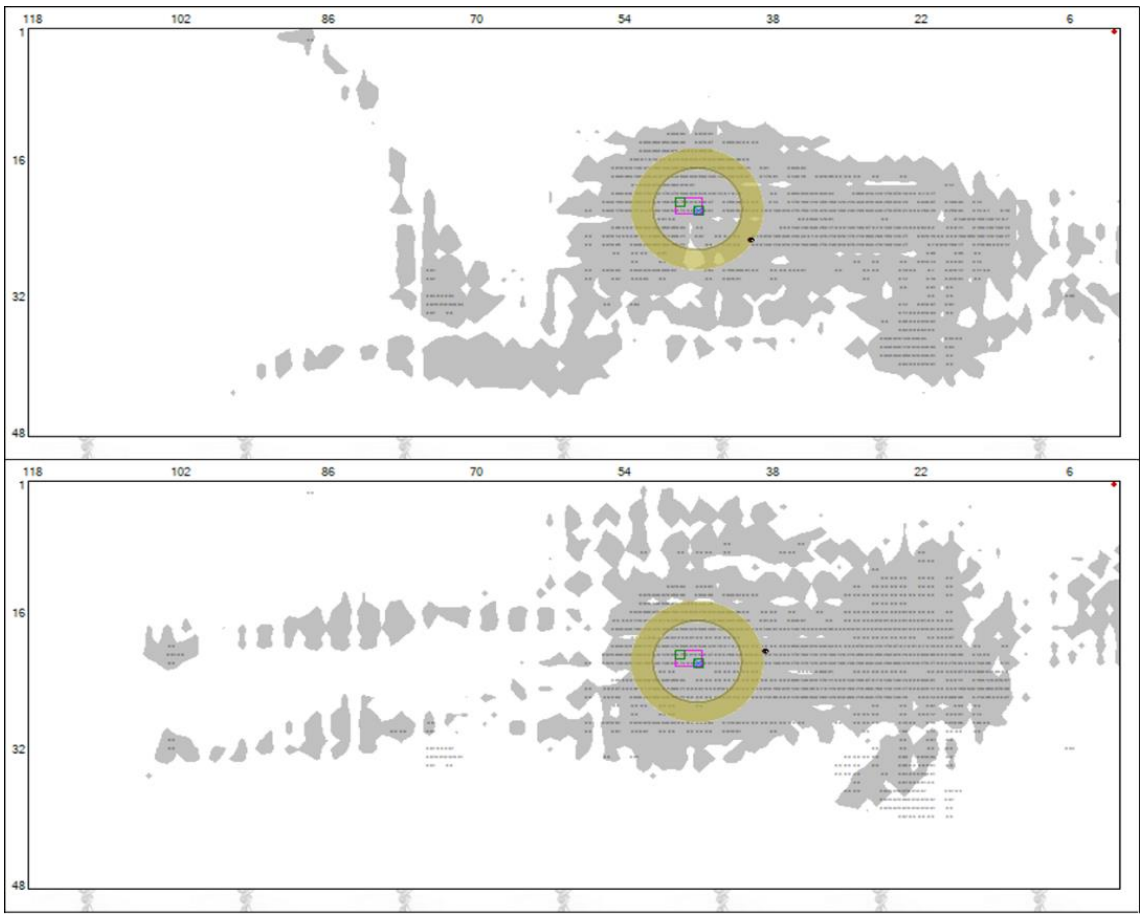

Figure 6-9: Indicators showing at risk areas on SCI 2 in top, the lateral posture and, below, in supine posture. In the lateral posture, an at risk region was identified around the great trochanter. Subsequently, the individual changed to the supine posture but the risk status remained at the identical pressure sensors, identified around the sacrum. The indicator was dependent on the accumulation of pressure in the corresponding pressure sensors, as opposed to the position of the subject, rather.

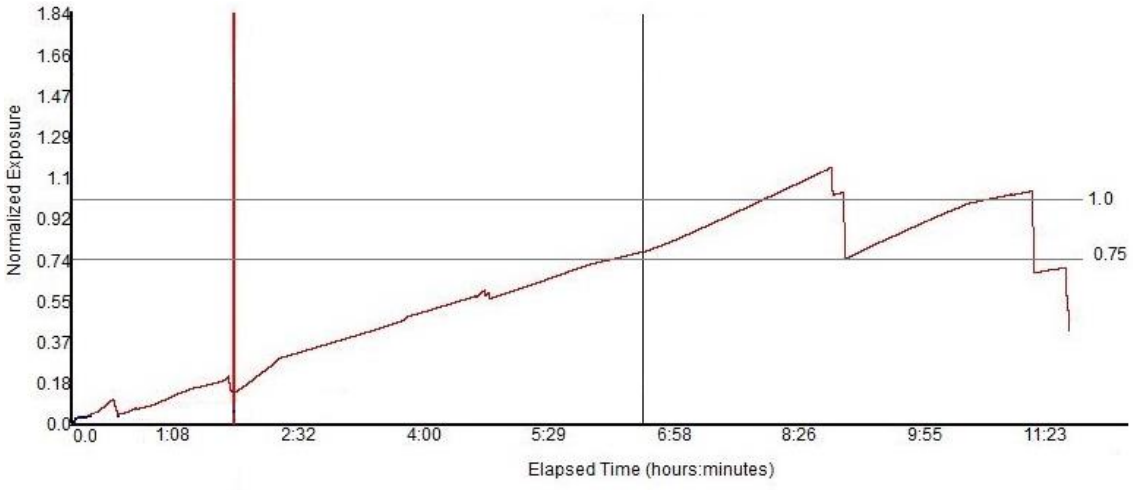

Figure 6-10: Normalised pressure exposure over the monitoring period. The normalised exposure thresholds of 0.75 and 1.0, corresponding to pressure values of 150 and 200mmHg, respectively, are also reported. A constant increase in the pressure exposure characterises the monitoring period. For values exceeding the exposure thresholds, yellow and/or red indicators indicate the at risk areas.

These examples provide evidence of the limitations of the algorithms currently used in the pressure monitoring system to detect vulnerable body areas and therefore promote repositioning. Indeed, the algorithm identifies at risk areas based purely on the combination of pressure and time that exceed thresholds, which have been arbitrary selected over a single pressure sensing element. In addition, the algorithm clearly does not reliably recognise when individuals are repositioned. Therefore, there is a need for objective, robust and custom – based indicators of posture and mobility, in combination with the assessment of skin by health professionals or carers to identify PU risk on specific individuals.

6.3 Discussion

The present chapter has evaluated the frequency and magnitude of postural changes in a small case study series of spinal cord injured subjects. Examining patients cases represent a challenge as frequency and magnitude of movements recommended for PU prevention are generally not strictly followed (Defloor et al. 2005, Woodhouse et al. 2019), and specialised mattresses which influence the trends of the pressure parameters are used. To author's knowledge, this is the first study in detecting patients posture and mobility with a developed semi – automated methodology which combined deep learning and machine learning algorithms.

The analysis involved the application of an integrated methodology, based on derivative of the most robust signals for the detection of postural changes, deep learning e.g. CNN and machine learning algorithms for detecting adopted postures. As there was no prior knowledge of the adopted postures, CNN was used to support normalisation of signals prior to classification.

The postural changes were detected by using the combined derivative signals with a mattress – specific threshold, derived from Chapter 5 (Table 5-2). Derivative signals revealed that in all cases variations in the magnitude exceeded the corresponding threshold values indicative of postural changes. In addition, smaller scale perturbations were observed, potentially related to postural adjustments as exemplified in Figures 6-2, 6-3 and 6-4. However, as no prior knowledge of the postures exists, it was difficult to assess the accuracy of the selected thresholds used to detect changes in posture and misdetection might have incurred.

Based on the events detected as postural changes, frequency of repositioning was evaluated, with respect to the total monitoring period (Table 6-2). In addition, interval of time in between two subsequent postural changes was also examined. It appeared that for two subjects e.g. SCI 1 and SCI 3, some static postures were maintained for 5 hours (Figures 6-2 and 6-4, Table 6-2), not reflecting the recommended frequency of 2 – 4 hour intervals (NPUAP/EPUAP/PPPIA 2019).

It is of note that also small variations in the magnitude of the derivative signals, which did not exceed the corresponding threshold values, were visible in all cases. These variations were associated to postural adjustments throughout the monitoring period, which could occur during

a static posture. However, it was difficult to determine whether each of these small-scale movements corresponded to either a false negative result or a reaction of the individual to prolonged posture. Regardless, these movements represent a potential strategy to allow tissue reperfusion and prevent tissue breakdown.

Static postures detection was initially performed involving images classification with CNN to identify postures performed in different anatomical planes i.e. sagittal and transverse planes. Subsequently, the corresponding signals were normalised. Naïve – Bayes and KNN algorithms were then applied to classify postures with respect to the training model of data derived from random postures performed on a foam mattress where individual signals were projected (Figure 6-5). Despite the accuracy in classifying postures could not be determined, some differences in classification between Naïve – Bayes and KNN were visible in all cases (Figures 6-6 and 6-7, Figures L-1 to L-4).

The translation of this novel algorithm may have been limited by the postures adopted in the clinical settings, which inevitably would have varied from the controlled postures prescribed in the lab – based tests. These differences would have influenced the distribution of pressures and the resulting magnitude of the derived signals, which is strongly dependent on both demographics, e.g. contact area and the position of the individuals on the mattress surface bed, e.g. COP. As evident in Figure 6-6, some individuals adopted a diagonal orientation on the mattress, which could have affected the posture predictions. In the present analysis, signals were processed through normalisation prior to classification, which modified their magnitude. Normalisation relied on CNN results in distinguishing between postures performed on the sagittal and transverse planes. Accordingly, if a misclassification occurred during the CNN step, this would have influenced the magnitude of the signals as result of normalisation. In addition, the use of training data from healthy cohorts may not reflect all postures adopted in clinical settings.

Limitations of the existing pressure monitoring algorithm for identifying vulnerable areas were demonstrated with clinical examples in the light of the skin integrity examined prior to and following the pressure recordings (Table 6-3 and Figures 6-8 and 6-9). The presence of the indicators of risk was examined for each of the SCI cases. It emerged that, following a change in posture, the system still identified the area covered by the same sensor cells included in the at "risk" area (Figure 6-9). It is evident that the current algorithm programmed into the ForeSite PT system is not accurate in detecting when individuals moves. In addition, the interpretation of these clinical pressure data demonstrated that the system does not have the capacity to predict pressure ulcer risk in vulnerable groups, such as the SCI. Indeed, pressure mapping system did not indicate any sign of risk, despite some postures were sustained for prolong time period, as suggested by the events detected by the derivative. These were associated to high pressure gradients (Figure 6-8) over the area where skin marks were identified following the monitoring

period. The present analysis highlights the importance of developing robust and reliable thresholds, in conjunction with individual characteristics, to support the detection of adequate repositioning as advocated in the guidelines for PUs prevention (NPUAP/EPUAP/PPPIA 2019).

Literature reveals a number of studies which have investigated pressure relieving movements in SCI individuals (Bain and Ferguson-Pell 2002, Yang et al. 2009, Sprigle et al. 2019). The majority of these studies utilised parameters, such as COP and individual weight, to evaluate the frequency of weight shifts in sitting postures, as spatial or percentage changes in these parameters (Bain and Ferguson-Pell 2002, Yang et al. 2009, Sprigle et al. 2019). The different nature of the postural movements performed during sitting, with focus on the buttock region i.e. adjacent to the ischial tuberosities, do not facilitate the comparison with the methodology utilised in the present study for the detection of repositioning in lying. Nonetheless, it appeared from these previous studies that the pressure relief behaviour did not respect the frequency advised in the guidelines, as observed in the present study for some individuals.

Moreover, a number of studies have applied machine learning algorithms for postures classification in both lying and sitting postures (Table 4-10). However, these studies mainly involved healthy individuals. Of the few which involved patients, one study conducted by Dai et al. (2012) investigated the ability of peak pressure index, estimated from a custom - made system, to predict different sitting postures in a small cohort of SCI individuals. However, as opposed to the present study which considered prolonged lying, the sitting postures were performed in a prescribed sequence for a limited period of time (20 seconds). In addition, the estimation of the static postures did not result from the detection of postural changes. Accordingly, this would limit the translation of this analysis to prolonged postures and the understanding of evoked postural movements.

The present study demonstrated that when associated with intelligent data processing, continuous pressure monitoring systems have the potential to translate pressure data into reliable indicators of posture and mobility. Indeed, the methodology developed in the present study was capable of detecting both the frequency and magnitude of postural changes in a small cohort of SCI patients. It was clear that the biggest challenge to address involved the fact that the details of postures were not available. Indeed, with the present data, it was not practically possible to annotate the postures adopted, which would have required a constant attendant or video recording for each patient. Thus further studies, which will be described in Chapter 7, should include training and test cohorts of appropriate patients whose postures are either annotated by an attendant or visualised by video recording. This would allow the validation of this novel methodology, determining the accuracy of derivative, CNN and machine learning algorithms in detecting postural changes and corresponding static postures. In case of unlabelled test data, CNN could provide a means to annotate the postures adopted.

It is clear that the emergence of digital health strategies will necessitate the use of robust monitoring tools, associated with robust methodology. When integrated with additional feedback technologies (Tung et al. 2015, Cicceri et al. 2020), a more efficient practice and personalised approach could be promoted for the prevention of pressure ulcers.

Chapter 7: Discussion

The present chapter reviews the key findings of the thesis, highlighting the main scientific contributions. These will also be considered in terms of the current state of the art, implications for clinical practice, and future research avenues will be suggested to extend the work presented in this thesis.

7.1 General overview

Examining the efficacy of repositioning strategies represents an important clinical challenge in pressure ulcer prevention. International guidelines have promoted intervention strategies to prevent PUs for individuals with limited mobility deemed at risk, including regular repositioning (typically every 2 – 4 hours in bed), the use of pressure redistributing support surfaces, risk assessment tools and routine skin examinations (NPUAP/EPUAP/PPPIA 2019). Despite widespread consensus on best practice, the prevalence of pressure ulcers continues to be unacceptably high. Thus, there is a growing need for technology to support clinical practice and promote self – management of risk.

Several commercial sensing technologies, including systems to monitor both movements (actimetry) and interface conditions (pressure mapping), are currently available to continuously assess how individuals move in bed and/or chairs (Conti et al. 2018). However, despite their development and clinical utility, there are still significant limitations with regards to the analysis and interpretation of the data. In particular, current pressure mapping systems are typically utilised over short time periods, involving minutes of data acquisition, offering only a 'snap shot' of posture data with no indication of mobility. This has limited the understanding of long – term effects of supported postures, which is fundamental for pressure ulcer prevention. When pressure mapping is used for prolonged periods in excess of 24 hours, the high acquisition frequency and resolution of the systems result in large data, much of which are potentially redundant for posture and mobility tracking (Bogie et al. 2008). By contrast, actimetry data represent the reference for movements detection currently utilised in clinical research (Källman et al. 2016, Ifedili et al. 2018, Pickham et al. 2018). Although they can be combined with snap shots of pressure data to evaluate the efficacy of repositioning in off-loading vulnerable body areas (Stinson et al. 2018), data from actimetry are not representative of conditions at the loaded interface. Accordingly, actimetry is not considered appropriate to evaluate the efficacy of pressure relieving strategies.

Despite the advances in technologies, commercial pressure mapping systems e.g. ForeSite PT are often programmed with algorithms based on arbitrary threshold values, for example 32 mmHg, which represents the closing pressure of capillaries in the nail fold (Landis 1930). Thus, this threshold value has little or no relevance to vulnerable tissue sites associated with PUs e.g.

the sacrum and heels. The corresponding software platform also requires manual input from clinicians and carers to specify exposure thresholds i.e. product of pressure and time from a given sensor. In addition, the time interval during which tissues are exposed to pressure relies on the manual resetting of a risk timer on the user interface, typically triggered following evoked postural movements. These variables are integrated within a pressure – time function, clearly relying on inappropriate thresholds (Figure A-1), on the basis of which vulnerable body areas are identified (Figure 2-3) and repositioning is advised. This has limited the impact offered by the use of these technologies to reduce both the prevalence and incidence of PUs (Gunningberg et al. 2017).

Nonetheless, monitoring systems provide the opportunity to estimate temporal biomechanical parameters at the body-support interface, creating a unique insight into conditions which could predispose vulnerable individuals to pressure ulcers. In order to release their potential, intelligent data processing is required to manage the large volume of data and provide clinically relevant interpretation (Bogie et al. 2008). Thus, there is a compelling need for novel data analysis and improved methodologies for indication of posture and mobility, thus promoting more appropriate interventions for pressure ulcer prevention.

Accordingly, this PhD project was designed to answer the following research question:

Can a lab – based methodology involving robust biomechanical parameters corresponding to body segment movements and/or interface pressure conditions predict posture and mobility during prolonged lying postures?

To answer this, a series of studies were conducted to evaluate a number of analytical approaches to address the following aims, which correspond to the experimental phases outlined in Section 2.7:

- **Aim 1:** Examine the potential of a range of biomechanical parameters to detect postural movements;
- **Aim 2:** Create a robust methodology and analytical framework for predicting both the frequency and magnitude of movements in lying postures;
- **Aim 3:** Validate these approaches with consideration of random postures and different support surfaces;
- **Aim 4:** Translate the methodology for use with clinical data.

The different studies required the development of an experimental design and implementation of different levels of signal analysis and processing. These are outlined in a schematic illustrated in Figure 7-1, which provides an overview of the developments in each of the experimental chapters.

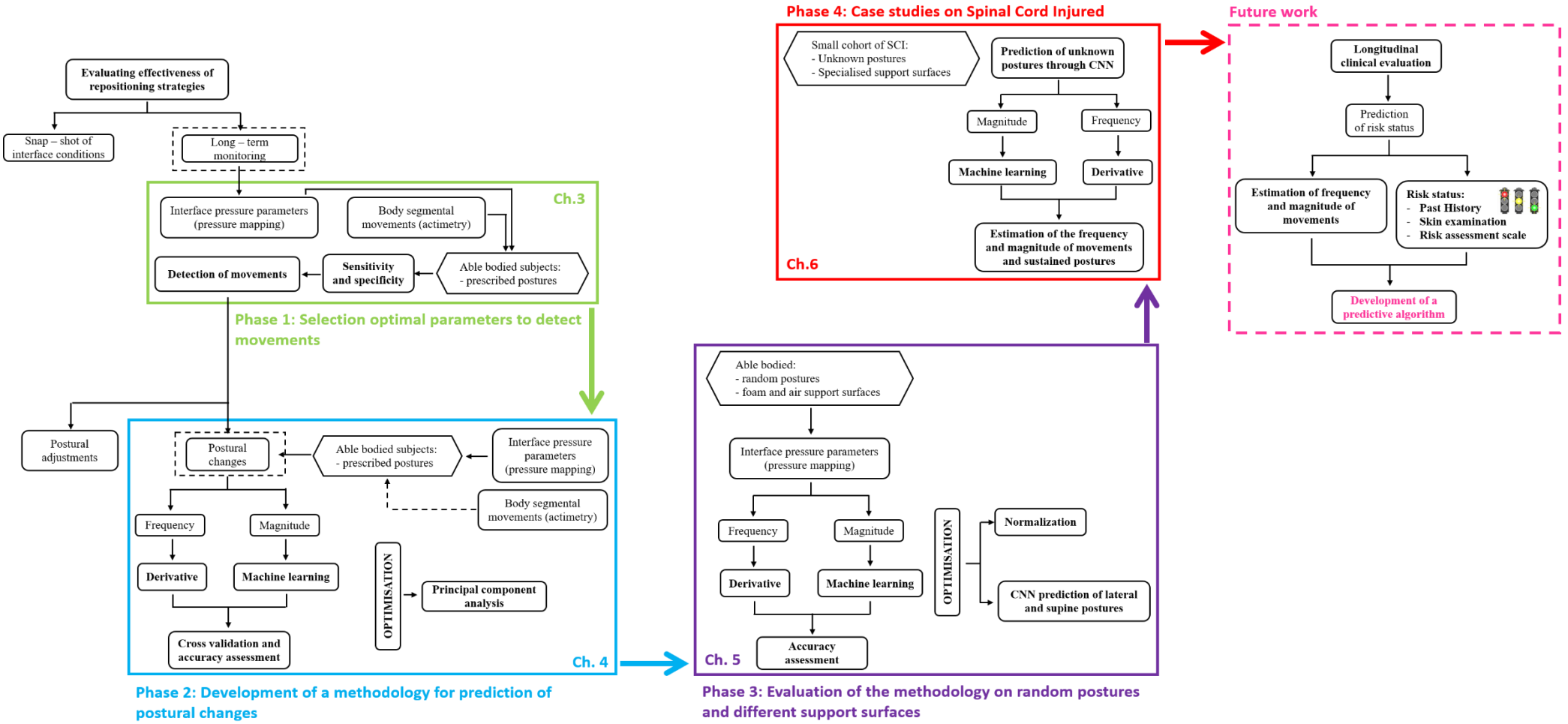

Figure 7-1: Overview of the experimental approaches undertaken in the present thesis.

An experimental approach detailed in Chapter 3, determined the most robust biomechanical parameters for the detection of postural movements in a cohort of able – bodied subjects. To the author's knowledge this is the first study to have evaluated the sensitivity and specificity of parameters from pressure measuring systems in detecting defined postural movements (Caggiari et al, 2019). Distinct pressure signals estimated from different regions of the body were sensitive to changes in postures. These relative changes in pressure parameters were observed to occur in the absence of significant signal drift. This was in concordance with a standardised calibration test to appraise the performance of the pressure monitoring system detailed in Appendix B and Chapter 3.

The potential of the pressure parameters were compared with those of signals estimated from actimetry systems, which represent a standard for movements tracking. The Receiver Operating Characteristics (ROC) analysis provided a robust tool to select the optimal parameters (Caggiari et al. 2019), thereby achieving **Aim 1** (Tables 3-11 and 3-12). The parameters with the highest sensitivity and specificity from the ROC analysis were examined in the light of a statistical procedure based on principal component analysis (PCA), which provided a means to reduce the high dimensionality and redundancy observed in the data. This approach resulted in a successful reduction of the large volume of data from both pressure mapping and actimetry systems and identified, at a minimal computational cost, the most relevant parameters indicative of postural movements.

While it is well known that actimetry systems provide a reference for position and movement detection (Edwardson et al. 2016, Lyden et al. 2016), there is limited current evidence that parameters estimated from pressure distribution could predict postures and movements with a high degree of accuracy. Thus, an analytical approach, as detailed in Chapter 4, was developed by considering a combination of both actimetry and pressure data and pressure data alone. The detection method was based on derivatives which provided high accuracy in detecting the frequency of postural changes. The parameters were then used within established machine learning algorithms to detect specific postures adopted by able – bodied subjects. The approach based on the derivative of biomechanical parameters has been successfully applied to other areas of clinical research, including gait analysis (Taborri et al. 2016) and QRS complex detection in the analysis of electrocardiograms (Elgendi et al. 2014). The translation of this approach to lying postures notably demonstrated the potential of pressure parameters alone in identifying postures and mobility, contributing to the development of a robust methodology for the detection of frequency and magnitude of lying postures, thus achieving **Aim 2**.

The movements detection and posture prediction was further assessed on a random sequence of postures performed on different support surfaces (foam and air cell mattresses). This analysis was detailed in Chapter 5. To the author's knowledge, this was the only study in having considered the implication of postures' order and different support surfaces for the detection of

magnitude and frequency of postures. Indeed, as observed in the present analysis, order of postures affected the changes in the magnitude of the pressure parameters, leading to a high variability between subjects. Optimisation of signals performed through a normalisation process efficiently reduced the inter – subject variability (Jacobs and Ferris 2015, Ghazwan et al. 2017). This was successful in validating posture and mobility tracking approach for random sequence of postures on different support surfaces, thus achieving **Aim 3**.

This achievement represented an important advance in translating the analytical approaches to clinical settings, where the adoption of postures follows a random order and can occur on a number of specialised reactive and active support surfaces (Section 1.10.2), and where the frequency and magnitude of movements do not routinely follow the current guidelines (Defloor et al. 2005, Woodhouse et al. 2019). Pressure data acquired in clinical settings can be influenced by specific patient characteristics, such as fixed postures syndrome and different morphologies, and by the use of wedges, lateral rotation systems and profiling beds, which are typically used to promote movements.

As pressure parameters demonstrated both a high inter– and intra– subject variability, an approach was examined involving image classification through the convolutional neural network (CNN) algorithm, associated with deep learning. As detailed in Chapter 5, this proved capable of distinguishing between postures occurring in different anatomical planes, e.g. sagittal and transverse planes. The CNN approach was subsequently integrated with the derivative and machine learning algorithms for the prediction of frequency and magnitude of postures in a small cohort of spinal cord injured subjects, whose individual profiles were acquired with no prior knowledge of postures. This integrated methodology, as described in Chapter 6, demonstrated a successful translation to a small cohort of patient data (**Aim 4**), demonstrating capability for analysing their long-term behaviour in terms of posture and mobility. To the author's knowledge, this advance has not been achieved in previous studies and provides an encouraging platform for future work, which is detailed later in this chapter.

It is clear that each study was successful in achieving the corresponding aims and their evolution contributed to successfully answering the global research question of the PhD project.

7.2 Scientific contributions

The overall project has yielded a number of novel contributions to the scientific field, with specific reference to the potential of bioengineering technologies for pressure ulcer prevention. These include:

1. A sensitivity and specificity evaluation of a series of biomechanical parameters for the detection of lying postures;
2. The development of a derivative approach for tracking the frequency of lying movements;

3. A machine learning approach for the prediction of lying postures in both sagittal and transverse planes of movement;
4. A semi – automated work – flow of data acquisition, processing and prediction of posture and mobility;
5. The translation of this analysis tool to a limited cohort of clinical data to demonstrate the potential added value to clinicians and end users.

This novel research can provide a means to use long-term pressure monitoring systems more effectively in clinical practice, so that they may contribute to predict the level of individual risk of pressure ulcer development, based on objective data with respect to posture and mobility. To date, these technologies do not reliably recognise when individuals are repositioned. The present work proposed a methodology based on objective and reliable parameters to detect when individuals move, with a view to delivering effective strategies for personalised care. To the author's knowledge, this is the first integrative approach which involves automated methods for prediction of postures and mobility associated with continuous monitoring of pressure data.

7.3 Limitations

One of the main limitations in the project was the use of relatively small cohort of able – bodied participants (n=11), recruited for the assessment of sensitivity and specificity study (phase 1 study). This number was further reduced in the subsequent training data involving machine learning to remove individuals who were unable to remain still in static postures (phase 2 study). Moreover, the use of a predominately young able – bodied cohort with fairly comparable anthropometric characteristics (Tables 4-1 and 4-2) for both the lab – studies will also question whether all the findings can be generalised to the wider population. Indeed, this cohort did not match specific sub – populations of individuals deemed to be at risk of developing pressure ulcers, often involving the extremes of age and body mass index (Margolis et al. 2003, Hyun et al. 2014).

A further small cohort of able – bodied participants (n=14) was used as training data for the detection of random sequence of static postures on different mattresses (phase 3 study). Such relatively limited number of individuals may have affected the accuracy results. However, no strict indications in terms of the amount of training data required for machine learning exists. Indeed, this may depend on several factors such as: i) the complexity of the classification problem; and ii) the complexity of the algorithms used, namely the principles underpinning each algorithm. Thus, a further evaluation would be required to determine the optimum training cohort size through a "learning curve", which is designed to depict the performance of the training model as function of the cohort size, thus to create a more robust and efficient model.

The same training cohort of healthy individuals utilised in phase 3 was then used for the detection of clinical postures (phase 4 study). Postures adopted by the training cohort may have

not completely reflected the range of postures adopted in clinical settings. In addition, it was not practically possible to annotate the postures adopted in the clinical data, which would have required a constant attendant for each patient during the recording period. This limited the predictive ability of CNN and machine learning classifiers and the estimation of the accuracy in classification (Figures 6-6 and 6-7). In addition, this affected the estimation of the occurrence of postural changes in terms of false positives, namely, movements corresponding to postural adjustments which occurred during static postures. Thus, a further study should include training cohorts of appropriate patients whose posture and mobility are annotated or video recorded. This would provide the means to assess the predictive ability of both CNN and classifiers. Future studies could also include a control in the signals magnitude immediately prior to and after a detected event to provide a more precise estimation as to whether the change represented a true positive or false positive. The discrimination between large (macro-) and small (micro-) scale movements would be an important step in identifying the profiles of interface pressure conditions, which could have an impact on pressure ulcers development. It is of note that in the earlier controlled studies, large scale movements were facilitated by the fact that able – bodied individuals were instructed to remain as still as possible and postures were evoked using adjustments of the bed frame and an automated tilting device.

It is well accepted that overfitting is a common issue with respect to the CNN algorithm, which belongs to its layers (Figure 5-15). This can influence the validation accuracy in training a model. Indeed, overfitting can happen when the neural network cannot generalise beyond the training data. To prevent overfitting it is important to select the correct number of layers and kernels and apply some regularization process. One example involves the drop out process (Figure 5-15) which randomly “drops out” nodes of the layer in which is applied. However, it affects the validation accuracy of the training model. This inevitably influenced the prediction of postures in the present analysis as no control exists as to the choice of the nodes to activate.

7.4 Clinical implications

This project has yielded several important implications for clinical practice, highlighting a number of issues that are relevant for designers of commercial pressure monitoring systems. The present research has demonstrated that objective temporal pressure parameters can provide a robust means of evaluating movement behaviour, which is a major advance on previous strategies involving “snap shots” of ‘observational’ parameters i.e. peak pressures or contact area. It also represents an alternative to the subjective interpretation of the colour maps depicting the pressure distribution, which are often poorly interpreted. The proposed methodology can provide effective measures of mobility, which represent an important metric for improving patient’s self-management, as well as supporting safe and efficient clinical practice. Indeed, both clinicians and patients would benefit from automated mobility analyses and consistent posture assessment and tracking, promoting personalised care, particularly for

individuals with restricted mobility. This should encourage manufacturers to: i) free up the systems from manual input of pressure and time variables; ii) include in the commercial software an automated detection of posture and mobility; iii) provide equipment and efficient training for performing routine calibration in situ, as the performance of the systems could change with usage; iv) match support systems to the level of individual risk of PU development.

In the long-term, pressure monitoring systems could be improved to intelligently select those individuals who are less mobile, or have a change in mobility status. Thus, this technology could be employed in both the community and hospital settings for targeted clinical interventions (Tung et al. 2015). With the expanding sophistication and availability of computing and sensing technologies, new technologies to assist limited mobility in self-managed care are emerging. Posture and mobility monitoring could be added to the established digital health platforms used to manage populations with reduced mobility and complex co-morbidities (de Morton et al. 2008). This could also be integrated with support and feedback technologies to identify detrimental health signs, thus promoting situational awareness, adherence, and access to professional resources (Bodenheimer et al. 2002). Moreover, connecting home-based and wearable equipment will increasingly enable patients, carers and clinicians to predict and prevent events that would otherwise have led to hospitalisation. This will release staff time and provide safety prompts that will improve the quality of care provision, which is becoming increasingly digitalised (NHS 2019).

7.5 Future work

Despite the encouraging results in the present work with respect to the tracking of posture and mobility, it must be acknowledged that the biomechanical parameters alone will not be able to predict all the events that might result in skin damage. Therefore, the work could be extended in a series of studies to combine the developed methodology for tracking posture and mobility with other risk parameters associated with pressure ulcers, including tissue status and tolerance, co-morbidities, nutrition and local microclimate. The ultimate goal remains the development of an intelligent tool which could predict the level of risk (as indicated by the traffic light scheme in Figure 7-1) and support clinical practice in both delivering PU prevention strategies and managing skin health. This could be suitable for use in both community and hospital settings.

An initial study, in close collaboration with clinicians, would involve the identification of critical features indicative of risk factors, based on the recent expert consensus framework (Coleman et al. 2014 a). These intrinsic factors may include co-morbidities and changes in skin status, which will reduce the tissue tolerance to mechanical loads and increase the individual risk of pressure ulcers. Data indicative of posture and mobility could then be combined with objective features of risk to develop a predictive model. To support this, a practice-based assessment of long – term positioning would be necessary, involving patients in both acute and community settings. This could initially involve a sleep study supported by video recording to

evaluate patterns of posture and mobility over prolonged periods. Indeed, during night sleeping the frequency of evoked repositioning is drastically reduced compared to carer-evoked repositioning during day times (Källman et al. 2016). This would help to identify trends in natural positioning during supported postures and features indicative of levels of risk due to lack of mobility (Coleman et al. 2013). A subsequent assessment of both frequency and magnitude during evoked postural changes would be also required. Consideration of the influence of both pillow support and mattress type, which could influence the magnitude of pressure distribution and corresponding signals, would help to predict changes in posture and mobility considering the wide range of positioning delivered in clinical practice. Thus, a predictive model will be developed which will involve individual – specific patterns of natural and evoked movements in a range of postures and support surfaces, with due consideration of features indicative of risk status.

In the last decade, a number of healthcare manufactures have utilised technologies to enhance and publicise the performance of their specialised support surfaces. As an example, the incorporation of active internal air sensors to provide adequate mattress deformation and pressure relief in specific body areas, such as the sacrum and heels, of individuals deemed to be at high risk of developing PUs. The internal support pressures are designed to change features according to the contacting surface and the morphology/positioning of the individuals (Chai and Bader 2013). Therefore, a further study could involve the integration of posture and mobility tracking and the PU risk prediction tool with an instrumented support surface in a measurement array incorporating pressure, actimetry and microclimate sensors. Biomechanical and clinical features will be used to improve the PU risk feedback alert.

A further development would include the package of the predictive algorithm into a beta software version, prior to the further evaluation of its performance in a clinical setting. This will proceed following consultation with technologists and end-user stakeholders, such as clinicians and patients. They could inform design to provide automatic and real-time analysis of the data, to provide classification at the time of examination, via a traffic light signal or other easy-to-interpret indicator systems.

Both biomechanical and clinical features, identified from the predictive tool, involved a high spatial resolution pressure sensing array (12.7mm) recording at relatively high frequency (1Hz). Thus, the features were computed from the high dimensional data, demanding computational performance. Accordingly, future work could include the development of a new pressure technology which replaced the high-resolution array with an optimal set of sensors, strategically placed in order to provide the same classification accuracy. In addition, this will integrate different sensing tools. This will contribute to the development of a new sensing platform, which is relatively simple and more cost – effective with similar performance in posture and

mobility tracking. Integration of this novel sensing platform and the risk tool in a user – friendly app, could support the translation of this technology to a tool for general skin health.

Future work will also consider the translation of the technology into the assessment of sitting postures. For wheelchair-bound individuals, different strategies to transfer body weight by leaning either forward or to the side or lifting-off from the support surface are typically recommended every 15-30 minutes. The different nature of postural movements, with evaluation concentrated in the buttock region i.e. adjacent to the ischial tuberosities, would require a sensitivity and specificity analysis to determine the most accurate pressure parameters in detecting postural changes. For example, it was previously reported that COP has the potential to provide an objective measure of stability and inform about adjustment strategies (Fenety et al. 2000). However, sensitivity and specificity have not been evaluated for any sitting-related parameters.

The translation of posture and mobility tracking in sitting should carefully consider the acquisition frequency of the pressure measuring system and the frequency of repositioning. In particular, the pressure mapping system for sitting, such as the ForeSite SS (XSENSOR Technology Corporation, Canada), acquires pressure data with a sampling rate of 5 Hz, compared with 1 sample per second for the ForeSite PT system. In addition, repositioning in sitting is inevitably more frequent than in lying. Thus, the requirement for an increased sampling rate would produce an increased volume of data, and the high frequency of repositioning would limit the temporal amount of data for each static posture. This would require a modified protocol of data analysis, with particular focus on the down-sampling strategy.

In order to pursue this research, I will seek research funding in academia, working closely with industry and clinicians which I have enjoyed during this iCASE funded PhD.

Appendices

Appendix A Current algorithm of the ForeSite PT system

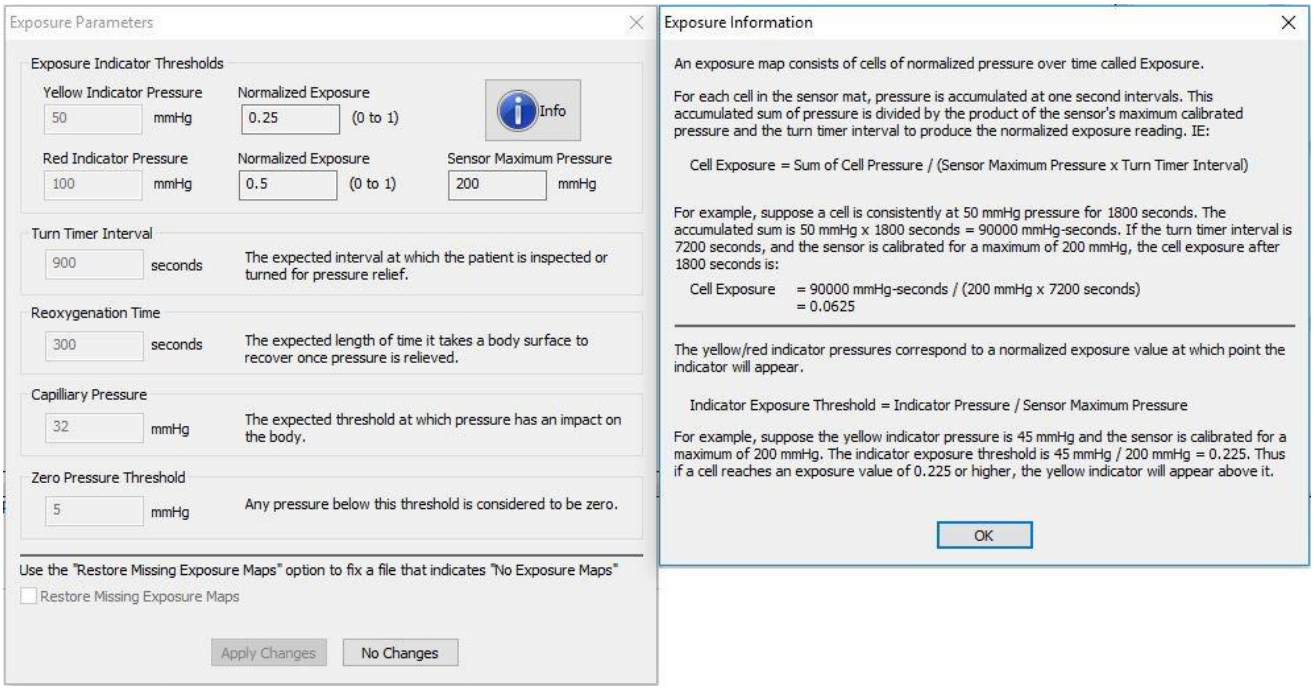

Figure A-1: Overview of the current algorithm incorporated in the ForeSite PT system. The left figure shows an overview of the arbitrary thresholds used. These are adjustable by the user and involve the exposure pressure thresholds and the turn timer interval. Capillary threshold is set at 32 mmHg. The right figure describes the principle beyond the identification of at risk body areas, based on the pressure thresholds previously selected.

Appendix B Evaluation of the pressure response of the ForeSite PT system under different loading and time regimens

Both static and quasi – static loading test have been designed to evaluate the response of the pressure cells within the ForeSite PT mat over different load conditions and time.

The static test involved loading through a phantom buttock model of 16 kg, which was placed in a convenient position on pressure mat for a total period of 24 hours. An additional weight of 22.5kg was subsequently located on top of the buttock model (Figure B-1) and a second static test was performed for 24 hours.

Figure B-1: A static test involving loading of a buttock model with an additional weight of 22.5 kg onto a foam mattress incorporating the ForeSite PT pressure mat.

The number of the sensor cells within the mat recording pressure values in intervals of 5 mmHg were estimated. A region of interest of 32x32 sensors which included the pressure distributions exerted by the loaded model was selected, for a total of 1024 pressure sensors. The static tests were designed to examine whether the number of the sensor cells reading intervals of pressure of 5 mmHg changes over the time, in different loading conditions. Eight separate times in 24 hours loading period were examined.

The results as presented in the histogram form relate the frequency of pressure values recorded by the 1024 sensors at different times (Figure B-3 and B-4). There is clearly minimal difference in the pressure distributions for both static loading conditions.

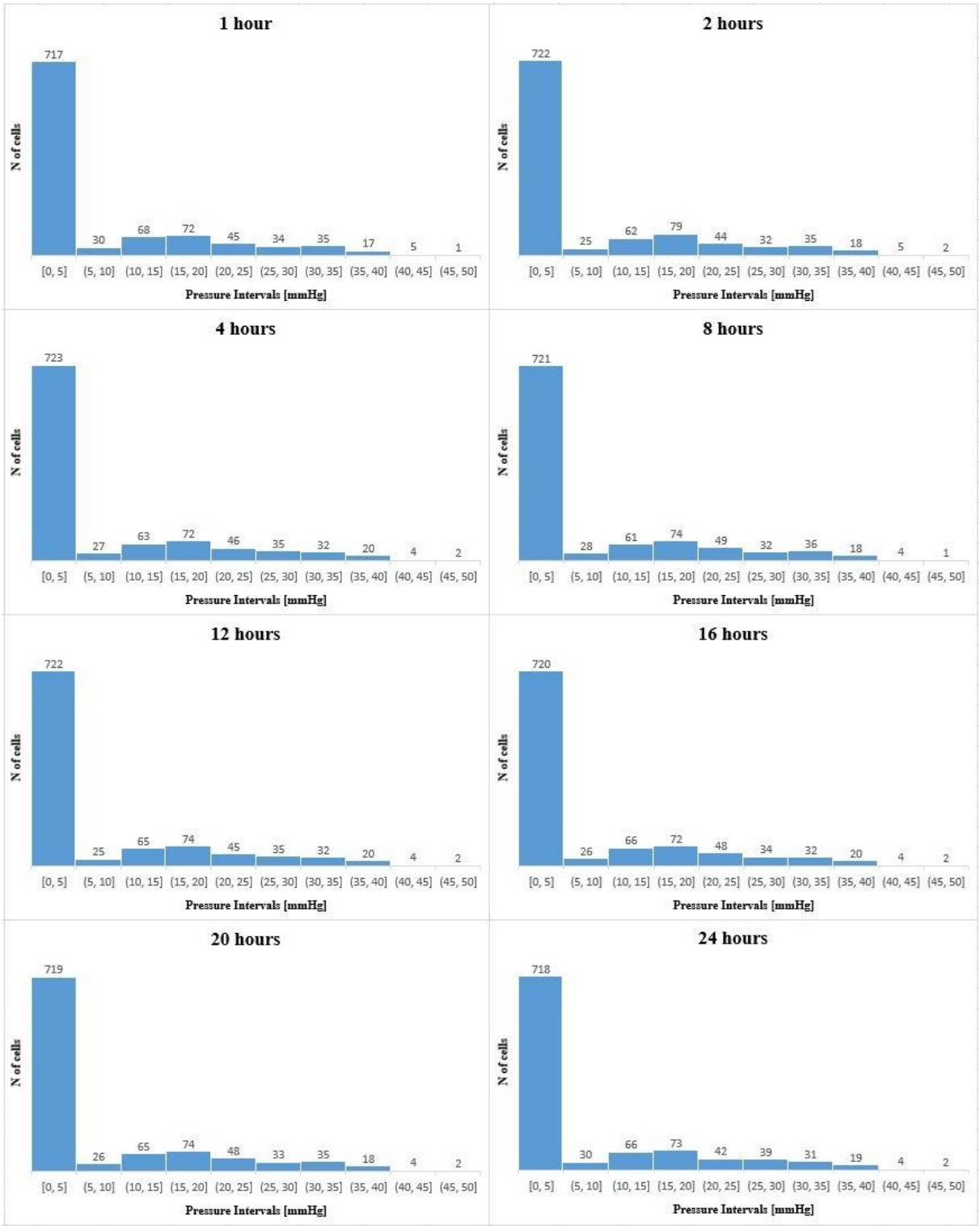

Figure B-2: Histograms representing the number of cells recording pressures in 5mmHg intervals over the 24 hour recording, for a static loading of 16kg.

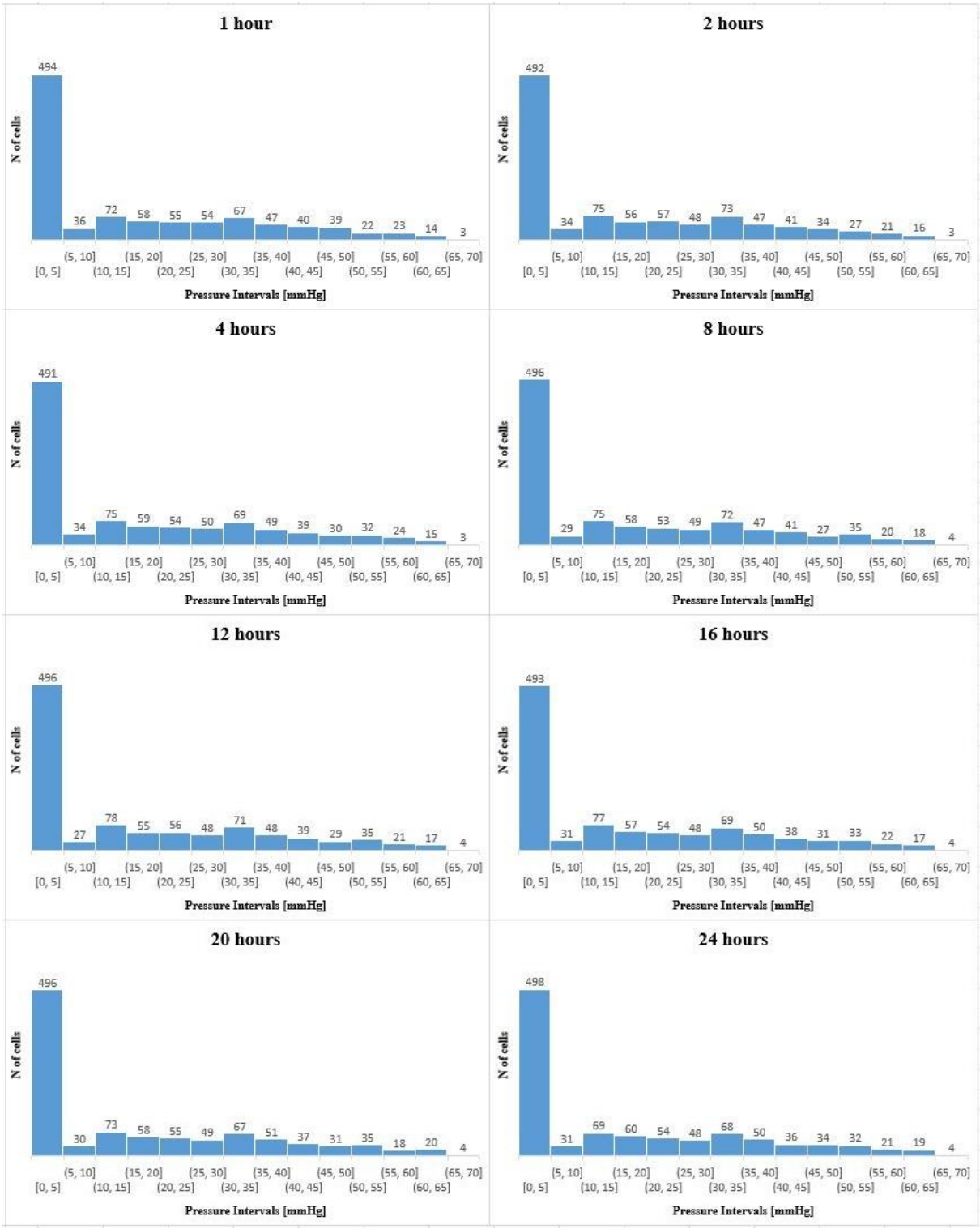

Figure B-3: Histograms representing the number cells recording pressures in 5mmHg intervals over the 24 hour recording, for a static loading of 38.5kg.

The quasi – static tests involved loading/unloading cycles via a spherical indenter using a series of increments of displacement. These were performed by using an electromechanical test machine (E10000, Instron Ltd, UK), which was programmed to activate the displacements and record the resulting loads. Simultaneously, the pressure mapping system recorded the pressure

magnitudes in two selected regions of the mat. A wooden spherical indenter (Area~1539 mm^2) was used to load the mat with a silicon gel sheet of 3mm inserted at the interface, as indicated in Figure B-4. The pressure map was located on top of a foam cushion (thickness of 110 mm), which was deformed under the load applied by the indenter (Figure B-4).

The quasi – static load protocol involved loading at five increments of displacement of 12mm, up to 50% compression of 60mm. At each increment, the displacement remains constant for 5 minutes (Figure B-5). The unloading cycles reversed the displacements. Before testing, the machine performed an initial test to automatically estimate the compressive stiffness of the composite of cushion, silicon sheet and pressure mat. The response revealed an estimated stiffness of 5.71 N/mm.

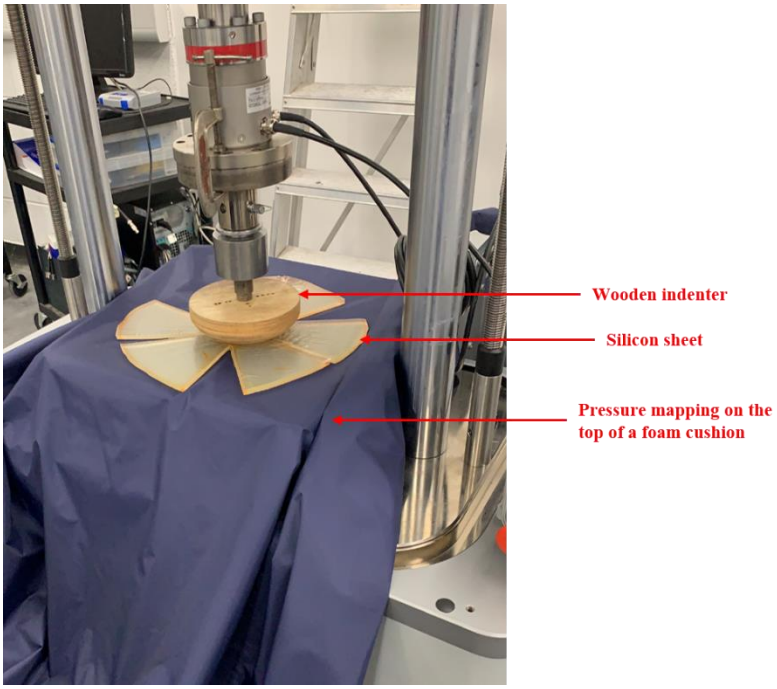

Figure B-4: Set up of the dynamic test where the pressure mapping system was placed on top of a foam cushion. A wooden indenter was used to perform a compressive test in displacement control, under whom load the cushion was deformed and the pressure mapping recording the corresponding applied pressure.

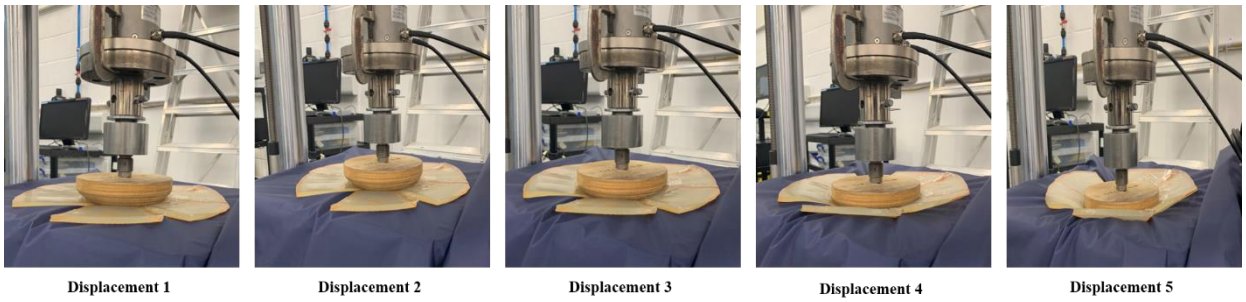

Figure B-5: Compressive displacements of the indenter in 12 mm increments to a maximum of 60 mm (displacement 5).

A region of interest incorporating 14x14 sensors under the spherical indenter was selected. For the maximum displacement of 60 mm, the maximum pressure recorded was approximately 170mmHg. In order to evaluate the pressure response of the mat, two pressure parameters were estimated. Peak pressure index (PPI) was calculated as the mean of values of pressure above specific thresholds of 5mmHg and 10mmHg. In addition, the contact area of all sensors above these two pressure thresholds was also calculated. The temporal profiles of PPI and contact area signals are shown in Figures B-6A and B, respectively. Both signals are characterised by incremental step changes which varied with the magnitudes of the displacement. It is also evident that there are differences in displacements for the loading and unloading phases in both parameters. During each increment there were minimal changes in either parameter over the 5 minutes period.

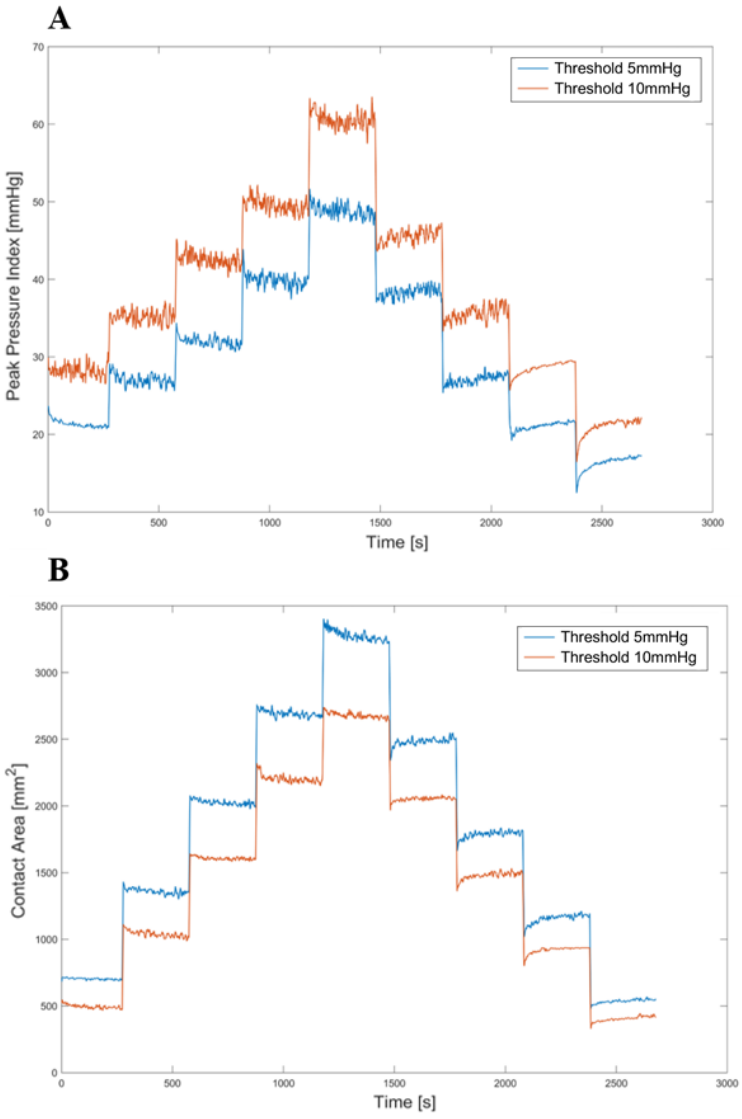

Figure B-6: Temporal trend of: peak pressure index (A), estimated as the mean of pressure values above a threshold of 5mmHg (curve in blue) and 10mmHg (curve in orange); contact area (B) estimated as the area covered a number of sensor cells recording a pressure value above the threshold of 5mmHg (blue curve) and 10mmHg (orange curve).

An elastic response is evident in the force signal recorded by the load cell, as indicated in in Figure B-7. This is characterised by incremental step changes which varied with the magnitude of the displacement. In addition, the load values revealed differences at similar increments for loading and unloading cycles. There was a clear force relaxation during the 5 minute period at each increment.

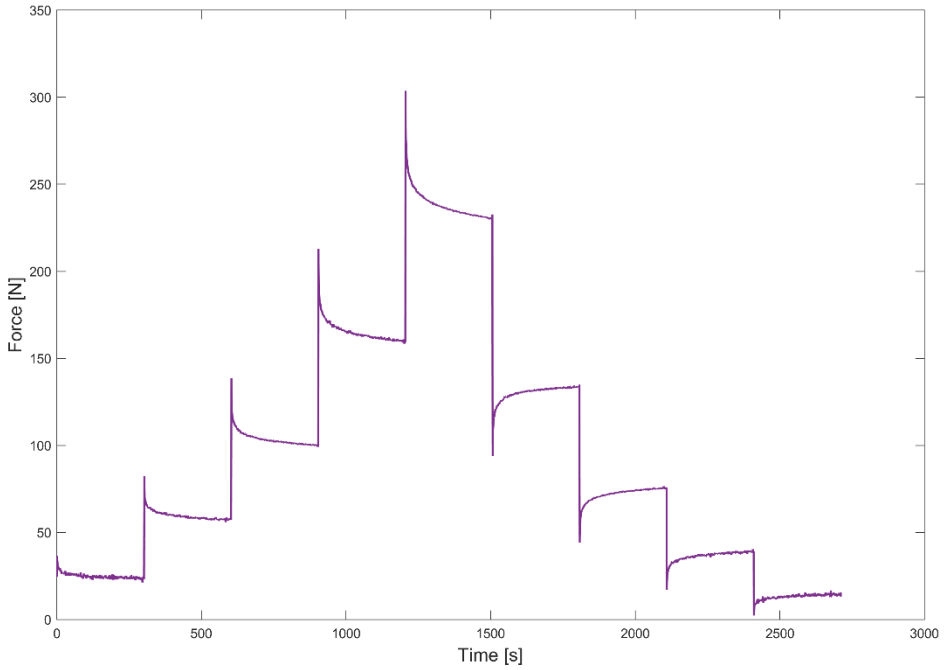

Figure B-7: Temporal trend of the force [N] recorded by the load cell, which clearly showed an elastic response in the transition from a displacement to the next.

In order to evaluate the accuracy of the mat, the peak pressure index response for the two threshold pressures were compared with the pressure exerted by the indenter, which was calculated as the force (Figure B-7) divided by the contact area estimated at 5 mmHg.

Signals of peak pressure index, force and contact area were subjected to an initial processing before comparison. In particular, the transitions between each step were not included as affected by elastic response. These were excluded by selecting the beginning and the end of the 5 minute period at each increment. Each period was then interpolated in order to encompass 300 data points, corresponding to 300 seconds, resulting in a total of 2700 data points per signal. The interpolation was applied in order to include signals and hence steps of equivalent length. Signal of force was then divided by contact area of pressure values ≥ 5mmHg, thus obtaining the metric N/mm^2 which was then converted to mmHg. Thus, peak pressure index signals estimated at 5mmHg and 10mmHg (signals in red – Figure B-8A and B) were compared with the pressure estimated at the indenter level (signal in green – Figure B-8A and B).

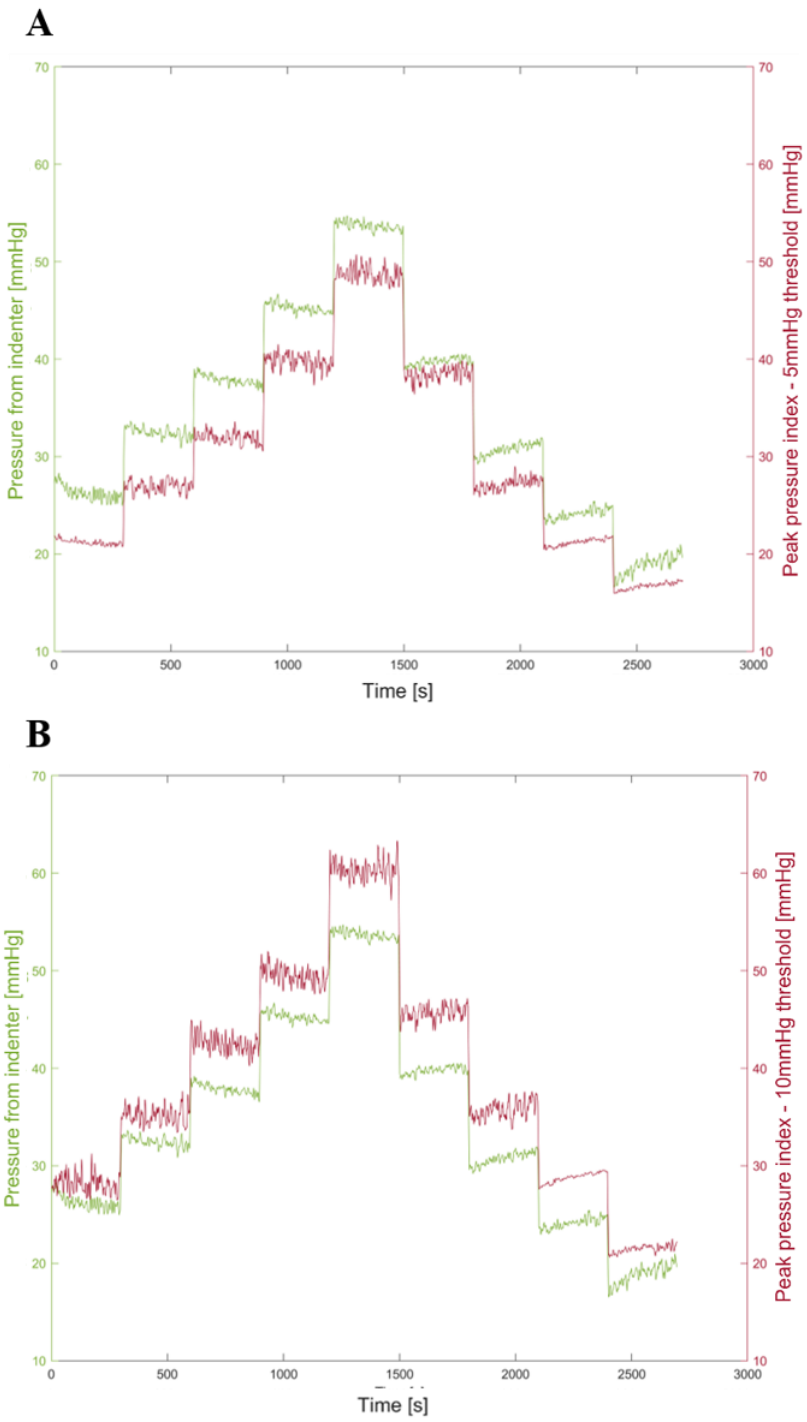

Figure B-8: Comparison between peak pressure index (signals in red) estimated at 5mmHg (A) and 10mmHg (B) and the pressure estimated at the indenter level (signals in green).

It is observed that that signal estimated from the indenter is higher in magnitude when compared with the peak pressure index signal estimated at 5mmHg. The differences between the two curves in the 5 minute periods at each increment are not constant (Figure B-8A). By contrast, peak pressure index signal estimated at 10mmHg and signal from the indenter have similar magnitudes for low increments. The difference in magnitude increases for high displacement of the indenter, remaining however constant in both loading and unloading phases.

Appendix C Sensing technologies to monitor lying postural changes

Participant Information Sheet

Study Title: Sensing technologies to monitor postural changes in bed

Researcher: Silvia Caggiari **Ethics number**: **26379**

Please read this information carefully before deciding to take part in this research. It is up to you to decide whether or not to take part. If you are happy to participate you will be asked to sign a consent form.

What is the research about?

This research project is being carried out by a PhD student, Silvia Caggiari (SC). The study aims to explore different lying and seated postures maintained for prolonged periods of time. This falls within the focus of our research team to prevent pressure ulcers in those individuals with limited mobility and sensation. In order to reduce the time and the amount of pressure sustained, and thus prevent pressure ulcers, frequent repositioning options are commonly applied by nurses and caregivers. Although repositioning is advised in national and international guidelines, the objective examination of the effect different postures has not been fully explained.

The aim of this research study is to establish how well technologies can detect changes in lying and sitting postures. These technologies include sensors that are worn on the body and that are placed between you and the support surface. Our study aims to describe how sensitive the technologies are to both large changes and small changes in posture. In addition, we will monitor how these measurements relate to changes in the health of your soft tissues when lying or sitting for prolonged periods.

Why have I been asked to participate?

Both men and women between the ages of 18 and 80 years are being invited to take part. However, there are certain conditions for which inclusion is contraindicated. These include:

- Current participation in another study
- Complaints of pain or discomfort directly before participation
- Medical history of any dermatological condition, including pressure ulcers
- History of disease associated with the skin, nervous system, musculoskeletal system,
- Not able to lie or sit for a continuous period of 150 minutes.

Do I have to take part?

It is up to you to decide whether or not to take part. If you do decide to take part, you will be given this information sheet to keep and be asked to sign a consent form. **If you do decide to take part, you are still free to withdraw at any time and without giving a reason.**

What will happen to me if I take part?

If you have expressed an interest in the study, you will be asked to come to Southampton General Hospital Tissue Viability laboratory where you can ask further questions about the project. If you decide to participate, you will be required sign a consent form and attend the laboratory on two occasions; session one will last approximately 180 minutes and session two will be 120 minutes. You will be asked to bring some loose fitting clothing, typically t-shirts and shorts/tracksuit bottoms, and change into them. A changing room facility will be provided next to the laboratory. Information about your age, gender, height and weight will be recorded. There will be one researcher (SC) present at all times during testing.

During data collection you will be asked to lie in a bed or sit in a chair. Sensors will then be placed around your upper chest, pelvis and leg using a Velcro strap, and these will measure your movements in the chair and bed. During data collection a sensing mat will be left between you and the support surface to measure the pressure. In addition, 4 small sensors will also be placed between you and the support surface to measure changes in temperature and humidity. All measurements are completely unpainful and non-invasive. Each of the sensors will remain in place during the testing period.

Visit 1: During the test sessions we will ask you to adopt several different postures. All the postures are safe and will be demonstrated by the researcher. Each posture will be held for a 10-15minute period. This will include:

- lying face upwards (supine)
- supine with the head of the bed increased by 10° up to 60° (5 postures)
- supine with the head of the bed decreased by 10° up to supine (5 postures)
- right side lying
- supine
- left side lying

You might feel in a seated position when the head of the bed is raised at angles greater than 40.

If at any point during the study you feel uncomfortable, you will be free to move and reposition yourself. In order to produce small movements in your muscles, two small self-adhesive electrodes will be attached to the skin on your thigh. The electrodes will be connected to a small battery powered machine that will provide a small electrical current, which you feel as a tingling sensation. This will help us prescribe a small movement in your legs. The stimulation will not be painful and will last only 2 minutes. We will record measurements throughout the different postures and also ask you to rate your comfort and safety.

After this time, you will be able to change back into your original clothing and leave the laboratory at your convenience. The researcher (Silvia Caggiari) will ensure that you are comfortable at all times. You will be able to stop the testing session at any time if you do not wish to proceed.

Visit 2: This visit will occur approximately four weeks after visit 1. During the second visit you will be asked to adopt fewer postures. The equipment used will be the same as that in visit one. However, we will make additional measurements of tissue health and temperature/humidity during this test session. During data collection a sensor will be attached to your lower back using an adhesive sensor ring attached to your skin, this will measure how much oxygen and carbon dioxide is in your skin and soft tissues. In order to establish baseline tissue health we will ask you to lie on your front for a 15 minute period. Once this is established you will then be asked to adopt five postures, which are similar to those which you have completed in visit 1. We will again ask you to rate your comfort during each posture.

The researcher (Silvia Caggiari) will ensure that you are comfortable at all times and will never do anything that you are not happy with. You will be able to stop the testing session at any time if you do not wish to proceed.

What are the risks involved in taking part?

There are very few risks in taking part in the study. You may feel uncomfortable in some of the postures we ask you to adopt. The researcher will take great care to avoid any discomfort, embarrassment, or harm.

What are the possible benefits of taking part?

There are no direct benefits to taking part in this study.

Will my participation be confidential?

In accordance with data protection policy of the Faculty of Health Sciences and the Data Protection Act 1998, all participant details will be removed from any documentation and a study specific code number assigned. Details of participants will be known only to the researcher and the senior investigators (Professor Dan Bader and Dr Peter Worsley, SC's supervisors) and stored securely in a locked filing cabinet, within a locked office within the research group, accessible only to the senior investigators. The anonymised data collected will be stored for subsequent off-line analysis. All analyses will be conducted within the research group. At the end of the study all documentation (i.e. study file, raw data, lab books) will be securely archived in accordance with University of Southampton policy with access only available to the senior investigator. Accordingly, the data will be stored for 10 years.

What happens if I change my mind?

You have the right to withdraw at any time, with or without reason.

What will happen to the results of the research?

The results of this study will be written up for publication in journals and presented at national and international research and industry events. The data will also be presented in a PhD thesis of SC which will be published in public records. We will only present anonymised data in order to protect your identity.

What happens if something goes wrong?

If you have any complaints or concerns during this study, you should inform the researcher immediately. In the unlikely event that something goes wrong during the study, indemnity insurance has been provided.

If you have a concern or a complaint about this study, you should contact the research governance team at the university (023 8059 5058, rgoinfo@soton.ac.uk). They will be able to support you regarding any complaints with the study or investigators.

Contact for Further Information

Silvia Caggiari

Faculty of Health Sciences

University of Southampton

E-mail: S.Caggiari@soton.ac.uk

You will be given a copy of this information sheet and a signed consent form to keep.

Thank you for taking the time to read this information.

Appendix D Sensitivity trends - Postural changes in the sagittal plane

Centre of Pressure (COP)

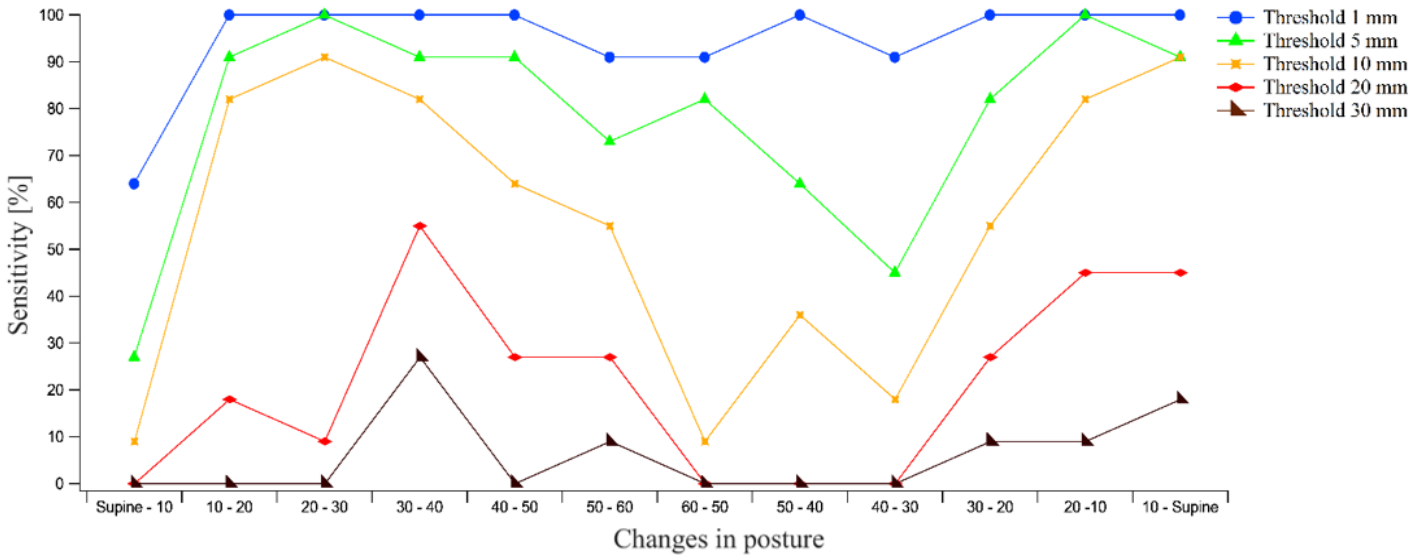

Figure D-1: Sensitivity trend in evaluating the sagittal changes in posture in the **whole body ROI** for COP displacements. Each curve represents the trend with respect a specific threshold value (1, 5, 10, 20, 30 mm). Each data point represents the sensitivity value [%], across all participants, for a specific threshold value.

Peak Pressure

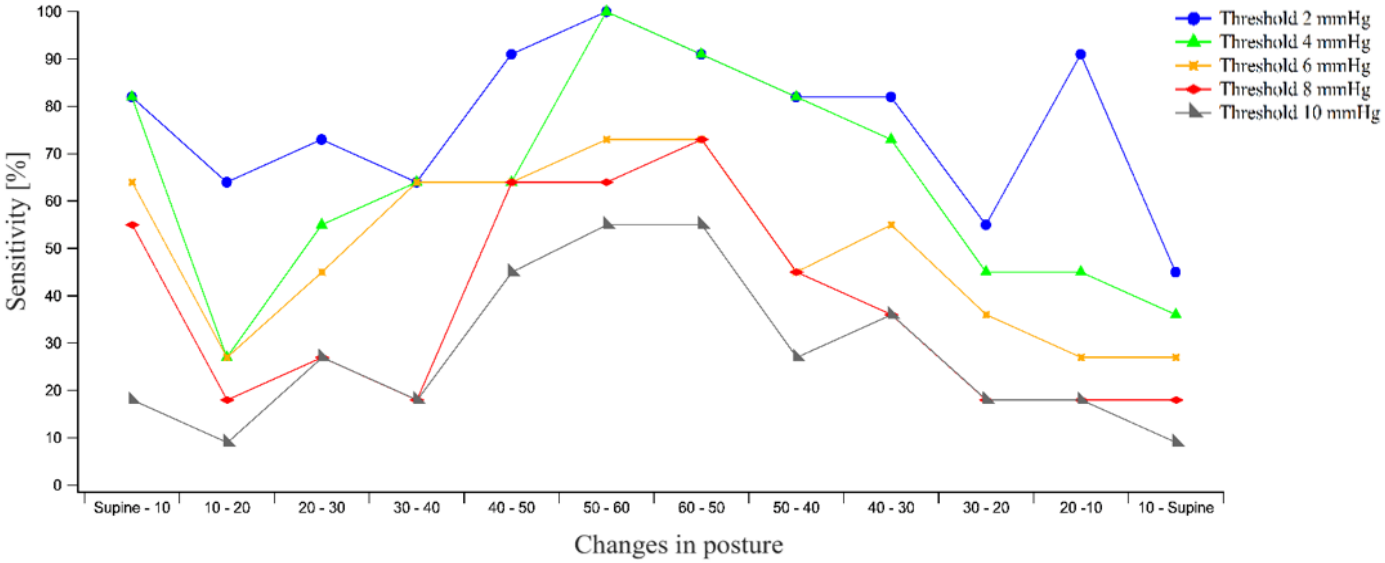

Figure D-2: Sensitivity trend in evaluating the sagittal changes in posture in the **whole body ROI** for peak pressures. Each curve represents the trend with respect a specific threshold value (2, 4, 6, 8, 10 mmHg). Each data point represents the sensitivity value [%], across all participants, for a specific threshold value.

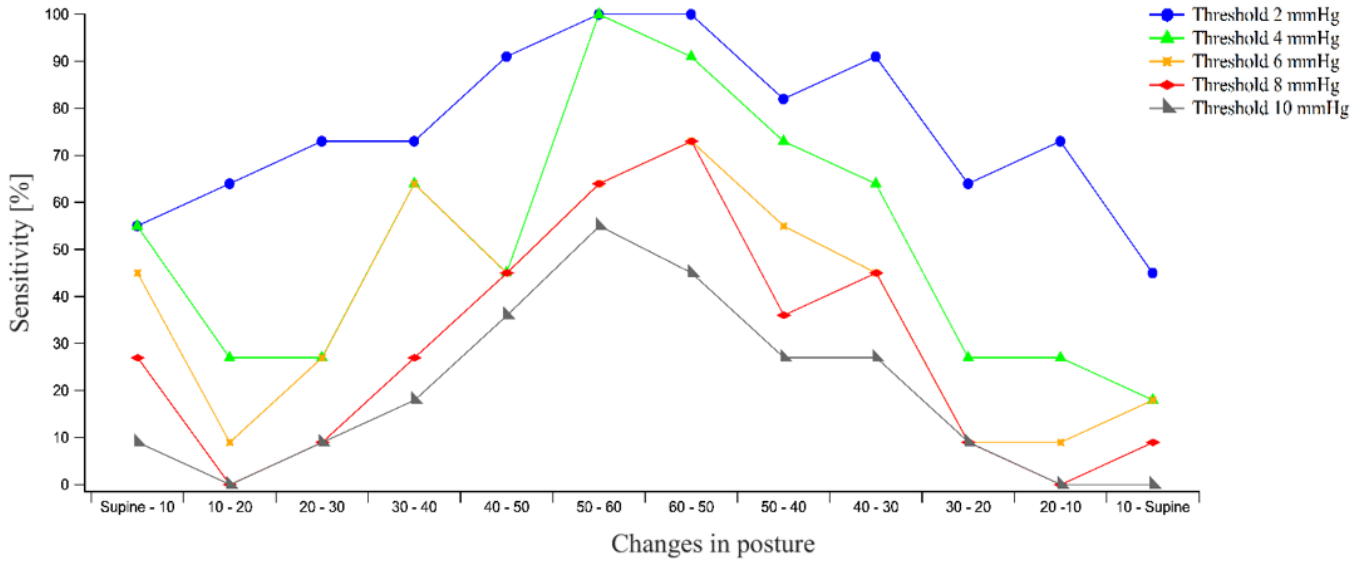

Figure D-3: Sensitivity trend in evaluating the sagittal changes in posture in the **buttock ROI** for peak pressures. Each curve represents the trend with respect a specific threshold value (2, 4, 6, 8, 10 mmHg). Each data point represents the sensitivity value [%], across all participants, for a specific threshold value.

Peak pressure gradient – Parallel direction with respect to the long axis of the mat

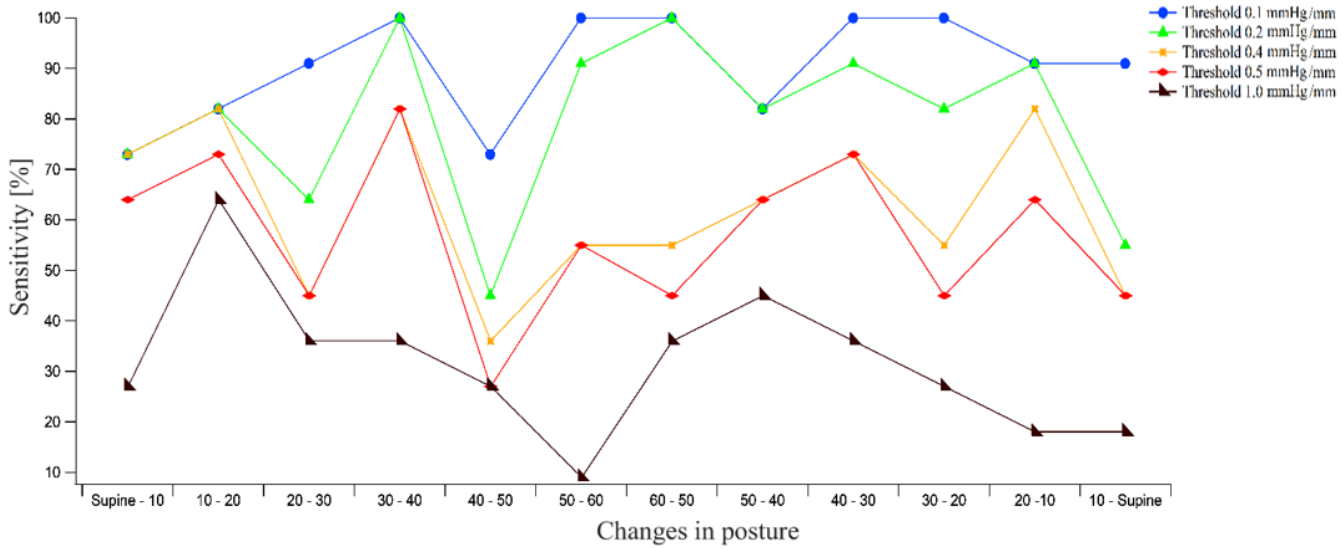

Figure D-4: Sensitivity trend in evaluating the sagittal changes in posture in the **whole body ROI** for peak pressure gradient estimated in the parallel direction. Each curve represents the trend with respect a specific threshold value (0.1, 0.2, 0.4, 0.5, 1.0 mmHg/mm). Each data point represents the sensitivity value [%], across all participants, for a specific threshold value.

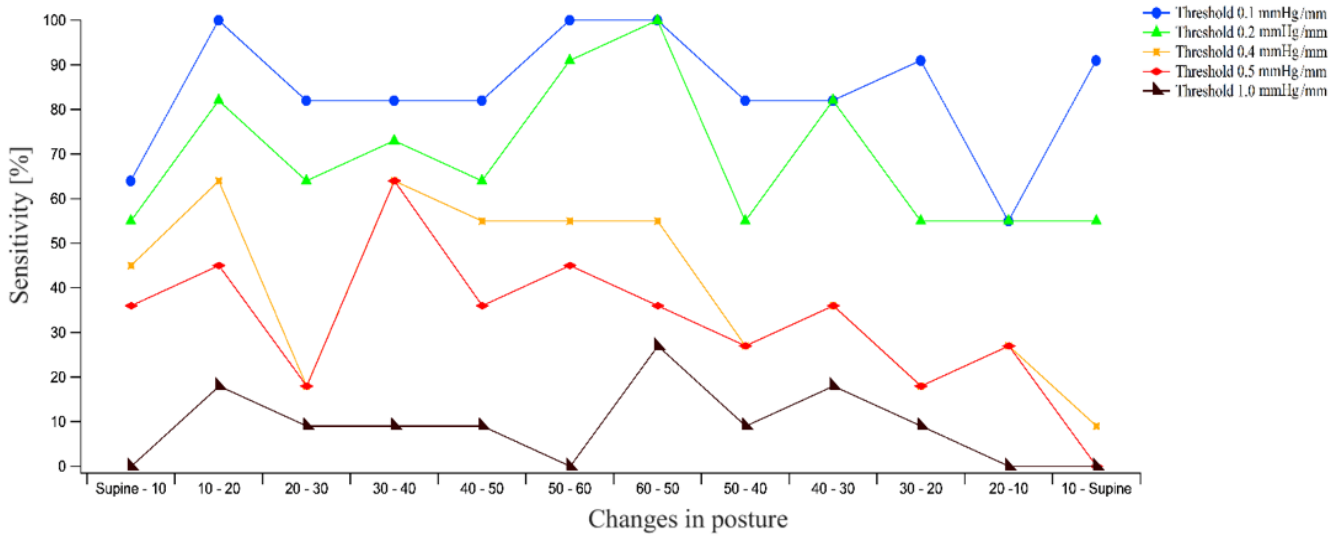

Figure D-5: Sensitivity trend in evaluating the sagittal changes in posture in the **buttock ROI** for peak pressure gradient estimated in the parallel direction. Each curve represents the trend with respect a specific threshold value (0.1, 0.2, 0.4, 0.5, 1.0 mmHg/mm). Each data point represents the sensitivity value [%], across all participants, for a specific threshold value.

Peak pressure gradient – perpendicular direction with respect to the long axis of the mat

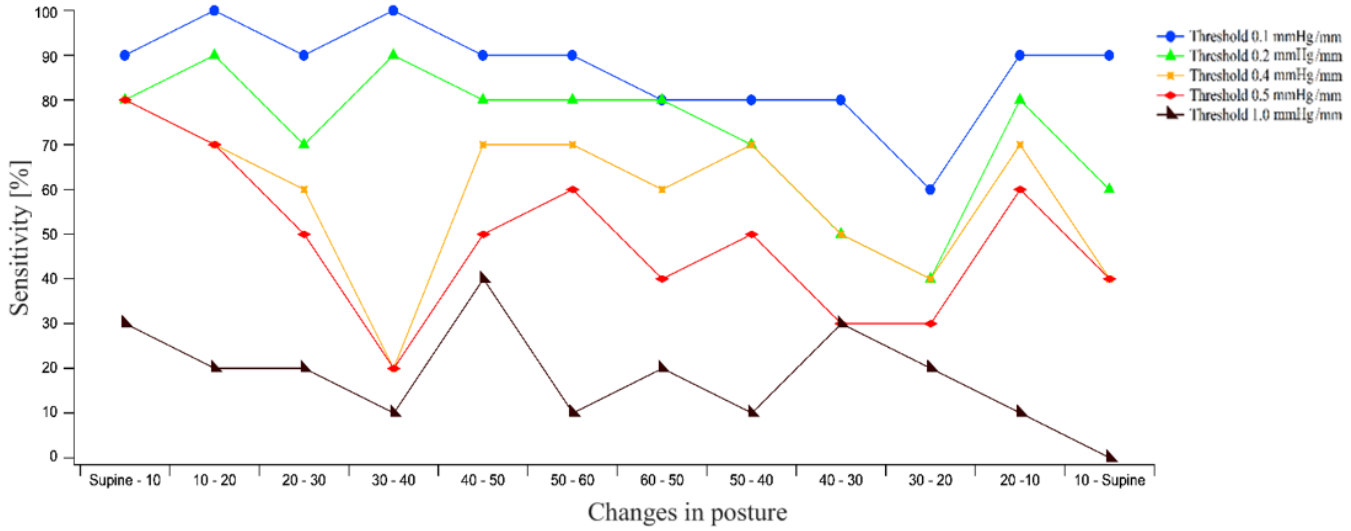

Figure D-6: Sensitivity trend in evaluating the sagittal changes in posture in the **whole body ROI** for peak pressure gradient estimated in the perpendicular direction. Each curve represents the trend with respect a specific threshold value (0.1, 0.2, 0.4, 0.5, 1.0 mmHg/mm). Each data point represents the sensitivity value [%], across all participants, for a specific threshold value.

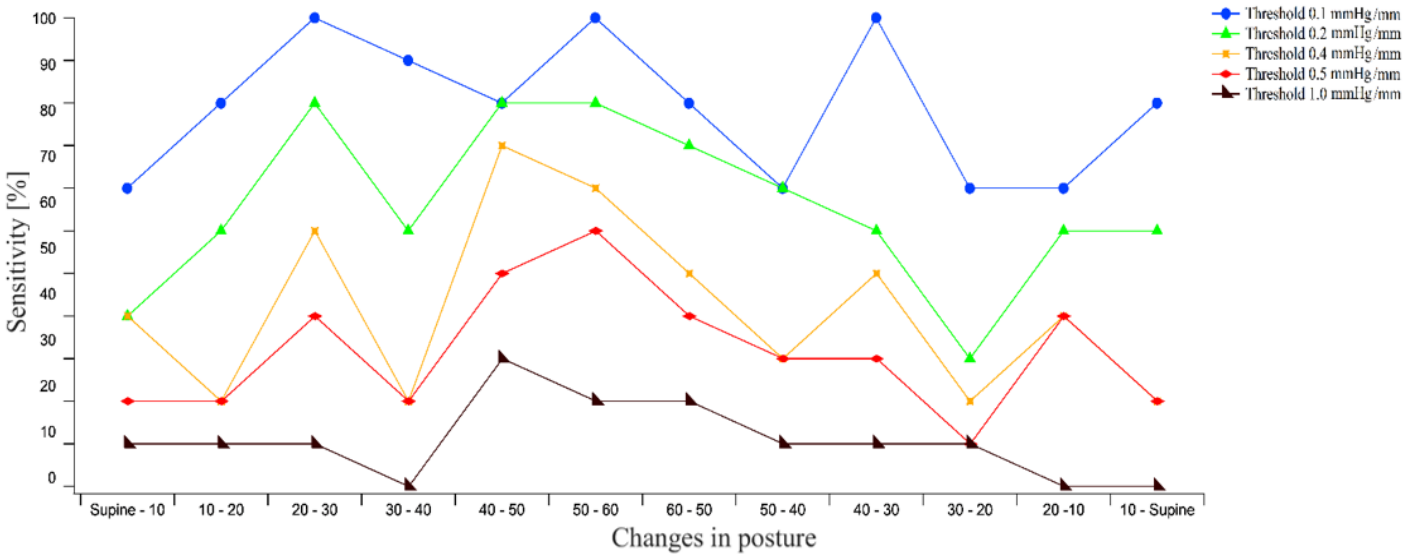

Figure D-7: Sensitivity trend in evaluating the sagittal changes in posture in the **buttock ROI** for peak pressure gradient estimated in the perpendicular direction. Each curve represents the trend with respect a specific threshold value (0.1, 0.2, 0.4, 0.5, 1.0 mmHg/mm). Each data point represents the sensitivity value [%], across all participants, for a specific threshold value.

Contact Area

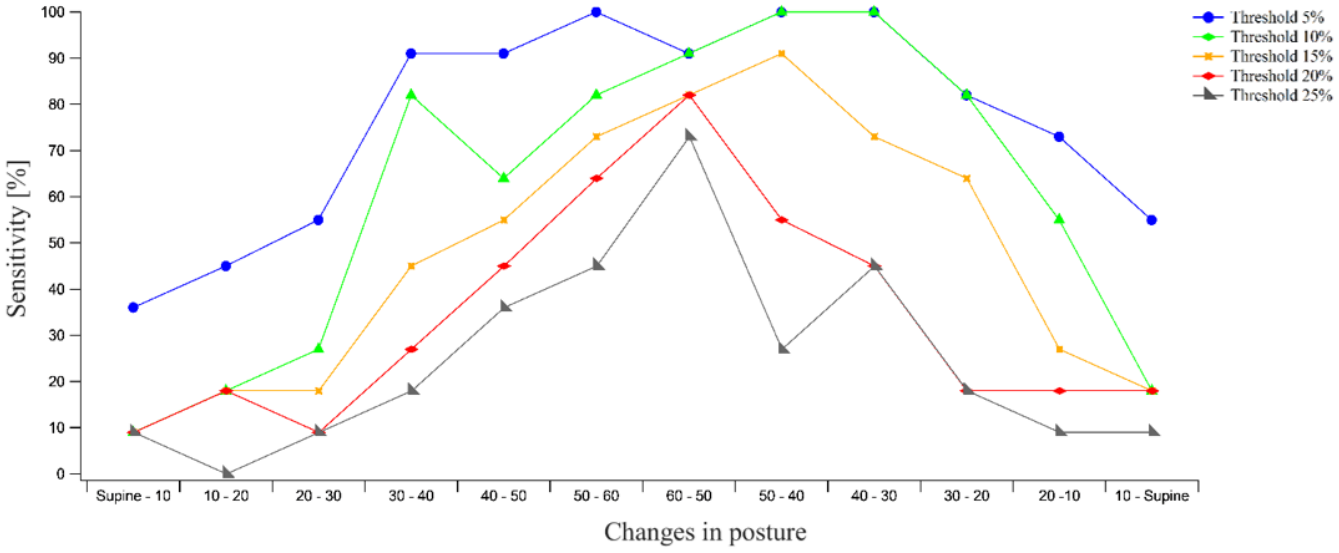

Figure D-8: Sensitivity trend in evaluating the sagittal changes in posture in the **whole body ROI** for contact area. Each curve represents the trend with respect a specific threshold value (5, 10, 15, 20, 25 %). Each data point represents the sensitivity value [%], across all participants, for a specific threshold value.

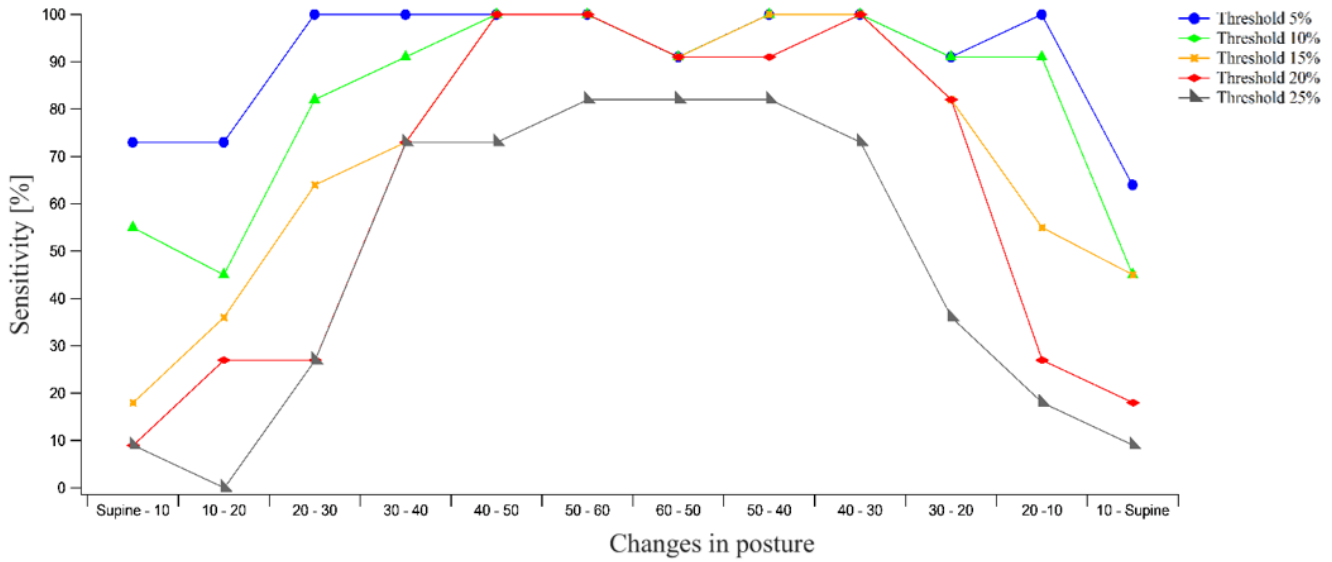

Figure D-9: Sensitivity trend in evaluating the sagittal changes in posture in the **buttock ROI** for contact area. Each curve represents the trend with respect a specific threshold value (5, 10, 15, 20, 25 %). Each data point represents the sensitivity value [%], across all participants, for a specific threshold value.

Tilt angles

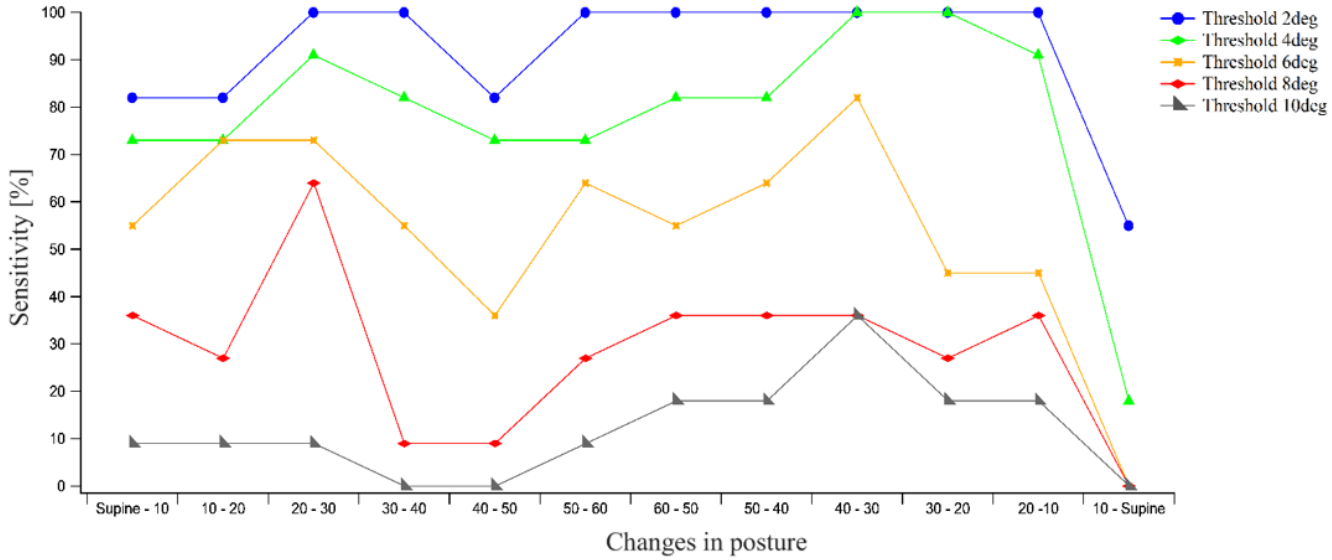

Figure D-10: Sensitivity trend in evaluating changes in posture for tilt angles estimated at the **waist location**. Each curve represents the trend with respect a specific threshold value (2, 4, 6, 8, 10 degree). Each data point represents the sensitivity value [%], across all participants, for a specific threshold value.

Appendix E Specificity trends - Postural changes in the sagittal plane

Centre of Pressure (COP)

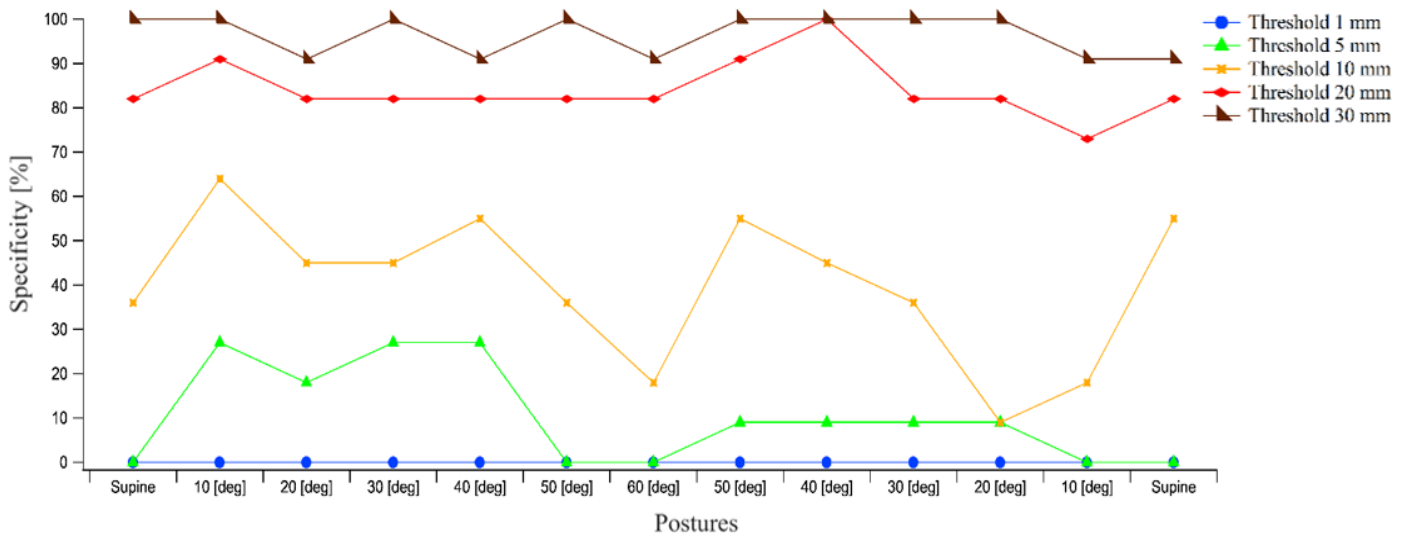

Figure E-1: Specificity trend in evaluating the movements within each postures in **whole body ROI** for COP displacements. Each curve represents the trend with respect a specific threshold value, ranging between 1 mm and 30 mm. Each data point represents the specificity value [%], across all participants, for a specific threshold value.

Peak Pressure

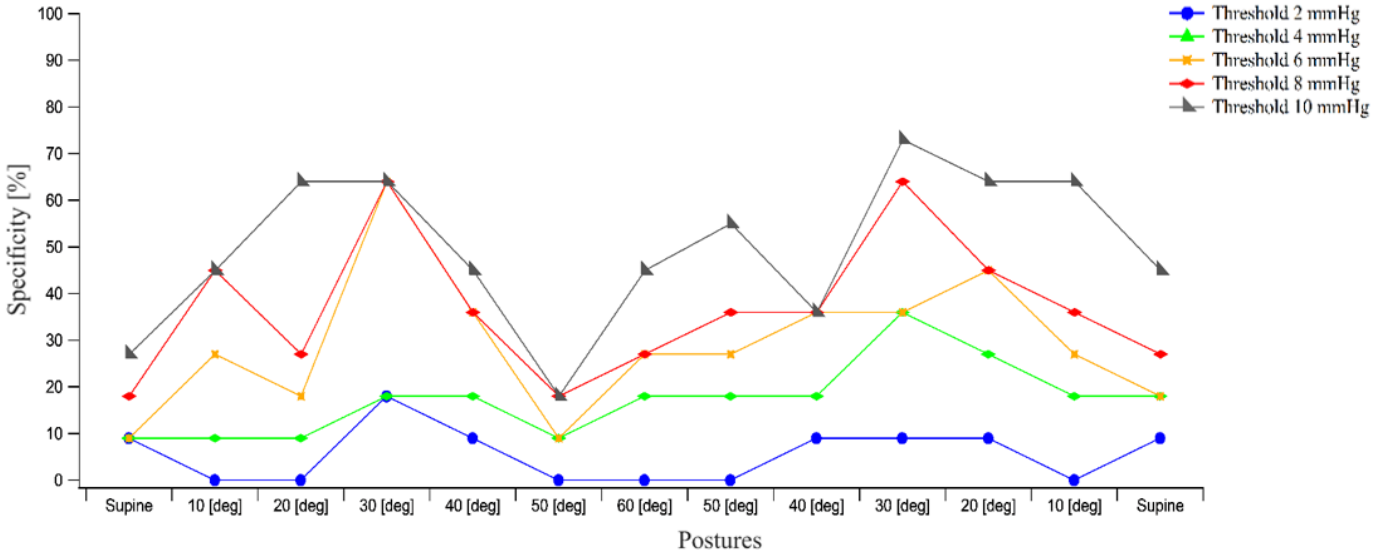

Figure E-2: Specificity trend in evaluating the movements within each postures in **whole body ROI** for peak pressures. Each curve represents the trend with respect a specific threshold value, ranging between 2 mmHg and 10 mmHg. Each data point represents the specificity value [%], across all participants, for a specific threshold value.

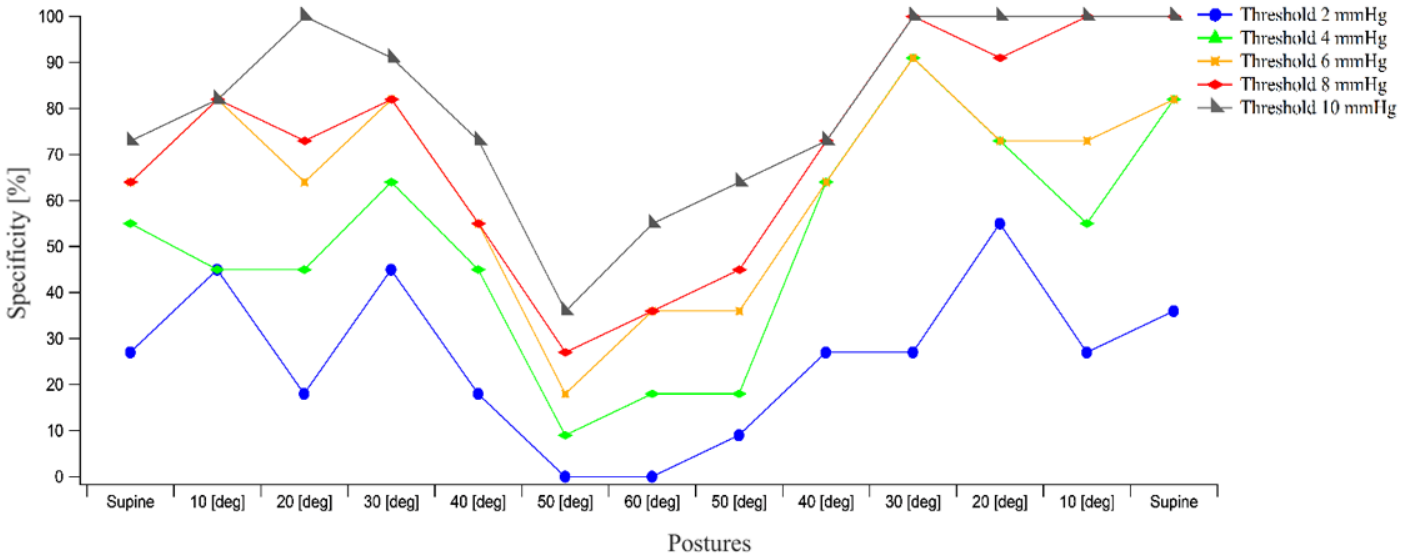

Figure E-3: Specificity trend in evaluating the movements within each postures in **buttock ROI** for peak pressures. Each curve represents the trend with respect a specific threshold value, ranging between 2 mmHg and 10 mmHg. Each data point represents the specificity value [%], across all participants, for a specific threshold value.

Peak pressure gradient – Parallel direction with respect to the long axis of the mat

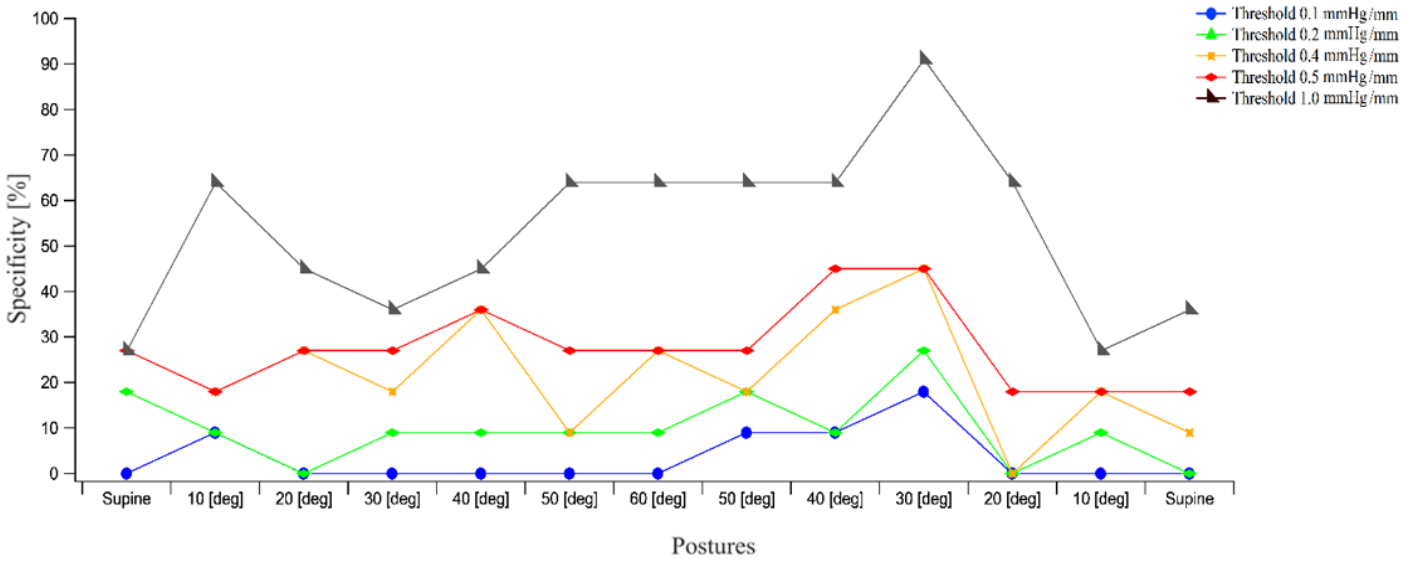

Figure E-4: Specificity trend in evaluating the movements within each postures in **whole body ROI** for peak pressure gradient estimated in the parallel direction. Each curve represents the trend with respect a specific threshold value, ranging between 0.1 mmHg/mm and 1.0 mmHg/mm. Each data point represents the specificity value [%], across all participants, for a specific threshold value.

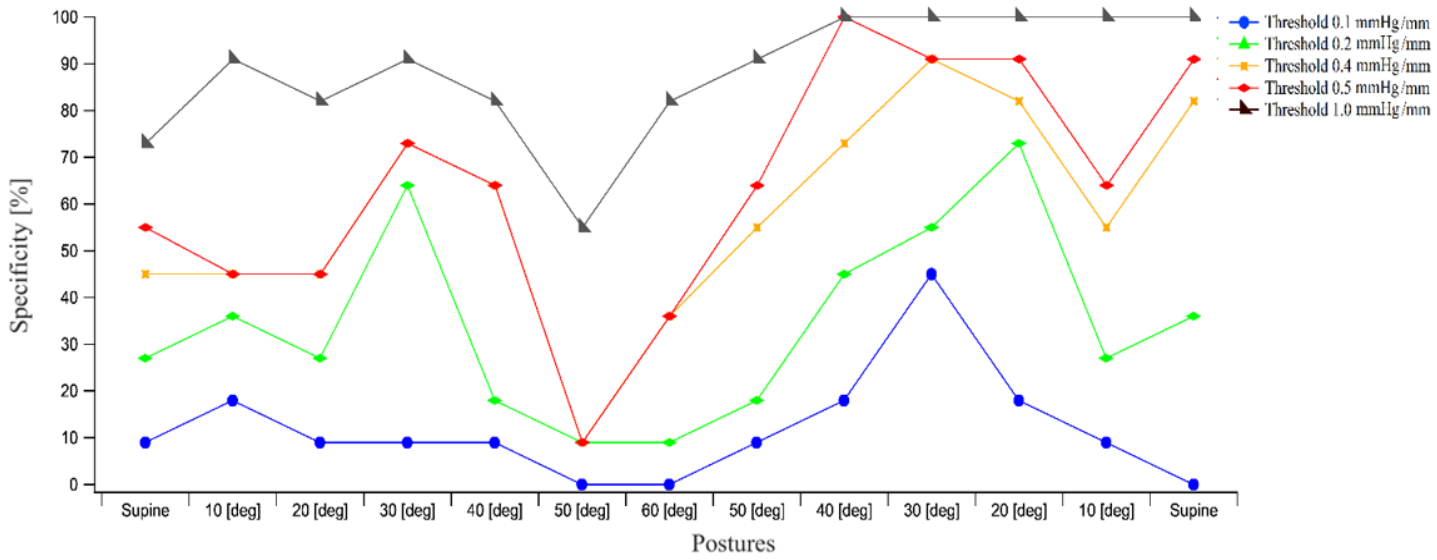

Figure E-5: Specificity trend in evaluating the movements within each postures in **buttock ROI** for peak pressure gradient estimated in the parallel direction. Each curve represents the trend with respect a specific threshold value, ranging between 0.1 mmHg/mm and 1.0 mmHg/mm. Each data point represents the specificity value [%], across all participants, for a specific threshold value.

Peak pressure gradient – Perpendicular direction with respect to the long axis of the mat

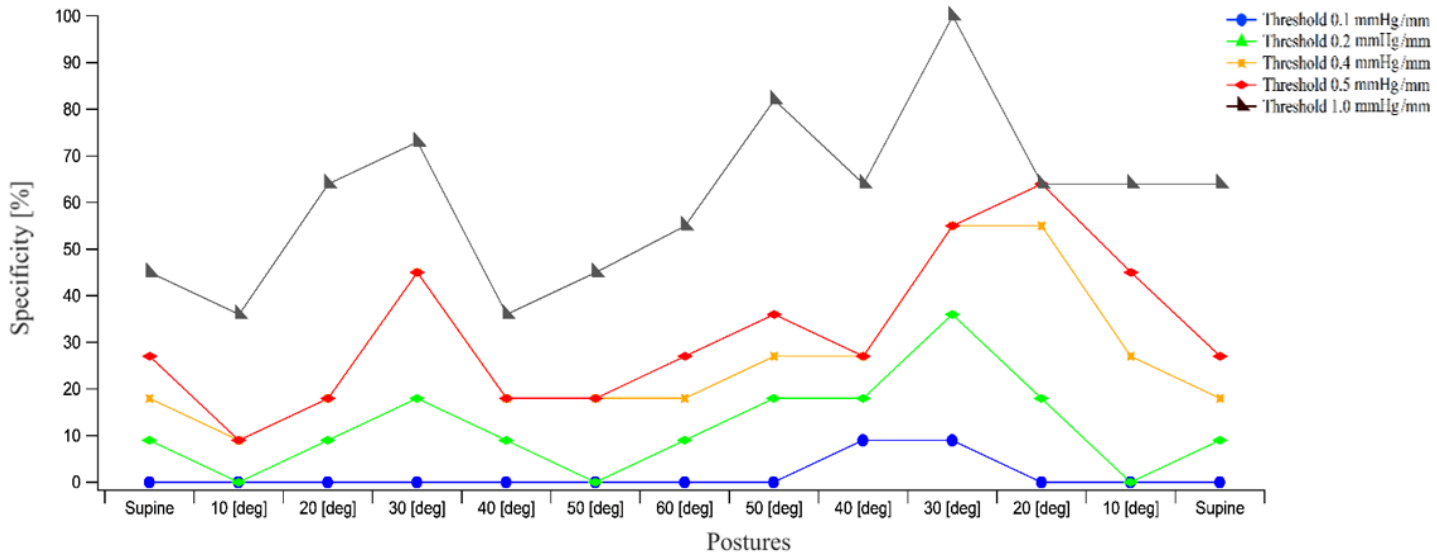

Figure E-6: Specificity trend in evaluating the movements within each postures in **whole body ROI** for peak pressure gradient estimated in the perpendicular direction. Each curve represents the trend with respect a specific threshold value, ranging between 0.1 mmHg/mm and 1.0 mmHg/mm. Each data point represents the specificity value [%], across all participants, for a specific threshold value.

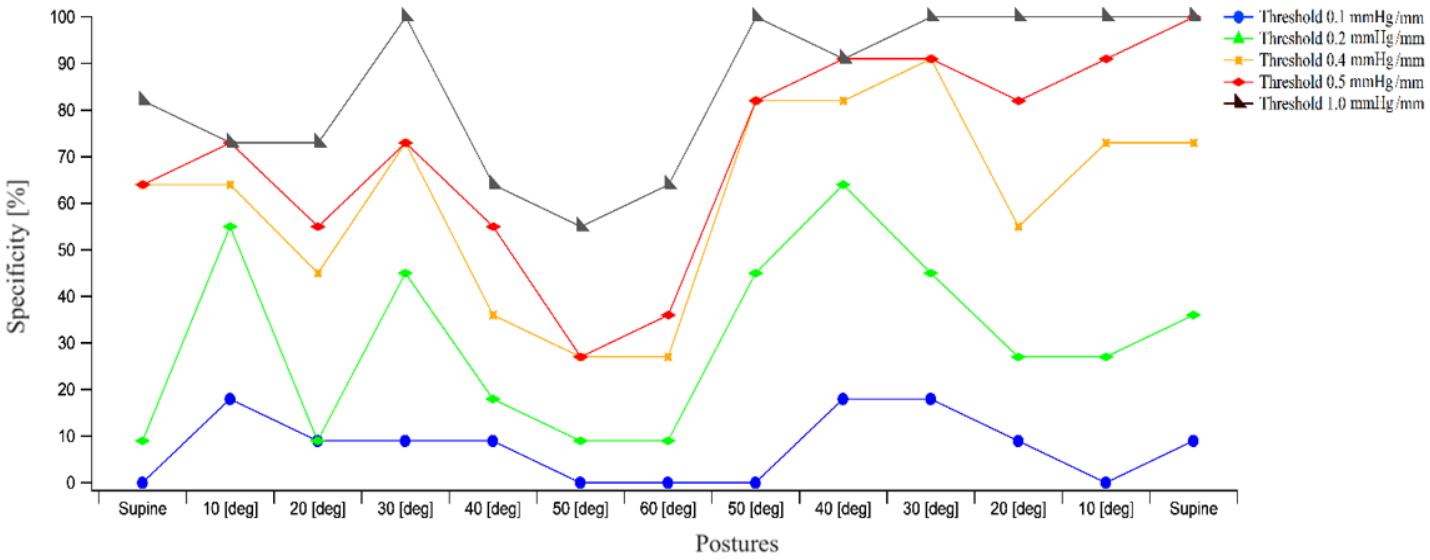

Figure E-7: Specificity trend in evaluating the movements within each postures in **buttock ROI** for peak pressure gradient estimated in the perpendicular direction. Each curve represents the trend with respect a specific threshold value, ranging between 0.1 mmHg/mm and 1.0 mmHg/mm. Each data point represents the specificity value [%], across all participants, for a specific threshold value.

Contact Area

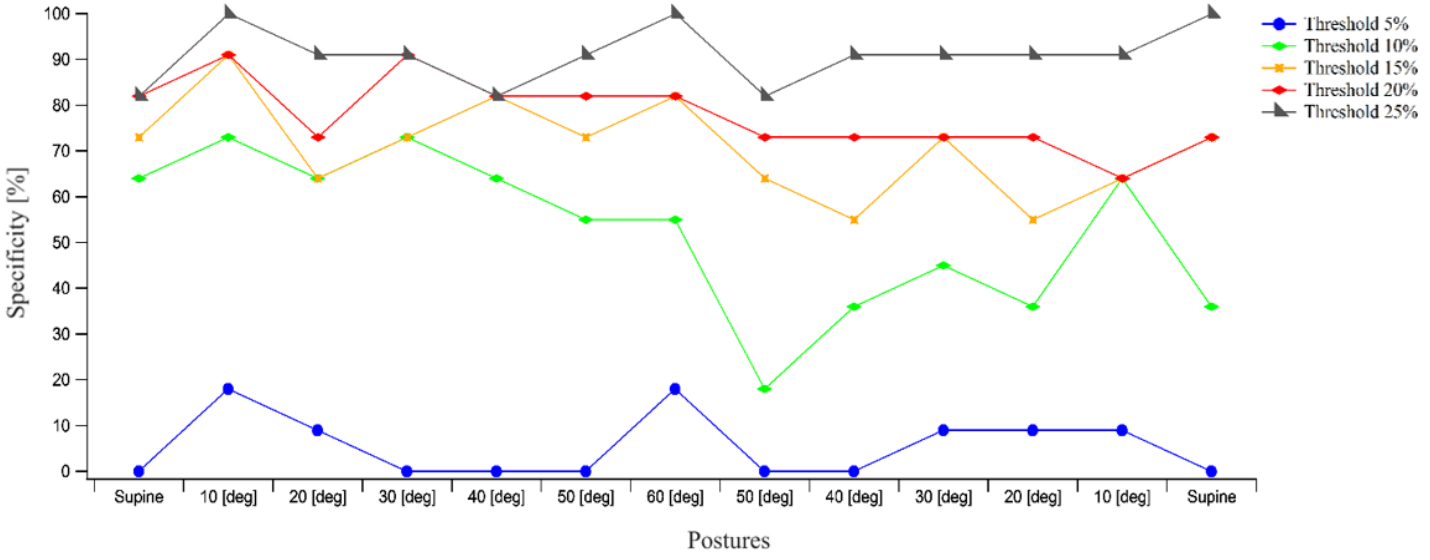

Figure E-8: Specificity trend in evaluating the movements within each postures in **whole body ROI** for contact area. Each curve represents the trend with respect a specific threshold value, ranging between 5% and 25%. Each data point represents the specificity value [%], across all participants, for a specific threshold value.

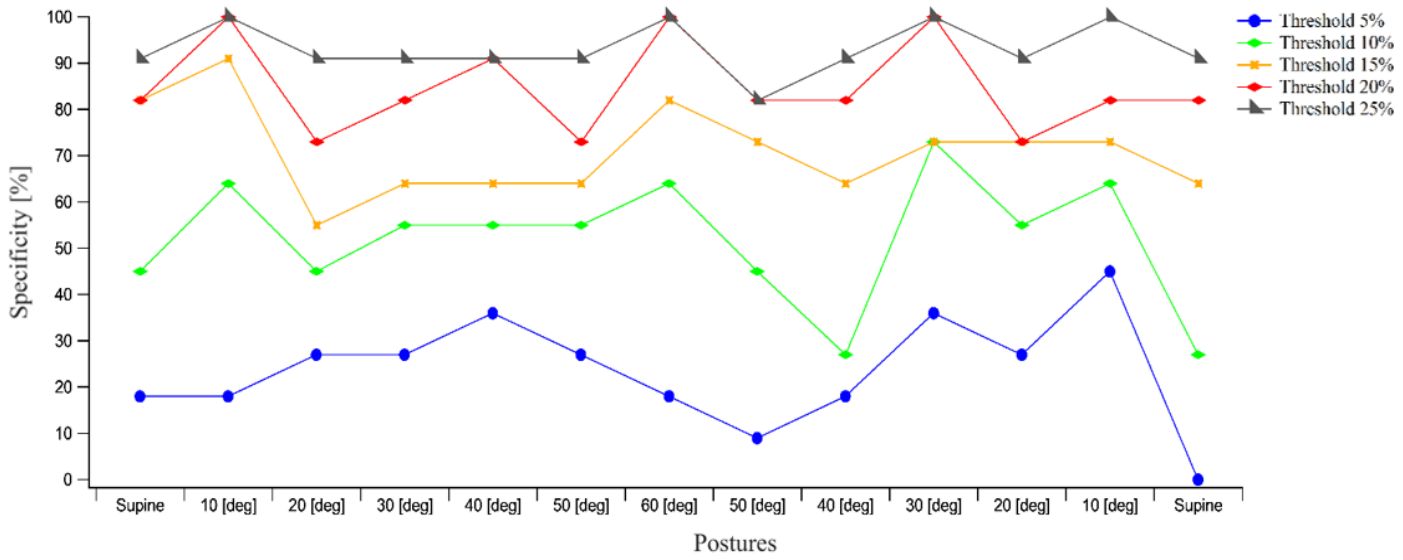

Figure E-9: Specificity trend in evaluating the movements within each postures in **buttock ROI** for contact area. Each curve represents the trend with respect a specific threshold value, ranging between 5% and 25%. Each data point represents the specificity value [%], across all participants, for a specific threshold value.

Tilt angles

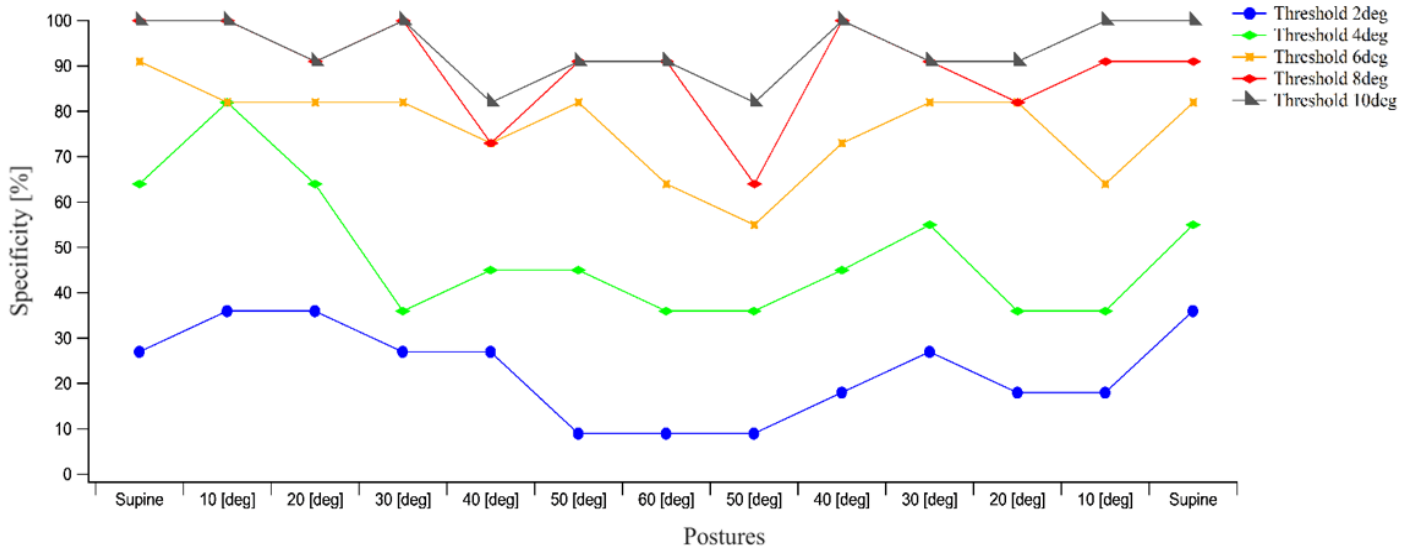

Figure E-10: Specificity trend in evaluating the **waist tilt angles** within each postures. Each curve represents the trend with respect a specific threshold value, ranging between 2 and 10°. Each data point represents the specificity value [%], across all participants, for a specific threshold value.

Appendix F Sensitivity trends - Postural changes in the transverse plane

Centre of Pressure (COP)

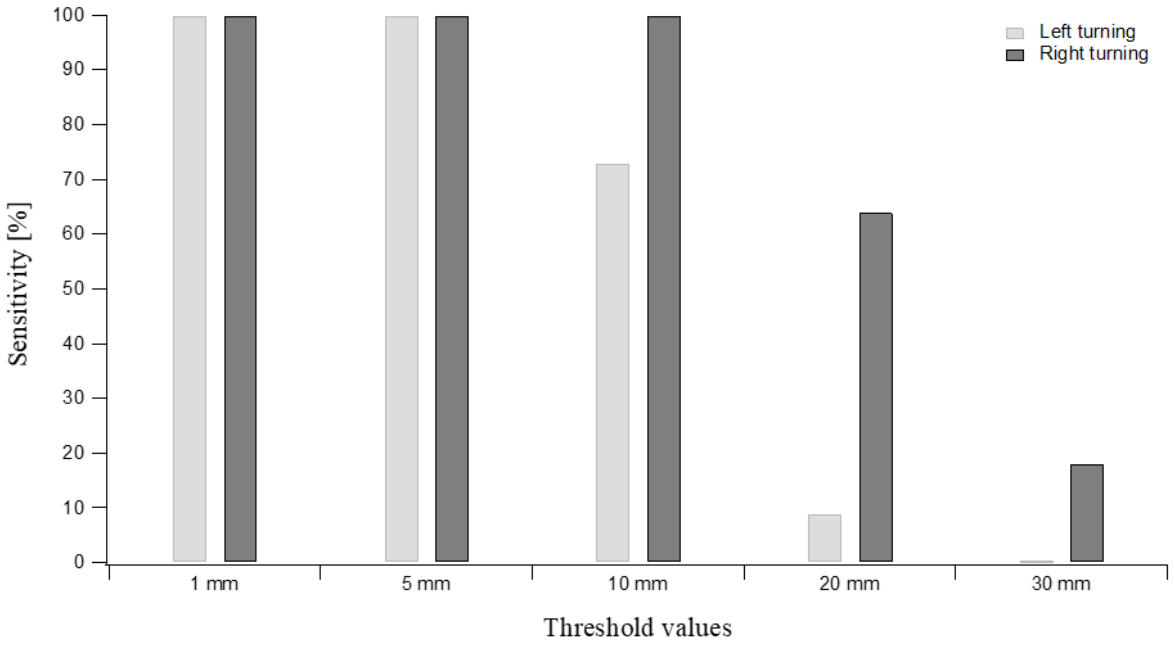

Figure F-1: Sensitivity values in detecting the lateral changes in posture during left and right turning for the **whole body COP** at four threshold values, ranging between 1 mm and 30 mm.

Peak pressure

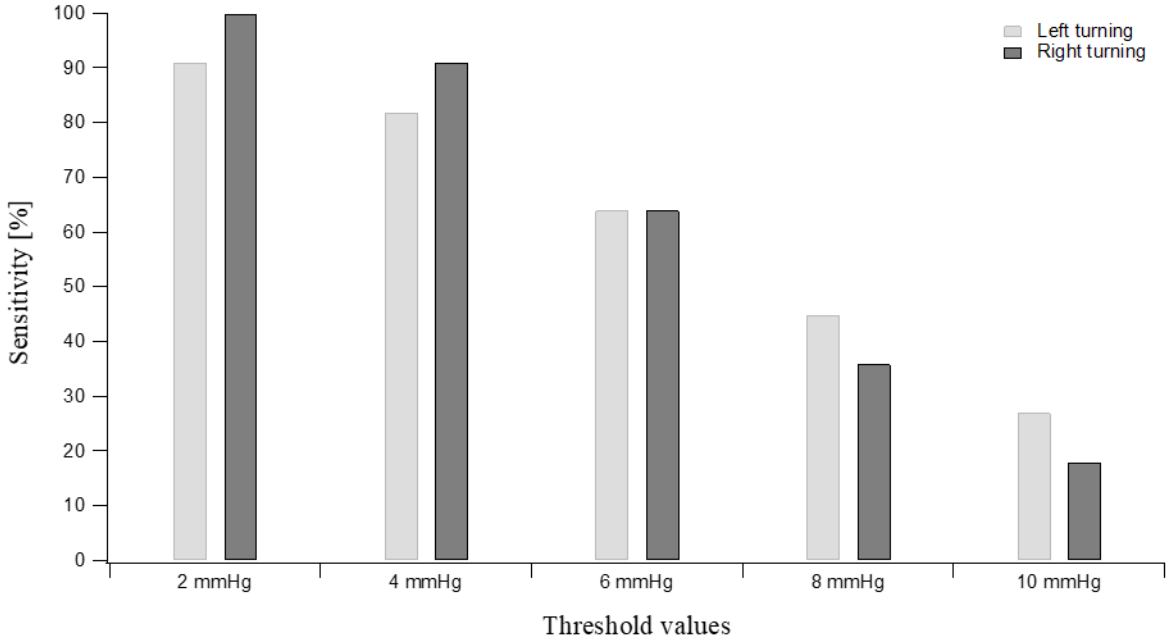

Figure F-2: Sensitivity values in detecting the lateral changes in posture during left and right turning for the **whole body peak pressures** at four threshold values, ranging between 2 mmHg and 10 mmHg.

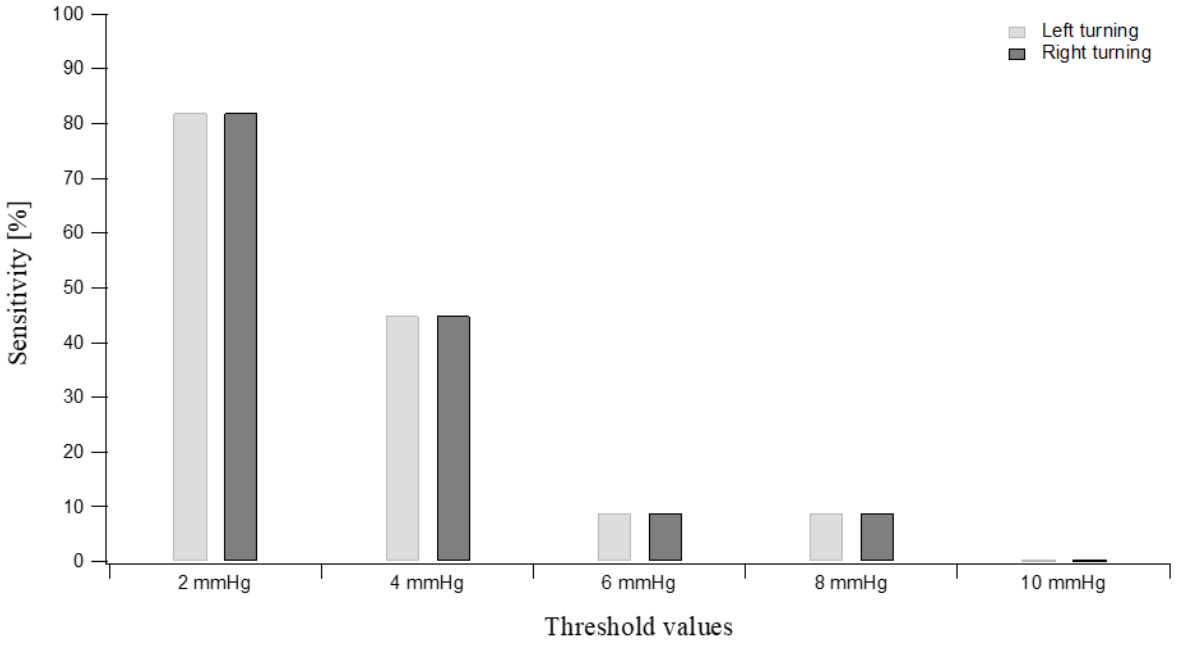

Figure F-3: Sensitivity values in detecting the lateral changes in posture during left and right turning for the **buttock peak pressures** at four threshold values, ranging between 2 mmHg and 10 mmHg.

Peak pressure gradient – Parallel direction with respect to the long axis of the mat

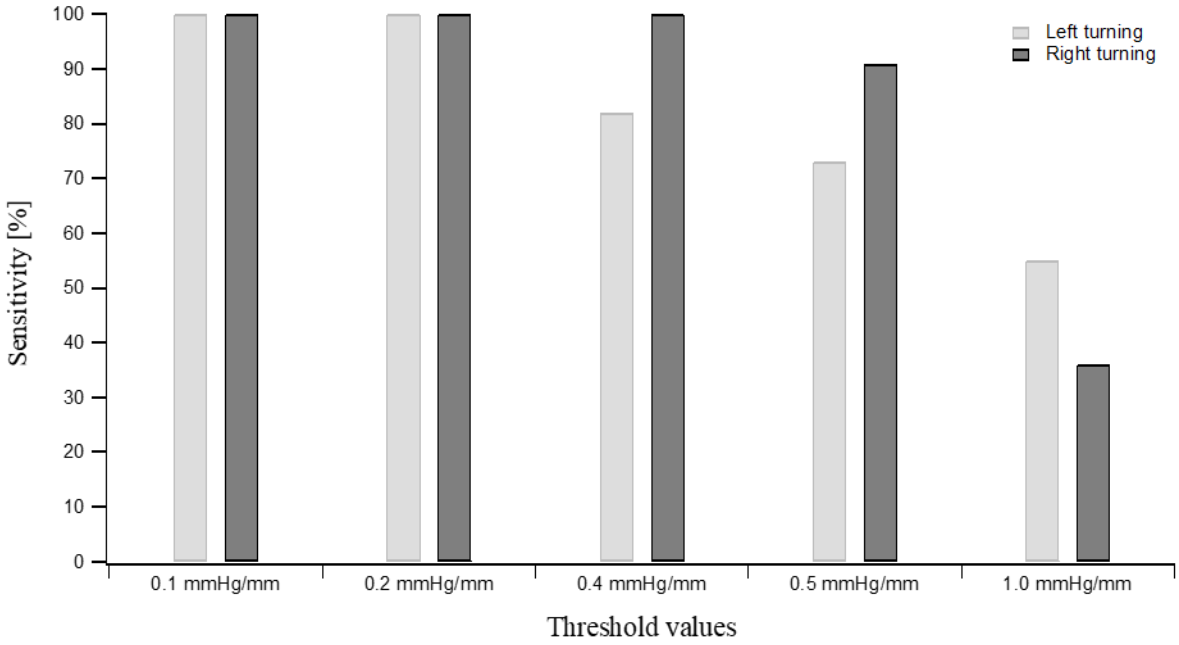

Figure F-4: Sensitivity values in detecting the lateral changes in posture during left and right turning for the **whole body peak pressure gradient** estimated in the parallel direction at four threshold values, ranging between 0.1 mmHg/mm and 1.0 mmHg/mm.

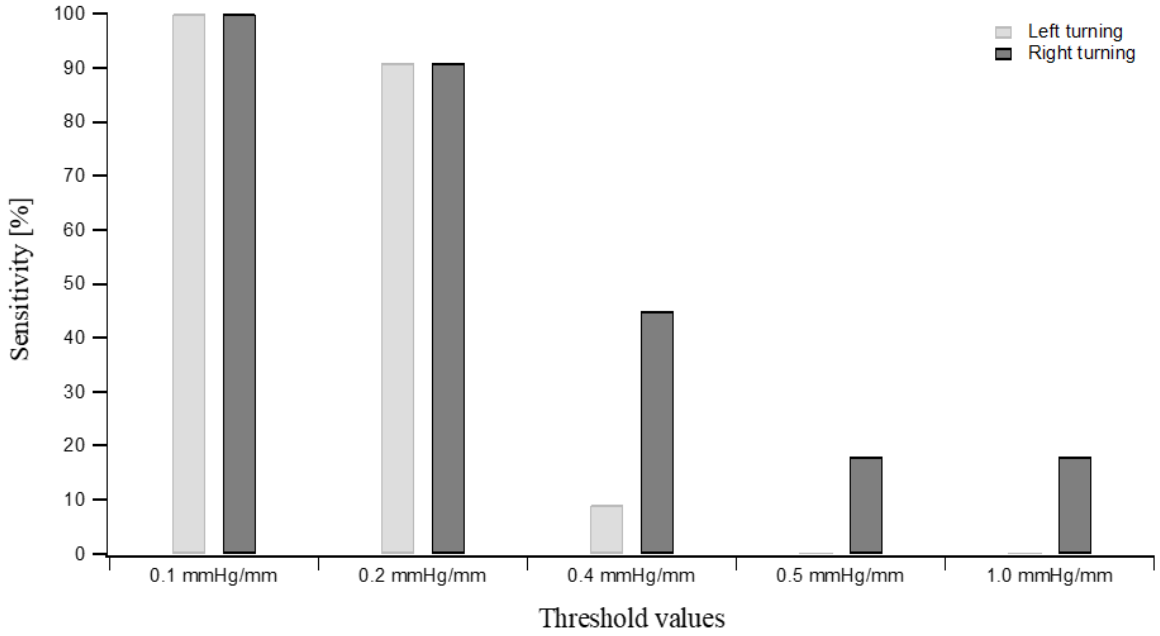

Figure F-5: Sensitivity values in detecting the lateral changes in posture during left and right turning for the **buttock peak pressure gradient** estimated in the parallel direction at four threshold values, ranging between 0.1 mmHg/mm and 1.0 mmHg/mm.

Peak pressure gradient – Perpendicular direction with respect to the long axis of the mat

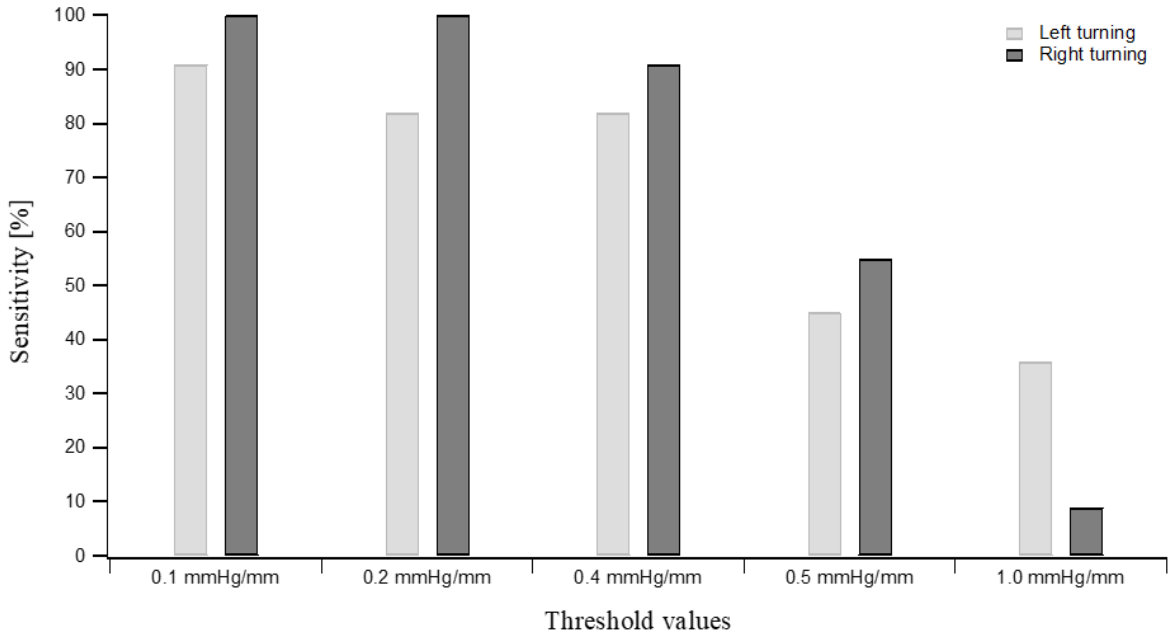

Figure F-6: Sensitivity values in detecting the lateral changes in posture during left and right turning for the **whole body peak pressure gradient** estimated in the perpendicular direction at four threshold values, ranging between 0.1 mmHg/mm and 1.0 mmHg/mm.

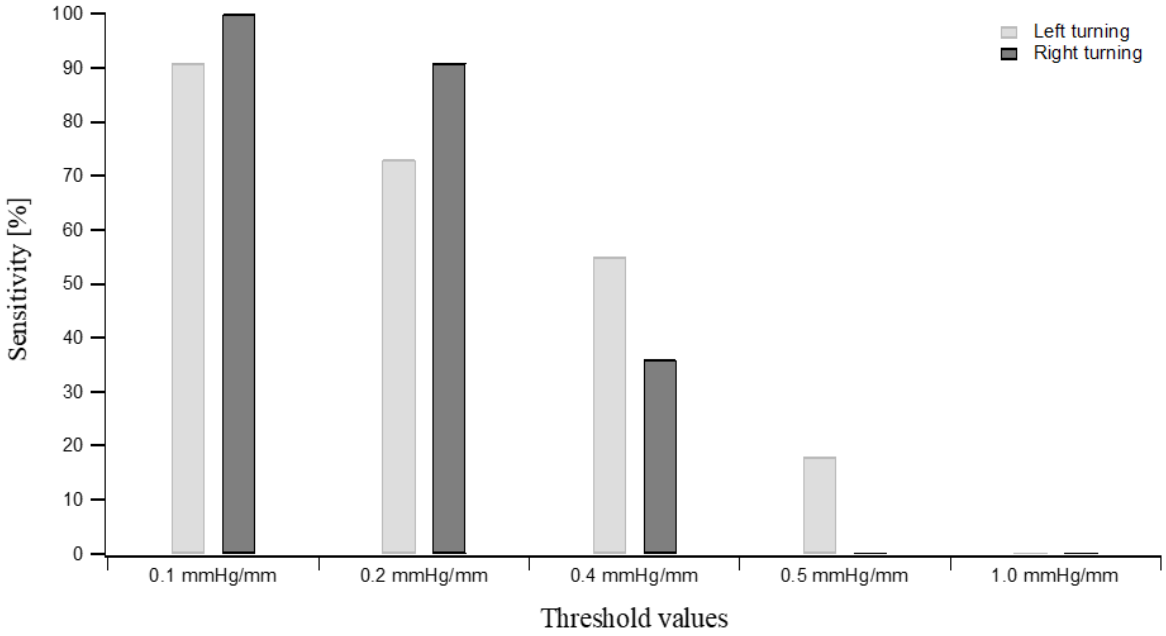

Figure F-7: Sensitivity values in detecting the lateral changes in posture during left and right turning for the **buttock peak pressure gradient** estimated in the perpendicular direction at four threshold values, ranging between 0.1 mmHg/mm and 1.0 mmHg/mm.

Contact Area

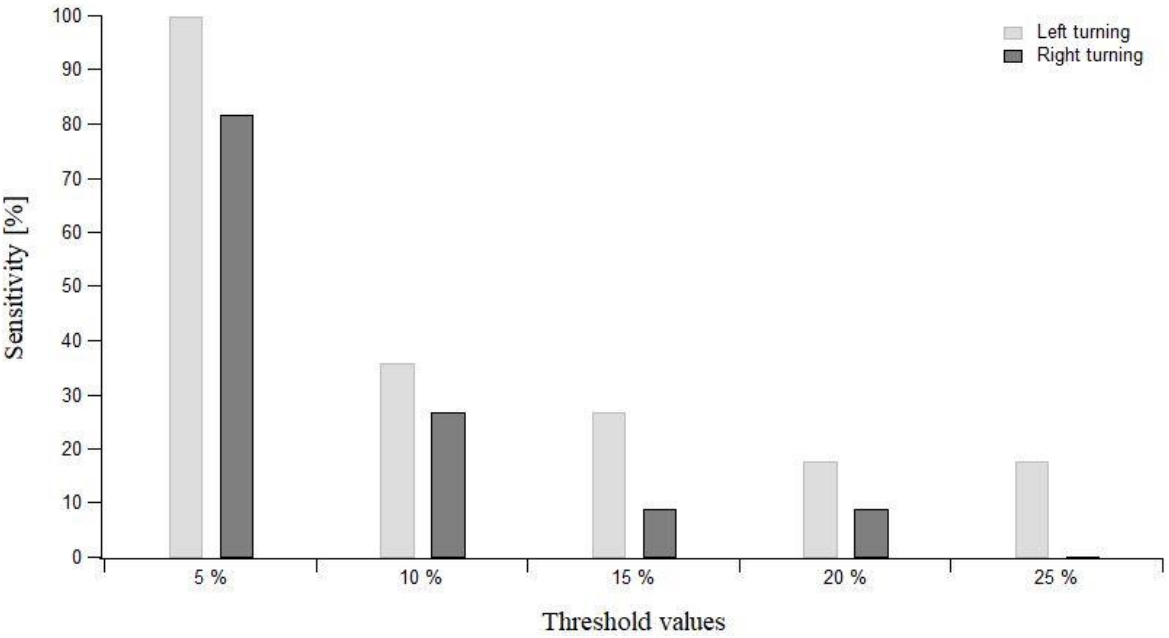

Figure F-8: Sensitivity values in detecting the lateral changes in posture during left and right turning for the **whole body contact area** at four threshold values, ranging between 5% and 25%.

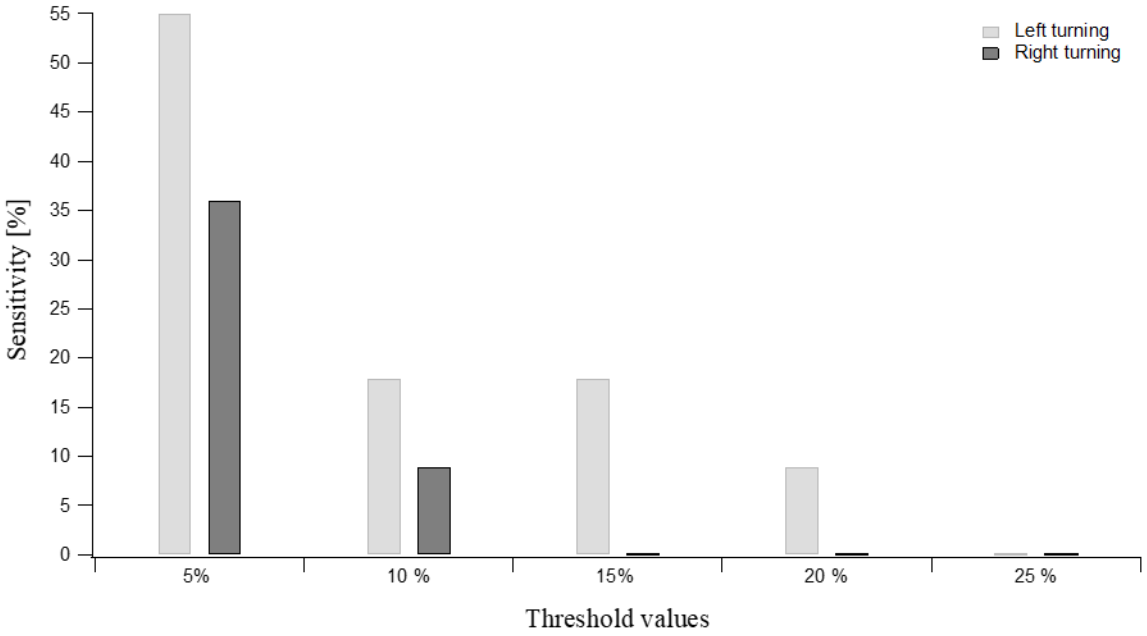

Figure F-9: Sensitivity values in detecting the lateral changes in posture during left and right turning for the **buttock contact area** at four threshold values, ranging between 5% and 25%.

Tilt angles

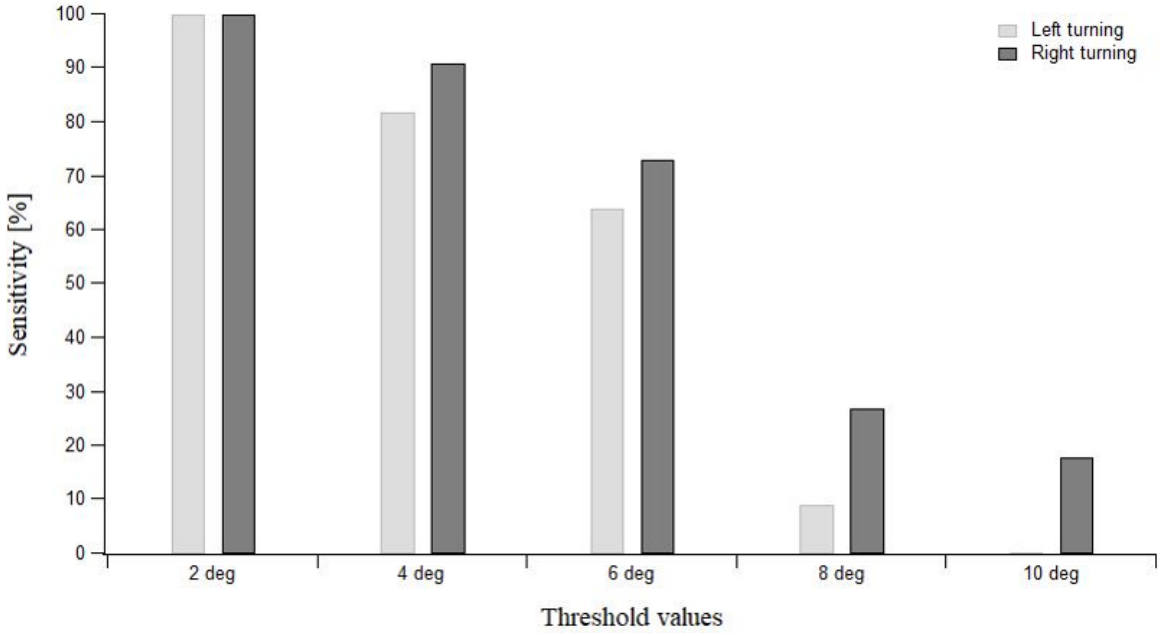

Figure F-10: Sensitivity values in detecting the lateral changes in posture during left and right turning for the **waist inclination angles** at four threshold values, ranging between 2^{o} and 10^{o}.

Appendix G ROC curves analyses

Centre of Pressure (COP)

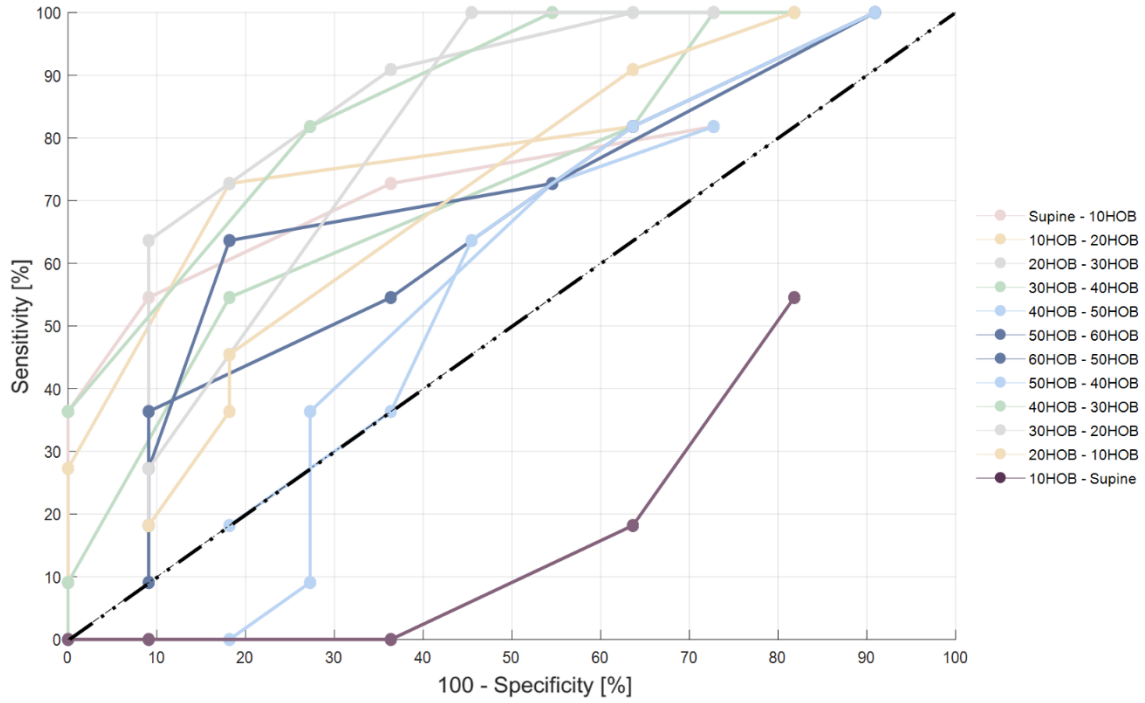

Figure G-1: ROC curves across all changes in posture for COP displacements at the **whole body ROI**. Each data point represents a sensitivity/specificity pair corresponding to a specific decision threshold. The threshold values increase from the right side to the left side of the curve.

Peak pressure

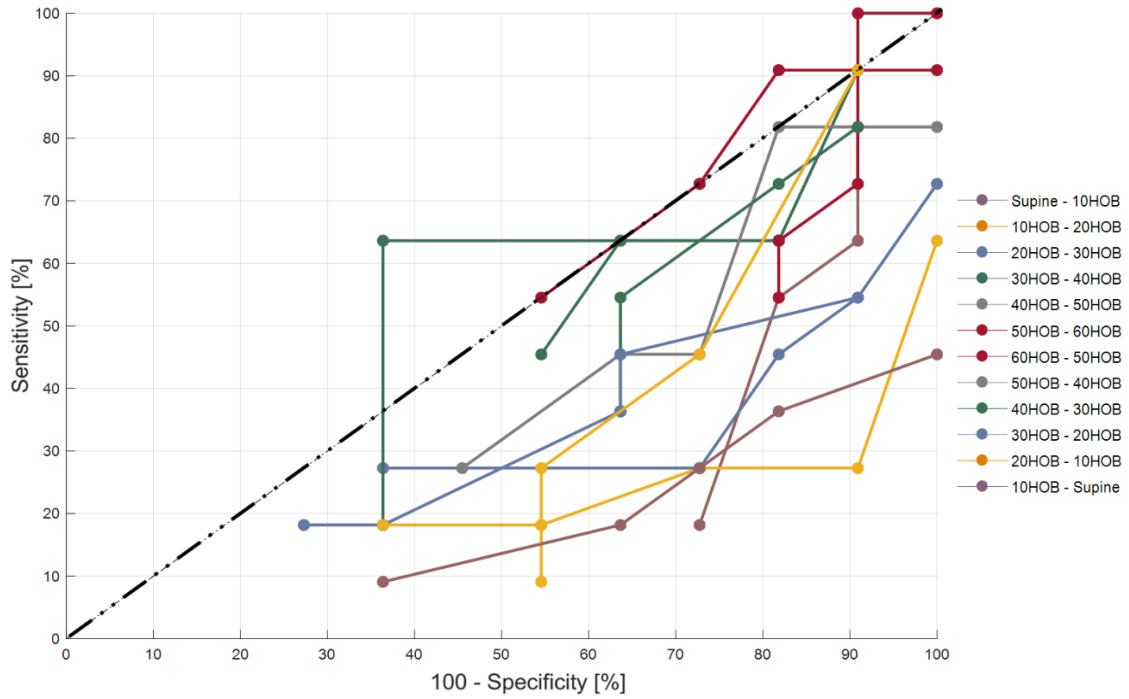

Figure G-2: ROC curves across all changes in posture for peak pressure at the **whole body ROI**. Each data point represents a sensitivity/specificity pair corresponding to a specific decision threshold. The threshold values increase from the right side to the left side of the curve.

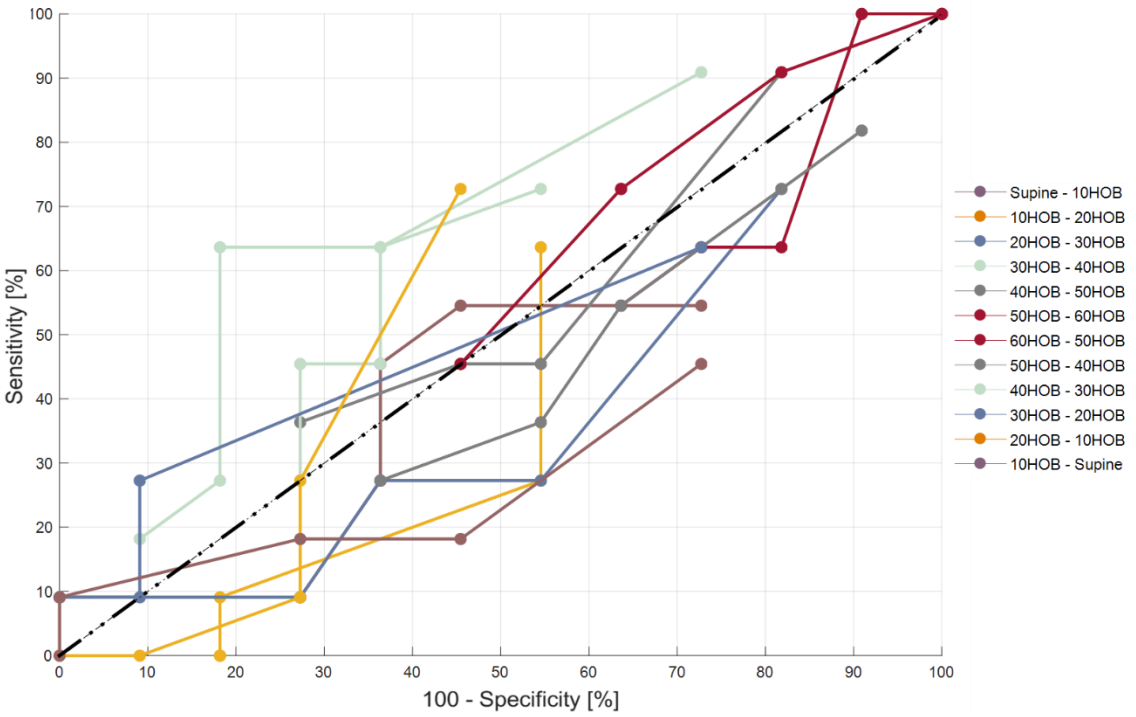

Figure G-3: ROC curves across all changes in posture for peak pressure at the **buttock ROI**. Each data point represents a sensitivity/specificity pair corresponding to a specific decision threshold. The threshold values increase from the right side to the left side of the curve.

Peak pressure gradient – Parallel direction with respect to the long axis of the mat

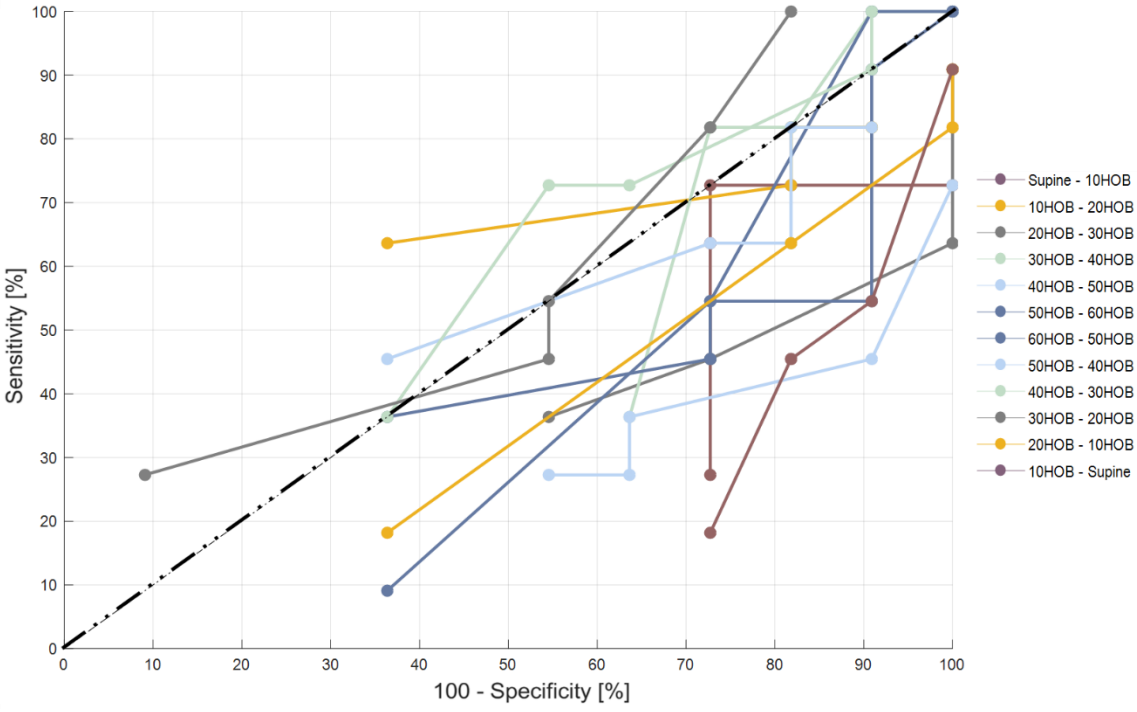

Figure G-4: ROC curves across all changes in posture for peak pressure gradient estimated in the parallel direction at the **whole body ROI**. Each data point represents a sensitivity/specificity pair corresponding to a specific decision threshold. The threshold values increase from the right side to the left side of the curve.

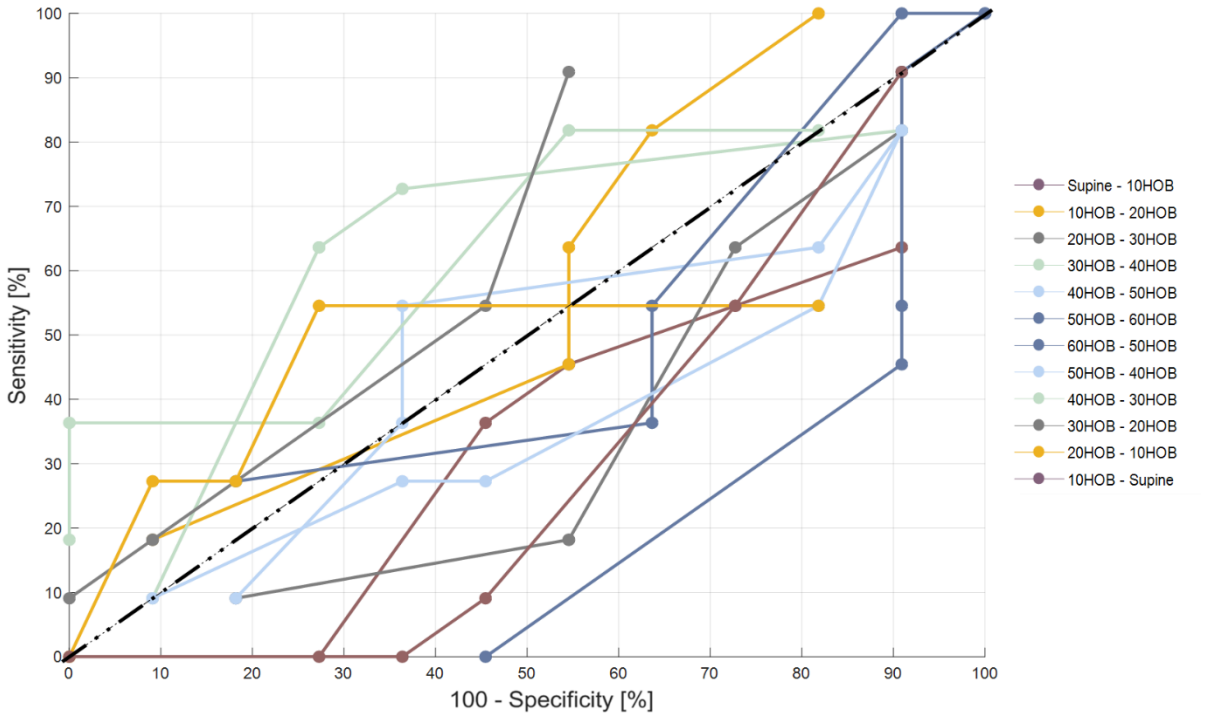

Figure G-5: ROC curves across all changes in posture for peak pressure gradient estimated in the parallel direction at the **buttock ROI**. Each data point represents a sensitivity/specificity pair corresponding to a specific decision threshold. The threshold values increase from the right side to the left side of the curve.

Peak pressure gradient – Perpendicular direction with respect to the long axis of the mat

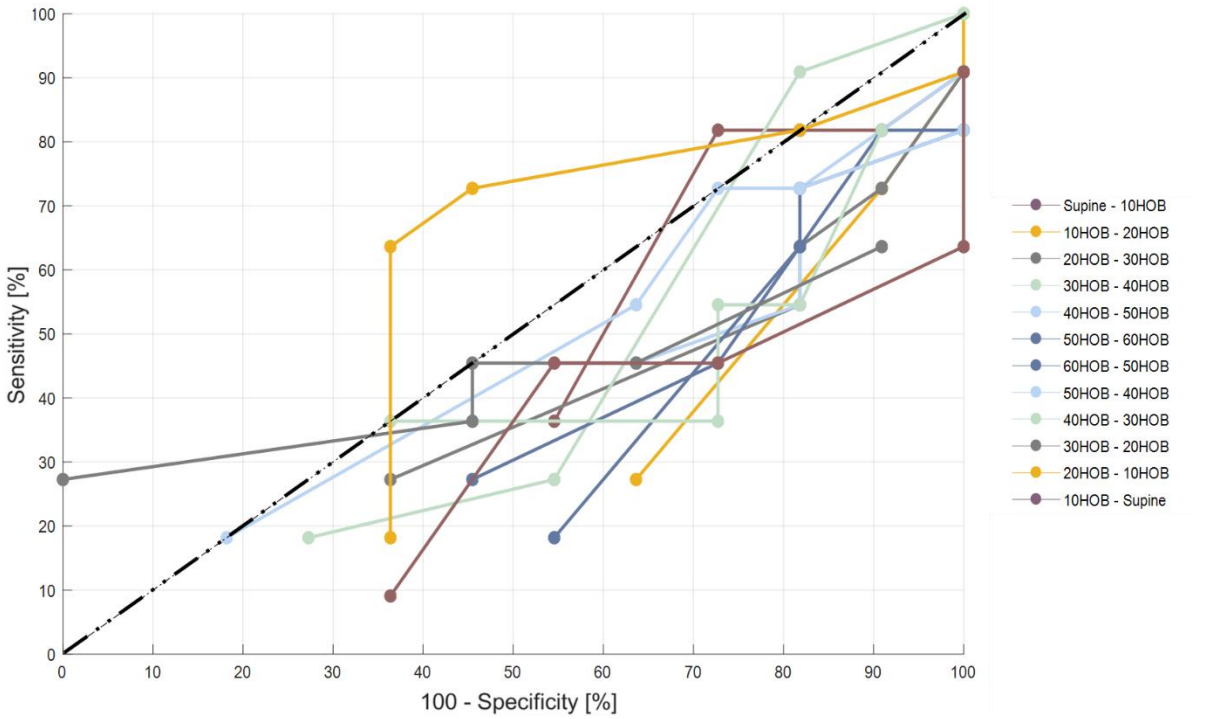

Figure G-6: ROC curves across all changes in posture for peak pressure gradient estimated in parallel direction at the **whole body ROI**. Each data point represents a sensitivity/specificity pair corresponding to a specific decision threshold. The threshold values increase from the right side to the left side of the curve.

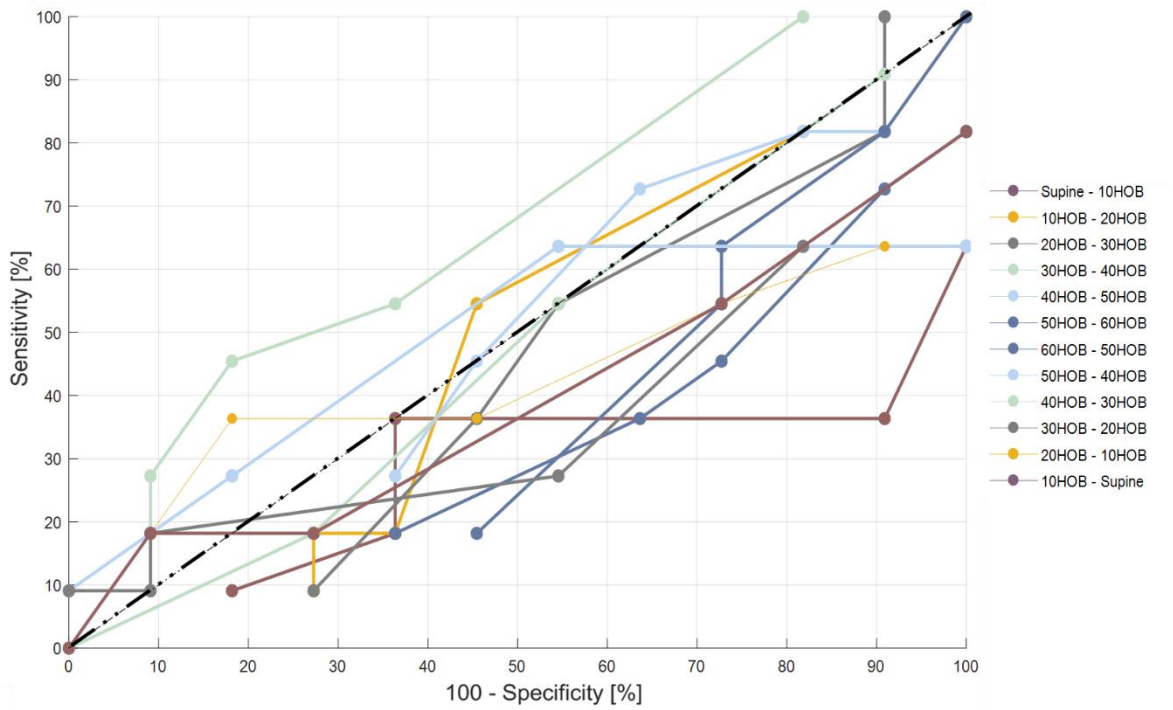

Figure G-7: ROC curves across all changes in posture for peak pressure gradient estimated in the parallel direction at the **buttock ROI**. Each data point represents a sensitivity/specificity pair corresponding to a specific decision threshold. The threshold values increase from the right side to the left side of the curve.

Contact Area

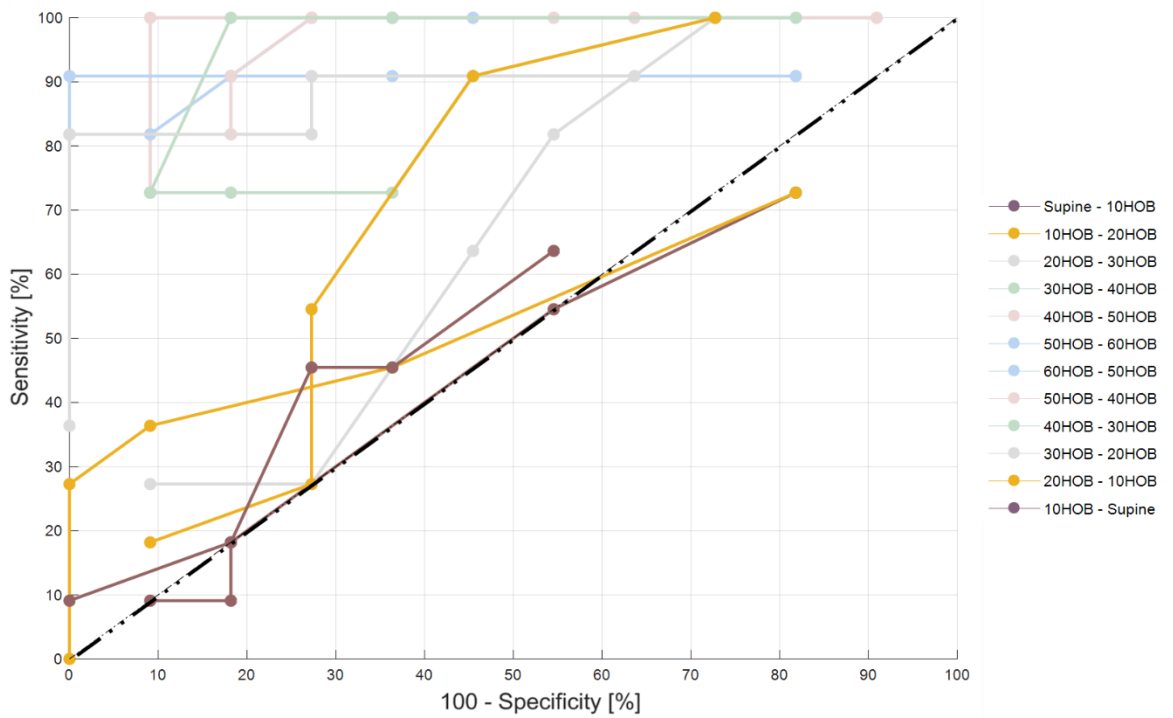

Figure G-8: ROC curves across all changes in posture for contact area at the **buttock ROI**. Each data point represents a sensitivity/specificity pair corresponding to a specific decision threshold. The threshold values increase from the right side to the left side of the curve.

Tilt angles

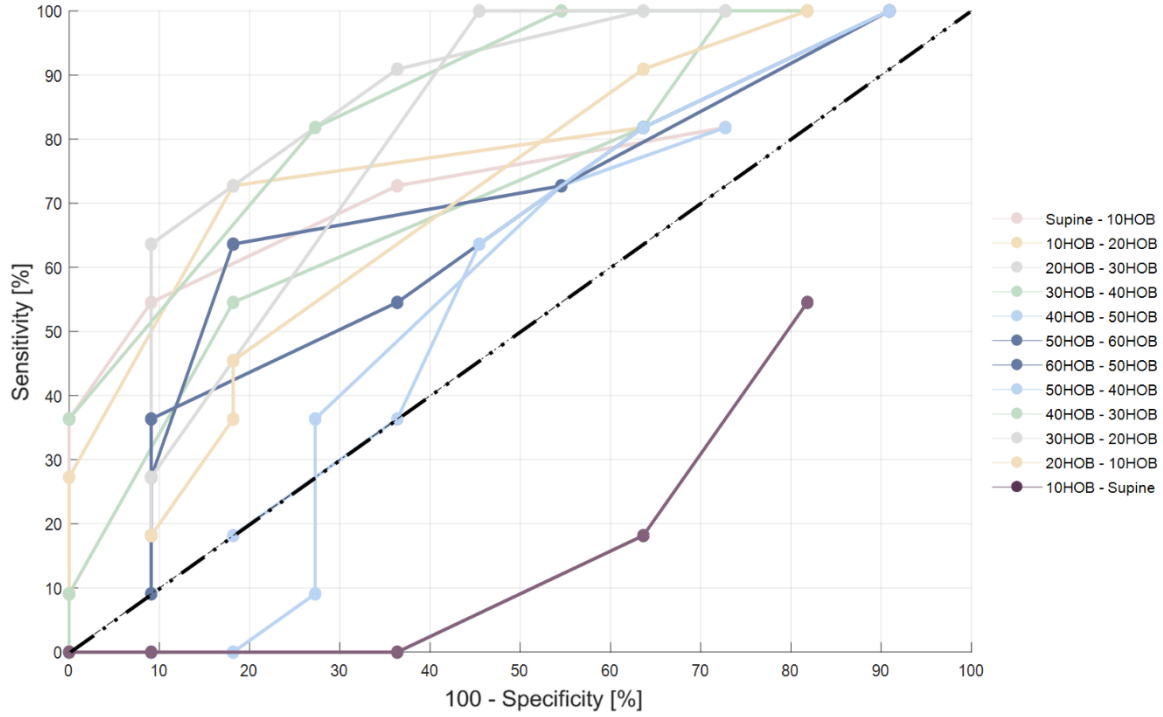

Figure G-9: ROC curves across all changes in posture for **tilt angles** evaluated at the **waist**. Each data point represents a sensitivity/specificity pair corresponding to a specific decision threshold. The threshold values increase from the right side to the left side of the curve.

Appendix H Custom software developed in Matlab for the detection of frequency and magnitude of changes in posture

Combined training data set - 20º HOB increments

% This script was used to project the training data set, including interface pressure and actimetry signals, into the PCs dimentional space, therby creating a training model

```
load('TrainDataSet.mat')
load('Label_TrainDataSet.mat')
[row, col] = size(TrainDataSet);

%Delete offset from contact area
for j = 1:4:col
   TrainDataSet(:,j) = TrainDataSet(:,j) - 100;
   TrainDataSet(:,j+1) = TrainDataSet(:,j+1) - 100;
end

% fixed sliding window of 60 secs
L = 60; % length window
nwindows = row/L;

for j = 1:col
   t0 = 1;
   t1 = 60;

   for p = 1:nwindows
      FeatureVector.Train.MEAN(p,j) =  mean(TrainDataSet(t0:t1,j));
      FeatureVector.Label(p,1) = mean(LabelnotransitionoptimizedDataSet(t0:t1,1));
      t0 = t1 + 1;
      t1 = t1 + 60;
   end
end

% Contact Area
j = 1:4:col;
ContactArea.Global.MEAN = [FeatureVector.Train.MEAN(:,j(1)) FeatureVector.Train.MEAN(:,j(2))
FeatureVector.Train.MEAN(:,j(3)) FeatureVector.Train.MEAN(:,j(4)) FeatureVector.Train.MEAN(:,j(5))
FeatureVector.Train.MEAN(:,j(6)) FeatureVector.Train.MEAN(:,j(7)) FeatureVector.Train.MEAN(:,j(8))
FeatureVector.Train.MEAN(:,j(9))];

% Tilt Angles - Sternum
j = 3:4:col;
Sternum.SagittalPlane.MEAN = [FeatureVector.Train.MEAN(:,j(1)) FeatureVector.Train.MEAN(:,j(2))
FeatureVector.Train.MEAN(:,j(3)) FeatureVector.Train.MEAN(:,j(4)) FeatureVector.Train.MEAN(:,j(5))
FeatureVector.Train.MEAN(:,j(6)) FeatureVector.Train.MEAN(:,j(7)) FeatureVector.Train.MEAN(:,j(8))
FeatureVector.Train.MEAN(:,j(9))];
j = 4:4:col;
Sternum.TransversePlane.MEAN = [FeatureVector.Train.MEAN(:,j(1)) FeatureVector.Train.MEAN(:,j(2))
```

```
FeatureVector.Train.MEAN(:,j(3)) FeatureVector.Train.MEAN(:,j(4)) FeatureVector.Train.MEAN(:,j(5))
FeatureVector.Train.MEAN(:,j(6)) FeatureVector.Train.MEAN(:,j(7)) FeatureVector.Train.MEAN(:,j(8))
FeatureVector.Train.MEAN(:,j(9))];

% Label

LabelTrain = [FeatureVector.Label; FeatureVector.Label; FeatureVector.Label; FeatureVector.Label; FeatureVector.Label;
FeatureVector.Label; FeatureVector.Label; FeatureVector.Label; FeatureVector.Label];
```

```
% Training data set
```

```
ContactArea.Global.AllSubjects = [ContactArea.Global.MEAN(:,1); ContactArea.Global.MEAN(:,2);
ContactArea.Global.MEAN(:,3); ContactArea.Global.MEAN(:,4); ContactArea.Global.MEAN(:,5);
ContactArea.Global.MEAN(:,6); ContactArea.Global.MEAN(:,7); ContactArea.Global.MEAN(:,8);
ContactArea.Global.MEAN(:,9)];

Sternum.SagittalPlane.AllSubjects = [Sternum.SagittalPlane.MEAN(:,1); Sternum.SagittalPlane.MEAN(:,2);
Sternum.SagittalPlane.MEAN(:,3); Sternum.SagittalPlane.MEAN(:,4); Sternum.SagittalPlane.MEAN(:,5);
Sternum.SagittalPlane.MEAN(:,6); Sternum.SagittalPlane.MEAN(:,7); Sternum.SagittalPlane.MEAN(:,8);
Sternum.SagittalPlane.MEAN(:,9)];

Sternum.TransversePlane.AllSubjects = [Sternum.TransversePlane.MEAN(:,1); Sternum.TransversePlane.MEAN(:,2);
Sternum.TransversePlane.MEAN(:,3); Sternum.TransversePlane.MEAN(:,4); Sternum.TransversePlane.MEAN(:,5);
Sternum.TransversePlane.MEAN(:,6); Sternum.TransversePlane.MEAN(:,7); Sternum.TransversePlane.MEAN(:,8);
Sternum.TransversePlane.MEAN(:,9)];

% DataSet with Global Area

DataSet_Train = [ContactArea.Global.AllSubjects Sternum.SagittalPlane.AllSubjects Sternum.TransversePlane.AllSubjects];
DataSet_Train(:,4) = LabelTrain;
```

```
% Considering changes in posture in 20HOB increments
```

```
sup = find(DataSet_Train(:,4) == 0);
HOB_20 = find(DataSet_Train(:,4) == 2);
HOB_40 = find(DataSet_Train(:,4) == 4);
HOB_60 = find(DataSet_Train(:,4) == 6);

Lat_L = find(DataSet_Train(:,4) == 7);
Lat_R = find(DataSet_Train(:,4) == 8);

Posture1 = DataSet_Train (sup,:);
Posture2 = DataSet_Train (HOB_20,:);
Posture3 = DataSet_Train (HOB_40,:);
Posture4 = DataSet_Train (HOB_60,:);
Posture5 = DataSet_Train (Lat_L ,:);
Posture6 = DataSet_Train (Lat_R ,:);

DataSet_Train_20HOB = [Posture1; Posture2; Posture3; Posture4; Posture5; Posture6];
```

```
% Projection in the PCA dimentional space
```

```
C = cov(DataSet_Train_20HOB(:,1:3)); % covariance matrix

[eigenvector,eigenvalues]=eig(C_); % eigenvectors and values

temp=DataSet_Train_20HOB(:,1:3)';
[r_temp c_temp] = size(temp);

for i = 1:r_temp
  Dmean_global(i,1) = mean(temp_global(i,:));
end

for j = 1:c_temp
   for i = 1:r_temp
      temp_global(i,j) = temp_global(i,j) - Dmean_global(i,1); % mean centering
   end
end

PC = eigenvector'*temp; % PC components

figure
plot(PC(3,sup),PC(2,sup),'or','MarkerFaceColor','r')
plot(PC(3,HOB_20),PC(2,HOB_20),'ob', 'MarkerFaceColor','b')
plot(PC(3,HOB_40),PC(2,HOB_40),'og', 'MarkerFaceColor','g')
plot(PC(3,HOB_60),PC(2,HOB_60),'ok','MarkerFaceColor','k')
plot(PC(3,Lat_L),PC(2,Lat_L),'om','MarkerFaceColor','m')
plot(PC(3,Lat_R),PC(2,Lat_R),'om', 'MarkerFaceColor','m')

axis ([-120 100 -40 40])
legend('Supine', '20 HOB', '40 HOB', '60 HOB', 'Lateral', 'Lateral')

[coeff_training,scores_training,pcvars_training] = pca(DataSet_Train_20HOB(:,1:3));

xlabel(['PC1-(',num2str(round(pcvars_training(1)/sum(pcvars_training)*100)),'%)'])
ylabel(['PC2-(',num2str(round(pcvars_training(2)/sum(pcvars_training)*100)),'%)'])

PC = PC';
```

Test data set

```
% This code was used to detect the occurance of changes in posture by examining the derivative signals of the parameters and to classify the range of postures by using three machnine learning algorithms
```

```
load('SternumSignals.mat')
load('AreaSignals.mat')

for i = 1:10
```

```
    Mat = sprintf('Mat%d',i);
    AreaSignals.Interpolate.Global.(Mat) = AreaSignals.Interpolate.Global.(Mat)';
    SternumSignals.Interpolate.Sternum.(Mat) = SternumSignals.Interpolate.Sternum.(Mat)';
end

for i = 1:10
    Mat = sprintf('Mat%d',i);
    S = sprintf('Subject%d',i);
    TestDataSet.(S) = [AreaSignals.Interpolate.Global.(Mat) SternumSignals.Interpolate.Sternum.(Mat)];
end
```

```
% Fixed sliding window to calculate mean and derivative
```

```
l = length(TestDataSet.Subject1);
[row col] = size(TestDataSetl.Subject1);
L = 60; % length window
nwindows = l/L;
nsubjects = 10;

for i = 1:nsubjects
    S = sprintf('Subject%d',i);
    for j = 1:col
        t0 = 1;
        t1 = 60;

        for p = 1:nwindows
            FeatureVector.Test.MEAN.(S)(p,j) = mean(TestDataSet.(S)(t0:t1,j));
            FeatureVector.Test.DERIVATIVE.(S)(p,j) = mean(diff(TestDataSet.(S)(t0:t1,j)));
            t0 = t1 + 1;
            t1 = t1 + 60;
        end
    end
end
```

```
% Processing of derivative signals - rectification
```

```
for s = 1:nsubjects
    S = sprintf('Subject%d',s);

    ind0 = find(FeatureVector.Test.DERIVATIVE.(S)(:,1)<0);
    FeatureVector.Test.DERIVATIVE.(S)(ind0,1) = abs(FeatureVector.Test.DERIVATIVE.(S)(ind0,1));
    ind1 = find(FeatureVector.Test.DERIVATIVE.(S)(:,2)<0);
    FeatureVector.Test.DERIVATIVE.(S)(ind1,2) = abs(FeatureVector.Test.DERIVATIVE.(S)(ind1,2));
    ind2 = find(FeatureVector.Test.DERIVATIVE.(S)(:,3)<0);
    FeatureVector.Test.DERIVATIVE.(S)(ind2,3) = abs(FeatureVector.Test.DERIVATIVE.(S)(ind2,3));
    FeatureVector.Test.DERIVATIVE.(S)(:,4) =
FeatureVector.Test.DERIVATIVE.(S)(:,2)+FeatureVector.Test.DERIVATIVE.(S)(:,3); % sum of the derivative signals from
actimetry signals estimated from sagittal and transverse planes
end
```

```
% Detection of the occurrence of changes in posture
```

```
thr = 0.10;

for s = 1:nsubjects
   S = sprintf('Subject%d',s);
   l = length(FeatureVector.Test.DERIVATIVE.(S)(:,4));
   for t = 1:length(thr)
      for i = 1:l
         if FeatureVector.Test.DERIVATIVE.(S)(i,4)>= thr(t)
            transitions.(S)(i,t)= 1;
         else
            transitions.(S)(i,t)= 0;
         end
      end
   end
end

close all

Npostures = 20;
for j = 1:nsubjects
   S = sprintf('Subject%d',j);
   index = find(transitions.(S)(:,1) == 1);
   l = length(index);
   for p=1:Npostures
      for i=1:l-1
         if (index(i+1)-index(i)) <= 10
            m1 = FeatureVector.Test.DERIVATIVE.(S)(index(i),4);
            m2 = FeatureVector.Test.DERIVATIVE.(S)(index(i+1),4);
            if m2>m1
               index(i) = index(i+1);
            else
               index(i+1) = index(i);
            end
         end
      end
   end
   index = unique(index);
   l = length(index);

   indexFirst = index(1);
   if (indexFirst - 1) < 4
      index(1) = 1;
      CP.(S) = [index];
   else
      CP.(S) = [1;index];
   end

   indexLast = length(transitions.(S)(:,1));
   if indexLast - index(end) < 4
      index(end) = indexLast;
      CP.(S) = [CP.(S)];
   else
```

```
        CP.(S) = [CP.(S);length(transitions.(S)(:,1))];
    end

    cp = length(CP.(S));
    figure
    plot(FeatureVector.Test.DERIVATIVE.(S)(:,4))
    for i = 1:cp
        hold on
        plot(CP.(S)(i), FeatureVector.Test.DERIVATIVE.(S)(CP.(S)(i),4),'or', 'MarkerFaceColor', 'r')
    end

end

% After the detection of the changes in posture, the static postures were
% identified

for j = 1:nsubjects
    S = sprintf('Subject%d',j);
    cp = length(CP.(S));
    n = 0;
    for i=1:cp-1
        P = sprintf('P%d',i);
        Postures.(S).(P) = FeatureVector.Test.MEAN.(S)(CP.(S)(i)+2:CP.(S)(i+1)-2,:);
    end
end
```

```
% Create the test data set for each subject
```

```
for s = 1:nsubjects
    S = sprintf('Subject%d',s);
    Postures.(S).TOT = [Postures.(S).P1; Postures.(S).P2; Postures.(S).P3; Postures.(S).P4; Postures.(S).P5; Postures.(S).P6;
Postures.(S).P7; Postures.(S).P8];
end
```

```
% Postures labelling
```

```
for j = 1:nsubjects
    S = sprintf('Subject%d',j);
    n = 0;
    LabelTest.(S) = [];
    for i=1:cp-1
        P = sprintf('P%d',i);
        lp = length(Postures.(S).(P));
        Label = n*ones(lp,1);
        LabelTest.(S) = [LabelTest.(S); Label];
        n = n + 2;
    end
end

for s = 1:nsubjects
    S = sprintf('Subject%d',s);
```

```
    [I] = find(LabelTest.(S) == 8);
    LabelTest.(S)(I,:) = 4;
    [I] = find(LabelTest.(S) == 10);
    LabelTest.(S)(I,:) = 2;
    [I] = find(LabelTest.(S) == 12);
    LabelTest.(S)(I,:) = 0;
    [I] = find(LabelTest.(S) == 14);
    LabelTest.(S)(I,:) = 7;
    [I] = find(DataSet_Train(:,4) == 8)
    DataSet_Train(:,4) = 7;
end
```

```
% Naïve – Bayes classifier – probability of each class
```

```
LabelLearn = DataSet_Train_20HOB(:,4);
Lableunique=unique(LabelLearn);
nc=length(Lableunique); % number of classes

% compute class probability
for i = 1:nc
    c = find(LabelLearn == Lableunique(i));
    classprobability(i) = sum(length(c))/length(LabelLearn);
end
```

```
for i = 1:nc
    class = sprintf('class%d',i);
    x.(class) = PC((LabelLearn==Lableunique(i)),1:3);
    x.(class) = x.(class)';
    len.(class) = length(x.(class));
end
```

```
% Projection of the test data points into the training PCs dimentional space
```

```
for s = 1:10

S = sprintf('Subject%d',s);
    C_test = Postures.(S).TOT(:,1:3);
    [row col] = size(C_test);
    temp_test = C_test';
    for i = 1:col
        Dmean_test(i,1) = mean(temp_test(i,:));
    end

    for j = 1:row
        for i = 1:3
            temp_test(i,j) = temp_test(i,j) - Dmean_test(i,1);

        end
    end

    PC_test.(S) = eigenvector'*temp_test; % projection in the training PCs dimentional space
    hold on
```

```
    plot(PC_test.(S)(3,:),PC_test.(S)(2,:),'om','MarkerFaceColor','m')

    PC_test.(S) = PC_test.(S)';
    TestPoint = PC_test.(S)(:,1:3);
    L = length (TestPoint);
```

```
% Conditional probability
```

```
    for i = 1:nc
        for l = 1:L
            class = sprintf('class%d',i);
            mu.(class) = mean(x.(class),2);
            X.(class) = x.(class) - mu.(class);
            Sigma.(class) = (1/(len.(class)-1))*(X.(class)*X.(class)');
            proba.(S).(class)(l,1)= (1/(sqrt(det(2*pi*Sigma.(class)))))* exp(-1/2*(TestPoint(l,:)'-
mu.(class))'*inv(Sigma.(class))*(TestPoint(l,:)'-mu.(class)));
        end
    end
```

```
    for j=1:length(proba.(S).class1)

        Prob.(S).class1(j,1)= (proba.(S).class1(j,1)* classprobability(1))/ (proba.(S).class1(j,1)*classprobability(1) +
proba.(S).class2(j,1)*classprobability(2) + proba.(S).class3(j,1)*classprobability(3) + proba.(S).class4(j,1)*classprobability(4)  +
proba.(S).class5(j,1)*classprobability(5));
        Prob.(S).class2(j,1) = (proba.(S).class2(j,1)* classprobability(2))/ (proba.(S).class1(j,1)*classprobability(1) +
proba.(S).class2(j,1)*classprobability(2) + proba.(S).class3(j,1)*classprobability(3) + proba.(S).class4(j,1)*classprobability(4) +
proba.(S).class5(j,1)*classprobability(5));
        Prob.(S).class3(j,1) = (proba.(S).class3(j,1)* classprobability(3))/ (proba.(S).class1(j,1)*classprobability(1) +
proba.(S).class2(j,1)*classprobability(2) + proba.(S).class3(j,1)*classprobability(3) + proba.(S).class4(j,1)*classprobability(4) +
proba.(S).class5(j,1)*classprobability(5));
        Prob.(S).class4(j,1) = (proba.(S).class4(j,1)* classprobability(4))/ (proba.(S).class1(j,1)*classprobability(1) +
proba.(S).class2(j,1)*classprobability(2) + proba.(S).class3(j,1)*classprobability(3) + proba.(S).class4(j,1)*classprobability(4) +
proba.(S).class5(j,1)*classprobability(5));
        Prob.(S).class5(j,1) = (proba.(S).class5(j,1)* classprobability(5))/ (proba.(S).class1(j,1)*classprobability(1) +
proba.(S).class2(j,1)*classprobability(2) + proba.(S).class3(j,1)*classprobability(3) + proba.(S).class4(j,1)*classprobability(4) +
proba.(S).class5(j,1)*classprobability(5));
        TotalProb.(S) = [Prob.(S).class1 Prob.(S).class2 Prob.(S).class3 Prob.(S).class4 Prob.(S).class5];
    end

    Scount = 0;

for i = 1:length(TotalProb.(S))

    [v,ind] = max (TotalProb.(S)(i,:));

    if ind == 1
        CurrentPosture.Bayes.(S)(i,1) = 0;
        if CurrentPosture.Bayes.(S)(i,1) == LabelTest.(S)(i,1)
            Scount = Scount + 1;
        end
    end
    if ind == 2
```

```
        CurrentPosture.Bayes.(S)(i,1) = 2;
        if CurrentPosture.Bayes.(S)(i,1) == LabelTest.(S)(i,1)
            Scount = Scount + 1;
        end
    end

    if ind == 3
        CurrentPosture.Bayes.(S)(i,1) = 4;
        if CurrentPosture.Bayes.(S)(i,1) == LabelTest.(S)(i,1)
            Scount = Scount + 1;
        end
    end
    if ind == 4
        CurrentPosture.Bayes.(S)(i,1) = 6;
        if CurrentPosture.Bayes.(S)(i,1) == LabelTest.(S)(i,1)
            Scount = Scount + 1;
        end
    end
    if ind == 5
        CurrentPosture.Bayes.(S)(i,1) = 7;
        if CurrentPosture.Bayes.(S)(i,1) == LabelTest.(S)(i,1)
            Scount = Scount + 1;
        end
    end

end

    Accuracy.Bayes(s,:) = round(100*(Scount/row));
```

```
end
```

Appendix I: Accuracy in classifying a range of postures adopted in a random sequence on different mattresses

Table I-4: Percentage accuracy for Naïve - Bayes classifier in classifying the range of postures on the foam mattress. For each subject the total accuracy is reported in addition with the accuracy in correctly classifying each static posture (in bold). It also includes the complementary percentage values which were misclassified for each of the static posture in bold.

		Accuracy [%] – Foam mattress															
		Naïve - Bayes															
Subjects	**Postures sequence**	**Supine**	20HOB	40HOB	60HOB	Lateral	Supine	20HOB	**HS**	60HOB	Lateral	Supine	20HOB	40HOB	60HOB	**Lateral**	**Total**
1	HS, Sup, Lat	**58**	12	12	0	18	0	0	**0**	0	100	0	0	6	0	**94**	**61**
2	Lat, Sup, HS	**0**	0	100	0	0	0	3	**0**	0	97	0	0	0	0	**100**	**29**
3	HS, Lat, Sup	**0**	0	0	0	100	0	0	**0**	0	100	0	0	0	98	**2**	**1**
4	Lat, HS, Sup	**0**	3	0	0	97	71	29	**0**	0	0	0	0	0	0	**100**	**32**
5	Lat, HS, Sup	**0**	0	0	0	100	0	0	**0**	0	100	0	0	0	0	**100**	**31**
6	HS, Sup, Lat	**0**	0	11	0	89	0	0	**0**	0	100	0	0	0	80	**20**	**6**
7	Lat, HS, Sup	**0**	0	0	0	100	0	0	**0**	0	100	0	25	75	0	**0**	**0**
8	Lat, HS, Sup	**89**	0	3	0	9	0	0	**0**	0	100	0	0	0	0	**100**	**57**
9	HS, Sup, Lat	**0**	0	0	0	100	0	0	**0**	0	100	0	0	0	0	**100**	**36**
10	Lat, Sup, HS	**0**	0	5	0	95	0	0	**0**	0	100	0	0	0	0	**100**	**28**
11	HS, Sup, Lat	**0**	0	14	0	86	0	0	**0**	0	100	0	0	4	0	**96**	**28**
12	Lat, Sup, HS	**0**	0	88	0	12	0	0	**0**	0	100	0	0	0	0	**100**	**34**
13	Lat, HS, Sup	**94**	0	0	0	6	0	0	**0**	0	100	0	0	0	0	**100**	**63**
14	Lat, HS, Sup	**0**	0	100	0	0	0	38	**0**	0	62	0	5	0	0	**100**	**34**

Table I-5: Percentage accuracy for Naïve - Bayes classifier in classifying the range of postures on the air cells mattress. For each subject the total accuracy is reported in addition with the accuracy in correctly classifying each static posture (in bold). It also includes the complementary percentage values which were misclassified for each of the static posture in bold.

		Accuracy [%] – Air cells mattress															
		Naïve - Bayes															
Subjects	**Postures sequence**	**Supine**	20HOB	40HOB	60HOB	Lateral	Supine	20HOB	**HS**	60HOB	Lateral	Supine	20HOB	40HOB	60HOB	**Lateral**	**Total**
1	Sup, HS, Lat	**0**	0	100	0	0	0	7	**0**	0	93	0	0	0	0	**100**	**40**
2	Lat, Sup, HS	**0**	0	28	72	0	0	53	**43**	4	0	3	0	91	0	**6**	**16**
3	Lat, HS, Sup	**3**	8	56	0	33	3	67	**22**	0	8	15	0	70	0	**15**	**13**
4	HS, Lat, Sup	**0**	0	0	0	100	0	0	**7**	0	93	68	0	32	0	**0**	**3**
5	Sup, Lat, HS	**0**	0	50	0	50	0	8	**0**	0	92	0	0	38	48	**14**	**5**
6	HS, Sup, Lat	**14**	14	14	0	58	0	0	**0**	0	100	0	0	0	0	**100**	**43**
7	Lat, HS, Sup	**0**	0	0	0	100	3	0	**0**	0	97	0	0	38	0	**62**	**17**
8	Sup, Lat, HS	**33**	0	37	0	30	0	0	**0**	0	100	0	0	0	0	**100**	**45**
9	HS, Sup, Lat	**7**	17	10	0	66	0	0	**0**	0	100	0	0	0	0	**100**	**41**
10	Sup, Lat, HS	**0**	59	0	11	0	0	0	**0**	0	100	0	0	0	0	**100**	**36**
11	Sup, HS, Lat	**0**	0	84	0	16	0	0	**0**	0	100	0	0	0	0	**100**	**32**
12	Sup, HS, Lat	**0**	0	24	3	73	0	57	**0**	0	43	0	55	30	0	**15**	**5**
13	HS, Lat, Sup	**0**	0	26	0	74	0	0	**0**	100	0	0	0	0	0	**100**	**38**
14	Sup, Lat, HS	**0**	0	0	0	100	0	0	**0**	100	0	0	0	0	0	**100**	**36**

Table I-6: Percentage accuracy for SVM classifier in classifying the range of postures on both the foam and air cells mattress. For each subject the total accuracy is reported in addition with the accuracy in correctly classifying each static posture (in bold).

		Accuracy [%] – SVM								
		Foam mattress					**Air cells mattress**			
Subjects	**Postures sequence**	Supine	HS	Lateral	**Total**	**Postures sequence**	Supine	HS	Lateral	**Total**
1	HS, Sup, Lat	0	0	100	**41**	Sup, HS, Lat	0	0	73	**29**
2	Lat, Sup, HS	0	0	100	**29**	Lat, Sup, HS	0	37	66	**35**
3	HS, Lat, Sup	0	0	87	**33**	Lat, HS, Sup	0	17	68	**27**
4	Lat, HS, Sup	0	0	0	**0**	HS, Lat, Sup	0	0	0	**0**
5	Lat, HS, Sup	0	0	24	**7**	Sup, Lat, HS	0	0	75	**29**
6	HS, Sup, Lat	0	0	80	**24**	HS, Sup, Lat	0	0	47	**18**
7	Lat, HS, Sup	0	0	0	**0**	Lat, HS, Sup	0	0	0	**0**
8	Lat, HS, Sup	0	0	0	**0**	Sup, Lat, HS	0	0	0	**0**
9	HS, Sup, Lat	0	0	98	**35**	HS, Sup, Lat	0	0	100	**38**
10	Lat, Sup, HS	0	0	100	**29**	Sup, Lat, HS	0	0	0	**0**
11	HS, Sup, Lat	0	0	100	**29**	Sup, HS, Lat	0	0	0	**0**
12	Lat, Sup, HS	0	0	0	**0**	Sup, HS, Lat	0	0	76	**24**
13	Lat, HS, Sup	0	0	0	**0**	HS, Lat, Sup	0	0	3	**1**
14	Lat, HS, Sup	0	5	0	**0**	Sup, Lat, HS	0	0	43	**15**

Appendix L Postures classification in SCI patients

Figure L-1: Grey scale images representing some of the static postures adopted by **SCI 1** on the air cell mattress. The captions represent the classification performed with the **KNN algorithm**.

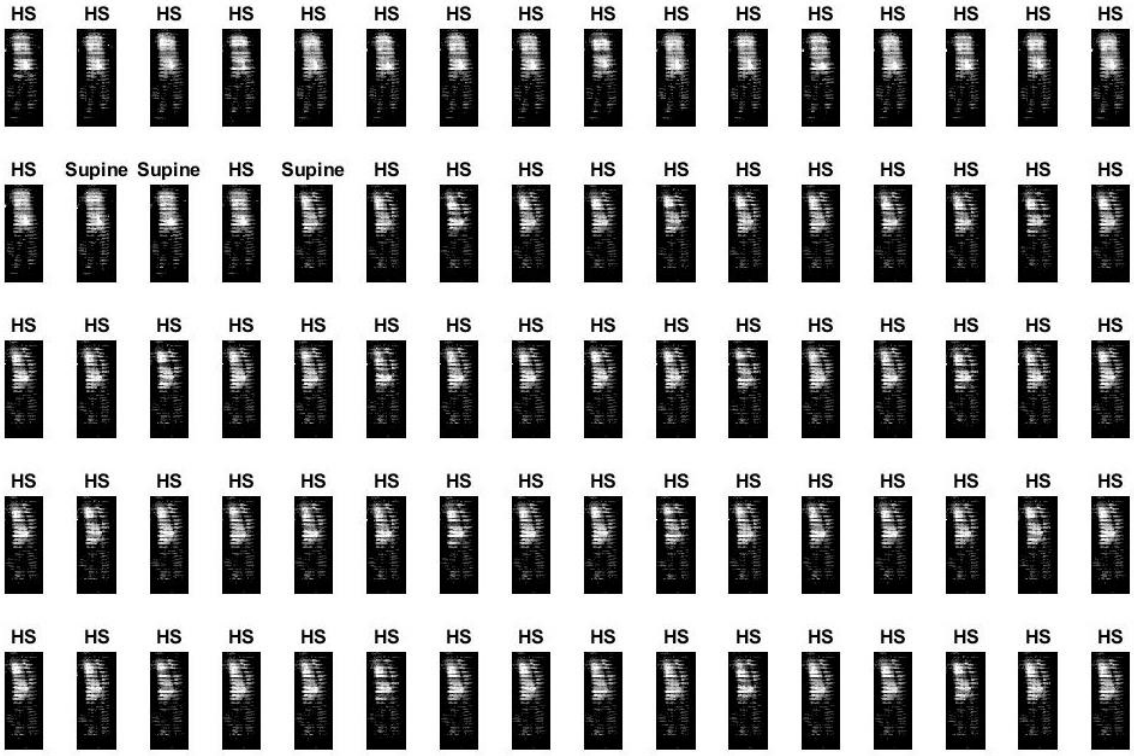

Figure L-2: Grey scale images representing some of the static postures adopted by **SCI 1** on the air cell mattress. The captions represent the classification performed with the **Naïve –Bayes algorithm**.

Figure L-3: Grey scale images representing some of the static postures adopted by **SCI 3** on the foam mattress. The captions represent the classification performed with the **KNN algorithm**. Captions in red indicates postures misclassified.

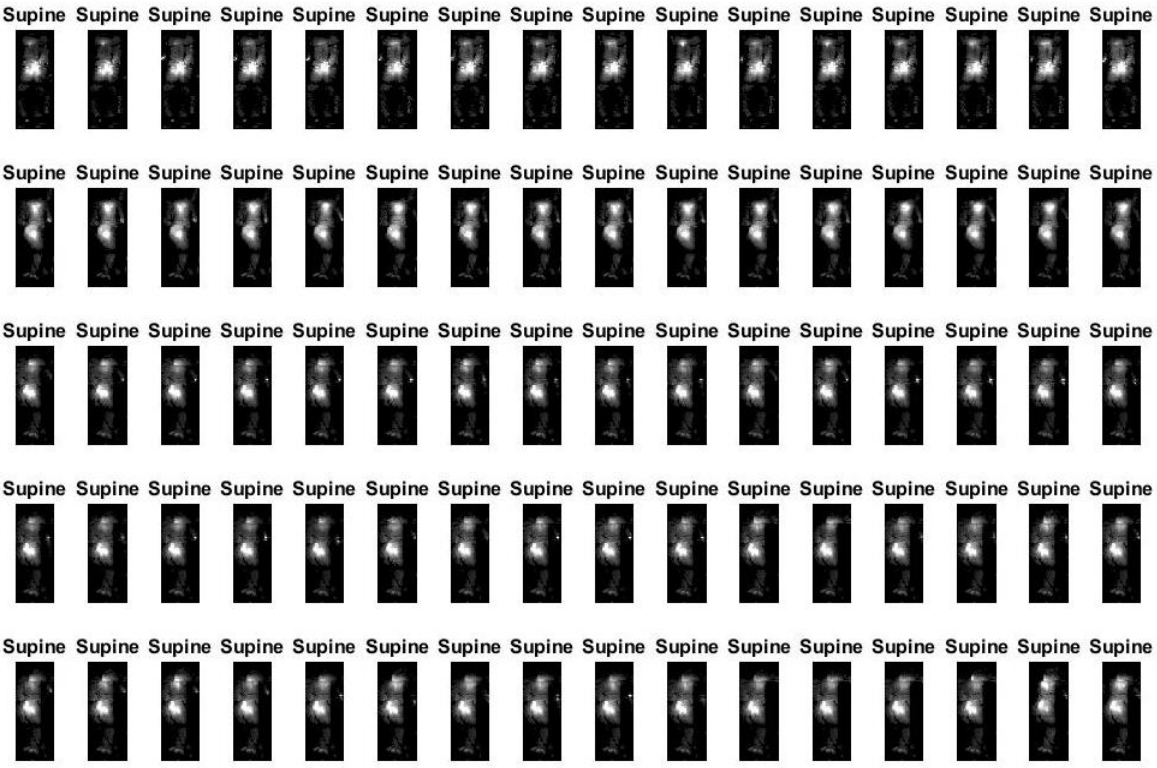

Figure L-4: Grey scale images representing some of the static postures adopted by **SCI 3** on the foam mattress. The captions represent the classification performed with the **Naïve – Bayes** algorithm.

References

International review. Pressure ulcer prevention: pressure, shear, friction and microclimate in context. A consensus document. London: Wounds International, 2010., 2010.

Abdel-Hamid, O., A. Mohamed, H. Jiang, L. Deng, G. Penn and D. Yu (2014). Convolutional Neural Networks for Speech Recognition. *IEEE/ACM Transactions on Audio, Speech, and Language Processing* 22(10): 1533-1545.

Akins, J., P. Karg and D. Brienza (2011). Interface shear and pressure characteristics of weelchair seat cushions. *Journal of Rehabilitation Research & Development* 48(3): 225-234.

Al Mutairi, K. B. and D. Hendrie (2018). Global incidence and prevalence of pressure injuries in public hospitals: A systematic review. *Wound Medicine* 22: 23-31.

Alhassan, S. and T. N. Robinson (2010). Defining accelerometer thresholds for physical activity in girls using ROC analysis. *Journal of physical activity & health* 7(1): 45-53.

Aylward-Wotton, N. and B. Kent (2017). Improving pressure damage detection in the community using continuous pressure monitoring of patients. Final report, Cornwall Partnership Foundation NHS Trust and University of Plymouth.

Bader, D. L. (1990). The recovery characteristics of soft tissues following repeated loading. *J Rehabil Res Dev.* 27(2): 141-150.

Bader, D. L. and P. R. Worsley (2018). Technologies to monitor the health of loaded skin tissues. *BioMed Eng OnLine* 17(40).

Bain, D. and M. Ferguson-Pell (2002). Remote monitoring of sitting behavior of people with spinal cord injury. *Journal of rehabilitation research and development* 39: 513-520.

Barrois, B., C. Labalette, P. Rousseau, A. Corbin, D. Colin, F. Allaert and J. L. Saumet (2008). A national prevalence study of pressure ulcers in French hospital inpatients. *Journal of Wound Care* 17(9): 373-379.

Bergstrom, N., B. Braden, A. Laguzza and V. Holman (1987). The Braden Scale for Predicting Pressure Sore Risk. *Nursing Research* 36(4): 205-210.

Black, J. M., J. E. Cuddigan, M. A. Walko, L. A. Didier, M. J. Lander and M. R. Kelpe (2010). Medical device related pressure ulcers in hospitalized patients. *International Wound Journal* 7(5): 358-365.

Bodenheimer, T., K. Lorig, H. Holman and K. Grumbach (2002). Patient Self-management of Chronic Disease in Primary Care. *JAMA* 288(19): 2469-2475.

Bogie, K., I. Nuseibeh and D. Bader (1995). Early progressive changes in tissue viability in seated spinal cord injured subjects. *Paraplegia* 33(3): 141-147.

Bogie, K., X. Wang, B. Fei and J. Sun (2008). New technique for real-time interface pressure analysis: Getting more out of large image data sets. *Journal of rehabilitation research and development* 45(4): 523-535.

Bosboom, E. M. H., C. V. C. Bouten, C. W. J. Oomens, H. W. M. van Straaten, F. P. T. Baaijens and H. Kuipers (2001). Quantification and localisation of damage in rat muscles after controlled loading; a new approach to study the aetiology of pressure sores. *Medical Engineering & Physics* 23(3): 195-200.

Bouten, C. V., C. W. Oomens, F. P. Baaijens and D. L. Bader (2003). The etiology of pressure ulcers: Skin deep or muscle bound? *Archives of Physical Medicine and Rehabilitation* 84(4): 616-619.

Bouten, C. V. C., M. M. Knight, D. A. Lee and D. L. Bader (2001). Compressive Deformation and Damage of Muscle Cell Subpopulations in a Model System. *Annals of Biomedical Engineering* 29(2): 153-163.

Breuls, R. G. M., C. V. C. Bouten, C. W. J. Oomens, D. L. Bader and F. P. T. Baaijens (2003). Compression Induced Cell Damage in Engineered Muscle Tissue: An In Vitro Model to Study Pressure Ulcer Aetiology. *Annals of Biomedical Engineering* 31(11): 1357-1364.

Brienza, D., J. Vallely, P. Karg, J. Akins and A. Gefen (2018). An MRI investigation of the effects of user anatomy and wheelchair cushion type on tissue deformation. *Journal of Tissue Viability* 27(1): 42-53.

Burges, C. J. C. (1998). A Tutorial on Support Vector Machines for Pattern Recognition. *Data Mining and Knowledge Discovery* 2(2): 121-167.

Caggiari, S., P. R. Worsley and D. L. Bader (2019). A sensitivity analysis to evaluate the performance of temporal pressure - related parameters in detecting changes in supine postures. *Medical Engineering & Physics* 69: 33-42.

Chai, C. Y. and D. L. Bader (2013). The physiological response of skin tissues to alternating support pressures in able-bodied subjects. *Journal of the Mechanical Behavior of Biomedical Materials* 28: 427-435.

Chai, C. Y., O. Sadou, P. R. Worsley and D. L. Bader (2017). Pressure signatures can influence tissue response for individuals supported on an alternating pressure mattress. *Journal of Tissue Viability* 26(3): 180-188.

Chi-Chun, H., H. Yu-Wei, C. Yu-Hsien and K. Chia-Hao (2008). Bayesian classification for bed posture detection based on kurtosis and skewness estimation. *HealthCom 2008 - 10th International Conference on e-health Networking, Applications and Services*: 165-168.

Cho, Y. K., S. G. Kim, D. Kim, H. J. Kim, J. Ryu, D. Lim, C.-Y. Ko and H. S. Kim (2014). Development of a shear measurement sensor for measuring forces at human–machine interfaces. *Medical Engineering & Physics* 36(12): 1721-1728.

Cicceri, G., F. De Vita, D. Bruneo, G. Merlino and A. Puliafito (2020). A deep learning approach for pressure ulcer prevention using wearable computing. *Human-centric Computing and Information Sciences* 10(1): 5.

Coggrave, M. J. and L. S. Rose (2012). A specialist seating assessment clinic: changing pressure relief practice. *Spinal Cord* 41: 692.

Coleman, S., C. Gorecki, E. A. Nelson, S. J. Closs, T. Defloor, R. Halfens, A. Farrin, J. Brown, L. Schoonhoven and J. Nixon (2013). Patient risk factors for pressure ulcer development: Systematic review. *International Journal of Nursing Studies* 50(7): 974-1003.

Coleman, S., E. A. Nelson, J. Keen, L. Wilson, E. McGinnis and C. Dealey (2014 b). Developing a pressure ulcer risk factor minimum data set and risk assessment framework. *Journal of Advanced Nursing* 70(10): 2339-2352.

Coleman, S., J. Nixon, J. Keen, L. Wilson, E. McGinnis, C. Dealey, N. Stubbs, A. Farrin, D. Dowding, J. M. G. A. Schols, J. Cuddigan, D. Berlowitz, E. Jude, P. Vowden, L. Schoonhoven, D. L. Bader, A. Gefen, C. W. J. Oomens and E. A. Nelson (2014 a). A new pressure ulcer conceptual framework. *Journal of Advanced Nursing* 70(10): 2222-2234.

Coleman, S., I. L. Smith, E. McGinnis, J. Keen, D. Muir, L. Wilson, N. Stubbs, C. Dealey, S. Brown, E. A. Nelson and J. Nixon (2018). Clinical evaluation of a new pressure ulcer risk assessment instrument, the Pressure Ulcer Risk Primary or Secondary Evaluation Tool (PURPOSE T). *Journal of Advanced Nursing* 74(2): 407-424.

Conti, M., S. Orcioni, N. M. Madrid, M. Gaiduk and R. Seepold (2018). A Review of Health Monitoring Systems Using Sensors on Bed or Cushion. I. Rojas, F. Ortuño and (eds). Book A Review of Health Monitoring Systems Using Sensors on Bed or Cushion. Bioinformatics and Biomedical Engineering. IWBBIO 2018, Lecture Notes in Computer Science. vol. 10814. Springer, Cham.

Cover, T. and P. Hart (1967). Nearest neighbor pattern classification. *IEEE Transactions on Information Theory* 13(1): 21-27.

Culhane, K. M., G. M. Lyons, D. Hilton, P. A. Grace and D. Lyons (2004). Long-term mobility monitoring of older adults using accelerometers in a clinical environment. *Clinical Rehabilitation* 18(3): 335-343.

Dai, R., S. E. Sonenblum and S. Sprigle (2012). A robust wheelchair pressure relief monitoring system. Book A robust wheelchair pressure relief monitoring system. 2012 Annual International Conference of the IEEE Engineering in Medicine and Biology Society.

Daniel, R. K., D. L. Priest and D. C. Wheatley (1981). Etiologic factors in pressure sores: an experimental model. *Archives of physical medicine and rehabilitation* 62(10): 492-498.

de Morton, N. A., D. J. Berlowitz and J. L. Keating (2008). A systematic review of mobility instruments and their measurement properties for older acute medical patients. *Health and quality of life outcomes* 6: 44-44.

Defloor, T., D. D. Bacquer and M. H. F. Grypdonck (2005). The effect of various combinations of turning and pressure reducing devices on the incidence of pressure ulcers. *International Journal of Nursing Studies* 42(1): 37-46.

Defloor, T. and M. F. Grypdonck (2005). Pressure ulcers: validation of two risk assessment scales. *Journal of Clinical Nursing* 14(3): 373-382.

Defloor, T. and M. H. F. Grypdonck (1999). Sitting posture and prevention of pressure ulcers. *Applied Nursing Research* 12(3): 136-142.

Demarré, L., A. Van Lancker, A. Van Hecke, S. Verhaeghe, M. Grypdonck, J. Lemey, L. Annemans and D. Beeckman (2015). The cost of prevention and treatment of pressure ulcers: A systematic review. *International Journal of Nursing Studies* 52(11): 1754-1774.

Dinsdale, S. M. (1974). Decubitus Ulcers: Role of pressure and friction causation. *Arch Phys Med Rehabil* 55: 147-152.

Do, N. H., D. Y. Kim, J.-H. Kim, J. H. Choi, S. Y. Joo, N. K. Kang and Y. S. Baek (2016). Effects of a continuous lateral turning device on pressure relief. *Journal of Physical Therapy Science* 28(2): 460-466.

Dowd, G., K. Linge and G. Bentley (1983). Measurement of transcutaneous oxygen pressure in normal and ischaemic skin. *J Bone Joint Surg Br* 65(1): 79-83.

Duvall, J., P. Karg, D. Brienza and J. Pearlman (2019). Detection and classification methodology for movements in the bed that supports continuous pressure injury risk assessment and repositioning compliance. *Journal of Tissue Viability* 28(1): 7-13.

Edwardson, C. L., A. V. Rowlands, S. Bunnewell, J. Sanders, D. W. Esliger, T. Gorely, S. O'Connell, M. J. Davies, K. Khunti and T. Yates (2016). Accuracy of Posture Allocation Algorithms for Thigh- and Waist-Worn Accelerometers. *Medicine & Science in Sports & Exercise* 48(6): 1085-1090.

Efron, B. (2013). Bayes' Theorem in the 21st Century. *Science* 340(6137): 1177.

Elgendi, M., B. Eskofier, S. Dokos and D. Abbott (2014). Revisiting QRS detection methodologies for portable, wearable, battery-operated, and wireless ECG systems. *PloS one* 9(1): e84018.

Farage, M. A., K. W. Miller, P. Elsner and H. I. Maibach (2013). Characteristics of the Aging Skin. *Advances in wound care* 2(1): 5-10.

Fenety, P. A., C. Putnam and J. M. Walker (2000). In-chair movement: validity, reliability and implications for measuring sitting discomfort. *Applied Ergonomics* 31(4): 383-393.

Ferguson-Pell, M. and M. D. Cardi (1993). Prototype Development and Comparative Evaluation of Wheelchair Pressure Mapping System. *Assistive Technology* 5(2): 78-91.

Ferris, A., A. Price and K. Harding (2019). Pressure ulcers in patients receiving palliative care: A systematic review. *Palliative Medicine* 33(7): 723-725.

Fortune, E., V. A. Lugade and K. R. Kaufman (2014). Posture and movement classification: the comparison of tri-axial accelerometer numbers and anatomical placement. *Journal of biomechanical engineering* 136(5): 051003.

Foubert, N., A. M. McKee, R. A. Goubran and F. Knoefel (2012). Lying and sitting posture recognition and transition detection using a pressure sensor array. *2012 IEEE International Symposium on Medical Measurements and Applications Proceedings*: 1-6.

Gawlitta, D., W. Li, C. Oomens, F. Baaijens, D. Bader and C. Bouten (2007 a). The Relative Contributions of Compression and Hypoxia to Development of Muscle Tissue Damage: An In Vitro Study. *Annals of Biomedical Engineering* 35(2): 273-284.

Gawlitta, D., C. W. J. Oomens, D. L. Bader, F. P. T. Baaijens and C. V. C. Bouten (2007 b). Temporal differences in the influence of ischemic factors and deformation on the metabolism of engineered skeletal muscle. *Journal of Applied Physiology* 103(2): 464-473.

Gefen, A. (2007 a). The biomechanics of sitting-acquired pressure ulcers in patients with spinal cord injury or lesions. *International Wound Journal* 4(3): 222-231.

Gefen, A. (2007 b). Pressure-sensing devices for assessment of soft tissue loading under bony prominences: technological concepts and clinical utilization. *Wounds* 19: 350-362.

Gefen, A. (2009 a). Reswick and Rogers pressure-time curve for pressure ulcer risk. Part 1. *Nursing standard (Royal College of Nursing (Great Britain) : 1987)* 23: 64, 66, 68 passim.

Gefen, A. (2009 b). Reswick and Rogers pressure-time curve for pressure ulcer risk. Part 2. *Nursing standard (Royal College of Nursing (Great Britain) : 1987)* 23: 40-44.

Gefen, A., B. van Nierop, D. L. Bader and C. W. Oomens (2008). Strain-time cell-death threshold for skeletal muscle in a tissue-engineered model system for deep tissue injury. *Journal of Biomechanics* 41(9): 2003-2012.

Ghazwan, A., S. M. Forrest, C. A. Holt and G. M. Whatling (2017). Can activities of daily living contribute to EMG normalization for gait analysis? *PloS one* 12(4): e0174670-e0174670.

Gilsdorf, P., R. Patterson, S. Fisher and N. Appel (1990). Sitting forces and weelchair mechanism. *Journal of Rehabilitation Research & Development* 27(3): 239-246.

Goossens, R. H. M., R. Zegers, G. A. H. van Dijke and C. J. Snijders (1994). Influence of shear on skin oxygen tension. *Clinical Physiology* 14(1): 111-118.

Gorecki, C., J. Nixon, A. Madill, J. Firth and J. M. Brown (2012). What influences the impact of pressure ulcers on health-related quality of life? A qualitative patient-focused exploration of contributory factors. *Journal of Tissue Viability* 21(1): 3-12.

Grant, P. M., C. G. Ryan, W. W. Tigbe and M. H. Granat (2006). The validation of a novel activity monitor in the measurement of posture and motion during everyday activities. *British Journal of Sports Medicine* 40(12): 992-997.

Gray, R. J., P. R. Worsley, D. Voegeli and D. L. Bader (2016). Monitoring contractile dermal lymphatic activity following uniaxial mechanical loading. *Medical Engineering & Physics* 38(9): 895-903.

Guest, J. F., N. Ayoub, T. McIlwraith, I. Uchegbu, A. Gerrish, D. Weidlich, K. Vowden and P. Vowden (2017). Health economic burden that different wound types impose on the UK's National Health Service. *International Wound Journal* 14(2): 322-330.

Guest, J. F., N. Ayoub, T. Mcllwraith, I. Uchegbu, A. Gerrish, D. Weidlich, K. Vowden and P. Vowden (2015). Heath economic burden that wounds impose on the National Health Service in the UK. *BMJ Open* 5(12): e009283.

Guest, J. F., G. W. Fuller, P. Vowden and K. R. Vowden (2018). Cohort study evaluating pressure ulcer management in clinical practice in the UK following initial presentation in the community: costs and outcomes. *BMJ Open* 8(7).

Gunningberg, L., C. Bååth and E. Sving (2018). Staff's perceptions of a pressure mapping system to prevent pressure injuries in a hospital ward: A qualitative study. *Journal of Nursing Management* 26(2): 140-147.

Gunningberg, L. and C. Carli (2016). Reduced pressure for fewer pressure ulcers: can real-time feedback of interface pressure optimise repositioning in bed? *International Wound Journal* 13(5): 774-779.

Gunningberg, L., I.-M. Sedin, S. Andersson and R. Pingel (2017). Pressure mapping to prevent pressure ulcers in a hospital setting: A pragmatic randomised controlled trial. *International Journal of Nursing Studies* 72: 53-59.

Gunningberg, L., N. A. Stotts and E. Idvall (2011). Hospital-acquired pressure ulcers in two Swedish County Councils: cross-sectional data as the foundation for future quality improvement. *International Wound Journal* 8(5): 465-473.

Gyi, D. E., J. M. Porter and N. K. B. Robertson (1998). Seat pressure measurement technologies: considerations for their evaluation. *Applied Ergonomics* 29(2): 85-91.

Harstall, C. (1996). Interface Pressure measurament systems for management of pressure sores. *Alberta Heritage Foundation for Medical Research (AHFMR)* 14.

Hermans, M. H. E. and E. Call (2015). Failure to Reposition After Sliding Down in Bed Increases Pressure at the Sacrum and Heels. *Wounds* 27(7): 191-198.

Herrman, E., C. Knapp, D. JC and R. Salcido (1999). Skin perfusion responses to surface pressure-induced ischemia: Implication for the developing pressure ulcer. *Journal of Rehabilitation Research & Development* 36(2).

Hijazi, S., R. Kumar and C. Rowen (2015). Using Convolutional Neural Networks for Images Recognition. *IP Group, Cadence*.

Hobson, D. A. (1992). Comparative effects of postures on pressure and shear at the body-seat interface. *Journal of Rehabilitation Research and Development* 29(4): 21-31.

Hu, B., P. C. Dixon, J. V. Jacobs, J. T. Dennerlein and J. M. Schiffman (2018). Machine learning algorithms based on signals from a single wearable inertial sensor can detect surface- and age-related differences in walking. *Journal of Biomechanics* 71: 37-42.

Husain, T. (1953). An experimental study of some pressure effects on tissues, with reference to the bed-sore problem. *The Journal of Pathology and Bacteriology* 66(2): 347-358.

Hyun, S., X. Li, B. Vermillion, C. Newton, M. Fall, P. Kaewprag, S. Moffatt-Bruce and E. R. Lenz (2014). Body mass index and pressure ulcers: improved predictability of pressure ulcers in intensive care patients. *American journal of critical care : an official publication, American Association of Critical-Care Nurses* 23(6): 494-501.

Ifedili, I. A., S. M. Kennerly, V. K. Sabol and T. L. Yap (2018). Implementing a visual cueing technology intervention in a nursing home: Nursing staff perceptions. *Geriatric Nursing* 39(5): 607-609.

Jacobs, D. A. and D. P. Ferris (2015). Estimation of ground reaction forces and ankle moment with multiple, low-cost sensors. *Journal of neuroengineering and rehabilitation* 12: 90-90.

Källman, U., S. Bergstrand, A.-C. Ek, M. Engström and M. Lindgren (2016). Nursing staff induced repositionings and immobile patients' spontaneous movements in nursing care. *International Wound Journal* 13(6): 1168-1175.

Kapp, S., C. Miller and N. Santamaria (2018). The quality of life of people who have chronic wounds and who self-treat. *Journal of Clinical Nursing* 27(1-2): 182-192.

Karatas, G. K., A. K. Tosun and U. Kanatl (2008). Center-of-Pressure Displacement During Postural Changes in Relation to Pressure Ulcers in Spinal Cord-Injured Patients. *American Journal of Physical Medicine & Rehabilitation* 87(3): 177-182.

Kim, J. H., X. Wang, C. H. Ho and K. M. Bogie (2012). Physiological measurements of tissue health; implications for clinical practice. *International Wound Journal* 9(6): 656-664.

Kim, Y., Y. Son, W. Kim, B. Jin and M. Yun (2018). Classification of Children's Sitting Postures Using Machine Learning Algorithms. *Applied Sciences* 8(8): 1280.

Knight, S. L., R. P. Taylor, A. A. Polliack and D. L. Bader (2001). Establishing predictive indicators for the status of loaded soft tissues. *Journal of Applied Physiology* 90(6): 2231-2237.

Kosiak, M. (1961). Etiology of decubitus ulcers. *Archives Of Physical Medicine And Rehabilitation* 42: 19-29.

Kottner, J., J. Black, E. Call, A. Gefen and N. Santamaria (2018). Microclimate: A critical review in the context of pressure ulcer prevention. *Clinical Biomechanics* 59: 62-70.

Kottner, J., A. Gefen and N. Lahmann (2011). Weight and pressure ulcer occurrence: A secondary data analysis. *International Journal of Nursing Studies* 48(11): 1339-1348.

Lahmann, N. A., R. J. G. Halfens and T. Dassen (2006). Pressure Ulcers in German Nursing Homes and Acute Care Hospitals: Prevalence, Frequency, and Ulcer Characteristics. *Ostomy Wound Management* 52(2): 20-33.

Landis, E. (1930). Micro-injection studies of capillary blood pressure inhuman skin. *Heart* 15: 209-228.

Laszczak, P., L. Jiang, D. L. Bader, D. Moser and S. Zahedi (2015). Development and validation of a 3D-printed interfacial stress sensor for prosthetic applications. *Medical Engineering & Physics* 37(1): 132-137.

Laszczak, P., M. McGrath, J. Tang, J. Gao, L. Jiang, D. L. Bader, D. Moser and S. Zahedi (2016). A pressure and shear sensor system for stress measurement at lower limb residuum/socket interface. *Medical Engineering & Physics* 38(7): 695-700.

Lee, C., J. Park, S. Park and C. H. Kim (2019). Fall-Detection Algorithm Using Plantar Pressure and Acceleration Data. *International Journal of Precision Engineering and Manufacturing*.

Lemmens, J. M., J. Broadbridge, M. Macaulay, R. W. Rees, M. Archer, M. J. Drake, K. N. Moore, D. L. Bader and M. Fader (2019). Tissue response to applied loading using different designs of penile compression clamps. *Medical devices (Auckland, N.Z.)* 12: 235-243.

Liao, F., S. Burns and Y.-K. Jan (2013). Skin blood flow dynamics and its role in pressure ulcers. *Journal of Tissue Viability* 22(2): 25-36.

Linder-Ganz, E., S. Engelberg, M. Scheinowitz and A. Gefen (2006). Pressure–time cell death threshold for albino rat skeletal muscles as related to pressure sore biomechanics. *Journal of Biomechanics* 39(14): 2725-2732.

Linder-Ganz, E. and A. Gefen (2007). The Effects of Pressure and Shear on Capillary Closure in the Microstructure of Skeletal Muscles. *Annals of Biomedical Engineering* 35(12): 2095-2107.

Lippoldt, J., E. Pernicka and T. Staudinger (2014). Interface Pressure at Different Degrees of Backrest Elevation With Various Types of Pressure-Redistribution Surfaces. *American Association of Critical-Care Nurses* 23(2): 119-126.

Loerakker, S., E. Manders, G. J. Strijkers, K. Nicolay, F. P. T. Baaijens, D. L. Bader and C. W. J. Oomens (2011). The effects of deformation, ischemia, and reperfusion on the development of muscle damage during prolonged loading. *Journal of Applied Physiology* 111(4): 1168-1177.

Loerakker, S., L. R. Solis, D. L. Bader, F. P. T. Baaijens, V. K. Mushahwar and C. W. J. Oomens (2013). How does muscle stiffness affect the internal deformations within the soft tissue layers of the buttocks under constant loading? *Computer Methods in Biomechanics and Biomedical Engineering* 16(5): 520-529.

Loerakker, S., A. Stekelenburg, G. J. Strijkers, J. J. M. Rijpkema, F. P. T. Baaijens, D. L. Bader, K. Nicolay and C. W. J. Oomens (2010). Temporal Effects of Mechanical Loading on Deformation-Induced Damage in Skeletal Muscle Tissue. *Annals of Biomedical Engineering* 38(8): 2577-2587.

Lyden, K., D. John, P. Dall and M. H. Grant (2016). Differentiating Sitting and Lying Using a Thigh-Worn Accelerometer. *Medicine & Science in Sports & Exercise* 48(4): 742-747.

Manini, A. and A. M. Sabatini (2010). Machine Learning Methods for Classifying Human Physical Activity from On-Body Accelerometers. *sensors* 10: 1154-1175.

Margolis, D. J., J. Knauss, W. Bilker and M. Baumgarten (2003). Medical conditions as risk factors for pressure ulcers in an outpatient setting. *Age and Ageing* 32(3): 259-264.

Matar, G., J. Lina and G. Kaddoum (2019). Artificial neural network for in-bed posture classification using bed-sheet pressure sensors. *IEEE Journal of Biomedical and Health Informatics*: 1-1.

Mathie, M. J., A. C. F. Coster, N. H. Lovell and B. G. Celler (2003). Detection of daily physical activities using a triaxial accelerometer. *Medical and Biological Engineering and Computing* 41(3): 296-301.

McInnes, E., A. Jammali-Blasi, S. E. M. Bell-Syer, J. C. Dumville, V. Middleton and N. Cullum (2015). Support surfaces for pressure ulcer prevention. *Cochrane Database of Systematic Reviews* 50(9): 419-430.

Merino, M., O. Rivera, I. Gómez, A. Molina and E. Dorronzoro (2010). A Method of EOG Signal Processing to Detect the Direction of Eye Movements. Book A Method of EOG Signal Processing to Detect the Direction of Eye Movements. 2010 First International Conference on Sensor Device Technologies and Applications.

Mervis, J. S. and T. J. Phillips (2019). Pressure Ulcers: Prevention and Management. *Journal of the American Academy of Dermatology* 81(4): 893-902.

Miller, G. and J. Seale (1981). Lymphatic clearance during compressive loading. *Lymphology* 14(4): 161-166.

Ming, Z. and V. C. Roberts (1993). The effect of shear forces externally applied to skin surface on underlying tissues. *Journal of Biomedical Engineering* 15(6): 451-456.

Mohammed, S., A. Samé, L. Oukhellou, K. Kong, W. Huo and Y. Amirat (2016). Recognition of gait cycle phases using wearable sensors. *Robotics and Autonomous Systems* 75: 50-59.

Moore, Z., S. Cowman and R. M. Conroy (2011). A randomised controlled clinical trial of repositioning, using the 30° tilt, for the prevention of pressure ulcers. *Journal of Clinical Nursing* 20(17-18): 2633-2644.

Moore, Z., S. Cowman and J. Posnett (2013). An economic analysis of repositioning for the prevention of pressure ulcers. *Journal of Clinical Nursing* 22(15-16): 2354-2360.

Nelissen, J. L., W. A. Traa, H. H. d. Boer, L. d. Graaf, V. Mazzoli, C. D. Savci-Heijink, K. Nicolay, M. Froeling, D. L. Bader, A. J. Nederveen, C. W. J. Oomens and G. J. Strijkers (2018). An advanced magnetic resonance imaging perspective on the etiology of deep tissue injury. *Journal of Applied Physiology* 124(6): 1580-1596.

NHS. (2019). NHS Long Term Plan. 2019.

Nixon, J., I. L. Smith, S. Brown, E. McGinnis, A. Vargas-Palacios and E. A. Nelson (2019). Pressure relieving support surfaces for pressure ulcer prevention (PRESSURE 2): clinical and health economic results of a randomised controlled trial [published online ahead of print September 3 2019].

Norton, D., R. McLaren and A. Exton-Smith (1962). An Investigation of Geriatric Nursing Problems in Hospital. *London: The National Corporation for the Care of Old People*.

NPUAP. (2007). Support Surface Standards (S3I) Terms and Definitions Related to Support Surfaces. From http://www.npuap.org/wp-content/uploads/2012/03/NPUAP_S3I_TD.pdf and https://www.npuap.org/wp-content/uploads/2012/01/Terms-and-Defs-Feb-5-2019-FINAL-3.12-2.pdf.

NPUAP/EPUAP/PPPIA. Prevention and Treatment of Pressure Ulcers: Clinical Practice Guideline. Emily Haesler (Ed.). Cambridge Media: Perth, Australia, 2019.

Oomens, C. W. J., O. F. J. T. Bressers, E. M. H. Bosboom, C. V. C. Bouten and D. L. Bader (2003). Can Loaded Interface Characteristics Influence Strain Distributions in Muscle Adjacent to Bony Prominences? *Computer Methods in Biomechanics and Biomedical Engineering* 6(3): 171-180.

Oomens, C. W. J., S. Loerakker and D. L. Bader (2010). The importance of internal strain as opposed to interface pressure in the prevention of pressure related deep tissue injury. *Journal of Tissue Viability* 19(2): 35-42.

Pancorbo-Hidalgo, P. L., F. P. Garcia-Fernandez, I. M. Lopez-Medina and C. Alvarez-Nieto (2006). Risk assessment scales for pressure ulcer prevention: a systematic review. *Journal of Advanced Nursing* 54(1): 94-110.

Papanikolaou, P., P. Lyne and D. Anthony (2007). Risk assessment scales for pressure ulcers: A methodological review. *International Journal of Nursing Studies* 44(2): 285-296.

Peeters, E. A. G., C. V. C. Bouten, C. W. J. Oomens and F. P. T. Baaijens (2003). Monitoring the biomechanical response of individual cells under compression: A new compression device. *Medical and Biological Engineering and Computing* 41(4): 498-503.

Peirce, S., T. Skalak and G. Rodeheaver (2000). Ischemia-reperfusion injury in chronic pressure ulcer formation: A skin model in the *Wound Repair and Regeneration* 8(1): 68-75.

Peterson, M., W. Schwab, K. McCutcheon, J. H. van Oostrom, N. Gravenstein and L. Caruso (2008). Effects of elevating the head of bed on interface pressure in volunteers. *Critical Care Medicine* 36(11): 3038-3042.

Peterson, M., W. Schwab, K. McCutcheon, J. H. van Oostrom, N. Gravenstein and L. Caruso (2013). Patient repositioning and pressure ulcer risk - Monitoring interface pressures of at-risk patients. *Journal of Rehabilitation Research & Development (JRRD)* 50(4): 477–488.

Phillips, L. and J. Buttery (2009). Exploring pressure ulcer prevalence and preventative care. *Nursing Times* 105(16): 34-36.

Pickham, D., N. Berte, M. Pihulic, A. Valdez, B. Mayer and M. Desai (2018). Effect of a wearable patient sensor on care delivery for preventing pressure injuries in acutely ill adults: A pragmatic randomized clinical trial (LS-HAPI study). *International Journal of Nursing Studies* 80: 12-19.

Rajan, V., B. Varghese, T. G. van Leeuwen and W. Steenbergen (2009). Review of methodological developments in laser Doppler flowmetry. *Lasers in Medical Science* 24(2): 269-283.

Reenalda, J., M. Jannink, M. Nederhand and M. Ijzerman (2009). Clinical Use of Interface Pressure to Predict Pressure Ulcer Development: A Systematic Review. *Assistive Technology* 21(2): 76-85.

Reswick, J. and J. Rogers (1976). Experience at Rancho Los Amigos Hospital with devices and techniques to prevent pressure ulcers. Bedsores Biomechanics. Cowden J.M. (eds) Kenedi R.M. Strathclyde Bioengineering Seminars, Palgrave, London

Rich, S. E., D. Margolis, M. Shardell, W. G. Hawkes, R. R. Miller, S. Amr and M. Baumgarten (2011). Frequent manual repositioning and incidence of pressure ulcers among bed-bound elderly hip fracture patients. *Wound Repair and Regeneration* 19(1): 10-18.

Rithalia, S. V. S. (2004). Evaluation of alternating pressure air mattresses: one laboratory-based strategy. *Journal of Tissue Viability* 14(2): 51-58.

Rus, S., T. Grosse-Puppendahl and A. Kuijper (2017). Evaluating the recognition of bed postures using mutual capacitance sensing. *Journal of Ambient Intelligence and Smart Environments* 9(1): 113 - 127.

Saripalle, S. K., G. C. Paiva, T. C. Cliett, R. R. Derakhshani, G. W. King and C. T. Lovelace (2014). Classification of body movements based on posturographic data. *Human Movement Science* 33: 238-250.

Scott, R. G. and K. M. Thurman (2014). Visual Feedback of Continuous Bedside Pressure Mapping to Optimize Effective Patient Repositioning. *Advances in Wound Care* 3(5): 376-382.

Shaked, E. and A. Gefen (2013). Modeling the Effects of Moisture-Related Skin-Support Friction on the Risk for Superficial Pressure Ulcers during Patient Repositioning in Bed. *Frontiers in bioengineering and biotechnology* 1: 9-9.

Shier, D., J. Butler and R. Lewis. Hole's human anatomy and physiology. McGraw-Hill: Boston, 2004

Shlens, J. (2014). A Tutorial on Principal Component Analysis. *arXiv:1404.1100v1 [cs.LG]*

Short, R. and K. Fukunaga (1981). The optimal distance measure for nearest neighbor classification. *IEEE Transactions on Information Theory* 27(5): 622-627.

Smits, E. J., E. A. H. Winkler, G. N. Healy, P. M. Dall, M. H. Granat and P. W. Hodges (2018). Comparison of single- and dual-monitor approaches to differentiate sitting from lying in free-living conditions. *Scandinavian Journal of Medicine & Science in Sports* 28(8): 1888-1896.

Spilsbury, K., A. Nelson, N. Cullum, C. Iglesias, J. Nixon and S. Mason (2007). Pressure ulcers and their treatment and effects on quality of life: hospital inpatient perspectives. *Journal of Advanced Nursing* 57(5): 494-504.

Sprigle, S., S. E. Sonenblum and C. Feng (2019). Pressure redistributing in-seat movement activities by persons with spinal cord injury over multiple epochs. *PloS one* 14(2): e0210978-e0210978.

Stephens, M., C. Bartley, R. Betteridge and R. Samuriwo (2018). Developing the tissue viability seating guidelines. *Journal of Tissue Viability* 27(1): 74-79.

Stevenson, R., M. Collinson, V. Henderson, L. Wilson, C. Dealey, E. McGinnis, M. Briggs, E. A. Nelson, N. Stubbs, S. Coleman and J. Nixon (2013). The prevalence of pressure ulcers in community settings: An observational study. *International Journal of Nursing Studies* 50(11): 1550-1557.

Stinson, M., R. Ferguson and A. Porter-Armstrong (2018). Exploring repositioning movements in sitting with 'at risk' groups using accelerometry and interface pressure mapping technologies. *Journal of Tissue Viability* 27(1): 10-15.

Stinson, M., R. Schofield, C. Gillan, J. Morton, E. Gardner, S. Sprigle and A. Porter-Armstrong (2013). Spinal Cord Injury and Pressure Ulcer Prevention: Using Functional Activity in Pressure Relief. *Nursing Research and Practice* 2013: Article ID 860396, 860398 pages.

Stinson, M. D., A. P. Porter-Armstrong and P. A. Eakin (2003). Pressure mapping systems: reliability of pressure map interpretation. *Clinical Rehabilitation* 17(5): 504-511.

Stockton, L., K. S. Gebhardt and M. Clark (2009). Seating and pressure ulcers: Clinical practice guideline. *Journal of Tissue Viability* 18(4): 98-108.

Taborri, J., E. Palermo, S. Rossi and P. Cappa (2016). Gait Partitioning Methods: A Systematic Review. *Sensors (Basel, Switzerland)* 16(1): 66.

Torra i Bou, J.-E., F. P. García-Fernández, P. L. Pancorbo-Hidalgo and K. Furtado (2006). Risk Assessment Scales for Predicting the Risk of Developing Pressure Ulcers. Science and Practice of Pressure Ulcer Management. Clark M. Romanelli M., Cherry G., Colin D., Defloor T. (eds) Springer, London 43-57.

Traa, W. A., M. C. van Turnhout, J. L. Nelissen, G. J. Strijkers, D. L. Bader and C. W. J. Oomens (2019). There is an individual tolerance to mechanical loading in compression induced deep tissue injury. *Clinical Biomechanics* 63: 153-160.

Tsaousi, G., G. Stavrou, A. Ioannidis, S. Salonikidis and K. Kotzampassi (2015). Pressure Ulcers and Malnutrition: Results from a Snapshot Sampling in a University Hospital. *Medical Principles and Practice* 24(1): 11-16.

Tubaishat, A., P. Papanikolaou, D. Anthony and L. Habiballah (2017). Pressure Ulcers Prevalence in the Acute Care Setting: A Systematic Review, 2000-2015. *Clinical Nursing Research* 27(6): 643-659.

Tung, J., B. Stead, W. Mann, B. Pham and M. Popovic (2015). Assistive technologies for self-managed pressure ulcer prevention in spinal cord injury: A scoping review. *The Journal of Rehabilitation Research and Development* 52: 131-146.

Vanderwee, K., T. Defloor, D. Beeckman, L. Demarré, S. Verhaeghe, T. Van Durme and M. Gobert (2011). Assessing the adequacy of pressure ulcer prevention in hospitals: a nationwide prevalence survey. *BMJ Quality & Safety* 20(3): 260-267.

Vanderwee, K., M. H. F. Grypdonck, D. D. Bacquer and T. Defloor (2007). Effectiveness of turning with unequal time intervals on the incidence of pressure ulcer lesions. *Journal of Advanced Nursing* 57(1): 59-68.

Wai, A. P., S. F. Foo, W. Huang, J. Biswas, C.-C. Hsia, K. Liou and P. Yap (2010). Lying Posture Classification for Pressure Ulcer Prevention. *Journal of Healthcare Engineering* 1(2): 217-238.

Walia, G. S., A. L. Wong, A. Y. Lo, G. A. Mackert, H. M. Carl, R. A. Pedreira, R. Bello, C. S. Aquino, W. V. Padula and J. M. Sacks (2016). Efficacy of Monitoring Devices in Support of Prevention of Pressure Injuries: Systematic Review and Meta-analysis. *Advances in Skin & Wound Care* 29(12): 567-574.

Wang, F., Y. Wang, Y. Tian, P. Zhang, J. Chen and J. Li (2019). Pattern recognition and prognostic analysis of longitudinal blood pressure records in hemodialysis treatment based on a convolutional neural network. *Journal of Biomedical Informatics* 98: 103271.

Waterlow, J. (1985). Pressure sores: a risk assessment card. *Nursing Times* 81(48): 49-55.

Wong, H., J. Kaufman, B. Baylis, J. M. Conly, D. B. Hogan, H. T. Stelfox, D. A. Southern, W. A. Ghali and C. H. Ho (2015). Efficacy of a pressure-sensing mattress cover system for reducing interface pressure: study protocol for a randomized controlled trial. *Trials* 16(1): 434.

Woodhouse, M., P. R. Worsley, D. Voegeli, L. Schoonhoven and D. L. Bader (2015). The physiological response of soft tissue to periodic repositioning as a strategy for pressure ulcer prevention. *Clinical Biomechanics* 30(2): 166-174.

Woodhouse, M., P. R. Worsley, D. Voegeli, L. Schoonhoven and D. L. Bader (2019). How consistent and effective are current repositioning strategies for pressure ulcer prevention? *Applied Nursing Research* 48: 58-62.

Worsley, P. and D. Voegeli (2013). Back to basics: biophysical methods in tissue viability research. *Journal of Wound Care* 22(8): 434-439.

Worsley, P. R., B. Parsons and D. L. Bader (2016). An evaluation of fluid immersion therapy for the prevention of pressure ulcers. *Clinical Biomechanics* 40: 27-32.

Worsley, P. R., D. Rebolledo, S. Webb, S. Caggiari and D. L. Bader (2017). Monitoring the biomechanical and physiological effects of postural changes during leisure chair sitting. *Journal of Tissue Viability* 27(1): 16-22.

Worsley, P. R., G. Smith, L. Schoonhoven and D. L. Bader (2016). Characteristics of patients who are admitted with or acquire Pressure Ulcers in a District General Hospital; a 3 year retrospective analysis. *Nursing open* 3(3): 152-158.

Yang, C.-C. and Y.-L. Hsu (2010). A review of accelerometry-based wearable motion detectors for physical activity monitoring. *Sensors (Basel, Switzerland)* 10(8): 7772-7788.

Yang, Y. S., G. L. Chang, M. J. Hsu and J. J. Chang (2009). Remote monitoring of sitting behaviors for community-dwelling manual wheelchair users with spinal cord injury. *Spinal Cord* 47(1): 67-71.

Yousefi, R., S. Ostadabbas, M. Faezipour, M. Farshbaf, M. Nourani, L. Tamil and M. Pompeo (2011). Bed posture classification for pressure ulcer prevention. *2011 Annual International Conference of the IEEE Engineering in Medicine and Biology Society*: 7175-7178.

Zemp, R., M. Tanadini, S. Pluss, K. Schnuriger, N. B. Singh, W. R. Taylor and S. Lorenzetti (2016). Application of Machine Learning Approaches for Classifying Sitting Posture Based on Force and Acceleration Sensors. *BioMed Research International* 2016.

Zhou, L., Q. Li, G. Huo and Y. Zhou (2017). Image Classification Using Biomimetic Pattern Recognition with Convolutional Neural Networks Features. *Computational Intelligence and Neuroscience* 2017: 12.